

Derivation of a traffic load model for the structural design of highway bridges in South Africa

by Pierre Francois van der Spuy

Dissertation presented for the degree of Doctor of Philosophy in the Faculty of
Engineering at Stellenbosch University



Supervisor:

Professor Roman Lenner

Examined by:

Professor Eugene O'Brien

University College Dublin

Professor Joan Ramon Casas

Universitat Politècnica de Catalunya

Professor Johan Retief

Stellenbosch University

March 2020

“I think that when we know that we actually do live in uncertainty, then we ought to admit it; it is of great value to realize that we do not know the answers to different questions. This attitude of mind - this attitude of uncertainty - is vital to the scientist, and it is this attitude of mind which the student must first acquire.”

- Richard Feynman

Declaration

By submitting this thesis/dissertation electronically, I declare that the entirety of the work contained therein is my own, original work, that I am the sole author thereof (save to the extent explicitly otherwise stated), that reproduction and publication thereof by Stellenbosch University will not infringe any third party rights and that I have not previously in its entirety or in part submitted it for obtaining any qualification.

Abstract

This study sets out to derive a new traffic load model for the design of highway bridges in South Africa, with novel contributions to the field of bridge traffic loading. The current code for bridge design in South Africa, Technical Methods for Highways 7 (TMH7), was published in 1981 and was shown by previous studies, and by this study, to be deficient at characteristic level. This is especially true for shorter spans. TMH7 does not give any indication of the levels of safety used to calibrate the code and it is therefore not clear whether the code is still providing the necessary safety margins. Several studies, outlined in this document, show that the Uniformly Distributed Load (UDL) and knife edge loads for type NA loading should be increased. NA is referred to in TMH7 as normal loading. Further to this, the legal limit for Gross Vehicle Weight (GVW) was increased to 56 t and the vehicle characteristics on our roads have changed significantly since 1981. TMH7 loading is widely regarded in industry as too complex to apply and engineers have called for a simplified load model. A study of this nature is therefore well motivated to ensure safety of road users and to increase design efficiency for bridge engineers.

Derivation of traffic load models requires measured traffic data. Previous studies showed that at least one year of Weigh in Motion (WIM) data is required to make accurate predictions of load effects at long return periods. Most WIM sensors in South Africa are located on National Route 3 (N3) and National Route 4 (N4) which are the major import and export routes in the country and which also carry the heaviest traffic. Stations along these routes are considered to be well calibrated. A WIM station along the N3 at Roosboom is chosen for this study, as seven years of traffic from 2010 to 2016 are available and the station is considered one of the heaviest loaded in the country. A comparison with other stations confirms this.

In contrast with TMH7, it is typical in international codes to provide a load model for the slow, or heavy, lane which is reduced transversely by Multiple Lane Factors (MLFs). To align with international norms, a slow lane model is derived in this study based on the seven years of data at the Roosboom station as discussed previously. This measurement record includes the identification of 12.5 million heavy vehicles. The slow lane in the direction from Durban to Johannesburg is studied as vehicles in this direction are heavier than vehicles travelling from Johannesburg to Durban. Span lengths that are investigated range from 5 m to 50 m in increments of 5 m. The model derived herein is not valid for span lengths outside these bounds. The load effects (LEs) that are investigated are hogging on two span structures and sagging and shear on single span structures. For characteristic loads a 5 % probability of exceedance in a 50 year reference period is selected, similar to the Eurocode and the South African building design codes. This leads to a characteristic return period of 975 years. A censored GEV distribution is introduced to model the LEs. The shape factor is almost always negative, indicating an underlying Weibull distribution. This confirms the finding of other researchers that traffic LEs are

bounded. The characteristic axle load amounts to 160 kN, which is used to calculate a UDL to replicate the characteristic load effects, resulting in a slow lane load model with a UDL of 13 kPa and a triple axle of 160 kN, spaced at 1.2 m.

To distribute the slow lane model transversely, it is necessary to derive MLFs which take into account the reduced probability of simultaneous heavy vehicles in adjacent lanes. A novel method is presented in this work in which multiple lane WIM data is used to calculate MLF factors. A WIM station in Pretoria at Kilner Park measures four lanes of traffic at 0.01 s accuracy. This is the only station in South Africa measuring more than two lanes. By studying concurrent characteristic LEs in adjacent lanes it is possible to determine MLFs, first for two lanes loaded, then three lanes loaded and finally for four lanes loaded. The resulting MLFs are 1.0; 0.78; 0.07; 0.00. This implies that traffic from the fourth lane does not contribute to the characteristic global LEs.

Vehicles that travel at speed, referred to as free flowing traffic, cause additional forces on bridge decks due to dynamic interaction between the vehicles and a bridge (Vehicle Bridge Interaction - VBI). To account for these increased loads, it is typical to multiply the static loads by a dynamic amplification factor (DAF) which is defined as the ratio between the total load effect to the static load effect. It is not the aim of this study to do an in depth investigation of dynamic amplification for South African bridges and it is therefore decided to adopt the values given in the ARCHES report D10, which are based on European traffic. It is reasonable to assume that South African roads conform to at least class B road profiles, implying a DAF of 1.4 up to 5 m span length and reducing linearly to 1.2 at a 15 m span length. Seeing that South African vehicles are heavier than in Europe and have more axles, it is reasonable to assume that the DAF for South African traffic would be lower than for Europe. The ARCHES values can therefore be considered to be conservative in the absence of a comprehensive VBI study and measurements.

To derive a design load model, it is necessary to establish Partial Factors (PFs) in accordance with structural reliability theory. Target 50 year β values are taken in accordance with the South African building design codes, which are based on extensive studies of historical practise in South Africa. For Ultimate Limit State (ULS), the 50 year β value is taken as 3.5 for a high consequence of failure and for Serviceability Limit State (SLS) as 1.5. The SLS value is in accordance with international standards. The reliability index is directly related to the probability of failure and hence it is possible to determine return periods of 435 years for SLS and 5040 years for ULS. For traffic loads, where the return periods for static loads are long, the probabilities of non-exceedance are close to 1.0 for characteristic, SLS and ULS. This leads to very small differences in load effects between characteristic and ULS return periods, especially when a censored GEV distribution is fitted which tends towards the Weibull distribution. When the LEs are near the bound of the fitted underlying Weibull distributions then there is hardly any uncertainty in the loading and all the uncertainty is located in the resistance. A new approach is

introduced to address statistical uncertainty in fitting parameters. As seven years of data is used it is not surprising to find very small statistical uncertainty. Final partial factors are a function of reliability based partial factors, model uncertainty and statistical uncertainty. These amount to 1.18 for SLS and 1.33 for ULS.

Chapter 8 presents a worked example for a typical bridge configuration for various widths and span lengths and considers both characteristic loads and ULS. The findings from this section are that the new model with DAF is always critical for all deck widths, for all span lengths and load effects when compared to normal loading in TMH7. The new model also exceeds LM1 in the Eurocode at characteristic and ULS levels. Although TMH7 abnormal and super loading is compared to the new model, it should be compared to a separate new model for abnormal loading which is outside the scope of this study.

Opsomming

Hierdie studie beoog om 'n nuwe verkeersbelastingmodel vir die ontwerp van snelweg brûe in Suid-Afrika af te lei, met nuwe bydraes tot die veld van brugverkeersbelasting. Die huidige kode vir brugontwerp in Suid-Afrika, Technical Methods for Highways 7 (TMH7), is in 1981 gepubliseer en volgens vorige studies, en deur hierdie studie, skiet dit tekort op karakteristieke vlak. Dit geld veral vir korter spanlengtes. TMH7 gee geen aanduiding van die veiligheidsvlakke wat gebruik is om die kode te kalibreer nie en dit is dus nie duidelik of die kode steeds die nodige veiligheidsmarges bied nie. Verskeie studies, wat in hierdie dokument uiteengesit word, toon dat die verspreide belasting en mesrandlaste vir tipe NA belasting verhoog moet word. NA word in TMH7 verwys na as normale belasting. Verder is die wettige perk vir die bruto voertuiggewig (GVW) tot 56 ton verhoog en die voertuigkenmerke op ons paaie het sedert 1981 aansienlik verander. TMH7 belasting word in die industrie as te kompleks beskou en ingenieurs het 'n beroep gemaak op vereenvoudigde lasmodel. 'n Studie van hierdie aard is dus goed gemotiveer om die veiligheid van padgebruikers te verseker en om die ontwerpdoeltreffendheid vir brugingenieurs te verhoog.

Afleiding van verkeersbelastingmodelle vereis gemete verkeersdata. Vorige studies het getoon dat ten minste een jaar data benodig word om akkurate voorspellings te maak van laseffekte by lang herhaalperiodes. Die meeste meetstasies in Suid-Afrika is op Nasionale Roete 3 (N3) en Nasionale Roete 4 (N4) geleë, wat die belangrikste invoer- en uitvoerroetes in die land is en wat ook die swaarste verkeer dra. Stasies langs hierdie roetes word as goed gekalibreer beskou. 'n Meetstasie langs die N3 by Roosboom word vir hierdie studie gekies, aangesien sewe jaar se verkeer van 2010 tot 2016 beskikbaar is en die stasie beskou word as een van die swaarste in die land. 'n Vergelyking met ander stasies bevestig dit.

In teenstelling met TMH7, is dit in internasionale kodes tipies om 'n lasmodel te bied vir die stadige of swaar baan wat dwars verminder word deur Multiple Lane Factors (MLF's). Om in lyn te kom met internasionale norme, word 'n stadige baanmodel afgelei in hierdie studie gebaseer op die sewe jaar data van die Roosboom stasie, soos vroeër bespreek. Hierdie meetrekord bevat die identifisering van 12.5 miljoen swaar voertuie. Die stadige baan in die rigting van Durban na Johannesburg word bestudeer omdat voertuie in hierdie rigting swaarder is as voertuie wat van Johannesburg na Durban ry. Spanlengtes wat ondersoek word, strek van 5 m tot 50 m in stappe van 5 m. Die model wat hierin afgelei is, is nie geldig vir spanlengtes buite hierdie grense nie. Die laseffekte (LE's) wat ondersoek word, is negatiewe buiging op twee spanstrukture en positiewe buiging en skuif op enkelspanstrukture. Vir karakteristieke laste word 'n waarskynlikheid van oorskryding van 5% in 'n verwysingsperiode van 50 jaar gekies, soortgelyk aan die Eurocode en die Suid-Afrikaanse gebouontwerpkodes. Dit lei tot 'n karakteristieke herhaalperiode van 975 jaar. 'n Gesensureerde GEV-verspreiding word ingestel om die LEs te modelleer. Die vormfaktor is byna altyd negatief, wat 'n onderliggende Weibull verdeling aandui.

Dit bevestig die bevindinge van ander navorsers dat LEs 'n eindige bogrens het. Die karakteristieke las beloop 160 kN, wat gebruik word om 'n verspreide las te bereken om die kenmerkende laseffekte te produseer, wat lei tot 'n verwysingsmodel met 'n verspreide las van 13 kPa en 'n drievoudige as konfigurasie van 160 kN elk, met 'n afstand van 1.2 m tussenin.

Om die stadige baanmodel dwars te versprei, is dit nodig om MLFs af te lei wat die verminderde waarskynlikheid van gelyktydige swaar voertuie in aangrensende bane in ag neem. In hierdie werk word 'n nuwe metode aangebied waarin gemete data in veelvuldige lane gebruik word om MLF faktore te bereken. 'n Meetstasie in Pretoria by Kilner Park meet vier bane van die verkeer met 'n akkuraatheid van 0,01 s. Dit is die enigste stasie in Suid-Afrika wat meer as twee bane meet. Deur gelyktydige karakteristieke LE's in aangrensende bane te bestudeer, is dit moontlik om MLF's te bepaal, eerstens vir twee bane belaaï, dan drie bane belaaï en laastens vir vier bane belaaï. Die resulterende MLFs is 1.0; 0.78; 0.07; 0.00. Dit impliseer dat verkeer vanaf die vierde baan nie bydra tot die karakteristieke globale LEs nie.

Voertuie wat vinnig ry, ook vry vloeiende verkeer genoem, veroorsaak ekstra kragte op brugdekke as gevolg van dinamiese interaksie tussen die voertuie en 'n brug. Om rekenskap te gee van hierdie verhoogde kragte, is dit tipies om die statiese laste te vermenigvuldig met 'n dinamiese versterkingsfaktor (DAF) wat gedefinieer word as die verhouding tussen die totale laseffek en die statiese laseffek. Dit is nie die doel van hierdie studie om 'n diepgaande ondersoek na dinamiese versterking vir Suid-Afrikaanse brûe te doen nie, en daarom is dit besluit om die waardes in die ARCHES-verslag D10, gebaseer op Europese verkeer, aan te neem. Dit is redelik om aan te neem dat Suid-Afrikaanse paaie aan ten minste klas B ISO profiel voldoen, wat 'n DAF van 1.4 op 'n 5 m spanlengte impliseer en lineêr verminder tot 1.2 op 'n spanlengte van 15 m. Aangesien Suid-Afrikaanse voertuie swaarder is as in Europa en meer asse het, is dit redelik om te aanvaar dat die DAF vir Suid-Afrikaanse verkeer laer sou wees as vir Europa. Die ARCHES-waardes kan dus beskou word as konserwatief in die afwesigheid van 'n uitgebreide studie en metings.

Om 'n ontwerpbelastingmodel af te lei, is dit noodsaaklik om parsiële faktore (PFs) af te lei in ooreenstemming met die betroubaarheidsteorie. Teikenwaardes vir 50 jaar β word geneem volgens die Suid-Afrikaanse bouontwerpkodes, wat gebaseer is op uitgebreide studies van historiese praktyk in Suid-Afrika. Vir Uiterste Limietstaat (ULS) word die 50 jaar β waarde as 3.5 beskou vir 'n hoë gevolg van faling en vir Dienslimietstaat (SLS) as 1.5. Die SLS waarde is in ooreenstemming met internasionale standaarde. Die betroubaarheidsindeks hou direk verband met die waarskynlikheid van faling en daarom is dit moontlik om herhaalperiodes van 435 jaar vir SLS en 5040 jaar vir ULS te bepaal. Vir verkeerslading, waar die herhaalperiodes vir belastings lank is, is die waarskynlikheid dat dit nie oorskry word nie, naby 1.0 vir karakteristiek, SLS en ULS. Dit lei tot baie klein verskille in LEs tussen karakteristiek, SLS en ULS herhaalperiodes, veral as 'n gesensureerde GEV-verdeling gebruik

word wat neig na die Weibull verdeling. As die LEs naby die bogrens van die onderliggende Weibull verdeling is, is daar amper geen onsekerheid in die belasting nie, en is die onsekerheid is meestal in die weerstand geleë. 'n Nuwe benadering word voorgestel om statistiese onsekerheid in verdelingsparameters aan te spreek. Aangesien daar sewe jaar data gebruik word, is dit nie verbasend om baie klein statistiese onsekerheid te vind nie. Finale parsieële faktore is 'n funksie van betroubaarheidsgebaseerde parsieële faktore, modelonsekerheid en statistiese onsekerheid. Dit beloop 1,18 vir SLS en 1,33 vir ULS.

Hoofstuk 8 bied 'n uitgewerkte voorbeeld vir 'n tipiese brugkonfigurasie vir verskillende wydtes en spanlengtes en neem beide karakteristieke laste en ULS in ag. Die bevindinge uit hierdie afdeling is dat die nuwe model met DAF altyd oorheers vir alle dekwydtes, vir alle spanlengtes en LEs in vergelyking met normale belasting in TMH7. Die nuwe model oorskry ook LM1 in die Eurocode op karakteristieke en ULS vlakke. Alhoewel abnormale en superbelasting met die nuwe model vergelyk word, moet dit vergelyk word met 'n aparte nuwe model vir abnormale belasting wat buite die bestek van hierdie studie val.

Acknowledgements

As a PhD culminates an engineer's academic training, it is only apt to thank those who not only made it possible, but also fun along the way.

Cara, you were born halfway through the first year of this project. You are an absolute joy and motivation.

To my wife, Adele, you recently reminded me that soon after we met eleven years ago I told you about my ambition to obtain a PhD. At that point I had only embarked on my master's! We had to overcome many challenges along this journey, but through your unwavering support we have made it. Only those that have attempted a PhD with a family will know what sacrifices a spouse must make to keep the ship afloat. Now we embark as a couple +1 on our next journey to the desert of Dubai and I hope that you can now also reap the rewards of your patience, love and support.

To my parents, Andre and Lorette, and my brother Christiaan, you are an inspiration and motivation. This has been a long road. Thirteen years of secondary education and thirteen years of university education. Thank you for the unwavering support and encouragement along this journey.

I was fortunate to be appointed as an adjunct faculty member during my time of study. It has been a joy to teach, and to see students flourish into industry. To my colleagues at the department, especially Roman, Celeste, Billy and Gideon, it has been great fun and I will miss the interesting lunchtime discussions.

After spending eight years in industry, it was financially almost impossible to resign and be a fulltime student again. I was immensely fortunate to receive substantial financial support from Aurecon and the Wilhelm Frank trust. Dr Gustav Rohde, retired Chief Operating Officer of Aurecon: that Skype call on a morning in October 2016 when you pledged the support changed my life, and that of my family, forever. Thank you also for the mentorship along the way and your keen interest in my career.

Living with bipolar disorder would normally make it very hard to attempt a project of this nature. To my doctors, Prof Piet Oosthuizen and Dr Louw Fourie, you showed me that it is indeed possible to live successfully with a serious condition, which at times felt impossible.

To my collaborators along the way, thank you for your patience and insights. Professor Tertius de Wet from the Department of Statistics and Actuarial Sciences at Stellenbosch University spent countless hours listening to my ideas which were sometimes useful and at other times not at all. Your enthusiasm and advice on extreme value statistics was invaluable along the way. Dr Colin Caprani of Monash University was equally helpful. Your immense intellect and insight into bridge traffic loading issues was humbling to say the least. Thank you.

Table of Contents

Declaration.....	i
Abstract.....	ii
Opsomming.....	v
Acknowledgements.....	viii
List of figures.....	xiii
List of tables.....	xvi
Abbreviations.....	xviii
1 Introduction, motivation and research methodology	1
1.1 Motivation.....	1
1.2 Goals.....	2
1.3 Conclusion	5
2 Background information for the derivation of bridge live load models.....	6
2.1 Principles of statistics and reliability	6
2.1.1 Basics of statistics for traffic loading.....	6
2.1.2 Basics of structural reliability	27
2.2 Dynamic amplification.....	33
2.3 Multiple lane presence	34
2.4 International code overview.....	36
2.4.1 Historical code development procedures	36
2.4.2 Canadian Standard	37
2.4.3 BS 5400.....	40
2.4.4 Eurocode	42
2.4.5 AASHTO LRFD	45
2.4.6 Australian Standard.....	47
2.4.7 Conclusion	51
3 Current TMH7 loading and comparison with WIM measurements.....	52
3.1 TMH7 models	52

3.1.1	NA loading.....	52
3.1.2	NB loading.....	54
3.1.3	NC loading.....	54
3.2	WIM data in South Africa.....	55
3.2.1	General recording of WIM data	55
3.2.2	WIM in South Africa	56
3.2.3	Cleaning of WIM data in South Africa	57
3.2.4	Calibrating WIM data in South Africa.....	57
3.3	Comparison of TMH7 with measured WIM data	58
3.3.1	Cleaning and calibrating of data	59
3.3.2	Span lengths investigated.....	59
3.3.3	Convoys and load effects calculated.....	59
3.3.4	Identification of a representative WIM station	62
3.3.5	Traffic composition at the Roosboom station	67
3.3.6	Return period	71
3.3.7	Extrapolation to return period for static free flow loads	71
3.3.8	Characteristic values for all span lengths and load effects.....	77
4	Development of a static load model.....	82
4.1	Notional lane width.....	82
4.2	Methodology	83
4.2.1	Choice of load model format	83
4.2.2	Characteristic axle load.....	84
4.2.3	Axle group configurations investigated	85
4.2.4	Calculation of distributed load.....	85
4.2.5	Resulting load model	87
4.3	Comparison of the new single lane model with measured load effects	88
4.4	Conclusions.....	89
5	Multiple lane presence	91
5.1	Introduction.....	91

5.2	MLF calculation methodology.....	91
5.2.1	Time history of load effects	96
5.2.2	Extrapolation to characteristic values	96
5.2.3	Procedure	97
5.3	Application to a WIM site in South Africa.....	99
5.3.1	Calculation of MLFs.....	100
5.4	Comparison with other codes.....	107
5.5	Comparison with Turkstra’s rule	108
5.6	Conclusions.....	109
6	Dynamic amplification.....	111
6.1	Factors that influence DAF.....	111
6.1.1	Condition of the road surface.....	111
6.1.2	Span length and Eigen frequencies	112
6.1.3	Bridge type.....	112
6.1.4	Bridge material and damping	112
6.1.5	Vehicle velocity	112
6.1.6	Vehicle weight	113
6.1.7	Number of axles	113
6.1.8	Number of vehicles	113
6.1.9	Vehicle suspension type.....	113
6.1.10	Dynamic amplification at ULS	114
6.2	Suggested DAF for South African traffic based on ARCHES report.....	114
6.3	Minimum DAF for the governing form of traffic	115
7	Partial factor calibration.....	119
7.1	Reference period and design life.....	119
7.2	Design life for bridges.....	119
7.3	Target reliability.....	120
7.4	Target reliability for design of new bridges in South Africa	122
7.5	Return periods and non-exceedance probabilities for SLS and ULS.....	124

7.6	PFs for the static load effect.....	125
7.6.1	MLE for evaluation of quantiles	125
7.7	Time invariant uncertainties.....	127
7.7.1	Model uncertainty	127
7.7.2	Statistical uncertainty in parameter estimates	128
7.8	Partial load factors	132
7.9	Discussion of partial factors.....	134
8	Model validation	136
8.1	Summary of load model.....	136
8.2	Analysis type and deck configurations	137
8.3	Results.....	138
8.3.1	Fixed deck width - Characteristic	139
8.3.2	Fixed span lengths - Characteristic	142
8.3.3	Characteristic summary.....	142
8.3.4	Fixed deck width - ULS	143
8.3.5	Fixed span lengths - ULS.....	145
8.3.6	ULS summary	146
8.4	Example discussion.....	147
9	Conclusions.....	148
10	Recommendations for future research	151
	Appendix.....	153
	Bibliography	170

List of figures

Figure 1 - Document structure	4
Figure 2 - Typical PDF for a standardised normal distribution	11
Figure 3 - Typical CDF for a standardised normal distribution.....	12
Figure 4 - Typical normal probability plot showing good straight line adherence of the data	19
Figure 5 - Axle 3 histogram for 6 axis vehicles	22
Figure 6 - Bimodal PDFs for axle 3 of 6 axle vehicles.....	23
Figure 7 - Failure zone of the limit state function for normally distributed random variables (Lenner, 2014).....	29
Figure 8 - Normalized joint PDF in U-space (Lenner, 2014)	30
Figure 9 - MOT standard load train (O'Connor & Shaw, 2000)	36
Figure 10 - Standard MOT load curve (O'Connor & Shaw, 2000)	37
Figure 11 - Canadian MOL curve (O'Connor & Shaw, 2000)	38
Figure 12 - OHBD Truck load (O'Connor & Shaw, 2000)	38
Figure 13 - CHBDC Truck (O'Connor & Shaw, 2000).....	39
Figure 14 - CHBDC Lane Load (O'Connor & Shaw, 2000).....	39
Figure 15 - HB load configuration (O'Connor & Shaw, 2000)	41
Figure 16 - Eurocode LM1 (CEN, 2003).....	43
Figure 17 - Eurocode LM2 (CEN, 2003).....	44
Figure 18 - AASHTO Design truck (AASHTO, 2007)	46
Figure 19 - Australian T44 truck (O'Connor & Shaw, 2000).....	47
Figure 20 - AS5100 A160 loading (Standards Australia, 2004).....	49
Figure 21 - AS5100 M1600 loading (Standards Australia, 2004)	49
Figure 22 - AS5100 S1600 loading (Standards Australia, 2004).....	50
Figure 23 - TMH7 NA loading curve (Committee of State Road Authorities, 1981)	53
Figure 24 - TMH7 NB loading (Committee of State Road Authorities, 1981)	54
Figure 25 - TMH7 NC loading (Committee of State Road Authorities, 1981)	55
Figure 26 - WIM sensors installed across South Africa	56
Figure 27 - Spatial arrangement of example WIM vehicles	60
Figure 28 - Hogging moment load effect.....	61
Figure 29 - Sagging moment load effect.....	61
Figure 30 - Shear load effect.....	62
Figure 31 - Measuring station comparison normalised to Roosboom	66
Figure 32 - Vehicle type distribution	67
Figure 33 - GVW PDFs and CDFs	68
Figure 34 - GVW cumulative distribution	70

Figure 35 - Axle weight cumulative distribution	70
Figure 36 - Histogram of daily maxima on a 30 m span length.....	73
Figure 37 - Monthly maxima for 30 m hogging	74
Figure 38 - Weekly maxima for 30 m hogging.....	75
Figure 39 - Daily maxima for 30 m hogging	75
Figure 40 - Secondly maxima for 30 m hogging	76
Figure 41 - Quantile plot for sagging on a 30 m span (Weibull)	77
Figure 42 – NA static vs Characteristic WIM load effects	80
Figure 43 - Typical 7 axle truck width (UD Trucks South West Africa).....	83
Figure 44 - Quantile plot for axle weights fitted to censored GEV distribution.....	85
Figure 45 - UDL calculation example for sagging on a 30 m span length	86
Figure 46 - UDL for various axle configurations	86
Figure 47 - Proposed load model for tridem and quad axle configurations	88
Figure 48 – Comparison of new model with characteristic measured WIM	89
Figure 49 - Comparison of new model with characteristic measured WIM (normalised to WIM)	89
Figure 50 - Definition of MLF application	93
Figure 51 - Transverse influence line for 40 m sagging with load on edge beam	94
Figure 52 - Transverse distribution of lane loads.....	95
Figure 53 - WIM site lane arrangement	100
Figure 54 - Quantile plot for Lane 1 monthly maxima hogging moments	100
Figure 55 - Dynamic Amplification Factor based on ARCHES	115
Figure 56 - Required DAF for European traffic	117
Figure 57 - New model with DAF compared to static measurements	118
Figure 58 - Variation of reliability index with cost ratio for selected working life (Holicky, 2011)..	123
Figure 59 - Model uncertainty concept	128
Figure 60 - Normal plots of the sample quantiles at SLS (shear in kN)	130
Figure 61 - Normal plots of the sample quantiles at ULS (shear in kN)	131
Figure 62 - New static load model	137
Figure 63 – Typical single span grillage model for sagging and shear.....	138
Figure 64 - Typical two span grillage model for hogging	138
Figure 65 - Graphical results for 9 m deck width characteristic	154
Figure 66 - Graphical results for 6 m deck width characteristic	155
Figure 67 - Graphical results for 3 m deck width characteristic	156
Figure 68 - Graphical results for 10 m span length characteristic	157
Figure 69 - Graphical results for 20 m span length characteristic	158
Figure 70 - Graphical results for 30 m span length characteristic	159
Figure 71 - Graphical results for 40 m span length characteristic	160

Figure 72 - Graphical results for 50 m span length characteristic	161
Figure 73 - Graphical results for 9 m deck width ULS.....	162
Figure 74 - Graphical results for 6 m deck width ULS.....	163
Figure 75 - Graphical results for 3 m deck width ULS.....	164
Figure 76 - Graphical results for 10 m span length ULS	165
Figure 77 - Graphical results for 20 m span length ULS	166
Figure 78 - Graphical results for 30 m span length ULS	167
Figure 79 - Graphical results for 40 m span length ULS	168
Figure 80 - Graphical results for 50 m span length ULS	169

List of tables

Table 1 - CHBDC multiple lane reduction factors (Canadian Standards Association, 2014)	40
Table 2 - Lane factors for BS5400 and BD37/88	41
Table 3 - AASHTO multiple presence factors (AASHTO, 2007)	46
Table 4 - AASHTO dynamic load allowance (AASHTO, 2007)	47
Table 5 - AS5100 lane factors (Standards Australia, 2004).....	50
Table 6 - Example of Record Type 13	57
Table 7 - Example of two following vehicles from a WIM file.....	60
Table 8 – Roosboom characteristic load effects	78
Table 9 - Distribution bounds for censored GEV	79
Table 10 - Load effects for static NA loading	79
Table 11 - Extrapolated single lane load effects	101
Table 12 - Extrapolated two lane load effects.....	102
Table 13 - MLF values for two lanes loaded	103
Table 14 - Extrapolated three lane load effects.....	104
Table 15 - MLF values for three lanes loaded	105
Table 16 - Extrapolated four lane load effects	105
Table 17 - MLF values for four lanes loaded.....	106
Table 18 - Final MLFs	106
Table 19 - Final MLFs per load effect	107
Table 20 - Comparison of MLF values	107
Table 21 - MLFs calculated by Turkstra's rule	109
Table 22 - Design working life of structures according to ISO2394	120
Table 23 - ISO2394 target beta values (lifetime values).....	121
Table 24 – EN1990 consequence classes.....	121
Table 25 – EN1990 target beta values for CC2	122
Table 26 - Reliability based partial factors for hogging	126
Table 27 - Reliability based partial factors for sagging	127
Table 28 - Reliability based partial factors for shear	127
Table 29 - Statistical uncertainty partial factors for all load effects and span lengths.....	132
Table 30 - Partial factors for hogging	133
Table 31 - Partial factors for sagging.....	133
Table 32 - Partial factors for shear.....	134
Table 33 – Results table for 9 m deck width.....	139
Table 34 – Results table for 6 m deck width.....	140
Table 35 – Results table for 3 m deck width.....	141

Table 36 – Results table for 9 m deck width.....	143
Table 37 – Results table for 6 m deck width.....	144
Table 38 – Results table for 3 m deck width.....	145

Abbreviations

AASHTO	American Association for State Highway Transport Officials
ADR	Assessment Dynamic Ratio
ADTT	Average Daily Truck Traffic
ARCHES	Assessment and Rehabilitation of Central European Highway Structures
CC	Consequence Class
CDF	Cumulative Distribution Function
CEN	Comité Européen de Normalisation (French)
CHBDC	Canadian Highway Bridge Design Code
CSA	Canadian Standards Authority
CSRA	Committee for State Roads Authority
DAF	Dynamic Amplification Factor
DLA	Dynamic Load Allowance
EM	Expectation Maximization
EV	Extreme Value
FMM	Finite Mixture Model
FORM	First Order Reliability Method
GEV	Generalized Extreme Value
GMM	Gaussian Mixture Model
GVW	Gross Vehicle Weight
HPC	High Performance Computer
iid	independently and identically distributed
ISO	International Standards Organization
LE	Load Effect
LRF	Load and Resistance Factor
MLE	Maximum Likelihood Estimation
MLF	Multiple Lane Factor

MOL	Maximum Observed Load
MOT	Ministry of Transport
MR	Mean Rank
NCHRP	National Cooperative Highway Research Program
OHBDC	Ontario Highway Bridge Design Code
P	Probability
PDF	Probability Density Function
PF	Partial Factor
RC	Reliability Class
SANRAL	South African National Roads Agency Limited
SLS	Serviceability Limit State
TMH	Technical Methods for Highways
TT	Truck Tractor
UDL	Uniformly Distributed Load
ULS	Ultimate Limit State
VBI	Vehicle Bridge Interaction
WIM	Weigh in Motion

1 Introduction, motivation and research methodology

Traffic loading on short to medium span bridges is governed by free flowing traffic. Subsequent to the derivation of most international norms, including TMH7, WIM technology has been developed which enables the derivation of load models with superior accuracy. Further to this development, traffic volumes and weight increase over time and it is imperative that traffic load models for bridges are revised or replaced periodically.

TMH7 has been the code of practice for bridge design in South Africa since 1981 when it was first introduced (CSRA, 1981; Van der Spuy, 2014). It is based on modern principles and closely followed design codes such as the CEB-FIP Model Code for Concrete Structures of 1978, the British bridge design code known as BS5400 and the National Building Code of Canada. Limited information is available on the development of TMH7 and as such it is not clear how the design codes mentioned were incorporated. It is at least clear from inspection that the TMH7 traffic load model was based on that of BS5400. TMH7 consists of three parts (CSRA, 1981):

- Part 1 : General Statement
- Part 2 : Specification for Loads
- Part 3 : Design of Concrete Structures

TMH7 was the first bridge design code to be introduced in South Africa based on the limit state design philosophy and is considered to be a major improvement over the previously used Factor of Safety principles on which its predecessors were based (CSRA, 1981). Limit state design was enabled through the introduction of probabilistic analysis of resistance and load effects. TMH7 specifies PFs explicitly without any allowance for specifying safety levels on a case specific basis.

1.1 Motivation

Since its introduction in 1981, and with the subsequent availability of more complete traffic data, several studies have been performed on the continued validity of the code. The following list provides a summary of these efforts:

- Liebenberg in 1978, when deriving the code, stated that a probabilistic study of extreme truck events was not viable due to a lack of statistical information at the time (Anderson, 2006). It is therefore not clear if the loading was treated probabilistically at all. Extreme truck events tend to govern bridge LEs on short and medium span bridges and sufficient information is now available to perform a fully probabilistic study.
- Revisions and corrections to the code were issued in 1988, but Oosthuizen et al. (1991) showed there are still shortcomings for normal traffic on narrow and short span bridges. It was found

that TMH7 underestimates the bending moments for spans between 4 m and 9 m. Oosthuizen *et al.* (1991) also showed that shear forces are underestimated on span lengths below 23 m.

- A committee was formed in 1991 to investigate the simplification of the current traffic loading model by achieving similar results, but with a much simpler application (Oosthuizen *et al.*, 1991). Although the load curve with the aggregate loaded length concept was retained for the distributed NA load, it was proposed that the knife edge load be increased by 25 %. This, together with fixing the notional lane widths to 3 m, would address the shortcomings on short and narrow bridges identified by Ullmann in 1988. It was proposed to retain the abnormal load model, but to fix the variable axle spacing to 6 m. None of the recommendations made by this committee were implemented in the code. These deficiencies are confirmed in Chapter 3 where static TMH7 loading is compared to WIM data.

The 1989 axle weight limit, on which the above proposed revisions were based, was 8.2 t according to the Road Traffic Act 29 of 1989. In 1996, after receiving requests from industry, the Department of Transport decided to increase the allowable Gross Vehicle Weight (GVW) to 56 t and Axle Load to 16 t for vehicles on South African roads. TMH7 was never updated nor checked to allow for this increase.

It is the opinion in industry, and from the author's own experience, that the TMH7 load model for normal traffic is too complicated to apply in day-to-day design. As a consequence, various different applications of the code are seen in practice, varying from one engineer to the next. The complexity, as discussed in detail in section 3.1.1, is caused by the aggregate loaded length concept and the partial loading of influence lines.

TMH7 does not specify load application patterns for traffic loads. This is especially problematic for skew decks where it can be difficult to determine the critical loading positions. This problem is compounded by the partial loading of influence lines and the aggregate loaded length concept. Malan & Van Rooyen (2013) show that it is especially difficult to obtain the critical load patterns for transverse bending and twisting moments. Specialised software is needed to apply NA loading accurately. Software of this kind is not available generally, especially not in smaller consulting engineering practices.

It is unclear what reliability performance can be expected from TMH7 with its current set of PFs and whether the reliability is compliant with international norms.

1.2 Goals

It is safe to conclude that TMH7 needs to be revised and carefully checked with the current traffic characteristics and prescribed reliability in line with international norms. This is also the sentiment from a 2008 summit hosted by the South African Institution of Civil Engineering (SAICE) on the adoption of the Eurocodes in South Africa. There is also strong motivation for the simplification of the current

load model. As vehicle characteristics in South Africa are different to those in Europe, it is not advisable to adopt the Eurocode traffic load models as is (Lenner, de Wet & Viljoen, 2017). The purpose of this work is not to simply recalibrate TMH7 with new traffic data, but rather to use modern and novel techniques to identify and address the critical issues in the derivation of a traffic load model to propose a new live load model for short to medium span highway bridges for South Africa by

1. Studying TMH7 and critically evaluating its suitability for modern bridge design
2. Establish static load effects based on WIM data
3. Critically investigate methods to obtain characteristic values from static LEs by applying state-of-the-art distribution fitting techniques not previously used in this context
4. Develop a reference lane load model based on characteristic LEs which addresses concerns raised previously
5. Develop a novel procedure to account for the reduced probability of heavy vehicles in adjacent lanes simultaneously through the use of multiple lane WIM data
6. Critically evaluate the state-of-the-art for dynamic amplification
7. Calibrate partial factors based on international and South African norms
8. Provide a comprehensive worked example

Figure 1 shows an outline of the document structure and the main components of the study.

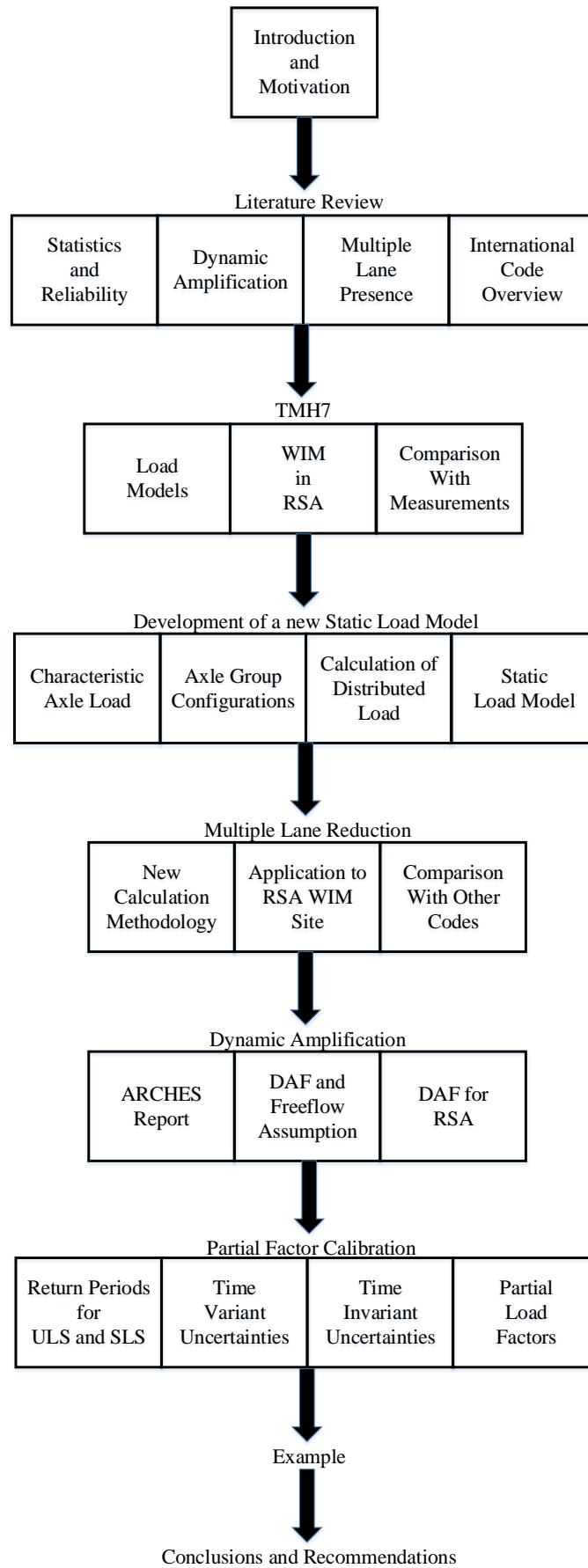


Figure 1 - Document structure

1.3 Conclusion

Chapter 1 presents a summary of past studies on the continued validity of the traffic load models in TMH7 and the complexity thereof. Many studies show that TMH7 is unconservative, especially on short span bridges. Changes to legal limits of vehicles and axles are discussed which adds to the motivation that the traffic load models in the code should be revised.

When deriving TMH7, the author noted that statistical information on load effects were not available at the time and the load models can therefore not be considered as fully probabilistic. South Africa possesses a large amount of WIM data and a fully probabilistic study is now possible and developed in this work.

Using WIM data load effects can be calculated for various span lengths and LEs. This work makes use of this technique and, together with state of the art statistical methods, LEs are determined for long return periods. By observing these LEs a load model is proposed which is not a real vehicle, but a configuration which replicates the LEs best.

Figure 1 shows a structure of the envisaged development of the load model. In addition to the static LEs, this work also considers multiple lane presence, dynamic amplification, calibration of partial factors and a comprehensive application of the proposed model.

2 Background information for the derivation of bridge live load models

This section discusses the background of the components needed to derive a new load model. These include the principles of statistics and reliability, dynamic amplification, multiple lane presence and an overview of current international codes.

2.1 Principles of statistics and reliability

Statistics and reliability are necessary to predict loads and uncertainties thereof over long periods. The concept of reliability is necessary to quantify uncertainty associated with a new load model at serviceability and ultimate limit states. The background to the statistics and reliability principles are discussed here.

2.1.1 Basics of statistics for traffic loading

Statistics deals with the collection, presentation, analysis and use of data to make decisions, solve problems, and design products and processes (Montgomery & Runger, 2010). In the analysis of traffic data it may be necessary to process millions of vehicle data records obtained from WIM stations, unless simplified procedures are used. It is essential to use statistical methods to process and draw conclusions from these large volumes of data. This section discusses some basic principles of statistics which are needed to understand the current research in the field as well the formulation of the traffic load model later in the document.

2.1.1.1 Sample spaces and random variables

A sample space constitutes all the possible outcomes of a random experiment and is denoted by S . An event is a subset of the sample space of a random experiment.

A random variable is defined as a function which assigns a real number to each outcome in the sample space of a random experiment and is denoted by X . Otherwise stated, it is a variable whose possible values are numerical outcomes of a random experiment. Random variables can be either discrete or continuous.

A continuous random variable is one which has an interval of real numbers for its range and the realisation can lie anywhere within this range. In the context of WIM data and load model derivation these are usually measurements, for example axle weights, measured on a WIM sensor. Measuring axle weights on a WIM sensor can be considered to be a random experiment and the value of results can fall above zero and will be real.

A discrete random variable is one which can only take on a countable number of distinct values. The results of a random experiment can therefore only yield a finite and countable number of results. (Nowak & Collins, 2002; Faber, 2009a; Montgomery & Runger, 2010).

The random variables used in the derivation of a traffic load model for bridges are continuous in nature and discrete random variables are not considered further in this work.

2.1.1.2 Probability

Probability is used to quantify the likelihood than an outcome of a random experiment will occur. For example, if a sample space is made up of N outcomes which all have an equal chance of occurring, then the chance of any outcome occurring is equal to $1/N$ (Montgomery & Runger, 2010). The value of a probability falls between 0 and 1, with 0 being the case that an outcome will never occur and 1 being the case when an outcome will occur with absolute certainty. Probability is indicated by $P(E)$ where P is the probability of occurrence of outcome E of a random experiment. Several definitions of probability exist and are discussed below (Nowak & Collins, 2002; Faber, 2009a,b; Montgomery & Runger, 2010).

Mathematical definition of probability

A set of axioms exist which provide a mathematical definition for probability. These are:

Axiom 1 – The probability of the entire sample space constituting an outcome is $P(S) = 1$.

Axiom 2 – The probability of an event E occurring is always larger or equal to 0 and smaller or equal to 1 i.e. $0 \leq P(E) \leq 1$.

Axiom 3 – If two events E_1 and E_2 are mutually exclusive then

$$P(E_1 \cup E_2) = P(E_1) + P(E_2) \quad (1)$$

This states that the probability of E_1 or E_2 occurring is equal to the sum of the probabilities of E_1 and E_2 occurring separately.

Frequentistic definition of probability

In the frequentistic interpretation of probability, the probability of an event E occurring is simply a function of the number of events occurring in n trials. The probability is calculated by dividing the number of events by the number of trials. It can be expressed as

$$P(E) = \lim_{n_{exp} \rightarrow \infty} \frac{N_E}{n_{exp}} \quad (2)$$

where

N_E the number of experiments where E occurred

n_{exp} the total number of experiments

It should be noted that experiments need to be performed to calculate the probability.

Classical definition of probability

The classical definition of probability can be formulated as

$$P(E) = \frac{n_E}{n_{tot}} \quad (3)$$

where

n_E number of equally likely ways an experiment could lead to E

n_{tot} total number of equally likely ways in the experiment

2.1.1.3 Descriptive statistics

Descriptive statistics are coefficients that provide a summary of a given sample space. It provides an indication of the central tendency of the data as well as the dispersion thereof. The most used descriptive statistical parameters are the mean, variance and standard deviation.

Sample mean

If the sample space is arranged in a vector $x = (x_1, x_2, x_3, \dots, x_n)$ then the sample mean is given by

$$\mu = \frac{1}{n} \sum_{i=1}^n x_i \quad (4)$$

where

n total number of random variables in a sample space

x_i values of the individual random variables that make up the sample space

The sample mean can be viewed as the central value of the sample space.

Sample variance and standard deviation

The sample variance and standard deviation are measures of the dispersion or variability about the mean of the random variables in a sample space. The variance s^2 is given by the following expression

$$s^2 = \frac{1}{n} \sum_{i=1}^n (x_i - \mu)^2 \quad (5)$$

where

n total number of random variables in a sample space

x_i values of the individual random variables that make up the sample space

μ the sample mean

The standard deviation is simply the square root of the variance. To compare different datasets the dimensionless coefficient of variation can be used and is defined as

$$v = \frac{s}{\mu} \quad (6)$$

where

s sample standard variation

μ the sample mean

Measures of correlation

When two or more random variables occupy a sample space it is useful to understand how these variables vary together. A standard way of expressing the relationship between random variables is known as the covariance. It is also regarded as a measure of the linear relationship or correlation between random variables. The covariance is expressed as

$$s_{XY} = \frac{1}{n} \sum_{i=1}^n (x_i - \bar{x})(y_i - \bar{y}) \quad (7)$$

where

\bar{x} sample mean for random variable X

\bar{y} sample mean for random variable Y

n total sample size

If the covariance is positive then X increases as Y increases. If the covariance is negative then Y decreases as X increases.

If the sample covariance is normalised with respect to the standard deviations of the constituting components it is called the sample correlation coefficient which is expressed as

$$r_{XY} = \frac{s_{XY}}{s_X s_Y} \quad (8)$$

where

s_X the sample standard deviation for the random variable X

s_Y the sample standard deviation for the random variable Y

The correlation coefficient is bounded inclusively by -1 and 1. For a value of -1 or 1 it implies that the random variables are perfectly correlated and a scatter diagram will show a perfectly straight line.

Dependence between random variables

Two correlated random variables are dependent if one outcome influences the probability of another outcome. A dependent event relies on another event to happen first. In short it can be said that all dependent random variables are also correlated, but not all correlated random variables are dependent.

Independent events, on the contrary, are events that have no connection of another event's probability of happening. Two events, A and B, can be said to be independent if the following conditions hold true:

$$P(A|B) = P(A) \quad (9)$$

$$P(B|A) = P(B) \quad (10)$$

$$P(A \cap B) = P(A)P(B) \quad (11)$$

Dependence is an important concept in bridge traffic loading as it is necessary to understand if adjacent or following traffic streams influence each other or not.

2.1.1.4 Probability density functions and cumulative distribution functions

Probability density functions are necessary to understand the spread of random variables. Cumulative distribution functions give an indication of the probability of a random event occurring.

Probability density functions

A probability density function (PDF) is a function of which the value at any point in the sample space gives a likelihood that the random variable would occur in that sample. It gives a simple description of the probabilities associated with a random variable. For a continuous random variable X the PDF, given by $f(x)$, is such that

$$f(x) \geq 0 \quad (12)$$

$$\int_{-\infty}^{\infty} f(x)dx = 1 \quad (13)$$

$$P(a \leq X \leq b) = \int_a^b f(x)dx \quad (14)$$

Thus the probability P of a random variable X falling between a and b is equal to the integral of the PDF between a and b . The shape of a PDF is a function of how the random variable is distributed.

Figure 2 below shows a typical PDF for a normally distributed random variable with a mean of 0 and a standard deviation of 1.

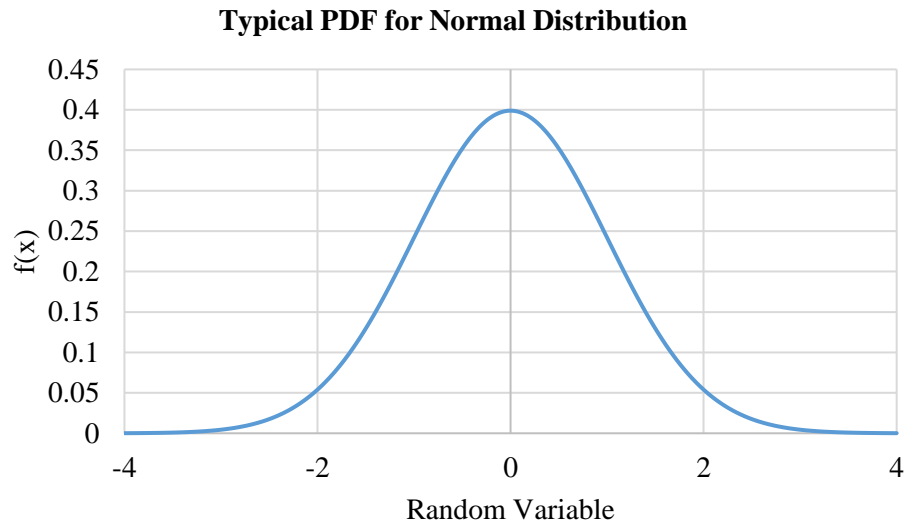


Figure 2 - Typical PDF for a standardised normal distribution

Cumulative distribution functions

A cumulative distribution function is a function which provides the probability that a random variable X will take on a value of equal to or less than x . It can also be viewed as the area under the PDF between negative infinity and x . It is denoted by $F(x)$ and expressed as

$$F(x) = P(X \leq x) = \int_{-\infty}^x f(u) du \quad (15)$$

where $-\infty \leq x \leq \infty$

Figure 3 below shows a typical CDF for a normally distributed random variable with a mean of 0 and a standard deviation of 1.

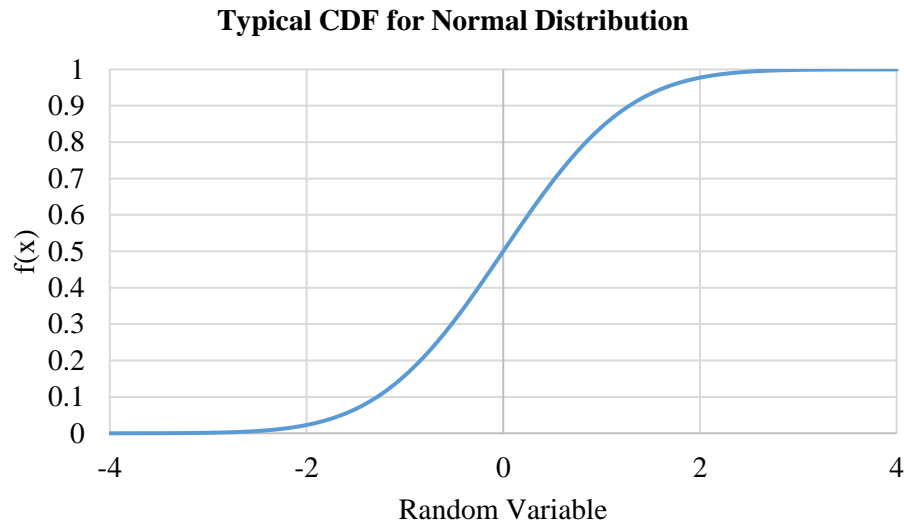


Figure 3 - Typical CDF for a standardised normal distribution

Probability distributions

The most common probability distributions used in the derivation of traffic load models and structural reliability are

- Gaussian (normal) distribution
- Lognormal distribution
- Extreme Value (EV) family of distributions
- Poisson distribution

Gaussian distribution

The Gaussian distribution is also known as the normal distribution. The Gaussian distribution is a perfectly symmetrical distribution with its center at the sample mean and its width determined by the standard deviation. The PDF and CDF of a Gaussian distribution are given by

$$f(x) = \frac{1}{\sqrt{2\pi}\sigma} e^{-\frac{(x-\mu)^2}{2\sigma^2}} \quad (16)$$

$$F(x) = \frac{1}{2} \left[1 + \operatorname{erf} \left(\frac{x-\mu}{\sigma\sqrt{2}} \right) \right] \quad (17)$$

$$\operatorname{erf}(x) = \frac{2}{\sqrt{\pi}} \int_0^x e^{-t^2} dt$$

where $-\infty \leq x \leq \infty$ and $\sigma > 0$

The normal distribution is denoted by $N(\mu, \sigma^2)$ where

μ the sample mean for random variable X

σ^2 the sample variance

A Gaussian distribution with $\mu = 0$ and $\sigma = 1$ is known as a standard Gaussian distribution. The calculation of the area under the Gaussian PDF requires complicated integration techniques and it is useful to use tables to read off probabilities. By standardizing the Gaussian distribution it possible to use only one table for all possible combinations of means and standard deviations. A normal random variable X can be transformed to a standard normal random variable Z , by performing the following transformation

$$Z = \frac{X - \mu}{\sigma} \quad (18)$$

where μ and σ is the mean and standard variation of the random variable X . The probability for a standard normal variable Z occurring is given by

$$P(X \leq x) = P\left(\frac{X - \mu}{\sigma} \leq \frac{x - \mu}{\sigma}\right) = P(Z \leq z) \quad (19)$$

It is common to denote the CDF of a standard Gaussian distribution by $\Phi(x)$ and the PDF by $\phi(x)$.

Lognormal distribution

If W is a Gaussian distributed random variable with mean θ and variance ω^2 , then a random variable $X = e^W$ is log-normally distributed. It can also be stated as $W = \ln(X)$. The PDF of a log-normally distributed random variable is given by

$$f(x) = \frac{1}{x\omega\sqrt{2\pi}} e^{-\frac{(\ln(x)-\theta)^2}{2\omega^2}} \quad (20)$$

where $0 \leq x \leq \infty$

The CDF is given by

$$F(x) = \Phi\left(\frac{\ln(x) - \theta}{\omega}\right) \quad (21)$$

The mean and variance of the log-normally distributed random variable X is given by

$$\mu = e^{\left(\theta + \frac{\omega^2}{2}\right)} \quad (22)$$

$$\sigma^2 = e^{(2\theta + \omega^2)}(e^{\omega^2} - 1) \quad (23)$$

The lognormal distribution is potentially useful to describe the probability density of axle weights or the strength of materials where negative values cannot occur.

Extreme Value distributions

Extreme value (EV) distributions are useful to predict the lowest and highest values of random variables. They are especially useful to extrapolate to larger return periods given a limited amount of data. The EV family of distributions is made up of the Gumbel distribution (Type 1 EV), the Frechet distribution (Type 2 EV) and the Weibull distribution (Type 3 EV).

Gumbel distribution

The Gumbel distribution is referred to as the Type 1 EV distribution and has a minimum version to predict extreme minimum values and a maximum version to predict extreme maxima. In this work it is only necessary to consider maximum values and the minimum version will therefore not be considered further. The Gumbel distribution is defined by a scale (α) and a location (v) parameter. The PDF for the Gumbel distribution is given by

$$f(x) = \frac{1}{\alpha} e^{\left[\frac{x-v}{\alpha} - e^{\left(\frac{x-v}{\alpha}\right)}\right]} \quad (24)$$

The CDF is given by

$$F(x) = e^{\left[-e^{\left(\frac{x-v}{\alpha}\right)}\right]} \quad (25)$$

The mean and variance for a Gumbel distribution is given by

$$\mu = v - \gamma\alpha \quad (26)$$

$$\sigma^2 = \frac{1}{6}\pi^2\alpha^2 \quad (27)$$

where γ is the Euler constant approximately equal to 0.57722.

The scale and location parameters of the Gumbel distribution can be estimated by the probability weighted moments method, maximum likelihood estimation (MLE), least squares and the method of moments (Huynh & Fang, 1989; Mahdi, 2005; Kernane & Raizah, 2010). The maximum likelihood method is described here for the Gumbel distribution, but the principle is also applicable to the other distributions.

The likelihood function of a specific distribution is a function that, when maximized, will yield the values for the unknown parameters of a distribution. The likelihood function is maximized when the derivative of the function is set to zero and the parameters are solved. It is often useful to use the logarithm of the likelihood function.

The log-likelihood function for the Gumbel distribution is given by

$$\ln L(\alpha, v) = -\sum_{i=1}^n \frac{x_i - v}{\alpha} - n \ln \alpha - \sum_{i=1}^n e^{-\left(\frac{x_i - v}{\alpha}\right)} \quad (28)$$

The log-likelihood function is differentiated with respect to both the scale and the location parameters and set to zero

$$\frac{\partial \ln L(\alpha, v)}{\partial v} = \frac{1}{\alpha} \left[n - \sum_{i=1}^n e^{-\left(\frac{x_i - v}{\alpha}\right)} \right] = \mathbf{0} \quad (29)$$

$$\frac{\partial \ln L(\alpha, v)}{\partial \alpha} = \sum_{i=1}^n \left(\frac{x_i - v}{\alpha^2} \right) - \frac{n}{\alpha} - \sum_{i=1}^n \left(\frac{x_i - v}{\alpha^2} \right) e^{-\left(\frac{x_i - v}{\alpha}\right)} = \mathbf{0} \quad (30)$$

The following equation is obtained with which α can be solved explicitly

$$\bar{x} = \alpha + \frac{\sum_{i=1}^n x_i e^{-\frac{x_i}{\alpha}}}{\sum_{i=1}^n e^{-\frac{x_i}{\alpha}}} \quad (31)$$

Once α has been solved v can be solved by

$$v = \alpha \left[\ln n - \ln \sum_{i=1}^n e^{-\left(\frac{x_i}{\alpha}\right)} \right] \quad (32)$$

Frechet distribution

The three parameter Frechet distribution, also known as the Type 2 EV distribution, is defined by three parameters namely the shape (β), the scale (α) and the location (v). The PDF is given by

$$f(x) = \frac{\beta}{\alpha} \left(\frac{x - v}{\alpha} \right)^{-1-\beta} e^{-\left(\frac{x-v}{\alpha}\right)^{-\beta}} \quad (33)$$

The CDF is given by

$$F(x) = e^{-\left(\frac{x-v}{\alpha}\right)^{-\beta}} \quad (34)$$

The location parameter is typically set to zero. In addition to MLE and other methods, a least squares estimation can be used to estimate the scale and shape parameters (Abbas & Tang, 2013) similar to what is described in the next section for the Weibull distribution. A linear transformation is applied to the CDF and least squares fitting is subsequently used to determine the parameters.

The mean and variance of a Frechet distribution is given by

$$\mu = v + \alpha \Gamma\left(1 - \frac{1}{\beta}\right) \text{ for } \beta > 1 \quad (35)$$

$$\sigma^2 = \alpha^2 \left[\Gamma\left(1 - \frac{2}{\beta}\right) - \Gamma^2\left(1 - \frac{1}{\beta}\right) \right] \text{ for } \beta > 2 \quad (36)$$

where $\Gamma(\mathbf{n})$ is a gamma function evaluated at \mathbf{n} .

The Frechet distribution is unbounded in nature and seldom used in traffic load modelling, which is widely accepted to be bounded. This is discussed in Section 3.3.7.

Weibull distribution

The Weibull distribution, also known as the Type 3 Extreme Value distribution, is defined by three parameters namely the shape (β), the scale (α) and the location (γ). The PDF is given by

$$f(x) = \frac{\beta}{\alpha} \left(\frac{x - \gamma}{\alpha} \right)^{\beta-1} e^{-\left(\frac{x-\gamma}{\alpha}\right)^\beta} \quad (37)$$

The CDF is given by

$$F(x) = 1 - e^{-\left(\frac{x-\gamma}{\alpha}\right)^\beta} \quad (38)$$

Various methods exist to determine the shape factor, the scale factor and the location of a Weibull distribution including graphical methods, MLE, Method of Moments and least squares (Tiryakioğlu, 2008; Genschel & Meeker, 2010; Marušić & Markovic, 2010; Bhattacharya, 2011; Carrillo, Cidrás, Díaz-Dorado & Obando-Montaño, 2014; Nwobi & Ugomma, 2014; Pobocikova & Sedliackova, 2014; Kantar, 2015). Only the graphical procedure with the Mean Rank (MR) method is described here, but MLE can also be performed as shown for the Gumbel distribution. The Weibull distribution for traffic data starts at the origin and the location parameter can be set to zero.

If Equation (38) is transformed both sides by $\ln\left(\frac{1}{1-x}\right)$ then

$$\ln\left(\frac{1}{1-F(x_i)}\right) = \left(\frac{x_i}{\alpha}\right)^\beta \quad (39)$$

so that

$$\ln\left[\ln\left(\frac{1}{1-F(x_i)}\right)\right] = \beta \ln x_i - \beta \ln \alpha \quad (40)$$

where x_i represents the order statistics $x_{(1)} < x_{(2)} < \dots < x_{(n)}$.

If $Y = \ln\left[\ln\left(\frac{1}{1-F(x_i)}\right)\right]$, $X = \ln x_i$ and $c = -\beta \ln \alpha$ then Equation (40) represents a simple linear regression function

$$Y = \beta X + c \quad (41)$$

An estimate of the scale parameter, α , can be calculated as

$$\alpha = e^{-\left(\frac{c}{\beta}\right)} \quad (42)$$

where c is the intercept of the linear regression. $F(x_i)$ can be approximated by the MR method

$$F(x_i) = \frac{i}{n+1} \quad (43)$$

By calculating $F(x_i)$, Y_i can be plotted as a straight line against $X_i = \ln x_i$. The slope of the line gives the shape parameter, β , and α can then be determined by Equation (42). The MR method can also be used with $F(x_i) = \frac{i-0.3}{n+0.4}$. It is important to note that the graphical estimation depends on the plot position. Although the graphical procedure is simple to use, MLE provides a more accurate analytical solution.

The mean and variance for the Weibull distribution is given by

$$\mu = \alpha \Gamma\left(1 + \frac{1}{\beta}\right) \quad (44)$$

$$\sigma^2 = \alpha^2 \left[\Gamma\left(1 + \frac{2}{\beta}\right) - \Gamma^2\left(1 + \frac{1}{\beta}\right) \right] \quad (45)$$

where $\Gamma(\mathbf{n})$ is a gamma function evaluated at \mathbf{n} .

The Weibull distribution is widely used in traffic load modelling due to its bounded nature. This is discussed in Section 3.3.7.

Generalized Extreme Value distribution (GEV)

The GEV distribution does not require a predetermined choice of the distribution family from one of the Weibull, Gumbel or Frechet EV distributions (Coles, 2001).

$$G(z) = \exp\left\{-\left[1 + \xi \left(\frac{z - \mu}{\sigma}\right)\right]^{-1/\xi}\right\} \quad (46)$$

Equation (46) gives the CDF of the GEV distribution for a random variable Z with μ being the location parameter, σ the scale parameter and ξ the shape parameter. The shape parameter describes the tail of the underlying data set and is negative for a Weibull (bounded) extreme value distribution and positive for a Frechet (unbounded) extreme value distribution. The Gumbel distribution is a special case of the GEV distribution with $\xi = 0$ (Coles, 2001). Many authors argue that due to the inherent bounded nature of traffic loading it is not unreasonable to allow only shape factors smaller than or equal to zero (OBrien, Schmidt, Hajializadeh, Zhou, Enright, Caprani, Wilson & Sheils, 2015).

***iid* Assumption for Extreme Value distributions**

Extreme Value theory is based on the condition that random variables are independently and identically distributed (*iid*) (Caprani, 2005; Caprani, OBrien & McLachlan, 2008; Caprani & OBrien, 2010a; Messervey, Frangopol & Casciati, 2011; Zhou, 2013). This implies that each random variable has the same probability distribution as the others and all are mutually independent. For random variables to be identically distributed there can be no overall trends in the data. Independent means that they are not connected in any way. When multiple vehicles occupy a lane simultaneously, the vehicles are not necessarily independent of each other. For example the position of the second vehicle could be dependent on the position of the first vehicle et cetera which violates the *iid* assumption. Furthermore, two-vehicle events and three-vehicle events, for example, could follow different distributions when the load effects are considered. Even single vehicle events are non *iid* if the events are produced by vehicles which are not from the same distribution. Therefore random variables in a traffic loading sample are not necessarily identically distributed. Although it is not possible to predict the outcome of fitting distributions to non *iid* data, conventional approaches fit EV distributions to these variables nonetheless.

The Block Maxima method is discussed in detail in a later section of this work. For now suffices to state the measurement period is divided into blocks of equal duration. The maximum value from each of these blocks are taken and an EV distribution is fitted to the data.

The *iid* condition and block size is investigated for South African traffic in Section 3.3.7.

Poisson distribution

The Poisson distribution is a discrete probability distribution which gives the probability of a certain amount of events occurring in a fixed time or space. An example of this would be the number of heavy vehicles which pass a weigh station in an hour. It is important to note that the intervals should be independent of one another. The Poisson distribution is important to understand early developments in multiple lane presence reduction. The PDF and CDF for the Poisson distribution is given by

$$f(x) = e^{-\lambda} \frac{\lambda^x}{x!} \quad (47)$$

$$F(x) = e^{-\lambda} \sum_{i=0}^x \frac{\lambda^i}{i!} \quad (48)$$

where λ is the average number of occurrences per time interval.

The mean and the variance are given by

$$\mu = \lambda \quad (49)$$

$$\sigma^2 = \lambda \quad (50)$$

An important observation is that the mean and variance of a Poisson distribution are equal.

2.1.1.5 Probability paper

Probability paper provides a graphical way of determining whether data fits a certain assumed distribution or not. The CDF is scaled to plot as a straight line, as opposed to the standard S-shape curve, by performing a linear transformation of the CDF (Allaix, 2007). If the data conforms to the assumed distribution, then a plot of the transformed CDF yields a straight line (Nowak & Collins, 2002; Caprani, 2005; Montgomery & Runger, 2010). For example it can be shown that the Weibull CDF in Equation (38) can be transformed to

$$\ln[-\ln(1 - F(x))] = \beta \ln x - \beta \ln \alpha \quad (51)$$

where the first term can be thought of as the y component of the equation for a straight line. The second term can be thought of as the mx component with the third term being the intercept on the vertical axis, or the c term. If one plots the first term on the vertical axis and the second term on the horizontal, then the line will be straight if the sample follows a Weibull distribution. This procedure can be applied to all distributions with two parameters. To plot a normally distributed random variable on normal probability paper the value of the random variable is plotted on the horizontal axis with the inverse standard normal value on the vertical. An example of this is shown in Figure 4 for an arbitrary normal distribution, with the straight line indicating that the data approximately conforms to a normal distribution.

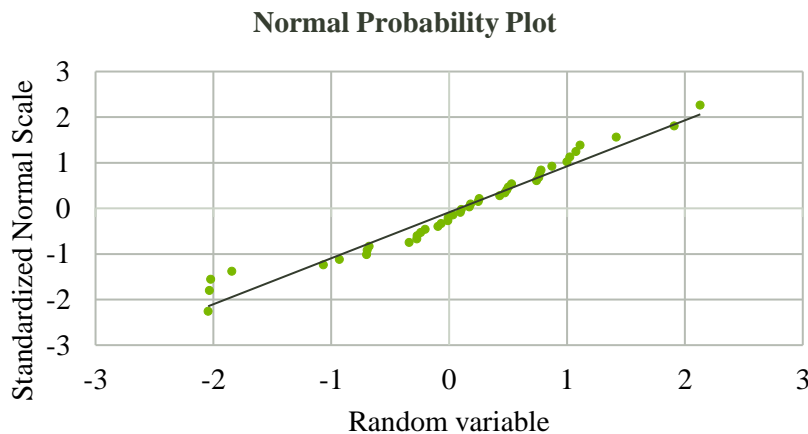


Figure 4 - Typical normal probability plot showing good straight line adherence of the data

2.1.1.6 Gaussian Mixture Modelling

Gaussian mixture modelling (GMM) is a sub category of Finite Mixture Modelling (FMM) which deals with the presence of more than one mode (or cluster) in a sample. It is especially important in the

analysis of traffic data as samples often consist of loaded and unloaded vehicles and different vehicle types which follow separate distributions. FMM is a way of identifying different distributions (often Gaussian) within samples. In this work the parameters for the mixtures are determined with the Expectation Maximization (EM) algorithm as well as with Bregman Soft Clustering. Bregman Soft Clustering gives similar results to the EM algorithm. Bregman Hierarchical Clustering is used to identify the number of components in a mix. Only the fundamental principles are given here.

Finite Mixture Modelling

The formulation of Finite Mixture Modelling is provided by various authors (McLachlan & Peel, 2000; Figueiredo & Jain, 2002; Picard, 2007; Steenbergen & Morales Napoles, 2012; Zhang & Huang, 2015).

Let $\mathbf{Y} = [Y_1, \dots, Y_d]^T$ be a d -dimensional random variable with $y = [y_1, \dots, y_d]^T$ being one particular outcome of \mathbf{Y} . \mathbf{Y} follows a mixture distribution with k components if its PDF can be written as

$$p(y|\theta) = \sum_{m=1}^k \alpha_m p(y|\theta_m) \quad (52)$$

where

$\alpha_1, \dots, \alpha_k$ are the mixing probabilities of which the sum can't be greater than 1.0

θ_m the set of parameters defining the m -th component

θ the complete set of parameters needed to define the mixture

Given a set of *iid* samples $\mathcal{Y} = \{y^{(1)}, \dots, y^{(n)}\}$ the log-likelihood for a k -component mixture is

$$\log p(\mathcal{Y}|\theta) = \log \prod_{i=1}^n p(y^{(i)}|\theta) = \sum_{i=1}^n \log \sum_{m=1}^k \alpha_m p(y^{(i)}|\theta_m) \quad (53)$$

To determine the parameters of the mixture it is necessary to maximize the function above. This is not possible analytically so the EM algorithm is used together with Bregman Soft Clustering for verification (Banerjee, Merugu, Dhillon & Ghosh, 2005; Garcia, Nielsen & Nock, 2010; Lucic, Bachem & Krause, 2015).

EM Algorithm

The EM algorithm is an iterative procedure which is used to calculate MLE which are not possible to solve analytically, and when there is missing data (Borman, 2004) or multiple populations. An example is Equation (53) where the parameters of mixture models need to be solved. The EM algorithm was first introduced in 1977 by Dempster (Dempster, Laird & Rubin, 1977) which states that each iteration of the algorithm consists of an expectation step (E-step) followed by a maximization step (M-step).

First an assumption of the mixture parameters is made. Then, the E-step calculates missing data based on the assumed parameters and is achieved using the conditional expectation. In the M-step the likelihood function is maximized and a new set of parameters are calculated. The process is repeated until convergence is reached. Convergence is guaranteed since the likelihood is increased at each iteration.

Bregman Soft Clustering

Clustering is the concept of arranging objects in groups so that objects in the same group (cluster) are more similar to each other than those in other groups. There exists a bijection between exponential families and Bregman divergences which enables the use of Bregman divergences to separate mixtures of data through the use of the Bregman Soft Clustering algorithm (Banerjee *et al.*, 2005; Lucic *et al.*, 2015). To define the Bregman Soft Clustering algorithm it is necessary to define Bregman divergence. Let $\varphi: S \rightarrow \mathbb{R}$ be a strictly convex function defined on a convex set $S \subseteq \mathbb{R}^d$ such that φ is differentiable on the interior of S . The Bregman divergence $D_\varphi: S * \text{int}(S) \rightarrow [0, \infty)$ is defined as

$$D_\varphi(\mathbf{x}, \mathbf{y}) = \varphi(\mathbf{x}) - \varphi(\mathbf{y}) - \langle \mathbf{x} - \mathbf{y}, \nabla\varphi(\mathbf{y}) \rangle \quad (54)$$

where $\nabla\varphi$ is the gradient of φ .

Bregman divergences are characterised by the fact that a mean of a set of points minimizes the sum of Bregman divergences between these points and any other point. To calculate mixture parameters it is necessary to maximize the likelihood function or, equivalently, minimize the log-likelihood. This can be shown to be equivalent to minimizing the corresponding Bregman divergence.

jMEF

The author acknowledges the jMEF Java library coded by Vincent Garcia and Frank Nielsen which implements the EM algorithm, Bregman Soft Clustering and Bregman Hierarchical Clustering.

As an example of the implementation of FMM, Figure 5 shows a typical axle weight distribution. The histogram clearly shows signs of bimodality which is due to the presence of empty and fully laden vehicles. Figure 6 shows the fitting of a bimodal normal distribution to the histogram using jMEF.

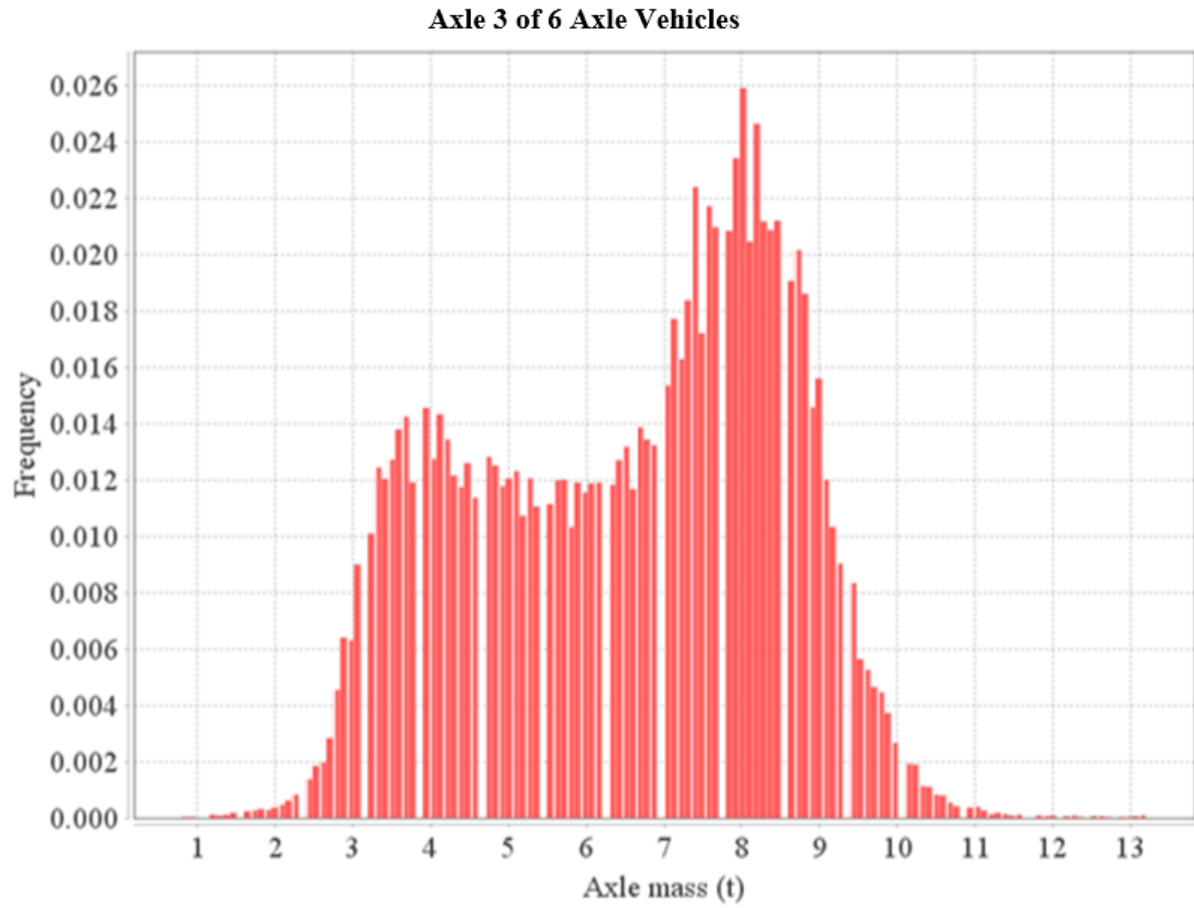


Figure 5 - Axle 3 histogram for 6 axis vehicles

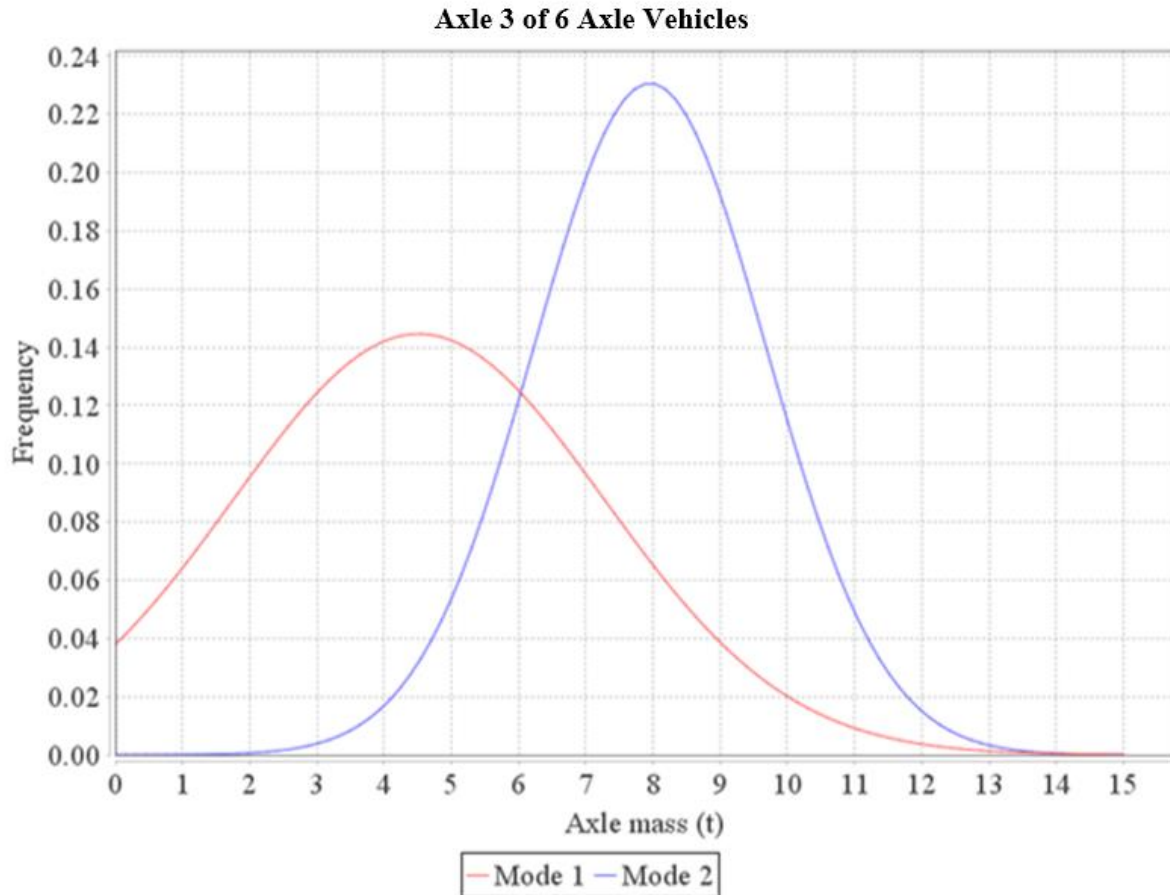


Figure 6 - Bimodal PDFs for axle 3 of 6 axle vehicles

2.1.1.7 Probability of exceedance and return period

The probability of exceeding any value in any one time period defines the return period for an event. If the probability of exceeding a value z in any one year is p , then the return period of z in years is described by

$$R(z) = \frac{1}{p} \quad (55)$$

This is the mean recurrence time of z (Ang & Tang, 1975; Enright, 2010).

If Z is defined as a value with a probability α of being exceeded in N years, and assumed the probability of Z being exceeded in 1 year is p , then the probability of Z not being exceeded in a year is $(1 - p)$. The probability of Z not being exceeded in N years is

$$(1 - p)^N = \left(1 - \frac{1}{R(Z)}\right)^N \quad (56)$$

It can be shown that

$$\left(1 - \frac{1}{R(Z)}\right)^N \approx e^{-\frac{N}{R(Z)}} \quad (57)$$

Therefore

$$\alpha = 1 - (1 - p)^N = 1 - \left(1 - \frac{1}{R(Z)}\right)^N \approx 1 - e^{-\frac{N}{R(Z)}} \quad (58)$$

Finally the return period is given by

$$R(Z) = \frac{1}{1 - (1 - \alpha)^{1/N}} \quad (59)$$

2.1.1.8 Determining fractiles at return periods

WIM data is typically only available for a couple of weeks or years. When determining characteristic values for bridge traffic loading it is necessary to extrapolate the measured data to some acceptable return period using some statistical distribution. As there are many sub populations of different vehicle types in the WIM data only the upper tail, consisting of the heaviest vehicles, of a parent distribution contributes significantly to the extrapolated value at the return period (Bailey, 1996; Zhou, Schmidt & Jacob, 2012; Zhou, 2013). It is difficult to determine the tail lengths of data accurately for non *iid* populations. For simplification, various tail lengths have been investigated including the upper $2\sqrt{n}$, upper 5 % and upper 30 % of values (Enright & OBrien, 2012; OBrien, O'Connor & Arrigan, 2012; Zhou, 2013; OBrien *et al.*, 2015; Heitner, OBrien, Schoefs, Yalamas, Décatoire & Leahy, 2016; Soriano, Casas & Ghosn, 2016; Anitori, Casas & Ghosn, 2017, 2018). Soriano *et al.* (2016) and Anitori *et al.* (2017, 2018) fit a normal distribution to the upper 5 % of maxima. This result could not be reproduced for South African traffic data. Enright (2010) found that by fitting a Weibull distribution to the upper 30 % of maxima gives a slightly more conservative value compared to $2\sqrt{n}$. However, a tail length of $2\sqrt{n}$, where n is the number of blocks in the block maxima data, is used most extensively in bridge traffic load models.

The tail length assumption of $2\sqrt{n}$ originated from Castillo (1988) where he states that $2\sqrt{n}$ is a good choice for high speed convergence. Castillo's study was not performed on bridge traffic load data which could have a different tail length from the data that he used. The validity of this assumption for South African bridge loading is discussed in more detail in Section 3.3.7.

To extrapolate to return periods a distribution is fitted to the tail and a quantile is taken which corresponds to the return period.

Many different techniques have been investigated including

- Block maxima method with Generalized Extreme Value (GEV) distribution (Getachew & O'Brien, 2007; Caprani *et al.*, 2008; Enright, Caprani & O'Brien, 2011; Enright & O'Brien, 2012; Zhou *et al.*, 2012; Hellebrandt, Blom & Steenbergen, 2014; Leahy, O'Brien & O'Connor, 2015; O'Brien *et al.*, 2015; Heitner *et al.*, 2016). Fitting the GEV distribution to the tail of load effect data has the advantage that the user does not need to choose between the Gumbel, Weibull or Frechet distributions.
- Block maxima method with Weibull distribution (Bailey, 1996; Bailey & Bez, 1999; Grave, 2001; Caprani, Belay & O'Connor, 2003; O'Connor & O'Brien, 2003; O'Brien, O'Connor, *et al.*, 2012; Enright & O'Brien, 2012; O'Brien, Hajjalizadeh, Donovan & Enright, 2012; Leahy, O'Brien, Enright & Hajjalizadeh, 2015; O'Brien *et al.*, 2015; Heitner *et al.*, 2016). It is reasonable to assume that traffic load effects are bounded due to the capacity of pavements to resist high axle loads, the capacity of tyres to withstand high pressures and geometric limitations. The Weibull maximum distribution has an upper bound and it is therefore reasonable to assume that traffic load effects follow this distribution. A further motivation for an upper bound is the legal weight limitations imposed on GVW and axle loads. This is explored in Chapters 3 and 4.
- Block maxima method with Gumbel distribution (Caprani *et al.*, 2003; O'Connor & O'Brien, 2003; Fu & You, 2009; O'Brien, Enright & Getachew, 2010; Sivakumar, Ghosn & Moses, 2011; Enright & O'Brien, 2012; O'Brien, O'Connor, *et al.*, 2012; Hellebrandt *et al.*, 2014; O'Brien *et al.*, 2015; Heitner *et al.*, 2016). The Gumbel distribution is a special case of the GEV distribution with a shape factor of zero and has been used to describe traffic load effects. It is not as well justified as the Weibull distribution as it does not have an upper bound, but it has been used partly because it yields more conservative results than a Weibull distribution and also as an upper limit where the tail of load effects indicate unbounded Frechet behaviour.
- Peaks-over-threshold (POT) method with Generalized Pareto distribution (GPD) (Crespo-Minguillón & Casas, 1997; Zhou *et al.*, 2012; O'Brien *et al.*, 2015). The POT method chooses a threshold above which data is fitted to the GPD distribution. The major drawback of this method is that the threshold is difficult to determine.
- Mixture peaks-over-threshold approach (Zhou, Schmidt, Toutlemonde & Jacob, 2016). This method makes provision for a mixture of different sub populations in traffic load effect data which are non *iid*, but it suffers from the same drawbacks of the traditional POT approach.
- Fitting Gaussian distribution to the tail (Nowak & Hong, 1991; Nowak, 1993, 1994; Nowak, Nassif & DeFrain, 1993; Flint & Jacob, 1996; Sivakumar, Moses & Ghosn, 2008; Kozikowski, 2009; Nowak & Rakoczy, 2013; Doan, Sparling & Feldman, 2016; Soriano *et al.*, 2016; Anitori *et al.*, 2017). This method was used widely in the calibration of the AASHTO code and the

Eurocode and has been found to fit the upper 5 % of daily maxima well for the traffic data studied. There is, however, no theoretical justification for fitting block maximum data to the tail of a normal distribution.

- Predictive likelihood (Caprani & O'Brien, 2010b). The application of predictive likelihood is shown to require a strict definition of acceptable safety levels, as the more usual return period definition does not yield the same results in general.
- Composite distribution statistics (Caprani & O'Brien, 2010a; Enright *et al.*, 2011). This method accounts for non *iid* sub populations from an extreme value perspective. It is useful when different vehicle types occupy a bridge longitudinally and transversely simultaneously or for daily maxima caused by different sub populations. When overloaded vehicles and permit vehicles are present in the data it may be difficult to identify these sub populations.
- Rice formula with the level crossing method (Cremona, 2001; Getachew, 2003; O'Connor & O'Brien, 2005; O'Brien *et al.*, 2015). This method is based on the conditions that the load effects are stationary and Gaussian, which have both been shown not to be the case. The Rice formula is fitted to level crossing histograms. Note that it is a parametric fit and that the optimal fitting corresponds to the largest number of class intervals verifying a confidence level for the Kolmogorov-Smirnov test.
- Raising the parent distribution to a power (Crespo-Minguillón & Casas, 1997; Ghosn, Moses & Wang, 2003; Fu & You, 2009; Soriano *et al.*, 2016; Anitori *et al.*, 2017, 2018). A way to analyse the maximum value of a variable over a long period is based on the knowledge of the CDF of the maximum value of this variable over a shorter basic period. Assuming that the maximum effect in each basic period is an independent variable equally distributed in all periods, then the CDF of the basic period can be raised to a power of N periods, typically the return period for characteristic values, SLS or ULS. The condition that load effects are equally distributed over many periods is not necessarily true for non-stationarity and changes in vehicle characteristics over time.
- Box-Cox approach (Caprani & O'Brien, 2010a). This approach aims to address the limitations of the traditional EV and POT approaches and the need to choose between the two. The Box-Cox-GEV distribution is a more generalised form of the standard GEV distribution and includes a fourth parameter namely the model parameter. The performance of this method for traffic load effects is not well established, although it seems as if it predicts larger load effects than the more conventional EV approaches.

The EV approaches (GEV, Weibull and Gumbel) are well researched and established. Fitting the GEV distribution to the tail of load effects has the advantage that it is not necessary to choose between the

constituent distributions (Gumbel, Frechet and Weibull). Some authors, however, state that the tail of traffic load effects are best suited to a Weibull distribution as traffic load effects are a physical process and therefore bounded in nature (Bailey, 1996; Caprani *et al.*, 2003; O'Brien, O'Connor, *et al.*, 2012; O'Brien *et al.*, 2015). The resulting load effects are bounded largely due to the capacity of pavements, pressure limitations of tyres and geometric constraints on the width, length and height of vehicles. It is thus expected that the GEV distribution will indicate underlying Weibull behaviour. The POT method is not considered further in this work due to the apparent difficulty in choosing a threshold.

2.1.2 Basics of structural reliability

It is not possible to make any structure one hundred percent safe. Rather, an acceptably low probability of failure over the design life of the structure is decided upon, which determines a resistance value below which a structure will fail, and a loading above which a structure will fail.

ISO2394 (ISO, 2015) and EN1990 (CEN, 2002) define reliability as the ability of a structure, or structural element, to fulfil the specified requirements, including the working life or reference period, for which it has been designed. The Eurocode further states that “*a structure shall be designed and executed in such a way that it will, during its intended life with appropriate degrees of reliability and in an economic way:*

- *Remain fit for the use for which it is required*
- *Sustain all actions and influences likely to occur during execution and use*”

By satisfying the above conditions, a structure is deemed reliable. The definitions above include some important considerations needed to define reliability:

- Performance requirements
- Design life or reference period
- Acceptable probability of failure
- The use that a structure is exposed to

2.1.2.1 Limit states

A limit state is that condition beyond which a structure no longer fulfils its purpose. There exist mainly two limit states for structural design:

- **Serviceability Limit State.** At SLS, a structure has not experienced loss of equilibrium, but rather a loss of functionality related to normal use. Loss of functionality mainly includes excessive cracking leading to durability problems, excessive deflections and excessive vibrations. Unsatisfactory appearance of a structure can also be included under SLS. SLS

exceedance can be irreversible when the limit state remains permanently exceeded after the loads causing the exceedance are removed (Holicky, 2009). SLS can also be deemed as reversible where the structure returns to its original state after the load is removed. SLS does not normally lead to a complete loss of functionality.

- Ultimate Limit State. At ULS a structure could lose equilibrium and collapse entirely. Exceedance of the capacity of a cross section can lead to yielding, rupture or excessive deformations, which in turn lead to the structure not being usable. Capacity exceedance of cross sections can lead to redistribution of forces and hence a change in the overall static behaviour of a structure. Exceedance of the ULS is irreversible and requires a major repair or a demolition. Cost of repairs is significant and loss of human life could occur. Examples of ULS failures include exceeding the moment capacity of a structure, formation of a plastic hinges, crushing of concrete in compression, loss of overall stability, buckling of a flange, buckling of a web and weld rupture (Nowak & Collins, 2002).

2.1.2.2 Safety margins and β values

If the load on a structure is denoted as E , and the resistance as R , then failure will occur when E exceeds R , or $E > R$. For a probabilistic analysis, both E and R are random variables which can each be described by some probability distribution.

Let M be $R - E$ so that failure occurs when E exceeds R and M becomes negative. M is called the safety margin and is shown to the right on Figure 7. If R and E both follow a normal distribution, then M will also be normally distributed. $f(r)$, $f(e)$ and $f(m)$ are the PDF's of the load, resistance and safety margin distributions. The probability of failure, P_f , is

$$P_f = P(E > R) = P(M < 0) = \Phi_M(0) \quad (60)$$

From Figure 7 it is clear that the probability of failure, P_f , is the area under $f(m)$ below zero on the horizontal axis. The CDF of M , evaluated at zero, equals the probability of failure P_f .

M can be transformed to the standardized normal distribution, U , so that

$$u_0 = \frac{0 - \mu_M}{\sigma_M} = -\frac{\mu_M}{\sigma_M} \quad (61)$$

The term $-u_0$ is known as the reliability index β and the probability of failure can hence be described by Equation (62) as

$$P_f = \Phi_U(u_0) = \Phi_U(-\beta) \quad (62)$$

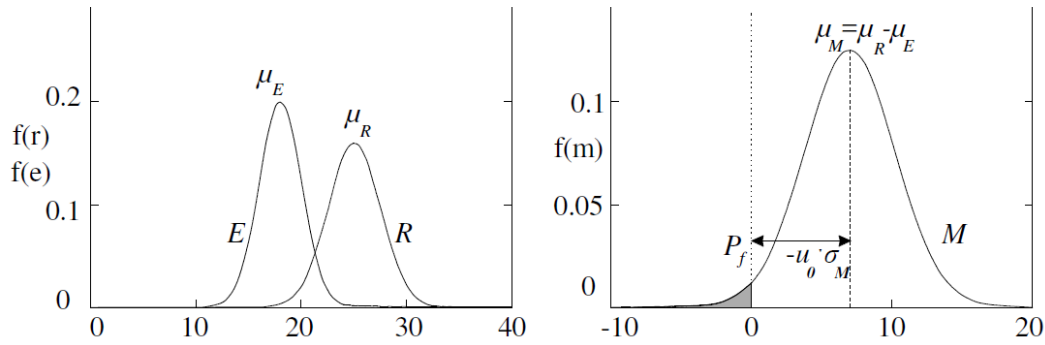


Figure 7 - Failure zone of the limit state function for normally distributed random variables (Lenner, 2014)

In the case of independent normally distributed random variables, β can be calculated explicitly as

$$\beta = \frac{\mu_M}{\sigma_M} = \frac{\mu_R - \mu_E}{\sqrt{\sigma_R^2 + \sigma_E^2}} \quad (63)$$

β (or $-u_0$) can be interpreted as the number of standard deviations from the mean to zero for the limit state function M , shown in Figure 7. A higher β value implies a smaller probability of failure P_f .

2.1.2.3 FORM analysis

To find P_f requires mathematical integration of functions that do not necessarily have closed form solutions. This is the case when either one or both the resistance PDF or the load effect PDF are non-normal.

For the general case the load, E , and the resistance, R , can be represented as functions of random variables

$$R = f_1(\mathbf{X}) \quad (64)$$

$$E = f_2(\mathbf{X}) \quad (65)$$

then the safety margin, M , can be written as

$$M = R - E = f_1(\mathbf{X}) - f_2(\mathbf{X}) = g(\mathbf{X}) \quad (66)$$

where $g(\mathbf{X})$ is known as the limit state function. If $g(\mathbf{X}) \leq 0$ failure occurs and if $g(\mathbf{X}) > 0$ a structure or component can be deemed safe.

If $f_{\mathbf{X}}(\mathbf{x})$ represents the joint PDF of $f_1(\mathbf{X})$ and $f_2(\mathbf{X})$ for \mathbf{X} then the probability of failure can be found by integrating over the failure domain as per Equation (67).

$$P_f = \int_{g(\mathbf{x}) \leq 0} f_{\mathbf{X}}(\mathbf{x}) d\mathbf{x} \quad (67)$$

To solve the integral in Equation (67) is not trivial and numerical approximations are needed. One such method is the First Order Reliability Method (FORM) (CEN, 2002; Holicky, 2009). The method is

based on the assumption of a linear or linearized limit state function and independent normal random variables for the load effect and the resistance.

As the load effect and/or resistance are usually not normally distributed, they have to be transformed into standard normal space. The transformation to standard normal space is achieved through Equations (68) and (69).

$$U_1 = \frac{R - \mu_R}{\sigma_R} \quad (68)$$

$$U_2 = \frac{E - \mu_E}{\sigma_E} \quad (69)$$

Equation (66) can be rewritten by substitution of Equations (68) and (69) to give

$$G = R - E = (U_1\sigma_R + \mu_R) - (U_2\sigma_E + \mu_E) = 0 \quad (70)$$

$$G = R - E = (\mu_R - \mu_E) + U_1\sigma_R + U_2\sigma_E = 0 \quad (71)$$

Once the random variables of the resistance and load have been transformed to standard normal space, the joint PDF can be shown in U -space by Figure 8. The reliability index, β , is the smallest distance between the origin and the failure surface $g(u)$. The design point is defined as the point on the failure surface closest to the origin, denoted in Figure 8 as u^* with intercepts U_{1d} and U_{2d} .

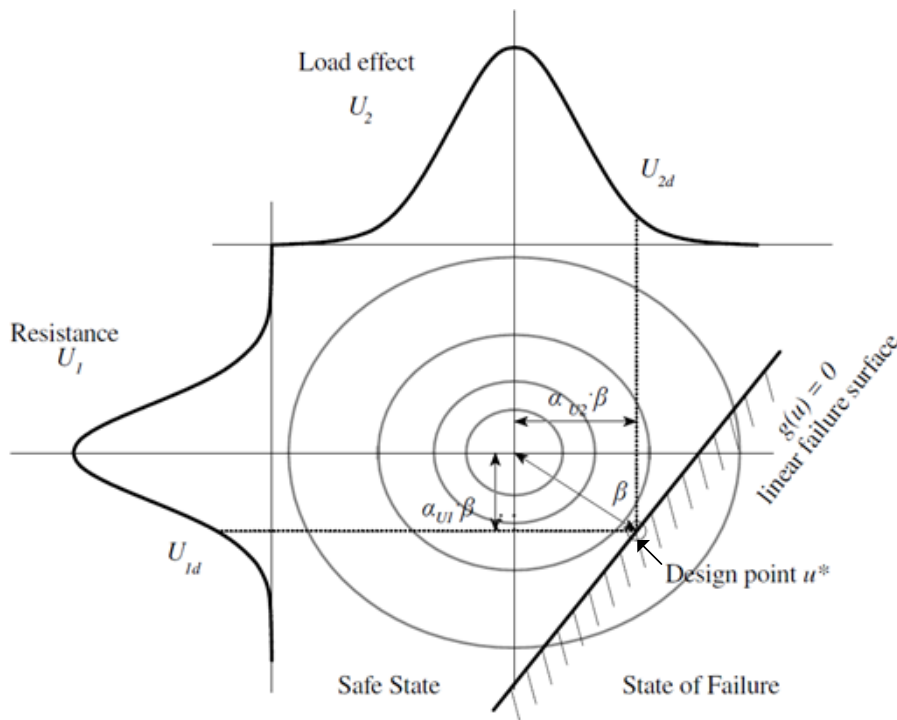


Figure 8 - Normalized joint PDF in U-space (Lenner, 2014)

It follows from Figure 8 that

$$\beta = \sqrt{U_{1d}^2 + U_{2d}^2} \quad (72)$$

$$U_{1d} = -\alpha_{U1}\beta \quad (73)$$

$$U_{2d} = \alpha_{U2}\beta \quad (74)$$

where the α factors are sensitivity factors describing the direction of the β vector. As $\alpha_{U1} = \alpha_R$ and $\alpha_{U2} = \alpha_E$, the design point for normal distributions can be found in original space by substituting Equations (73) and (74) into Equations (68) and (69) to give

$$R_d = -\alpha_R\beta\sigma_R + \mu_R \quad (75)$$

$$E_d = \alpha_E\beta\sigma_E + \mu_E \quad (76)$$

where R_d and E_d are the coordinates of the design point in original space. EN1990 (CEN, 2002) and ISO2394 (ISO, 2015) allows approximations of the sensitivity factors of $\alpha_E = -0.7$ and $\alpha_R = 0.8$. To apply this load sensitivity factor to traffic loading it is assumed that traffic loading is the dominant load component. If another load becomes dominant, for example selfweight for longer span lengths, then α_E should be multiplied by 0.4 (Holicky, 2009). Even this is an approximation as α_E is in reality a function of the load ratio for which a study falls outside the scope of this work. These values were nevertheless first introduced by Konig & Hosser (1982) and are a function of the standard deviations of the load and resistance functions, as indicated in Equations (77) and (78) specifically for normally distributed random variables.

$$\alpha_E = -\frac{\sigma_E}{\sqrt{\sigma_E^2 + \sigma_R^2}} \quad (77)$$

$$\alpha_R = \frac{\sigma_R}{\sqrt{\sigma_E^2 + \sigma_R^2}} \quad (78)$$

The approximations are valid, provided that

$$0.16 < \sigma_E/\sigma_R < 7.3$$

To evaluate the validity of this expression requires that the resistance must be modelled probabilistically as well. If this is not known then it is conservative to take $\alpha_E = 1.0$ which implies that all the uncertainty is located in the load component. Note that values of -0.7 and 0.8 are already conservative as

$$\sqrt{\alpha_E^2 + \alpha_R^2} > 1$$

The load and resistance distributions are often not normal and a more generic description of the design point is given by Ditlevsen & Madsen (2007) as

$$X_d = F_X^{-1}[\Phi(\alpha\beta)] \quad (79)$$

where X represents either E or R where F_X^{-1} is the inverse CDF of the effect or the resistance.

The sensitivity factors are discussed in more detail in Chapter 7.

2.1.2.4 Calibration of partial factors

The design format followed in this work is the semi-probabilistic format. Two PFs are applied for the load and the resistance respectively (Schneider, 1997). These factors, PFs, ensure that the applied load effects are below the resistance of a structure by a sufficient margin, determined by β . The characteristic load effects are multiplied by the PFs for SLS and ULS to determine the design load effects.

By assuming a value for α_E it becomes possible to evaluate the reliability of the load effects separate from that of the materials.

The partial factor format for transient loads is described in fib Bulletin 80 (fib, 2016) as

$$\gamma_E = \gamma_{Ed,M} \gamma_e \quad (80)$$

where

γ_E the partial factor for loading, in this case traffic loading

$\gamma_{Ed,M}$ the partial factor accounting for model uncertainty in the estimation of the load effect from the load model. Model uncertainty is the uncertainty related to imperfect knowledge or idealizations of the mathematical models used or uncertainty related to the choice of probability distribution types for the stochastic variables

γ_e is the reliability based partial factor accounting for variability of the traffic loads and uncertainties relating to the model of variable action

It is custom to model the loading with an EV distribution as per 2.1.1.8. The design point of the load effect, also denoted as E_d , can be found from Equation (79) or by extrapolating to the return period which corresponds to the chosen β value. E_c denotes the characteristic value for the same load effect. The reliability based partial factor, γ_e , is given by Equation (81) (Holicky, 2009; fib, 2016).

$$\gamma_e = \frac{E_d}{E_c} \quad (81)$$

In the design of structures, $\gamma_{Ed,M}$ is typically assumed as 1.12 for unfavourable variable actions (fib, 2016). EN1990 (CEN, 2002) specifies a range for $\gamma_{Ed,M}$ between 1.05 and 1.15 which can vary according to a country's national annex.

2.2 Dynamic amplification

The motion of vehicles cause additional bending moments and shear forces due to dynamic interaction between vehicles and bridges, also known as Vehicle-Bridge Interaction (VBI). To account for these increased loads it is common to multiply the static loads by a DAF which is defined as the ratio of the total load effect, E_T , to the static load effect, E_S (Paultre, Chaallal & Proulx, 1992; González, Dowling, OBrien & Znidaric, 2010; Caprani, González, Rattigan & OBrien, 2011; Caprani, 2013, 2017; Deng, Yu, Zou & Cai, 2015).

$$DAF = \frac{E_T}{E_S} \quad (82)$$

Design codes typically specify a DAF based on a study of light and heavy vehicles. It has been shown that this approach is conservative as heavier vehicles, which govern the maximum load effects, tend to cause the lowest dynamic amplification (Paultre *et al.*, 1992; O'Connor & OBrien, 2003; González, Znidaric, Casas, Enright, OBrien, Lavric & Kalin, 2009; Ludescher & Bruhwiler, 2009; OBrien, Rattigan, González, Dowling & Žnidarič, 2009; Caprani *et al.*, 2011; Caprani, 2013, 2017; Deng *et al.*, 2015). Codes in general therefore fail to recognise the decreased probability of the maximum static load effects occurring simultaneously with the maximum dynamic amplification, leading to conservative results. Codes typically determine the DAF for single vehicle events, which are higher than for multiple vehicle events, although multiple vehicle events tend to govern the load effects on short to medium span bridges (Caprani *et al.*, 2011), leading to further conservatism.

To overcome this conservatism Caprani *et al.* (2011) suggest an assessment dynamic ratio (ADR) which compares characteristic total load effects, \hat{E}_T , to characteristic static load effects, \hat{E}_S . The ADR is defined as

$$ADR = \frac{\hat{E}_T}{\hat{E}_S} = \frac{G_T^{-1}(q)}{G_S^{-1}(q)} \quad (83)$$

where

G_T is the cumulative distribution function of the total load effects

G_S is the cumulative distribution function of the static load effects

q is the quantile of interest. If G_T and G_S are derived using daily maxima values then

$q = 0.999997$ for a 5 % exceedance probability in 50 years.

The ADR ensures that only the dynamic amplification values, which occur together with the heaviest vehicles, are included in assessment. Experimental research has shown that this leads to substantially smaller values than prescribed in design codes (OBrien, Cantero, Enright & González, 2010; Caprani *et al.*, 2011; Deng *et al.*, 2015; Caprani, 2017). The ADR approach is well suited to assessment of

existing structures where a number of parameters can be measured deterministically. The concept can also be applied to determine the DAF for new bridge codes.

2.3 Multiple lane presence

Another key aspect of developing a load model is the consideration of multiple lanes on a bridge deck as vehicles can occupy any lane at any time. Multiple lane presence reduction factors (MLFs) are widely used in traffic load models for bridge design to account for the reduced probability of multiple heavy vehicles occurring simultaneously in adjacent lanes (Jaeger & Bakht, 1987; Bakht & Jaeger, 1990; Nowak, 1993; Fu, Liu & Bowman, 2013; Zhou, Shi, Caprani & Ruan, 2018). A single lane traffic load model is typically calibrated for the slow, heavy lane. Loading in each additional notional lane on a bridge deck is typically reduced by a factor less than one. This factor decreases as probability of side-by-side events in all considered lanes decreases.

A summary of MLF development and assumptions used internationally in other codes follows:

- In the derivation of the AASHTO factors, assumptions were made based on observations of side-by-side occurrences and assumed correlations and dependence between vehicle weights in adjacent lanes (Nowak & Hong, 1991; Nowak & Szerszen, 1998) and without WIM data. As overloaded vehicles avoid weigh stations the results may not be representative of the most onerous conditions. This method only accounts for free flowing traffic and hence short to medium span bridges where congested traffic is considered less onerous.
- In the derivation of the Eurocode, Monte Carlo simulations, with inherent assumptions, were performed for multiple lane traffic based on recorded free flowing data at Auxerre in 1986 (Sedlacek, Merzenich, Paschen, Bruls, Sanpaolesi, Croce, Calgaro & Pratt, 2008). Free flowing and congested traffic states were simulated based on an assumed ratio of cars to trucks of 75:25. Zhou *et al.* (2018) note that many assumptions were made in the process. As congested traffic was checked in this method it is also applicable to longer spans. The results are based on concurrencies in simulations rather than on measured multiple lane concurrent load effects.
- Jaeger & Bakht (1987) and Bakht & Jaeger (1990) proposed a method based on the Poisson distribution to predict the simultaneous presence of vehicles in adjacent lanes. The method is based on the assumption that the probability of simultaneous presence at any one time is small and the number of successive time intervals is large. This method has been used in the derivation of the load models in the Canadian and Chinese codes (Zhou *et al.*, 2018). It does not account for the possibility of having more than one vehicle in a lane and is therefore only applicable to bridges shorter than about 20 m where single vehicle events cause the largest load effects. The authors note, however, that this is conservative. The proposed reduction factors are based on assumptions made regarding the governing form of traffic for different span lengths

and the estimates of the Poisson parameter, which is noted by the authors as subjective. The authors propose free flowing traffic for span lengths up to 125 m which is questionable since it is well known that congested traffic governs on longer spans (Caprani & O'Brien, 2008; Caprani, 2012). The method assumes that traffic in adjacent lanes is identically distributed which is not applicable in all cases (Zhou *et al.*, 2018). Correlation of traffic flows between adjacent lanes is achieved by parameters developed by Harman & Davenport (1976) based on 'most traffic conditions.'

- Soriano *et al.* (2016) and Anitori, Casas & Ghosn (2017, 2018) show that for New York WIM data the tail of load effects can be approximated by fitting a normal distribution to the upper 5 % of data points. The authors also show that there is no correlation between the weights of trucks in adjacent lanes and therefore also no dependence. This finding allows a convolution approach whereby PDFs of load effects in adjacent lanes are added together to produce a joint PDF. This PDF represents simultaneous load effects of two trucks on a bridge. Sivakumar, Ghosn & Moses (2011) observed that the percentage of trucks involved in multiple presence events are dependent on the Average Daily Truck Traffic (ADTT) with an increase in multiple presence events with an increase in ADTT and a reduction in headway. A range of ADTT values were investigated. These studies consider short and medium span bridges defined by span lengths up to 60 m. Some simplifications in these studies result in single trucks occupying any one lane at a time and that only two adjacent lanes are considered. This is based on the observation that the probability of having three side-by-side trucks contributing to the maximum load effect in a main girder is small.
- Fu *et al.* (2013) propose an empirical framework for multiple presence reduction based on span length, ADTT and number of lanes for fatigue and ultimate limit states separately. This is the first method that considers characteristic load effects and acknowledges the decreased probability of multiple heavy vehicles occurring in any one lane or adjacent lanes as the truck volume, span length and number of lanes increase. The authors use regression analysis of ADTT, number of lanes and span length to propose site specific formula's for MLFs.
- Zhou *et al.* (2018) propose a comprehensive framework which studies the dependence between lanes at coincident extreme values and takes the load distribution to the superstructure members into account. The method is applicable to free flow and congested traffic conditions and can calculate bespoke MLFs for any superstructure type, number of spans, span lengths and deck width. As this method uses the deck configuration to determine the MLF it is well suited to assessment of existing bridges where the configuration is known. For new bridges it would require an iterative procedure as both the ideal deck configuration and the MLFs are unknown.

2.4 International code overview

Bridge load models describe the nature of vehicle loading on bridges with regards to concentrated loads and uniformly distributed loads. Although these models do not represent actual vehicles, they should encapsulate the effects of all vehicle types and vehicle gaps for different span lengths and for different numbers of lanes. The return period plays a critical role in establishing the characteristic load. In this section the load models of the Canadian, British, European, USA and Australian codes are presented to provide background for the development of the new model in later chapters.

2.4.1 Historical code development procedures

The first load model that resembles modern load models was the British MOT loading train, introduced in 1922 (O'Connor & Shaw, 2000). The model, shown in Figure 9, consists of a tractor and four trailers with a total length of 22.9 m. The main axle of the tractor has a weight of 219 kN with the trailers having axle weights of 100 kN each. It is the heavy axle of the tractor which led to the concept of a knife edge load, with the closely spaced trailer wheels forming the uniformly distributed load component of modern load models.

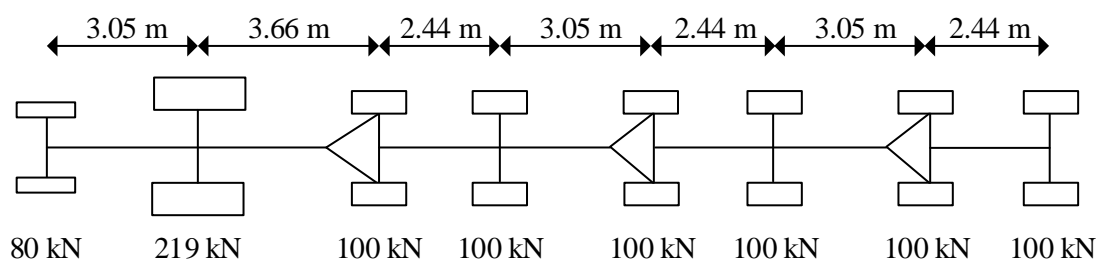


Figure 9 - MOT standard load train (O'Connor & Shaw, 2000)

An MOT standard load curve was introduced in 1931, consisting of a knife edge load and a uniformly distributed load. The intensity of the uniformly distributed load varied with loaded length, reducing as the span length increases. This reduction with loaded length is shown in Figure 10. The load curve was obtained by smearing the trailer axles over their spacing to give a load per unit area of 10.7 kPa. The main axle of the tractor, weighing 119 kN more than the other 100 kN axles, was divided by its contributing length, leading to a knife edge load of 39.2 kN/m over the spacing of the axle. A dynamic amplification of 50 % was allowed for which reduced beyond 22.9 m to 15 % at 122 m and zero at 762 m (O'Connor & Shaw, 2000). Beyond the 22.9 m train length, the UDL decreased to 3.4 kPa for span lengths equal or greater than 762 m. Even though the load model was not derived probabilistically, the load curve acknowledges the reduced probability of multiple heavy vehicles with an increase in span length.

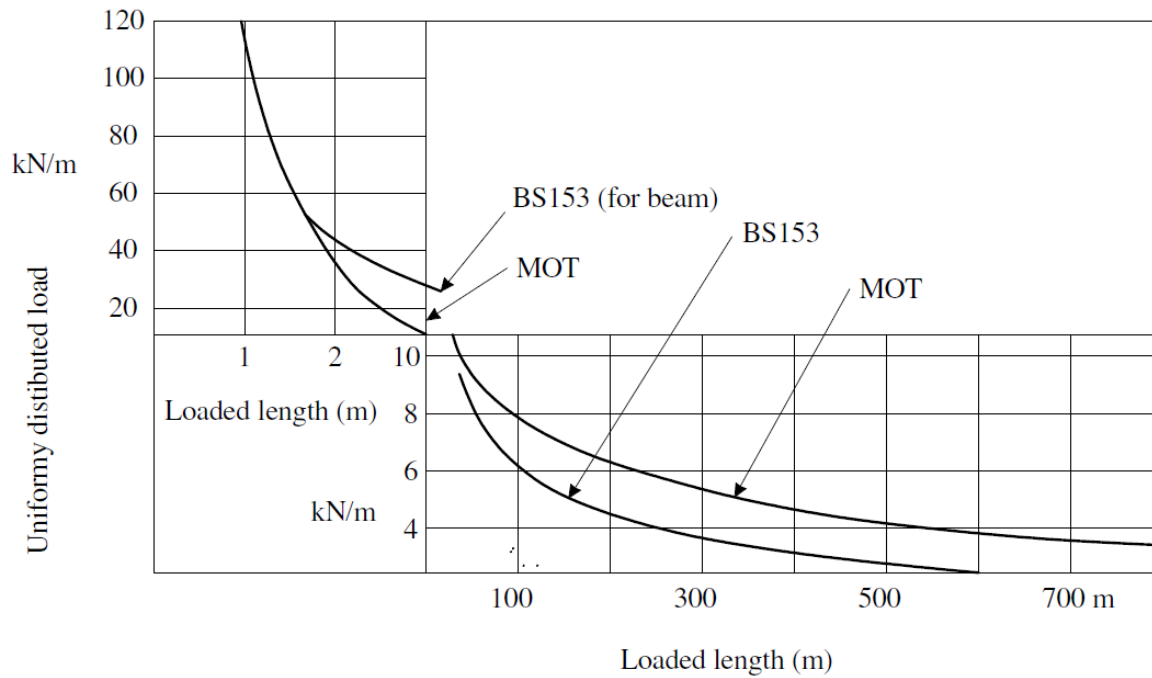


Figure 10 - Standard MOT load curve (O'Connor & Shaw, 2000)

The MOT standard load curve was replaced by BS 153 in 1958 which introduced different models for normal and abnormal loading. It is this concept which directly led to the HA and HB loading which, later appeared in BS 5400 between 1978 and 1983, and which led to NA and NB loading in TMH7. Before TMH7, MOT loading was used widely in South Africa (Stutterheim, 1988).

2.4.2 Canadian Standard

The Ontario Highway Bridge Design Code (OHBD), published in 1979, was a pioneer in the application of limit state design in bridge design codes. The load model was based on the legal limit of vehicles in Ontario, but influenced the load models in the remainder of Canada as well, as it is impossible to drive across Canada without travelling through the state of Ontario (O'Connor & Shaw, 2000).

A 1971 survey of vehicles in Ontario led to a Maximum Observed Load (MOL), in kN, given by Equation (84).

$$MOL = 9.806(20 + 3.0B_M - 0.0325B_M^2) \tag{84}$$

with B_M being an equivalent base length defined in the code. The MOL curve is shown in Figure 11, with the dashed line showing the maximum observed values for the corresponding equivalent base length. The MOL directly influenced the design truck of the OHBD, shown in Figure 12.

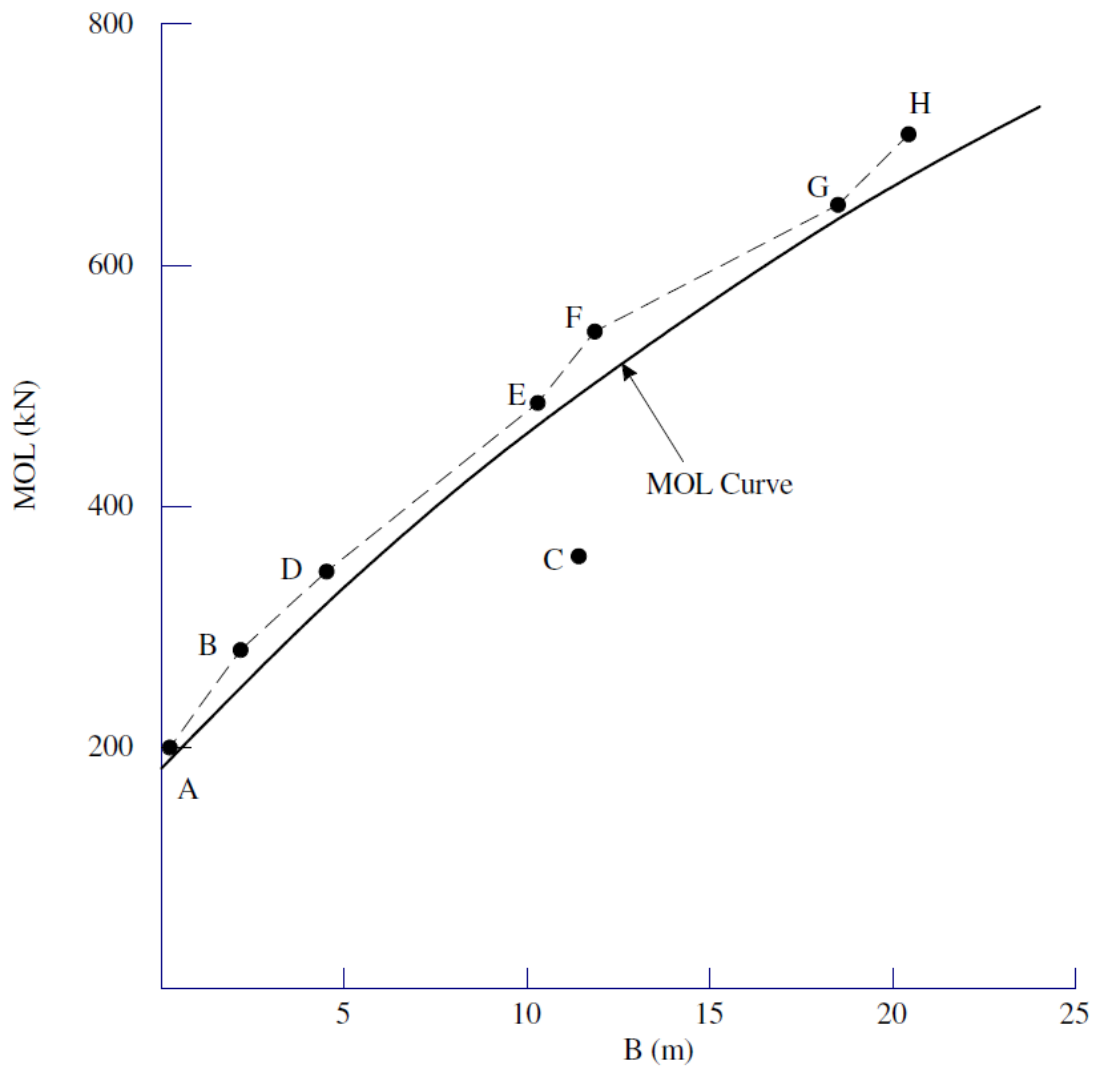


Figure 11 - Canadian MOL curve (O'Connor & Shaw, 2000)

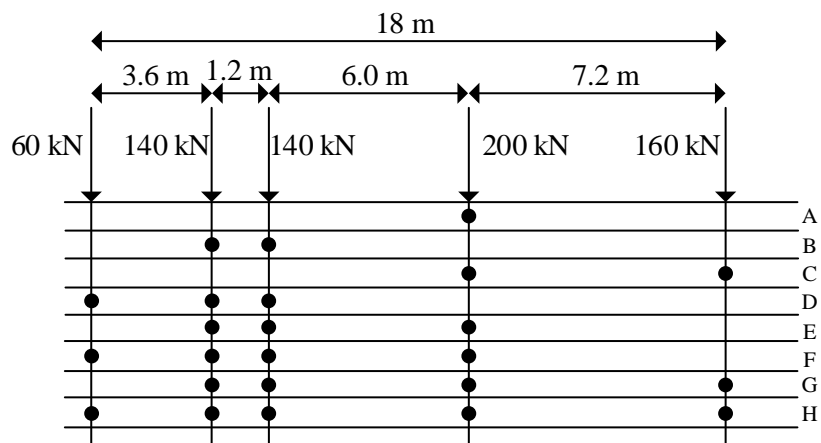


Figure 12 - OHBD Truck load (O'Connor & Shaw, 2000)

The model also had a design truck loading which was specified as 70 % of the Truck load together with a UDL of 10 kN/m. Characteristic extreme events were determined for a 50 year return period (Nowak & Grouni, 1984).

The OHBDC load models were reviewed in 1991 and were increased slightly with axles 2 and 3 of the design truck being increased from 140 kN to 160 kN. Characteristic extreme events were again determined for a 50 year return period, using an exponential distribution (Nowak & Grouni, 1994).

A memorandum of understanding (MOU) was signed by all provinces in 1988. This set the vehicle weight and dimension limits for all provinces in Canada and led to the CS-W loading, where W is the total vehicle weight in kN. This MOU was revised in 1991 and formed the basis of the live load model of the new Canadian Highway Bridge Design Code (CHBDC), of which the current version is CSA-S6 (Canadian Standards Association, 2014). CL-W loading consists of a CS-W Truck or the CL-W Lane Load and W is taken as not less than 625 kN. The CL-W Truck is a five axle idealised truck, shown in Figure 13.

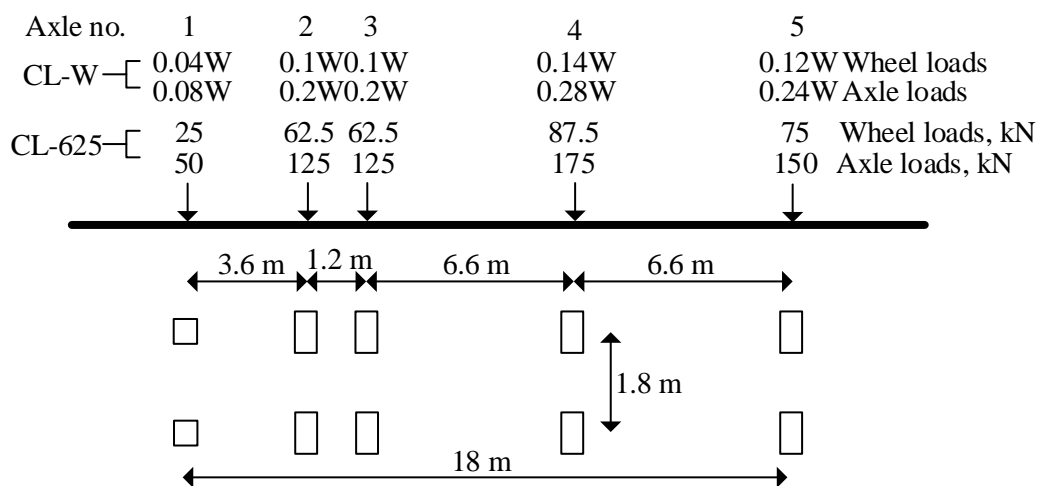


Figure 13 - CHBDC Truck (O'Connor & Shaw, 2000)

The CL-W Load Load consists of 80 % of a CL-W design truck with a UDL of 9 kN/m, shown in Figure 14.

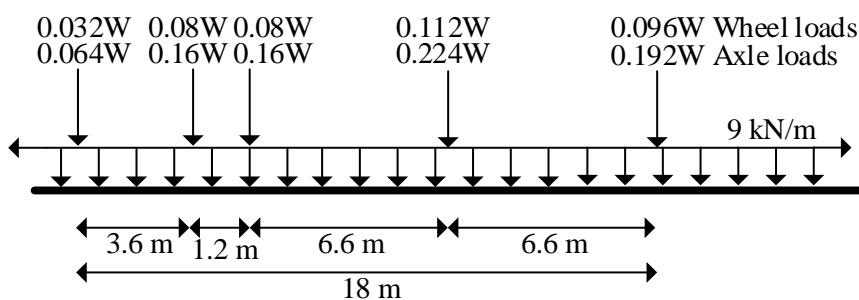


Figure 14 - CHBDC Lane Load (O'Connor & Shaw, 2000)

Truck axles that reduce the load effect under consideration are ignored and the Lane Load shall not be applied to loaded lengths which reduce the load effect to be calculated. A dynamic load allowance is to be applied only to the Truck with the following values

- 0.4 where only one axle of the truck is used
- 0.3 where any two axles of the truck are used, or where axles 1 and 3 are used
- 0.25 where three axles of the truck are used, except for axles 1 and 3, or more than three axles

This recognises the phenomena where an increase in the number of axles leads to a reduction of the dynamic amplification.

Multiple lane presence is represented by a modification factor in Table 1.

Table 1 - CHBDC multiple lane reduction factors (Canadian Standards Association, 2014)

Number of loaded design lanes	Modification factor
1	1.00
2	0.90
3	0.80
4	0.70
5	0.60
6 or more	0.55

2.4.2.1 Reliability calibration

The Canadian standard uses a target β of 3.5 for a 50 year design life (Agarwal & Cheung, 1987). An annual β value of 3.75 was calculated to be consistent with the 75 year design life beta of 3.5 (Canadian Standards Association, 2014).

2.4.3 BS 5400

Following from the MOT loading described in Section 2.4.1, BS5400 was published in 1978 (O'Connor & Shaw, 2000). It was the first British bridge design code to follow limit state design principles and consisted of a normal and abnormal load model. The characteristic normal load model, HA, consisted of a knife edge load of 120 kN together with a distributed load. For loaded lengths (L_{load}) up to 30 m the distributed load, W , was given as 30 kN/m, reducing to a minimum value of 9 kN/m at an L_{load} of 380 m. In 1988 the British Department of Transport issued a departemental standard BD37/88. HA loading was revised, keeping the knife edge load of 120 kN, but changing the UDL to

$$W = 336(L_{load})^{-0.67} \quad \text{for } L_{load} \leq 50 \text{ m}$$

$$W = 36(L_{load})^{-0.1} \quad \text{for } 50 \leq L_{load} \leq 1600 \text{ m}$$

The configuration of the abnormal load model, HB, remained unchanged from the previous edition, but the number of units of HB loading was increased from 25 to 45 on main roads. Figure 15 shows the configuration for HB loading with the centre spacing varying from 6 m to 26 m in 5 m increments, whichever creates the largest load effect. One unit of HB loading equals 2.5 kN per wheel leading to a 1800 kN vehicle weight for HB45 loading.

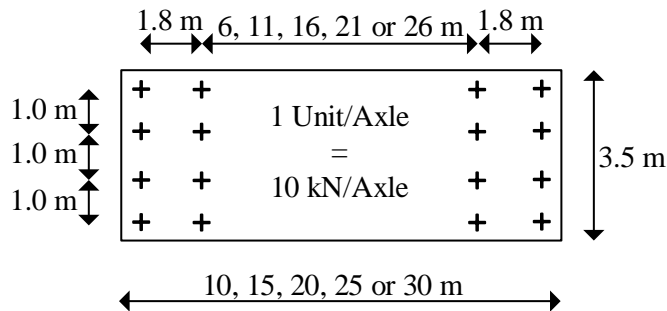


Figure 15 - HB load configuration (O'Connor & Shaw, 2000)

A dynamic allowance of 80 % was included and applied to the knife edge load of HA. No dynamic allowance was incorporated for HB loading. The multiple lane reduction factors β_n , shown in Table 2, are a function of span length L , number of notional lanes N and the width of the notional lanes b_L and can generally be taken as 1.0 for the first two lanes and 0.6 for subsequent lanes.

Table 2 - Lane factors for BS5400 and BD37/88

Loaded Length L m	First lane factor β_1	Second lane factor β_2	Third lane factor β_3	Fourth and subsequent
				lane factor β_n
$0 < L \leq 20$	α_1	α_1	0.6	$0.6\alpha_1$
$20 < L \leq 40$	α_2	α_2	0.6	$0.6\alpha_2$
$40 < L \leq 50$	1	1	0.6	0.6
$50 < L \leq 112$ & $N < 6$	1	$7.1/\sqrt{L}$	0.6	0.6
$50 < L \leq 112$ & $N \geq 6$	1	1	0.6	0.6
$L > 112$ & $N < 6$	1	0.67	0.6	0.6
$L > 112$ & $N \geq 6$	1	1	0.6	0.6

$$\alpha_1 = 0.274b_L \leq 1.0$$

$$\alpha_2 = 0.0137(b_L(40-L) + 3.65(L-20))$$

N shall be taken as the total number of notional lanes, except that for a bridge that carries traffic in one direction only the value of N shall be taken as twice the number of notional lanes. Note that the β referred to here is not the same as the symbol used to denote the reliability index elsewhere in this text.

2.4.4 Eurocode

With modern European road transport across European boundaries, it was concluded that co-operation between member countries was needed for evaluating the capacity of existing bridges (O'Connor & Shaw, 2000). This led directly to the composition of Eurocode 1 by the European Committee for Standardisation (CEN). Measured traffic data from across Europe was evaluated with regards to the composition of the traffic, traffic density, axle and vehicle loads, axle spacing and vehicle spacing. These evaluations dictated that the Eurocode load models must be comprised of a group of single loads and a UDL which must capture both local and global effects. The bridge loading model of the Eurocode is based on two weeks of data collected from a single station on the A6 freeway near Auxerre in France during 1986 (Hanswille & Sedlacek, 2007; Sedlacek *et al.*, 2008). Although the Auxerre station did not exhibit the largest axle loads, it did show the highest frequency of large axle loads. The values for the loads in the load models were determined through static and dynamic Monte Carlo simulations. Derivation of the transverse lane reduction is discussed in Section 2.3.

EN1991-2 (CEN, 2003) consists of four characteristic load models namely

- LM1 Normal traffic
- LM2 Verification for local effects
- LM3 Abnormal vehicles - specified in National Annex for each country
- LM4 Crowd loading - 5 kPa human loading applied

A half normal distribution was fitted to the measured axle weights and extrapolated to 1000 years (approximately 5 % probability of exceedance in 50 years). This produced a characteristic axle load of 300 kN, including dynamic effects (Croce, Sanpaolesi & Bruls, 1996; Sedlacek *et al.*, 2008). The Gumbel distribution and Monte Carlo simulations were also considered for extrapolation, but it is not clear if and how they were implemented. Traffic was simulated and run over various influence lines to record bending moments and shear forces at different span lengths. These forces were then used to calibrate the distributed loads.

2.4.4.1 Load Model 1

LM1 consists of a double axle and a UDL. The axle load in the first lane is specified as 300 kN with a UDL of 9 kPa, which reduces with each subsequent lane as the probability of having multiple heavy vehicles in adjacent lanes concurrently reduces. The loading arrangement for LM1 is shown in Figure 16. The α factors are adjustment factors, typically set to unity, which are specified in the national annex for each member country. For road bridges in lighter trafficked areas, or for member states with lighter loading, α can be reduced, but it is not recommended to be taken smaller than 0.8. α used here is not the same as the symbol used for the FORM sensitivity factor elsewhere in this text.

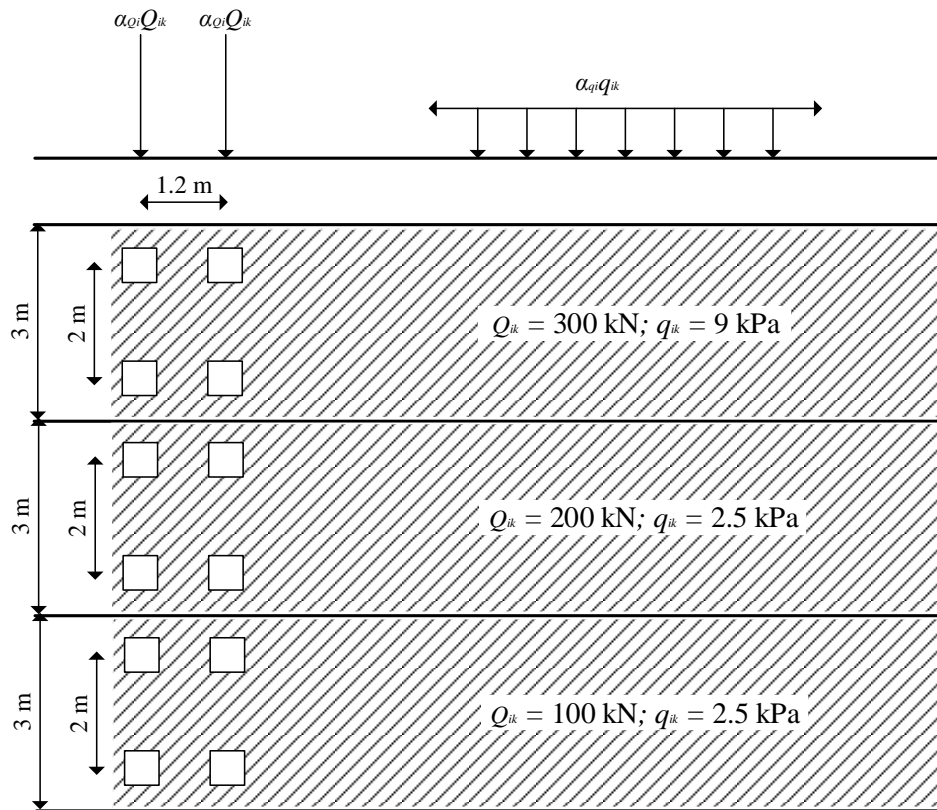


Figure 16 - Eurocode LM1 (CEN, 2003)

LM1, with a reference length of 11 m, can be interpreted as an assembly of

- A row of 450 kN vehicles in a jam situation with 5 m inter vehicle distances and one 900 kN vehicle in the first lane
- A 500 kN vehicle in the second lane with 120 kN vehicles in a row
- A 300 kN vehicle in the third lane with 120 kN vehicles in a row

2.4.4.2 Load Model 2

Load Model 2 (LM2) consists of a single axle of 400 kN which can be applied at any position on the deck in order to produce the most adverse loading. The axle load includes allowance for dynamic effects and is primarily intended for local verifications. Figure 17 shows the configuration of LM2, indicating that the axle can be located against the kerb.

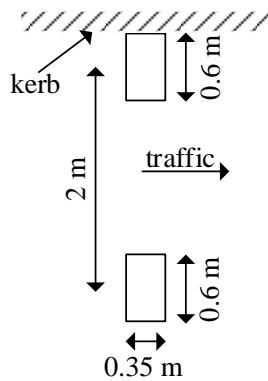


Figure 17 - Eurocode LM2 (CEN, 2003)

2.4.4.3 Dynamic amplification

In EN1991-2 the DAF is not stated explicitly, but is already included in the load model stipulated in the code. The DAF was determined using a medium quality pavement and a pneumatic vehicle suspension. It is a function of span length, number of loaded lanes and load effect.

One lane bridges

The DAF for one loaded lane is specified separately for bending and shear. Equations (85) and (86) give the DAFs for bending and shear respectively, where L is the span length.

$$DAF = \begin{pmatrix} 1.7 \text{ for } L \leq 5 \text{ m} \\ 1.85 - 0.03L \text{ for } 5 \text{ m} < L < 15 \text{ m} \\ 1.4 \text{ for } L \geq 15 \text{ m} \end{pmatrix} \quad (85)$$

$$DAF = \begin{pmatrix} 1.4 \text{ for } L \leq 5 \text{ m} \\ 1.45 - 0.01L \text{ for } 5 \text{ m} < L < 25 \text{ m} \\ 1.2 \text{ for } L \geq 25 \end{pmatrix} \quad (86)$$

Two lane bridges

The DAF for bending and shear are equal for bridges with two lanes and is shown in Equation (87).

$$DAF = \begin{pmatrix} 1.3 - \frac{0.4}{100}L \text{ for } L \leq 50 \text{ m} \\ 1.1 \text{ for } L > 50 \text{ m} \end{pmatrix} \quad (87)$$

Four lane bridges

For bridges with four lanes the DAF for moment and shear are both specified as 1.1.

Additional amplification near expansion joints

For cross sections near expansion joints an additional amplification factor, $\Delta\varphi$, shall be applied as per Equation (88). $\Delta\varphi$ shall not be taken as smaller than 1.0.

$$\Delta\varphi = 1.3 \left(1 - \frac{D}{26} \right) \quad (88)$$

where D is the distance at the cross section under consideration from the expansion joint.

The Eurocode fails to address the reduced probability of the static and dynamic extremes occurring simultaneously (Caprani *et al.*, 2011) and the DAFs are therefore high and conservative.

2.4.4.4 Reliability calibration of Eurocode

Partial factors for the Eurocode are determined for CC2 in accordance with Section 7.3. Although bridges have a design life of 100 years, Sykora, Holicky & Markova (2013) state that a β of 3.8 was used for the calibration of the partial factor which has a reference period of 50 years.

2.4.5 AASHTO LRFD

In 1986, the American Association for State Highway and Transport Officials (AASHTO) commissioned a major revision of United States bridge design practice. This led to the first Load and Resistance Factor Design (LRFD) code in 1994. The traffic load model is based on the weigh station measurement of 9250 vehicles from a single station in Ontario, Canada during 1975 (Nowak & Hong, 1991; Nowak & Szerszen, 1998; Leahy, OBrien, Enright, *et al.*, 2015). Load effects were calculated for the measured convoy and extrapolated normally to a 75 year return period to obtain characteristic values (Nowak & Rakoczy, 2013). With subsequent large volumes of WIM data becoming available the original model has been scrutinized and found to be conservative (Leahy, OBrien, Enright, *et al.*, 2015).

The AASHTO live load model is a combination of a truck and a lane load or a tandem and a lane load (AASHTO, 2007).

2.4.5.1 Design tandem

The characteristic design tandem consists of a pair of 110 kN axles spaced 1.2 m apart with the transverse spacing of the wheels being 1.8 m.

The design truck consists of a 35 kN axle followed by two 145 kN axles. The space between the 145 kN axles varies between 4.3 m and 9 m with the spacing between the front two axles being fixed at 4.3 m. A dynamic allowance of 33% must be added to this value for SLS and ULS. The design truck is shown in Figure 18.

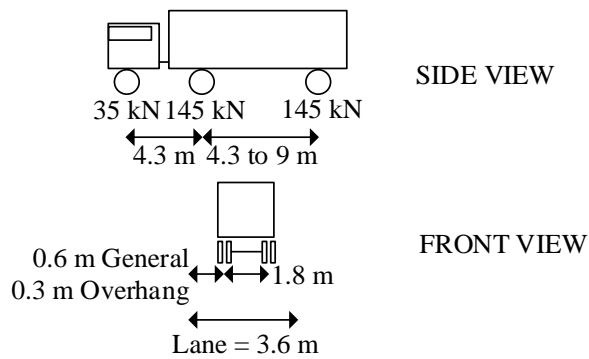


Figure 18 - AASHTO Design truck (AASHTO, 2007)

To determine the maximum negative moment between points of contraflexure under a uniform load on all spans, and the reactions at interior piers, two design trucks per lane may be used spaced 15 m apart with the distance between the 145 kN axles fixed at 4.3 m.

2.4.5.2 Design lane load

The characteristic design lane load consists of a longitudinal line load of 9.3 kN/m spread over a 3 m width.

2.4.5.3 Multiple lane presence

To account for the reduced probability of all lanes being loaded with the maximum load, AASHTO specifies multiple presence factors which are to be multiplied by the truck, tandem and lane loads. The factors are given in Table 3. The derivation of the MLFs was discussed in Section 2.3.

Table 3 - AASHTO multiple presence factors (AASHTO, 2007)

Number of loaded lanes	Multiple presence factors, m
1	1.2
2	1
3	0.85
>3	0.65

As opposed to other codes which use 1.0 as the MLF for the heaviest loaded lane, AASHTO uses the second highest loaded lane for the reference case, and 1.2 for the heaviest lane. This implies that, for single lane loading, the load model must be scaled up by 20 %.

2.4.5.4 Dynamic amplification

AASHTO (1992) specified the dynamic impact factor (IM) as a function of the bridge span length in meters. AASHTO (1994) replaced the IM with a dynamic load allowance (DLA) which is a function of

the limit state and components. The DLA is independent of the span length and is not applied to the lane load. Table 4 describes the values used in AASHTO.

Table 4 - AASHTO dynamic load allowance (AASHTO, 2007)

Component	Limit state	DLA %
Joints	All limit states	75
All other components	Fatigue and fracture	15
	Other	33

2.4.5.5 Reliability calibration of AASHTO

The load and resistance factors in AASHTO are based on statistical parameters from the 1970s and early 1980s. Load factors in the AASHTO LRFD specifications were selected so that the factored load corresponds to two standard deviations from the mean value. If the reliability level for ULS is back calculated a β of approximately 3.5 is obtained (Kulicki, Prucz, Clancy, Mertz & Nowak, 2007; Nowak & Iatsko, 2017).

2.4.6 Australian Standard

Early versions of the traffic load model for Australia were based on the AASHTO code (O'Connor & Shaw, 2000). The T44 truck loading, shown in Figure 19, was introduced in 1976, together with the L44 uniformly distributed lane loading, leading to an increase in load of 33 %. L44 consisted of a UDL of 12.5 kN/m and a knife edge load of 150 kN.

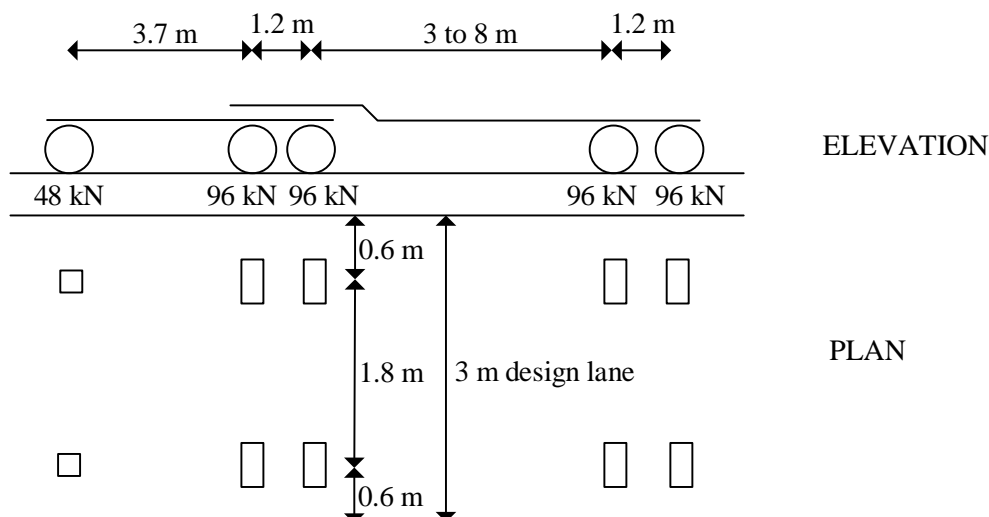


Figure 19 - Australian T44 truck (O'Connor & Shaw, 2000)

In 1992 the first limit state bridge design code was introduced in Australia. The code retained the T44 loading, but L44 lane loading was specified together with a 70 kN wheel load acting over an area of 500 mm in the longitudinal direction by 200 mm in the transverse direction.

Studies by Heywood, Gordon & Bouilly (2000) showed that load effects predicted by T44 loading was being encountered on a daily basis. In 2004, the new SM1600 load model was introduced and formalised in AS5100.2 (Standards Australia, 2004). The new model completely replaced the old T44 and L44 loadings. The approach followed in the derivation of SM1600 is somewhat unconventional. Where other codes are based on WIM or weigh station measurements, an upper load limit was considered based on available freight task, vehicle technology, safety and pavement damage for Australia's future economic needs. This upper load limit also constitutes the upper limit for overloading that can physically be achieved. By taking the physical upper limit, and considering that vehicles used as the basis for the model were loaded to 75 % of maximum freight density, a judgement was made to set the PF at 1.8. This is higher than in other codes discussed in this document, and together with the high characteristic loads the current Australian code is one of the heaviest in the world (Heywood *et al.*, 2000).

The minimum length between extreme axles of 25 m comfortably exceeded the length of the T44 vehicle and the total load of 1440 kN exceeded the old 388 kN.

Characteristic SM1600 consists of four load types namely

- W80 Wheel load
- A160 Axle load
- M1600 Moving traffic load
- S1600 Stationary traffic load

2.4.6.1 W80 loading

W80 loading consists of a single wheel load of 80 kN uniformly distributed over an area of 400 mm x 250 mm. The wheel load can be applied anywhere on the roadway surface for all structural elements for which a wheel load is critical. Dynamic amplification of 40 % is applied.

2.4.6.2 A160 loading

The A160 load represents a single axle load of 160 kN with the configuration shown in Figure 20. Dynamic amplification of 40 % is applied.

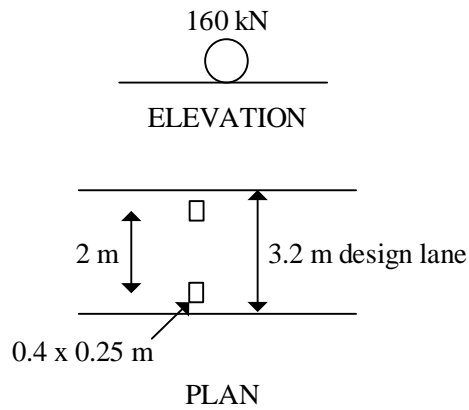


Figure 20 - AS5100 A160 loading (Standards Australia, 2004)

2.4.6.3 M1600 loading

M1600 loading represents a moving stream of traffic and consists of a uniformly distributed load and a truck load. The uniformly distributed part shall be continuous or discontinuous and of any length as may be necessary to produce the most adverse effects. Where a single tri-axial group from the M1600 moving traffic load, including the uniformly distributed load, governs a dynamic amplification of 35 % should be applied to the UDL and the truck. Otherwise a 30% dynamic amplification must be applied. The configuration of the M1600 load is shown in Figure 21.

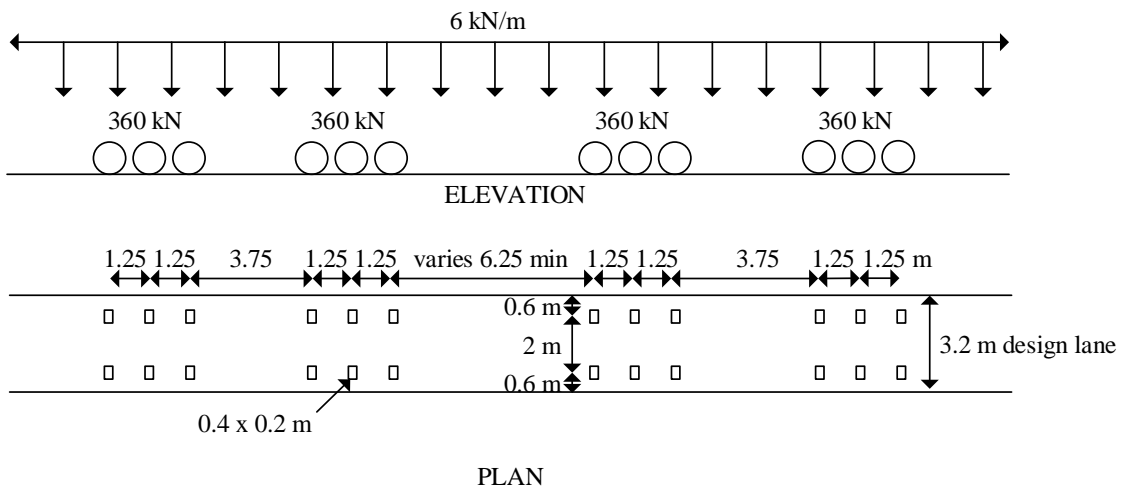


Figure 21 - AS5100 M1600 loading (Standards Australia, 2004)

2.4.6.4 S1600 loading

S1600 loading represents stationary traffic and therefore no dynamic effects are accounted for. The load consists of a uniformly distributed load together with a truck load as shown in Figure 22.

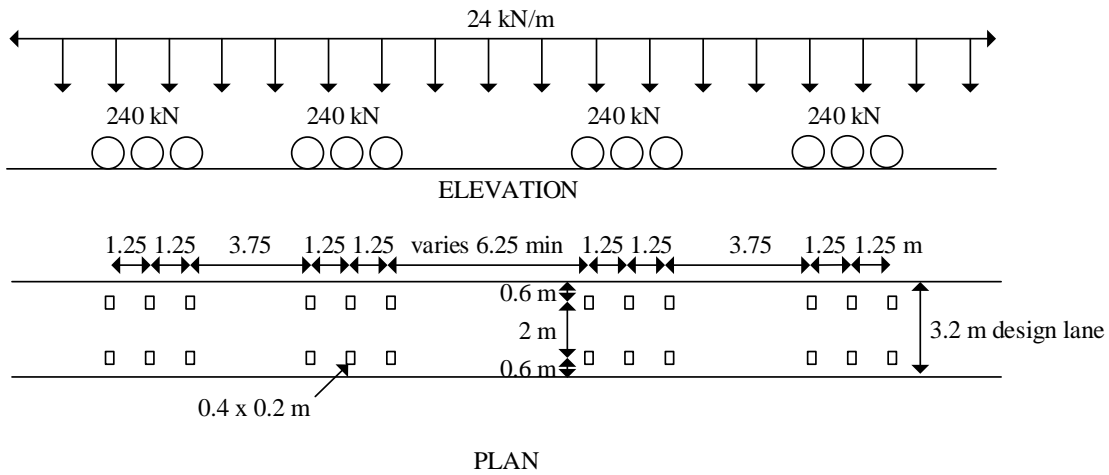


Figure 22 - AS5100 S1600 loading (Standards Australia, 2004)

The uniformly distributed part shall be continuous or discontinuous and of any length to produce the most adverse effects.

2.4.6.5 Multiple lane presence

To account for the reduced probability of all lanes being loaded with the maximum load, AS5100.2 specifies lane factors which are applied laterally to the A160, M1600 and S1600 models. The factors are shown in Table 5.

Table 5 - AS5100 lane factors (Standards Australia, 2004)

Accompanying Lane Factors	
Standard design lane number, n	Accompanying lane factor, ALF _i
1 lane loaded	1.0
2 lanes loaded	1.0 for first lane; and 0.8 for second lane
3 or more lanes loaded	1.0 for first lane; 0.8 for second lane; and 0.4 for third and subsequent lanes

2.4.7 Conclusion

The following codes are presented in this chapter:

- Canadian (CSA-S6)
- British (BS5400)
- European (EN1991-2)
- USA (AASHTO)
- Australia (AS5100.2)

All of these employ load models consisting of a combination of axle loads and distributed loads. It appears as if this configuration evolved from the very early MOT load trains which had a tractor, with one heavy axis and one lighter axis, towing a number of trailers. The heavy axis of the tractor evolved into the axle load (or knife edge load) in current models. The axle loads of the trailers, when spread over the axle spacings, led to the distributed load used in modern load models.

Although all the models employ axle loads combined with distributed loads, there exists great variability in the amount of axles and the spacings between them.

The level of reliability is not known for all the standards, but for those that are known there exists great variability, not only in the target β , but also in the reference periods. The AASHTO code was calibrated so that the design values are two standard deviations above the mean. Retrospectively, this relates to a target β of 3.5 for a 75 year design life, which is the level of reliability in the Canadian code also. The Eurocode is calibrated to a target β of 3.8 in a 50 year reference period for ULS.

It is surprising to note the relatively limited measured traffic data on which the Eurocode and AASHTO are based. The Eurocode is based on two weeks of WIM data at a single station near Auxerre in France. AASHTO is based on static weigh station measurement of 9250 vehicles in Ontario. It is well known that many heavy vehicles avoid weigh stations which introduces bias into the measurements (Nowak & Szerszen, 1998).

3 Current TMH7 loading and comparison with WIM measurements

It has been suggested that TMH7 is unconservative especially for shorter span bridges. This chapter introduces the current TMH7 load model and to assess the code from a modern perspective, current traffic as recorded by WIM systems is benchmarked against the NA load model. It is therefore necessary to provide an overview of WIM data in South Africa, how it is cleaned and calibrated and how individual vehicles and convoys are used to calculate load effects so that a comparison can be drawn.

3.1 TMH7 models

TMH7 consists of three vehicle loading components (CSRA, 1981) namely

- NA Normal traffic
- NB Abnormal traffic
- NC Super loading

As TMH7 is based on the BS5400 code of the time, the loading closely resembles HA and HB loading.

3.1.1 NA loading

Type NA loading represents normal traffic loading and consists of a distributed load plus a concentrated axle load per notional lane, or two 100 kN nominal wheel loads only. The distributed loading is a function of the loaded length and can be applied to the whole or parts of the length of any notional lane or combination of such lanes. The distributed part of NA loading is shown in Figure 23, as taken directly from the code. The load curve was derived by distinguishing between spans shorter and longer than 40 m. For spans shorter than 40 m a moving convoy of five vehicles weighing up to 228 kN was used. This convoy was preceded and followed by a line load of 6 kN/m (Anderson, 2006).

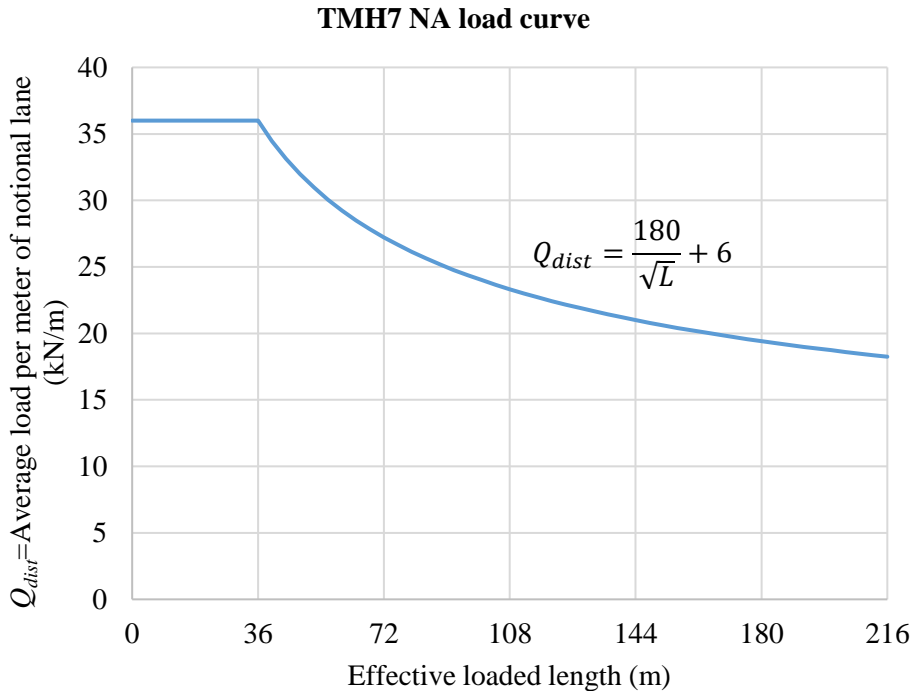


Figure 23 - TMH7 NA loading curve (Committee of State Road Authorities, 1981)

The distributed load, Q_{dist} , can either be applied to the full span lengths contributing to the maximum load effect under consideration as a lower average value or can be applied to partial span lengths at its real higher value, known as partial loading of influence lines. It can occur that shorter loaded lengths at higher intensities cause larger load effects than longer loaded lengths loaded at lower intensities. If entire influence lines are loaded at lower, average intensity, then an additional correction factor should be applied based on the shape of the influence line. This is in accordance with Section 2.A.2.2 of the code and is a function of the shape of the influence line. It is simpler to load the entire span with an average value, but the use of the correction factor is cumbersome for many load scenarios. It is, on the contrary, also difficult to apply the alternative of partial loading of influence lines, as it requires a detailed analysis of the influence surfaces and hence the optimal load patterns as only the parts of influence surfaces which contribute to the maximum LE are loaded. Both options are difficult to implement manually in a grillage model and require the use of sophisticated software for accurate results. Engineers in industry often resort to their own methods to simplify the issue, leading to inconsistent results amongst designers. This adds as motivation to simplify the current model.

The concentrated part of NA loading is known as knife edge loads. The values of these loads decrease with an increase in the number of loaded lanes and are placed at the position of maximum influence for each load effect. The expression for the knife edge load is $144/\sqrt{n}$ (kN) where n is the number of the notional lane under consideration. Only one knife edge load is applied per lane.

NA loading already contains provision for dynamic effects and no further adjustments should be made. Dynamic amplification is included as per the Swiss formula and is dependent on equivalent span length, L_s . It is not clear from the code what is meant by “equivalent span length” and the Swiss formula is unreferenced, but given in the code as

$$DAF = 0.05 \left(\frac{100 + L_s}{10 + L_s} \right) \quad (89)$$

Equation (89) leads to a DAF of 1.35 for a span length of 5 m which reduces linearly to 1.125 for a span length of 50 m.

3.1.2 NB loading

NB loading is a unit loading representing a single abnormally heavy vehicle as shown in Figure 24.

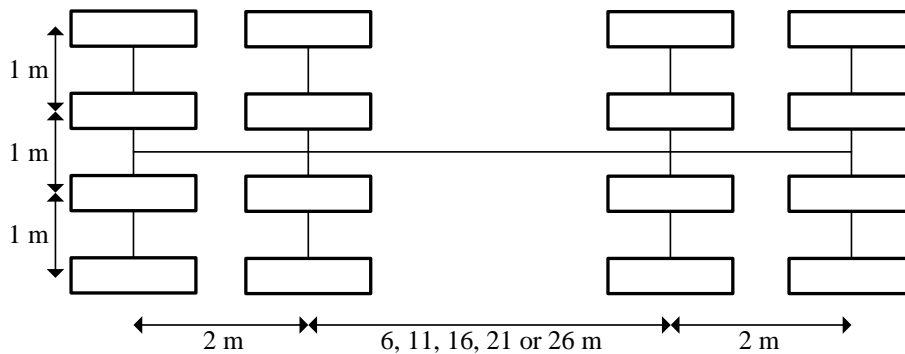


Figure 24 - TMH7 NB loading (Committee of State Road Authorities, 1981)

Only one NB vehicle is allowed on a bridge at a time and usually acts without any other forms of vehicular loading on a bridge. It can occupy any transverse position on a carriageway.

NB loading is typically applied in two magnitudes namely NB24 and NB36, with the number referring to the number of units applied. NB24 has an axle load of 240 kN and NB36 an axle load of 360 kN. The magnitude of NB loading is determined by the class of road and the relevant authority. No allowance is made for dynamic effects.

3.1.3 NC loading

NC is referred to as super loading and at any one time there can only be one of these vehicles on a bridge. An NC vehicle may only travel along the centreline or a maximum of 1 m to either side. It represents multi-wheeled trailer combinations with controlled hydraulic suspension and steering intended to transport very heavy indivisible payloads. The configurations of the NC vehicle is shown in Figure 25.

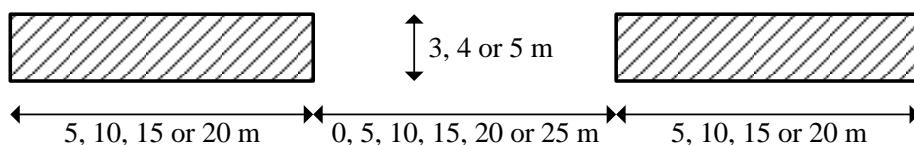


Figure 25 - TMH7 NC loading (Committee of State Road Authorities, 1981)

The loading is uniformly distributed over the area shown with an intensity of 30 kPa. No further allowance for dynamic effects is to be applied. Two thirds of NA loading can act in conjunction with NC loading.

An envelope of NA, NB and NC loading is taken as the critical traffic loading.

3.2 WIM data in South Africa

It is often convenient to examine LEs on bridges by using WIM data. Many countries do not have the luxury of WIM data, but South Africa has in excess of one hundred WIM stations, most of which are well calibrated. These WIM stations are mostly owned by toll concessions which monitor vehicles for overloading.

3.2.1 General recording of WIM data

The ability to measure vehicle characteristics such as GVW and axle loads at speed is known as WIM technology (Miao & Chan, 2002; Quilligan, 2003; O'Connor & O'Brien, 2005; Slavik, 2007; Jacob & Feypell-de La Beaumelle, 2010; O'Brien, O'Connor, *et al.*, 2012; Steenbergen & Morales Napoles, 2012; Leahy, O'Brien & O'Connor, 2015). WIM data enables authorities to collect large amounts of data undetected. This prevents drivers from purposely bypassing the weigh stations (Quilligan, 2003; Sivakumar *et al.*, 2008; Soriano *et al.*, 2016). This is a major benefit over the traditional weigh stations which allowed truck drivers to bypass the weigh stations to avoid overload detection and the accompanying sanctions (Nowak, 1994; Gindy & Nassif, 2007). The bypassing of heavy vehicles causes the frequency distribution of the GVW to be incomplete. To derive a load model for bridge design it is important to capture the heaviest vehicles along with their frequencies. This is captured by continuous WIM measurement.

A distinction is made between High Speed WIM sensors and Low Speed WIM sensors (Quilligan, 2003). Both types of WIM sensors are present in South Africa and each has distinct advantages and disadvantages. High speed WIM systems are more vulnerable to dynamic effects where low speed WIM systems require the drivers to slow down significantly, usually down to 10km/h which gives a permissible error band of 1-5 % (Quilligan, 2003). Other authors (Jacob & Feypell-de La Beaumelle, 2010) report that the operating speeds of low speed WIM sensors are in the range of 5 km/h to 15 km/h with an accuracy of 3 to 5 %. High speed WIM sensors are reported provide a lower accuracy of 10 to 25 % because of dynamic interaction between the road and the trucks (Jacob & Feypell-de La

Beaumelle, 2010). De Wet (2010b) shows that WIM errors in South Africa are generally less than 10 %. The accuracies mentioned here fall within the B(10) accuracy class of COST 323 which are suitable for the development of bridge live load models (Jacob, OBrien & Jehaes, 2002). O'Connor & OBrien (2005) show that an accuracy as low as C(15) does not have an appreciable effect on predicted extreme values. The errors reported here are in comparison with static weigh station values. Calibration is performed to convert the measured dynamic values to static values which can be used in pavement analysis and bridge load models. Several such methods have been developed for South African data (Slavik, 2007; de Wet, 2010a) and are discussed in Section 3.2.4.

3.2.2 WIM in South Africa

Figure 26 below shows the WIM sensors currently installed in South Africa. It is clear that the most sensors are located on the N3 between Durban and Johannesburg and also on the N4 between Maputo and Johannesburg. These are the heaviest freight routes which transport import and export freight between the ports of Richard's Bay, Durban and Maputo to the Gauteng province and back.

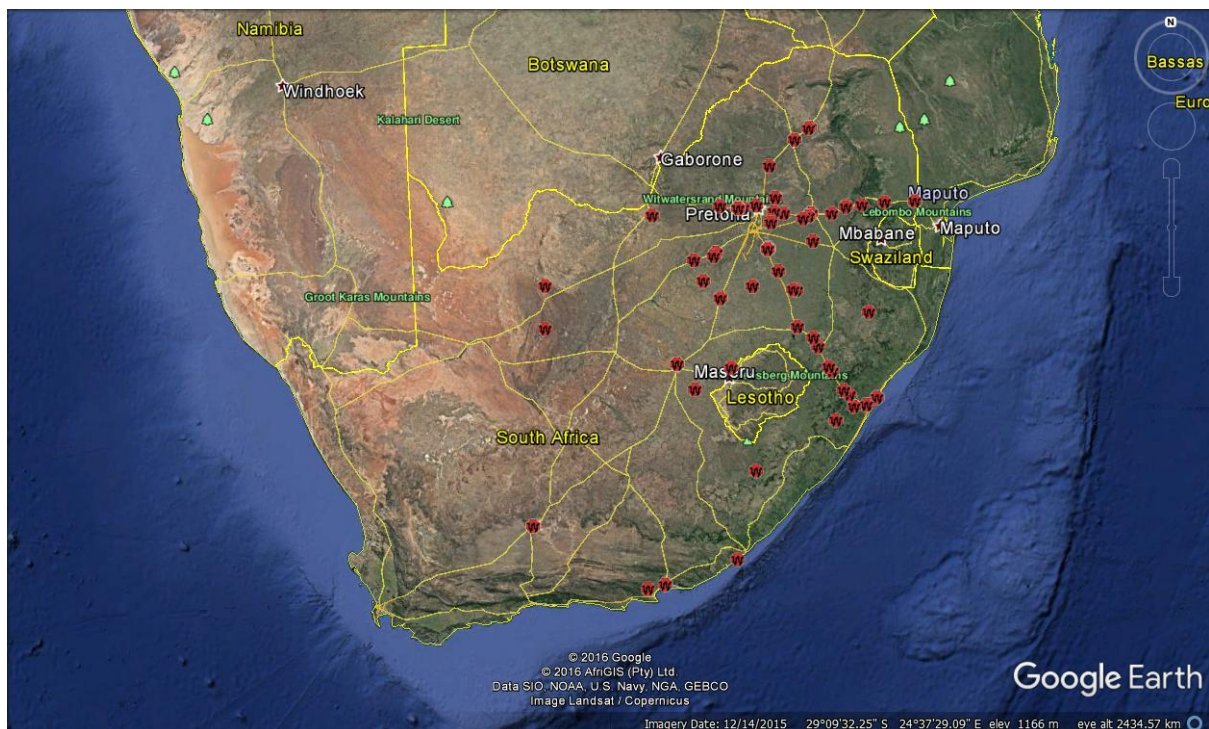


Figure 26 - WIM sensors installed across South Africa

The collection of WIM data in South Africa is governed by three specifications. TMH3 specifies the provision of WIM services (COTO, 2016) whereas TMH8 sets procedures for how traffic and axle load monitoring should be conducted (COTO, 2014). TMH14 specifies the data collection format and output. The format is known as the South African Standard Data Collection Format (COTO, 2013).

In 2007 it was reported that there were 56 permanent WIM stations on national and provincial roads in South Africa (Slavik, 2007). In 2010 it was reported that approximately 100 WIM sensors were installed in South Africa (de Wet, 2010a). Although there are some stations where more than one lane is measured in each direction, the majority of WIMs have a single sensor in the outer lane. This sensor is also only half a lane wide and only collects data from the outer row of wheels of vehicles (Slavik, 2007). Wheel loads are typically multiplied by a factor of 2.0 to determine the axle weights. This is known as Data Record 13 in the South African system and presents some inaccuracies due to the cross fall of roads.

Table 6 - Example of Record Type 13

Record Type	Data	Time	No of axles	Weight 1	Space 1	Weight 2	Space 2	Weight 3	Space 3	Weight 4	Space 4	Weight 5	Space 5	Weight 6	Space 7	Weight 7
13	150101	00011680	7	59	305	66	139	64	566	80	137	83	672	68	137	56

3.2.3 Cleaning of WIM data in South Africa

During WIM measurements, gross errors occur that have to be addressed. This is done by correcting values through calibration and by removing false recordings from the records (Enright & OBrien, 2011).

Although the derivation of the method is undocumented, Slavik developed a technique named Golem to specifically address sources of false recordings for South African data and according to the South African Standard Data Collection Format discussed in Section 3.2.1. Golem's rejection criteria, subsequently used in this work as follows:

- Any vehicle travelling at less than 5 km/h or more than 150 km/h
- Any truck length less than 4 m or greater than 26 m
- Any vehicle with fewer than two axles
- Vehicles with GVW less than 3.5 t
- Any vehicle with an individual axle weighing more than 16 t
- Any vehicle with an axle spacing less than 0.53 m or more than 10 m

3.2.4 Calibrating WIM data in South Africa

Static and dynamic effects are typically treated separately in bridge live load models (Nowak & Hong, 1991). It is typical to apply a DAF to the static loads to account for dynamic effects (Croce *et al.*, 1996; Caprani *et al.*, 2011; OBrien, O'Connor, *et al.*, 2012). WIM systems invariably measure a certain degree of dynamic effects due to vehicle dynamics and road surface irregularities (Ghosn & Moses, 1986; Nowak, 1993; Nowak & Szerszen, 1998, 2000; Slavik, 1998; Sivakumar *et al.*, 2008). These dynamic effects should not be confused with the DAF applied to bridges. This can be observed by comparing the GVW at a static weigh station with the GVW recorded by the WIM sensors (Sivakumar *et al.*, 2008).

To remove the dynamic component, WIM systems are calibrated to remove possible bias due to dynamic effects (OBrien & Enright, 2013).

In South Africa, De Wet and Slavik developed the Truck Tractor (TT) method which provides corrections for the systematic errors in WIM data (de Wet, 2010a,b). Systematic errors refer to the calibration of the WIM data. The application of this method results in a k-factor by which all axle weights are multiplied to suppress the systematic WIM error.

The systematic error causes a shift in the distribution of measured axle loads and the random error enlarges the dispersion of the distribution (Slavik, 1998). It is vital that the errors are addressed before using the data to determine a bridge load model. The TT method uses a sub population of six and seven axle trucks with a single steering axle and a double driving axle, called “eligible trucks.” It was found that the monthly average of TT loads is 21.8 t with a COV of 1.7 %. Measured “eligible trucks” are compared to the 21.8 t weight to calibrate the WIM data. The TT method is used in this study to correct the systematic WIM error.

The method has been accepted by the South African National Roads Agency Limited (SANRAL) and is included in Technical Methods for Highways 3 (TMH3) (Committee of Transport Officials South Africa, 2016).

3.3 Comparison of TMH7 with measured WIM data

The concerns raised in Chapter 1 about the performance of TMH7 live loading are critically evaluated here against measured WIM data. Single lane traffic loads are compared to traffic from a single notional lane by performing these steps:

1. Clean and calibrate the WIM data for all stations
2. Identify the span lengths to be investigated
3. Identify the LEs to be calculated
4. Identify a suitable representative reference WIM station by comparison
5. Decide on a suitable return period for characteristic loads
6. Determine the block size and a suitable probability distribution
7. Extrapolate the measured LEs to the return period
8. Calculate the same load effects and span lengths for TMH7 loading and draw a comparison

A comparison of this nature is necessary to evaluate the current performance of TMH7.

3.3.1 Cleaning and calibrating of data

Cleaning of WIM data to remove invalid readings is done according to the GOLEM criteria described in Section 3.2.3. The calibration of WIM data to remove the systematic error is done according to the TT method described in Section 3.2.4.

3.3.2 Span lengths investigated

Short to medium span lengths between 5 m and 50 m are investigated in this study since they, by inspection, form the majority of highway bridges in South Africa. Moreover these bridges are governed by free flowing traffic (Caprani & OBrien, 2010a). Span lengths within this range cover the majority of bridges in South Africa. For span lengths in excess of this range, the characteristic load effects are caused by congested traffic, rather than free flowing traffic with dynamic amplification. This is explored further in Chapter 6.

3.3.3 Convoys and load effects calculated

By using the time stamps and speeds it is possible to calculate the distance between vehicles and to assemble a convoy of axles for each day by using the date stamps. The distance between the rear axle of the front vehicle and the front axle on the following vehicle is calculated by using time difference and speed. The time stamp resolution from the Roosboom station is 0.01 s which is preferable (Enright, 2010). The increment distance for the convoys is implemented as 0.444 m which corresponds to a time step of 0.02 s at 80 km/h. This increment distance is deemed small enough to capture LEs accurately, especially on shorter bridges where a large increment can lead to a large error in the critical LE. Table 7 and Figure 27 shows an example of how two vehicles are placed in a convoy by using WIM data. The difference in time between the recordings and the speed of the front vehicle is used to calculate inter vehicle spacing between the front wheels of following vehicles.

Table 7 - Example of two following vehicles from a WIM file

	Vehicle 1	Vehicle 2	Units
Date	170101	170101	yymmdd
Time	00:06:38.60	00:12:20.70	hhmmss.ss
Speed	93	68	km/h
No of axles	2	7	[]
Axle 1 Weight	27	48	Tonnes x10
Spacing 1	608	298	cm
Axle 2 Weight	33	52	Tonnes x10
Spacing 2	N/A	137	cm
Axle 3 Weight	N/A	51	Tonnes x10
Spacing 3	N/A	706	cm
Axle 4 Weight	N/A	41	Tonnes x10

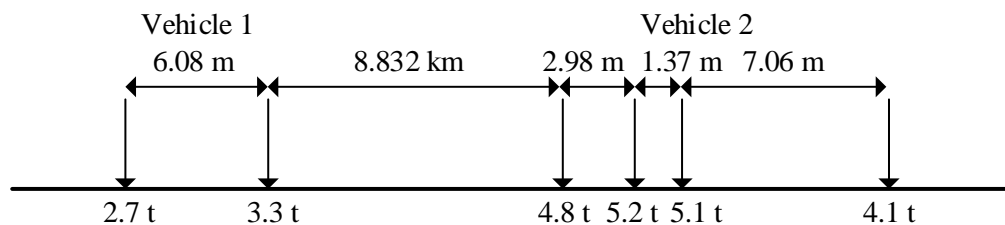


Figure 27 - Spatial arrangement of example WIM vehicles

Simplified studies utilise a single vehicle analysis (Nowak & Hong, 1991; Nowak, 1994; Anderson, 2006), but here continuous convoys of vehicles are passed over varying span lengths for the different load effects while recording the daily maximum values for each load effect and span length. The convoys contain all observed vehicles after cleaning of the data has been performed. This makes it possible to capture load effects resulting from multiple presence of heavy trucks in the same lane travelling at close distance. This provides more accurate results at longer span lengths.

When deriving traffic load models for bridges it is common to investigate hogging moments for two span structures as well as sagging moments and shear forces for single span structures (Caprani, 2005; Enright & OBrien, 2012; Lenner, 2014; Lenner, Keuser & Sykora, 2014). Nowak & Hong (1991) also consider shear on two span structures, but this is considered to be less onerous than for single span structures. Each axle in the convoy is treated individually and LEs from all axles on a bridge simultaneously are added together. The following symbols are used:

M Bending moment

V Shear force

P Point load

R Reaction

x Distance along span

The following sections 3.3.3.1 to 3.3.3.3 formulate the expressions for the hogging moment over the support on a two span structure (Figure 28), the sagging moment at mid span on a single span structure (Figure 29) and also the support shear on single span structures (Figure 30) due to a point load, P , at any point along the spans. These expressions are used in the Java computer program to calculate the LEs for axles at any point along the spans.

3.3.3.1 Two span hogging moment

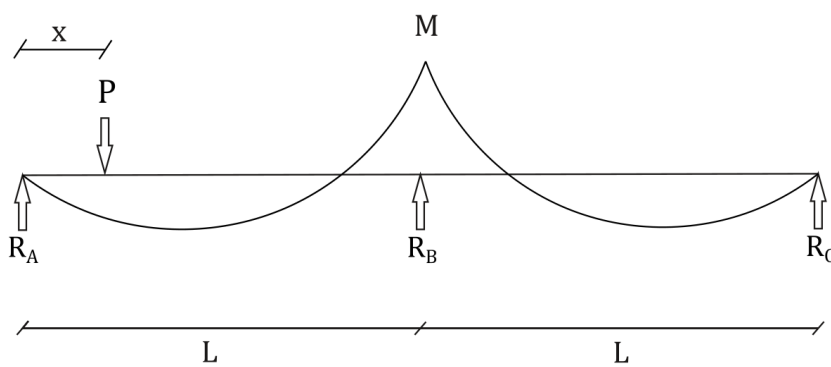


Figure 28 - Hogging moment load effect

$$M = \frac{P(L^2 - x^2)x}{4L^2} \text{ for } 0 < x < L \tag{90}$$

$$M = \frac{P(L^2 - (2L - x)^2)(2L - x)}{4L^2} \text{ for } L < x < 2L \tag{91}$$

3.3.3.2 Single span sagging moment

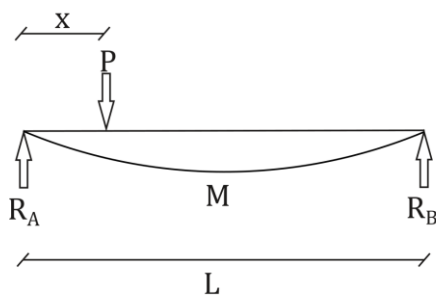


Figure 29 - Sagging moment load effect

$$M = \frac{Px}{2} \text{ for } x \leq \frac{L}{2} \tag{92}$$

$$M = -\frac{Px}{2} + \frac{PL}{2} \text{ for } x > \frac{L}{2} \quad (93)$$

3.3.3.3 Single span shear

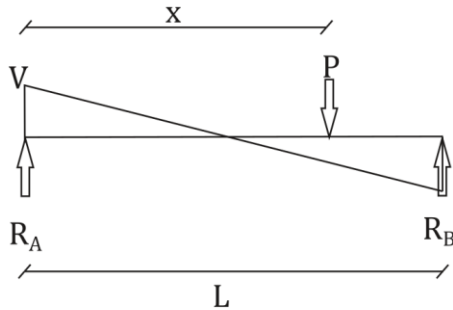


Figure 30 - Shear load effect

$$V = P \left(1 - \frac{x}{L}\right) \quad (94)$$

3.3.4 Identification of a representative WIM station

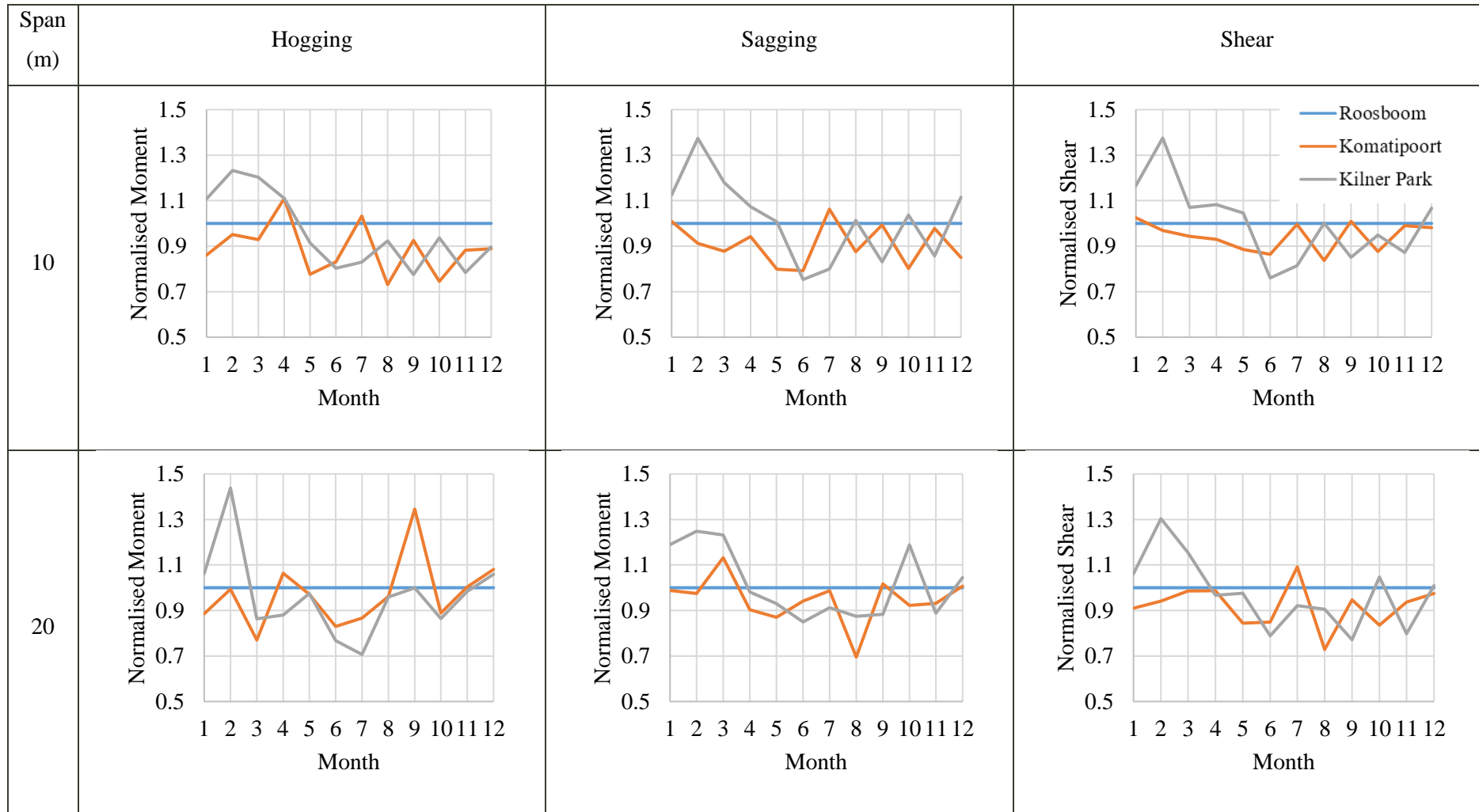
Various studies considered different minimum recording periods which are often limited by the amount of recording data, but at least one year of data is recommended by Sivakumar et al. (2008) for the derivation of load models. The Roosboom WIM station was chosen in previous studies (Lenner *et al.*, 2017) as a representative station for describing load effects and for comparing axle weights and GVWs with LM1 of the Eurocode. At the same time this station is located on National Route 3 (N3) which is considered to be one of the heaviest freight routes in South Africa (Anderson, 2006; Lenner *et al.*, 2017). It is further considered for the long measurement record of seven years from 2010 to 2016 which was made available for this study, measuring 12.5 million vehicles.

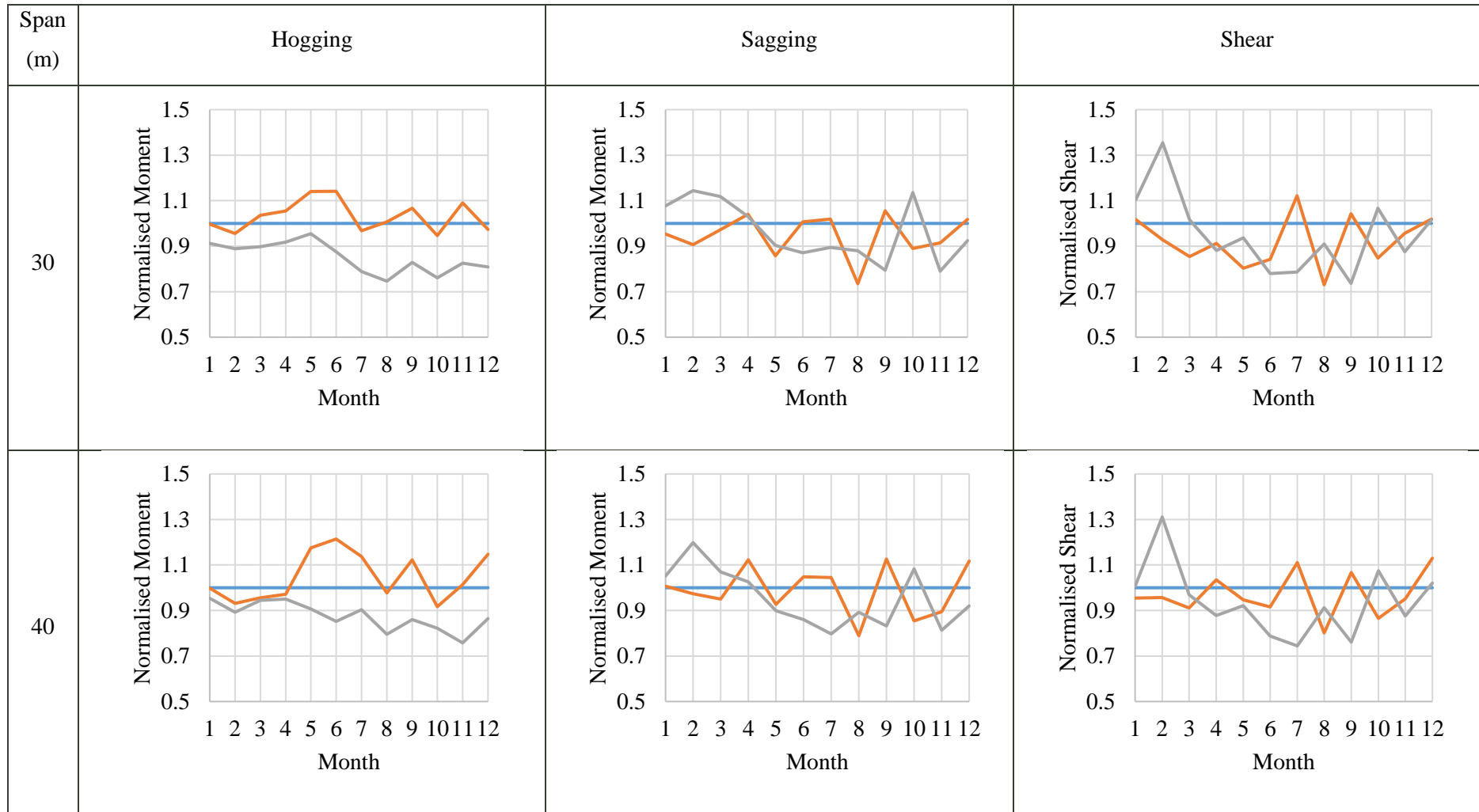
It is difficult to identify a single WIM station that produces the critical LEs over all time periods for all span lengths considered. A possible solution would be to aggregate stations, but combining data from different stations violates the *iid* condition for EV treatment of load effects.

To confirm that Roosboom is indeed one of the heaviest stations a comparison is made with two other stations. The moments and shears for the Roosboom station are compared to the Komatipoort station on the N4 and the Kilner Park station on National Route 1 (N1). The N1 and N4 are the other routes in South Africa that carry large volumes of heavy vehicles and are thereby selected as benchmarking stations. Monthly maxima is chosen here for overall comparison between stations. Figure 31 shows the results of the comparison with all moments and shear forces normalised to the Roosboom station for easier interpretation. The results show large variation of the comparative results across all span lengths and load effects. Generally it is shown that the Kilner Park station experiences lower monthly maximum

values except for the first three months of the annual measurement period. It is not clear why only the first three months, and especially February, produce these unusually large LEs, but a measurement error should not be excluded as a possible explanation. For span lengths of 10 m and 20 m the Roosboom station generally produces larger load effects than the Komatipoort station, but as the span length increases this effect becomes less pronounced. There is no clear indication that the Komatipoort station generally produces larger load effects than Roosboom and it is hence concluded that the Roosboom station is indeed representative of the heaviest traffic. Given the longer measurement record (Komatipoort has only one year of measured data), Roosboom with its seven years of data is the preferred station for further calibration in this study.

In the derivation of LM1 in the Eurocode, the length of the measurement period also played a deciding role in the choice of the Auxerre station in France, although the axle weights measured at Auxerre were lower than at other stations (Sedlacek *et al.*, 2008).





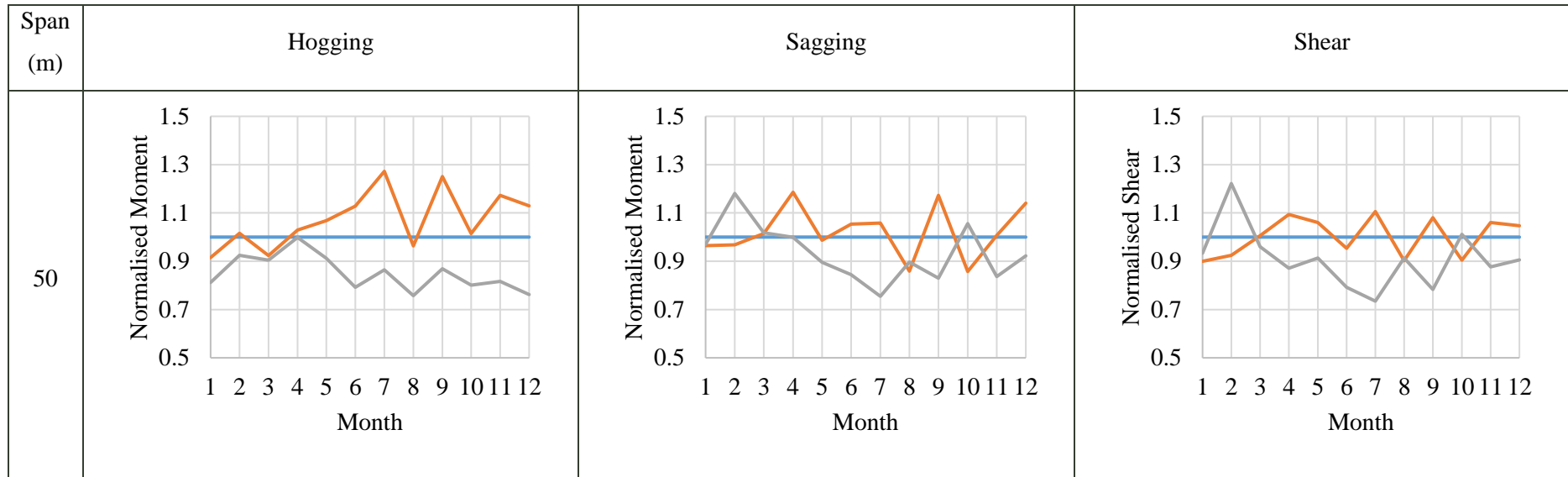


Figure 31 - Measuring station comparison normalised to Roosboom

3.3.5 Traffic composition at the Roosboom station

The number of recorded vehicles at Roosboom in the seven years of data is 12 511 698. Figure 32 shows the distribution GVW of vehicle types indicating that seven axle vehicles comprise the GVW tail. This is in contrast to Europe where five axle vehicles dominate the GVW tail. The tail for seven axle vehicles is shown in more detail in Figure 33.

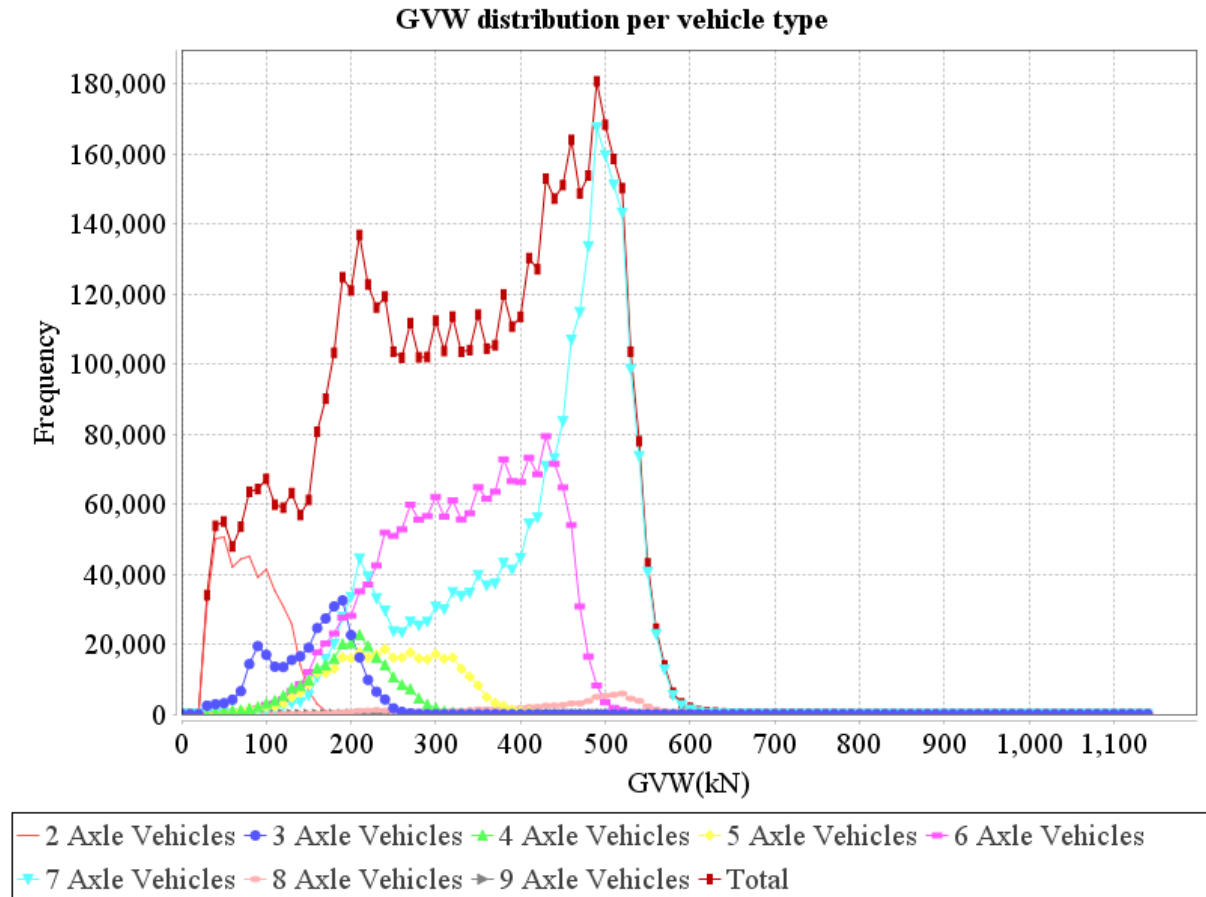


Figure 32 - Vehicle type distribution

Figure 33 zooms in on this by showing the PDFs and CDFs of the GVW for seven, eight and nine axle vehicles. GMM, described in Section 2.1.1.6, is used to separate the modes of the empty and the fully laden vehicles. For nine axle vehicles it is not possible to identify two modes, which indicates that these vehicles rarely operate unloaded. By observing the quantiles of the CDFs it can be said that

- 11 % of fully laden 7 axle vehicles exceed the legal limit
- 20 % of fully laden 8 axle vehicles exceed the legal limit
- 56 % of 9 axle vehicles exceed the legal limit

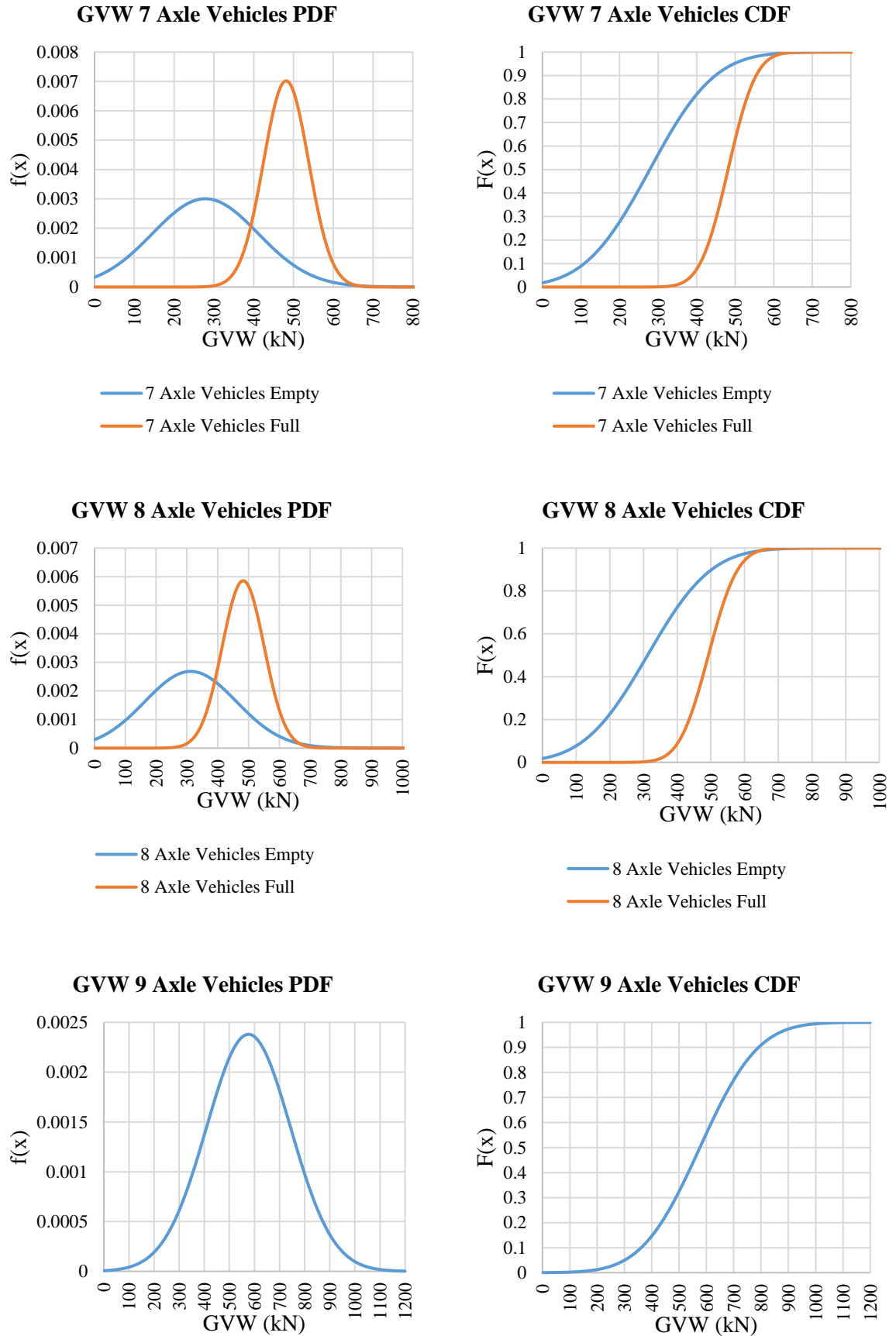


Figure 33 - GVW PDFs and CDFs

It is currently not clear whether the vehicles exceeding the legal limits are illegally overloaded vehicles or permit vehicles. OBrien *et al.* (2010) examine permit truck loading on bridges but assume that all extremely heavy trucks have permits, without differentiating between illegally overloaded standard trucks and permit trucks. A National Cooperative Highway Research Program (NCHRP) report which examines the use of US WIM data for bridge design (Sivakumar *et al.*, 2008), concludes that an approach which states that permit vehicles are all vehicles above a state's limit is best. Using the legal weight limits for South Africa would classify most heavy vehicles as permit vehicles due to the amount of illegal overloading. Since it is not possible to filter permit vehicles from the records, all vehicles are therefore included in the derivation of the proposed load model with no distinction between normal and permit vehicles. This necessarily implies that the load model is heavier compared to a model for normal traffic only with a separate model for abnormal vehicles. It does, however, cater for the population of vehicles that are actually on the roads.

Figure 34 and Figure 35 compare 1986 Auxerre data used for the development of LM1 in Eurocode with a year of WIM data from the N3 Roosboom station. In these figures, n_{30} is the number of vehicles with GVW above 30 kN and n_{10} represents the number of axle loads above 10 kN. The results show that measured South African vehicles, which typically have more axles, correlates with larger GVW and lower axle loads. This can be explained partially by a lower GVW limit in Europe, typically 40 t to 44 t, as opposed to 56 t prescribed in the National Road Traffic Act 93 of 1996 for South Africa. However, Lenner *et al.* (2017) concluded that it is not advisable to adopt LM1 as is due to the substantially different traffic characteristics such as frequency distribution of GVW and number of axles of individual vehicles. Seven axle vehicles in South Africa fulfil the role of the predominant five axle vehicles in Europe.

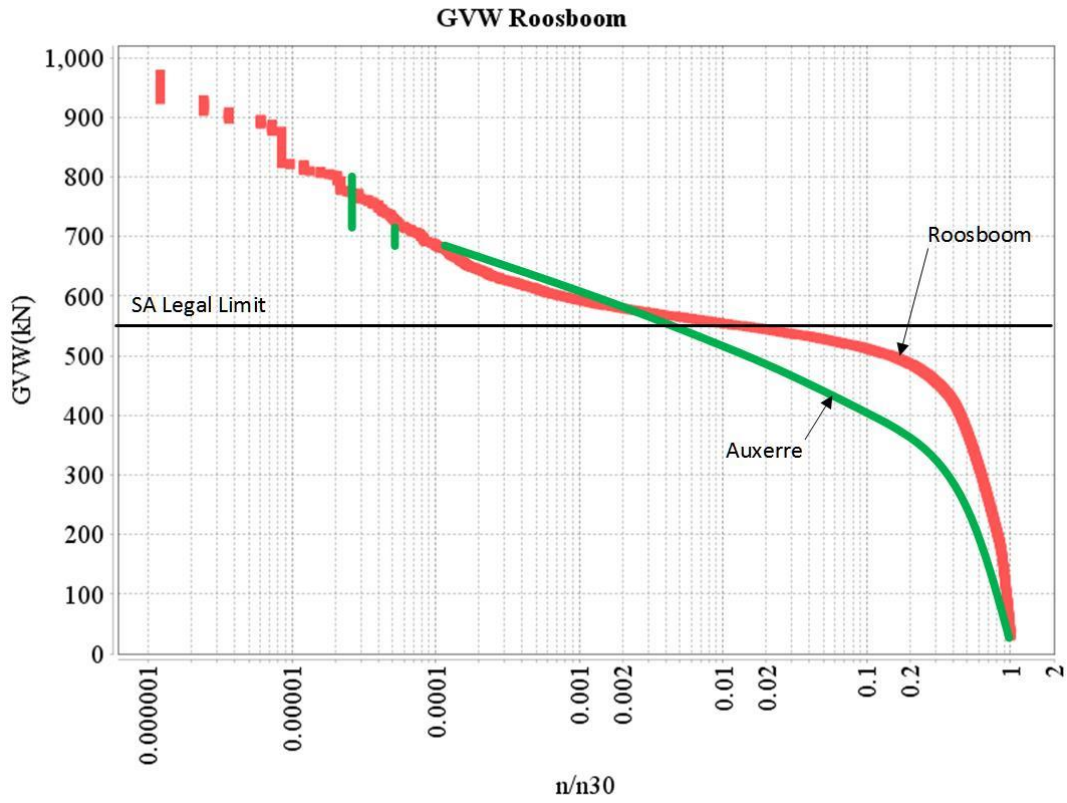


Figure 34 - GVW cumulative distribution

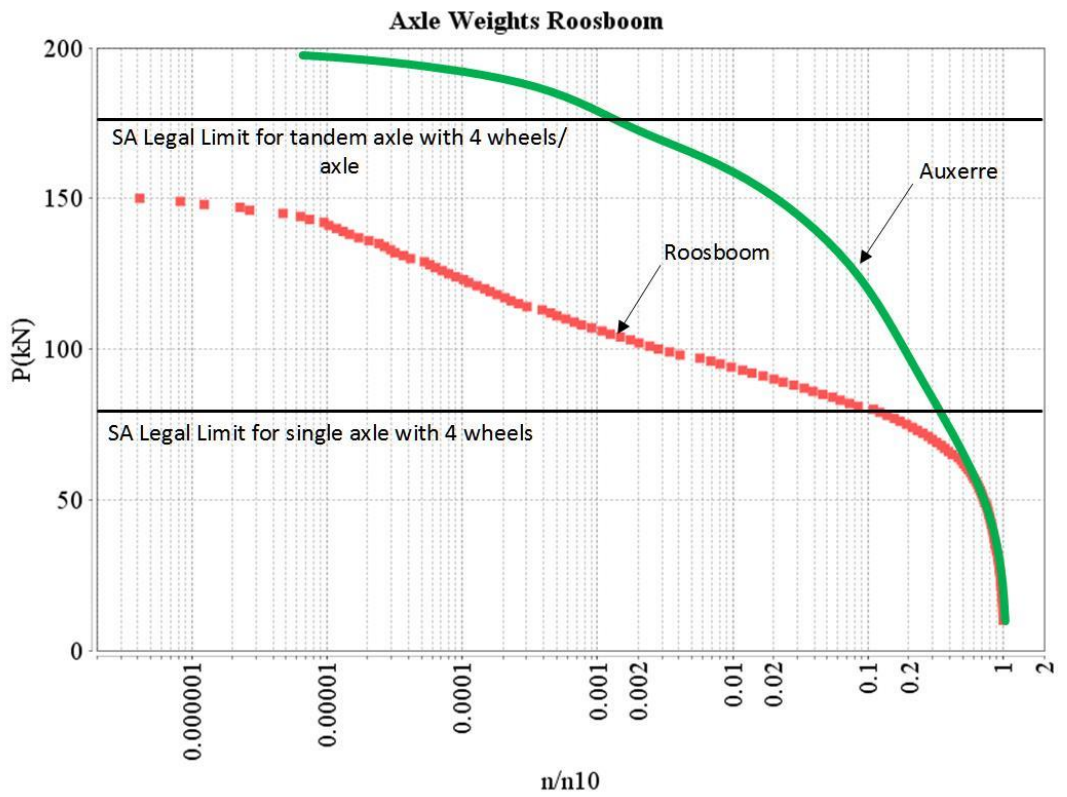


Figure 35 - Axle weight cumulative distribution

From Figure 34 it is important to again note the large amount of vehicles that exceed the legal limit of 56 t (or 550 kN) which further reinforces the notion of a single model for both normal and overloaded traffic.

3.3.6 Return period

TMH7 does not specify a return period nor a probability of exceedance. A 5 % probability of exceedance ($p = 0.05$ fractile) in a 50 year reference period or design working life is used in this study for characteristic values (Holicky, 2009), similar to EN1990. This is also the approach which is adopted in the South African building design codes (SABS, 2011). This return period is essential for characteristic values, but not at ULS or SLS which are functions of PFs and therefore of target reliability. Section 2.1.1.7 provides the methodology to calculate the return period. From Equation (59), the characteristic return period, R , is determined as

$$R = \frac{1}{1 - (1 - 0.05)^{\frac{1}{50}}}$$

$$= 975 \text{ years}$$

3.3.7 Extrapolation to return period for static free flow loads

Before extrapolation can commence, a probability distribution must be identified which fits the dataset most accurately. The Gaussian distribution was used in the original derivation of the AASHTO code (Nowak, 1993) and the Eurocode (Sedlacek *et al.*, 2008). Modern approaches tend to favour EV and studies have indicated that the tail of traffic load effects are best suited to the Weibull distribution (Bailey, 1996; Caprani *et al.*, 2003; OBrien, O'Connor, *et al.*, 2012; OBrien *et al.*, 2015). These studies assume that traffic load effects are *iid*. Additionally, the Weibull distribution is bounded per definition and it is therefore well suited to traffic loads which are a physical process and should in theory therefore have an upper limit (OBrien *et al.*, 2015). These assumptions are tested in this section for South African traffic data.

3.3.7.1 Distribution type

The data at hand determines the distribution type. As EV theory is preferred in this work, a GEV distribution is fitted to the tail of daily maxima load effects. In accordance with Section 2.1.1.4 the shape factor of the GEV distribution is negative for a Weibull distribution, zero for a Gumbel distribution and positive for a Frechet distribution if the parametrisation of Equation (46) is followed. It has already been argued that traffic load effects follow a Weibull distribution and it is expected that the shape factors for various span lengths and load effects will be negative. This implies a GEV distribution with a finite upper bound.

As the tail of the daily maxima is isolated as being *iid* and contains the critical LEs, a censored GEV distribution must be fitted to the *iid* tail, as opposed to an uncensored GEV distribution to the full sample which may in fact not be *iid*. All values to the left of the tail are censored, leading to left censoring. The censored fitting of the GEV distribution is a state-of-the-art approach to fitting to the tail of LE data. MLE, described for the Gumbel distribution in Section 2.1.1.4, maximises the log-likelihood function of a given distribution, or minimises the negative log-likelihood function to estimate distribution parameters. As all values left of the tail are censored, the likelihood function is adjusted from the standard GEV likelihood function. The tail length assumption of $2\sqrt{n}$ is confirmed in Section 3.3.7.2.

The log-likelihood function for the censored GEV is given by Phien & Fang (1989) in Equation (95).

$$L = \ln(N!) - \ln(k!) - \ln(m!) + m \times \ln(F(x_L)) + \sum_{i=1}^{2\sqrt{n}} \ln(f(x_i)) + k \times \ln(1 - F(x_R)) \quad (95)$$

where

- N the number of points in the full sample before censoring
- k the number of points censored above the tail, zero in this case
- m the number of points censored below the tail, $n - 2\sqrt{n}$ in this case
- x_L value below which left-censoring is applied, in this case the lowest observation in the tail
- x_R value above which right-censoring is applied, infinity in this case
- $f(x)$ PDF of the standard GEV distribution
- $F(x)$ CDF of the standard GEV distribution

By differentiating ($-L$) with respect to its partial derivatives and setting to zero, the location, scale and shape parameters of the censored GEV distribution are obtained.

Figure 36 shows a histogram of the daily maxima sagging moments on a 30 m span length with the $2\sqrt{n}$ tail indicated. A censored GEV is fitted to the tail only and indicated on the figure, indicating a visually good fit to the measured data. For the same case, Figure 41 indicates a quantile plot where the fitted distribution quantiles and the measured values show good straight line adherence, indicating a good fit. The shape parameter from the MLE results in $\xi = -0.06$ which, as expected, indicates an underlying Weibull distribution. An uncensored GEV fit is also shown for comparison which shows a particularly poor visual fit to the tail.

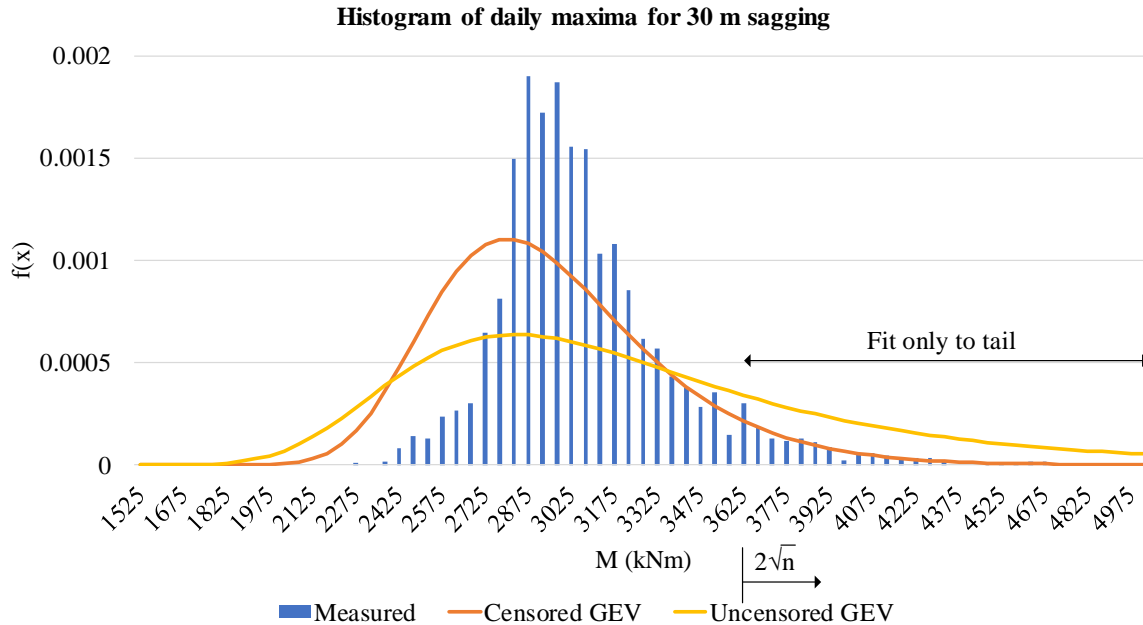


Figure 36 - Histogram of daily maxima on a 30 m span length

For hogging on span lengths of 25 m and above, the censored GEV distribution is no longer an appropriate fit to the daily maxima and indicates a shape factor $\xi > 0$. This implies that the underlying distribution would be Frechet and therefore unbounded, resulting in very large quantiles which are difficult to accept given the physical bounded nature of traffic loading. For hogging, the structure has two spans and thus twice the length over which convoys of vehicles are considered. This opens up the possibility that the maximum load effects are caused by more than one vehicle on a bridge simultaneously. These vehicles are not necessarily identically distributed and EV theory is not strictly applicable in these cases, hence the positive shape factor. For South Africa, with a large amount of illegally overloaded vehicles, it is not possible to identify and separate these populations sensibly. If it were possible to identify distinct populations that are *iid*, then composite distribution statistics (CDS), developed by Caprani (2005), is a solution which could be used to treat these events probabilistically. Lenner (2014) shows that the maximum load effects on longer span structures are dominated by the selfweight and are less sensitive to the traffic load. An unbounded Frechet tail is not allowed as it has been argued that traffic load effects are bounded in nature and all other load effects and span lengths indicate underlying Weibull distributions, shown in Section 3.3.8. For these ‘Frechet’ cases the shape factor is limited to $\xi = 0$ which implies a Gumbel distribution. Further to this, Chapter 4 shows that the load model itself is conservative for these cases as it is calibrated on shorter spans which are more critical.

3.3.7.2 Block maxima block size and tail length

The *iid* condition for the application of EV theory is discussed in Section 2.1.1.4. One approach is to fit EV distributions to maxima data within a certain time period, called the block size (Zhou, 2013). To ensure that data is independent it is essential to choose the block size such that successive blocks do not influence each other. The smallest block size is chosen so that the least amount of maxima is discarded. Figure 37, Figure 38, Figure 39 and Figure 40 show the monthly, weekly, daily and secondly maxima for seven years of the Roosboom station (2010 – 2016) respectively. The annual, monthly, weekly and daily maxima show no clear trends, indicating that any arbitrary block size would suffice. The secondly maxima show a clear trend between days with the load effects reducing during night time to indicate clear daily blocks. Autocorrelation is used to determine if a time series is dependent on its past and it is used to confirm trends in data and confirm these findings numerically. Annual, monthly, weekly and daily maxima produce autocorrelation coefficients between 0.25, 0.2, 0.1 and 0.2 respectively which are weak. A strong positive autocorrelation has a coefficient of 1.0 where a strong negative correlation has a coefficient of -1.0 which would indicate appreciable trends in data.

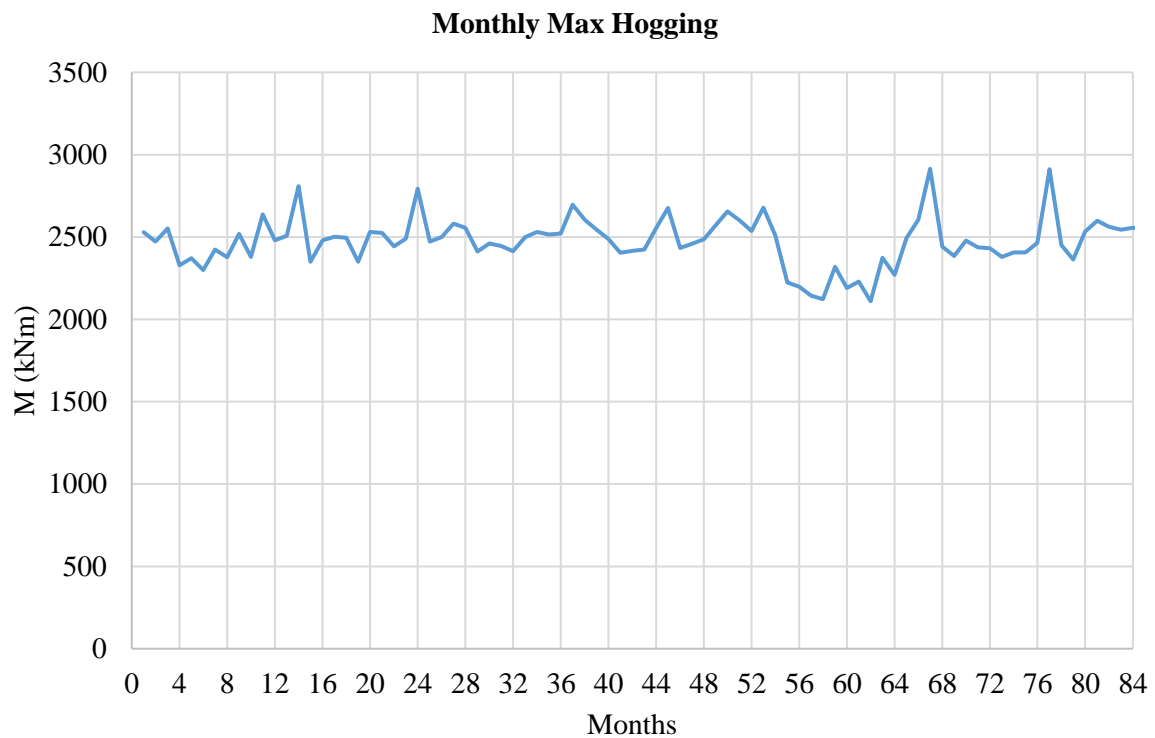


Figure 37 - Monthly maxima for 30 m hogging

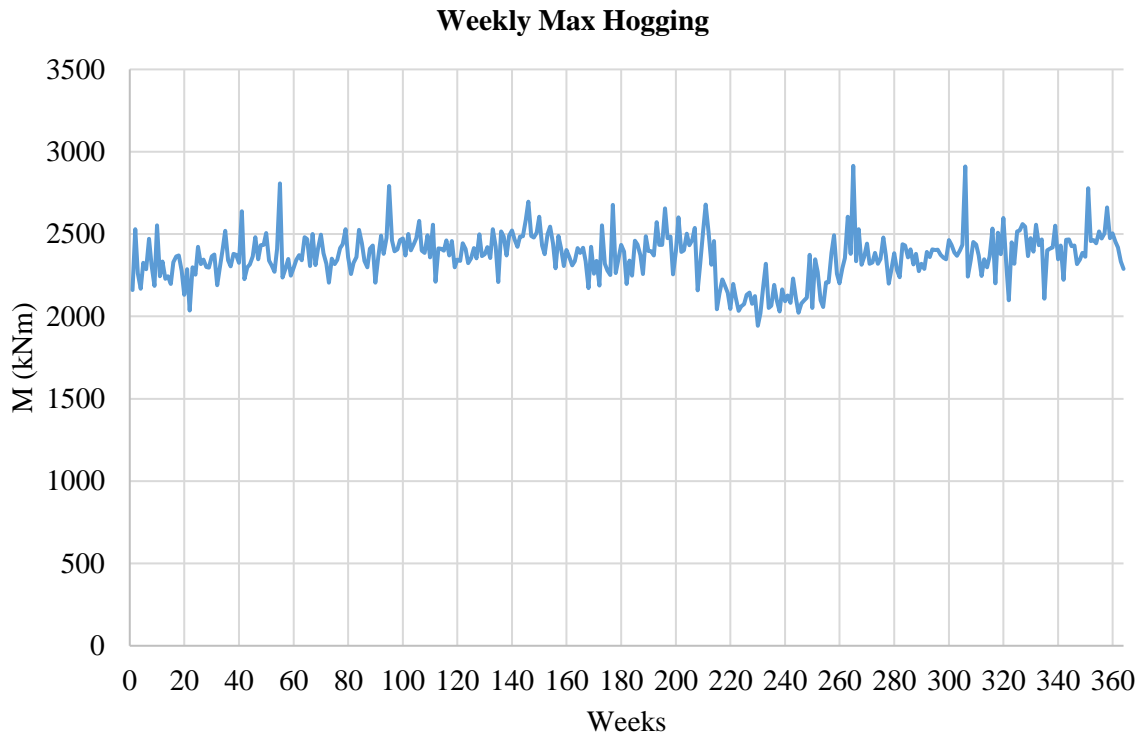


Figure 38 - Weekly maxima for 30 m hogging

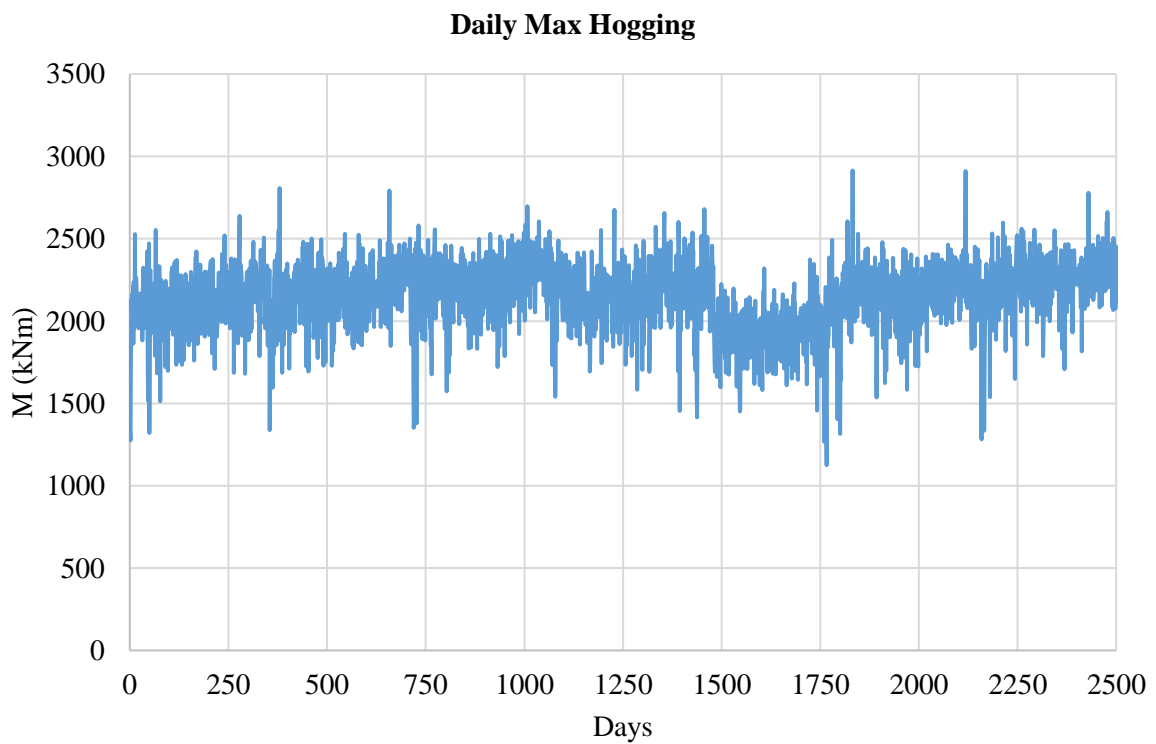


Figure 39 - Daily maxima for 30 m hogging

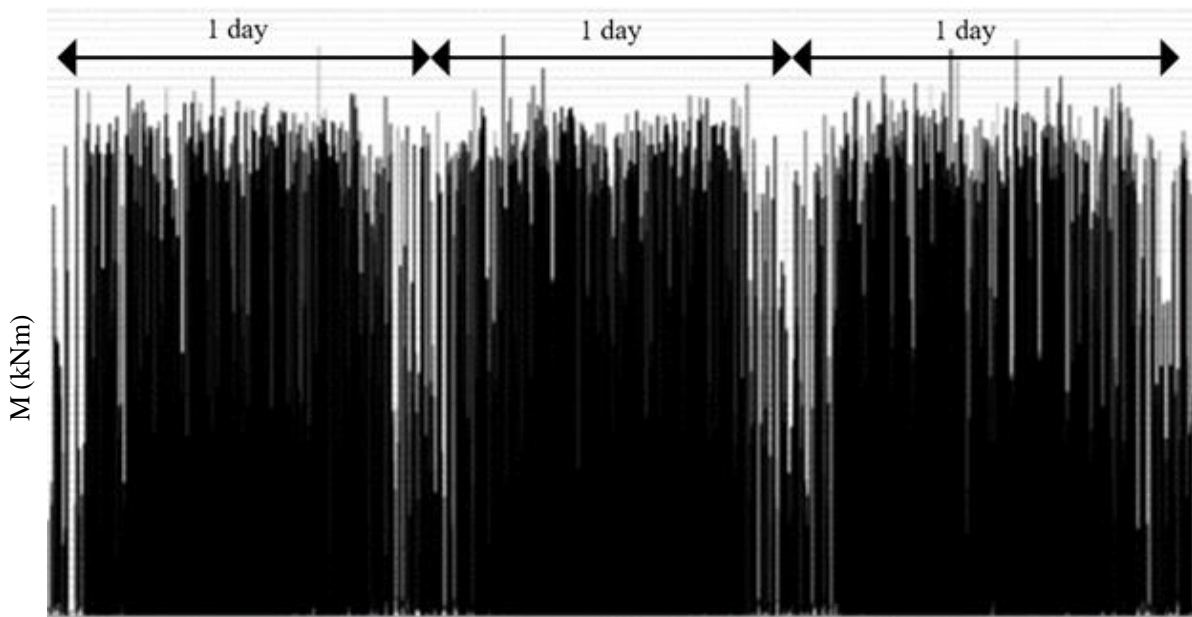


Figure 40 - Secondly maxima for 30 m hogging

To ensure that data is identically distributed it is essential that populations that are indifferently distributed in the data are separated, or that the critical population is isolated so that the data can be considered *iid*. Traffic load effects are by nature not *iid* as they are made up of load effects from different types of vehicles, which are not identically distributed. In accordance with Section 2.1.1.8, Castillo argues that by taking the upper $2\sqrt{n}$ of maxima, with n the number of maxima, isolates the tail sufficiently to ensure that all populations that are not critical are disregarded and that the tail can be considered to be identically distributed. This has become standard practice in the derivation of bridge live load models. Figure 41 shows a quantile plot for sagging on a 30 m span length where the upper $2\sqrt{n}$ of daily maxima is fitted to a censored GEV distribution. The figure shows that the points adhere well to a straight line and hence that the load effects are comprised of a sample which is identically distributed.

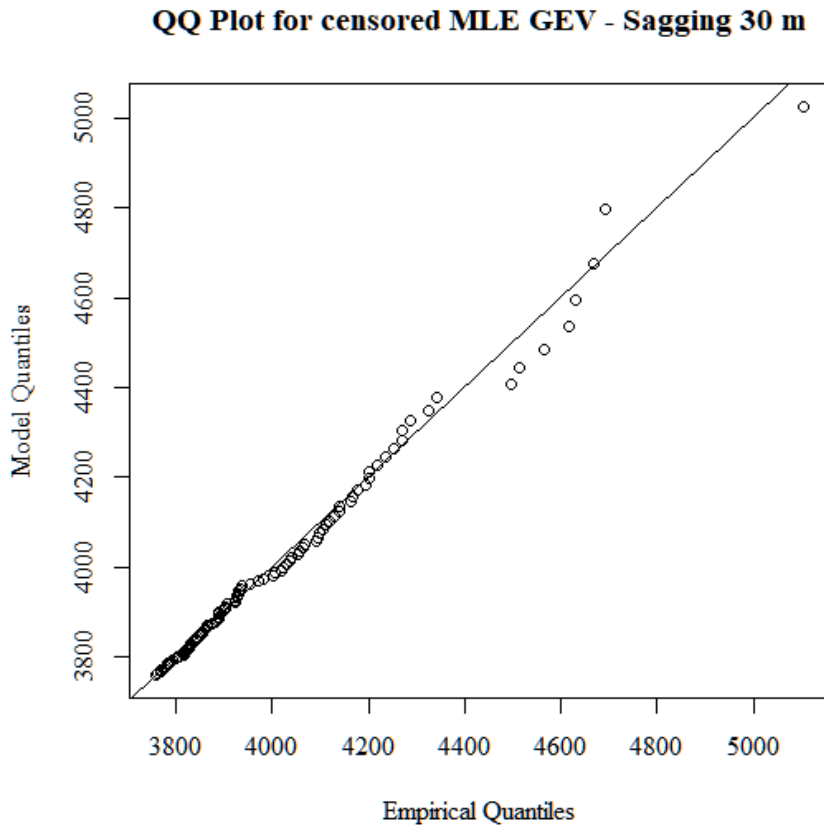


Figure 41 - Quantile plot for sagging on a 30 m span (Weibull)

It is therefore concluded that, through the use of daily maxima, and by considering the upper $2\sqrt{n}$ of daily maxima, the load effects can be considered to be *iid* and therefore amenable to EV theory. The distribution type is discussed in the next section.

3.3.8 Characteristic values for all span lengths and load effects

In South Africa heavy vehicles are allowed to travel on weekends and holidays for the total of 365 days a year. The specified characteristic return period of 975.3 years corresponds to a daily probability of non-exceedance, p , where

$$p = 1 - \frac{1}{975 \times 365} \quad (96)$$

The characteristic value (or quantile, Q) corresponding to a probability, p , for each load effect and span length for a GEV distribution, is calculated by Equation (97). The parameters are defined in Section 2.1.1.4.

$$Q(p; \mu, \sigma, \xi) = \begin{cases} \mu + \frac{\sigma((- \ln(p))^{-\xi} - 1)}{\xi} & \text{for } \xi \neq 0 \\ \mu - \sigma \ln(- \ln(p)) & \text{for } \xi = 0 \end{cases} \quad (97)$$

A summary of the characteristic load effects for bending moments and shear at various span lengths is provided in Table 8 for the censored GEV distribution for the Roosboom station. Cells shaded in grey are the cases discussed in Section 3.3.7.1 where quantiles are limited to the Gumbel distribution.

Table 8 – Roosboom characteristic load effects

Span Length (m)	Hogging (kNm)	Sagging (kNm)	Shear (kN)
5	250	401	336
10	841	1269	485
15	1779	2034	566
20	2490	3315	722
25	3160	4729	819
30	3178	6121	890
35	3907	7808	976
40	4547	9461	1045
45	5557	11459	1130
50	6749	13061	1151

Table 9 shows the upper bound of the censored GEV distributions with a negative shape parameter. The cases where distributions are limited to the Gumbel distribution do not have a finite upper bound and are indicated as infinity. For a 5 m span length the characteristic quantiles from Table 8 are close to the upper bound. For all other span lengths and load effects the quantiles are located away from the bound. The load effects on shorter spans are governed by axle loads rather than UDLs. It is further shown in Chapter 4 when the developed load model is discussed that the characteristic axle weight is located at the bound of the censored GEV distribution which explains why the load effects for shorter span bridges are located close to the upper bound. Longer spans are governed by UDLs which are to a large extent influenced by the GVW. Figure 32 and Figure 33 show that the GVW is in fact not truly bounded, which explains why the load effects on longer span bridges are further away from the bounds of the fitted GEV distributions.

Table 9 - Distribution bounds for censored GEV

Span Length (m)	Hogging (kNm)	Sagging (kNm)	Shear (kN)
5	262	460	339
10	1346	1518	497
15	2277	2214	604
20	3278	5378	920
25	∞	∞	993
30	∞	∞	1064
35	∞	39613	1285
40	∞	28213	1500
45	∞	48198	2445
50	∞	42583	2129

Table 10 provides the characteristic load effects as calculated for NA loading, with dynamic effects removed for comparison with the calibrated characteristic load effects from the WIM measurements. As only single lane loading is considered at this stage, NB and NC loading are not compared to measured values as they will not occur on a single design lane scenario.

Table 10 - Load effects for static NA loading

Span Length (m)	Hogging (kNm)	Sagging (kNm)	Shear (kN)
5	125	217	173
10	441	635	254
15	959	1262	337
20	1702	2100	420
25	2437	3150	504
30	3275	4413	588
35	4203	5889	673
40	5230	7913	791
45	6324	9508	845
50	7521	11212	897

Figure 42, a visual presentation of Table 8 and Table 10, shows a comparison between the characteristic load effects from the Roosboom station with characteristic load effects obtained from static NA loading. The load effects have been normalised to NA loading for easier interpretation.

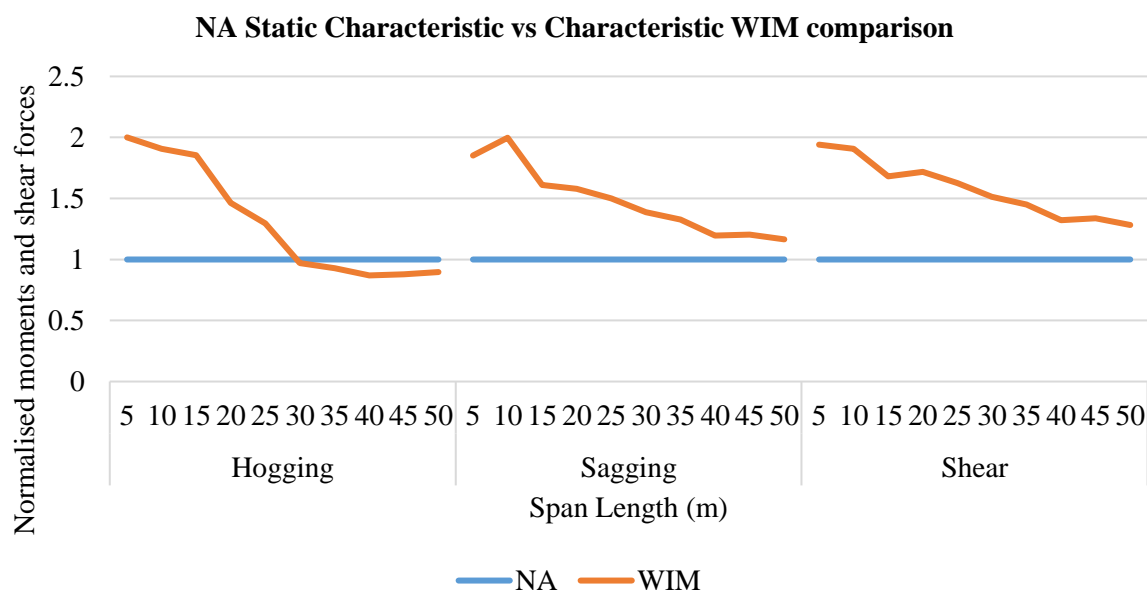


Figure 42 – NA static vs Characteristic WIM load effects

The following observations are made:

- The measured load effects exceed static NA loading for all load effects and span lengths, except for hogging on span lengths of 30 m and longer
- The exceedance is most pronounced in shorter spans where the measured load effects are up to twice those predicted by NA loading

This confirms the findings of previous authors, discussed in Chapter 1, that there are deficiencies in TMH7 NA loading at characteristic level. However, these results show that the situation may be more onerous than previously thought. This study is done almost 30 years after the previous studies and it is plausible that the traffic volumes, size and weight of the vehicles on South African roads have increased since then, leading to the more onerous results. This is supported by findings of Bosman (2004) and the deregulation of the South African road freight industry in the 1980's. This is further substantiated if one considers the poor state of the freight rail system in South Africa, leading to 70 % of cargo being transported by road. It is further not clear what level of safety was assumed in the derivation of TMH7 and it is possible that the 5 % probability of exceedance in 50 years used in this study for characteristic values has a lower probability of failure than that used for TMH7, and hence larger load effects. A full reliability based comparison is performed in Chapter 7.

At the same time, it must be highlighted that this is a comparison between an actual traffic lane and a notional lane in TMH7 which over exaggerates the ratio in the comparison, especially for shorter spans. TMH7 employs a variable width notional lane model and for narrow bridges it often occurs that a bridge which can realistically only accommodate two lanes of traffic is designed for three notional lanes. This

can, in part, explain why TMH7 is still performing reasonably well (Basson & Lenner, 2019). It is worth noting that the study by Basson & Lenner (2019) show that the smallest reliability is found for short spans.

In the next chapter a new static load model is derived which replicates the measured load effects from the Roosboom station.

4 Development of a static load model

In modern codes it is typical to develop a load model for the slow lane, and to extend this load model to other lanes using multiple presence factors. The previous chapter shows a clear motivation for updating of the South African load model, therefore this chapter aims at developing a load model for the slow lane based on the identified reference WIM station.

The content of this chapter has been published in *Structural Engineering International Volume 29 (2): 292-298* under the title *Towards a New Bridge Live Load Model for South Africa* (Van der Spuy & Lenner, 2019) and published and presented at *IABMAS 2018* under the title *Developing a new bridge live load model for South Africa* (Van der Spuy & Lenner, 2018).

4.1 Notional lane width

As the notion of a slow lane based load model is adopted here it is necessary to investigate the appropriate lane width.

Notional lanes are the parts of carriageways used only for the purpose of applying design loading and are not related to the actual road markings. The current TMH7 model makes provision for a variable notional lane width of between 2.4 m and 3.7 m. This is unrealistic as the width of the critical seven axle vehicles in South Africa is 2.917 m, shown in Figure 43. Using a narrow notional lane width such as 2.4 m can lead to more design lanes than actual traffic lanes, leading to unnecessarily conservative results. Using a notional lane width that is too wide can lead to fewer design lanes than actual traffic lanes, leading to an unsafe design. Another complexity of using a notional lane width that is too wide is that the loading has to be shifted laterally within a lane to create the most onerous LEs in critical elements. This is difficult to implement by hand and software is needed for accurate results.

It is proposed to accept a fixed notional lane width for the new load model. A 3 m notional lane width for South Africa is further motivated by Oosthuizen *et al.* (1991). The reasons being similar to those described above, but in addition that 2.4 m was less than the 2.6 m vehicle width limit in 1991 and that 3.7 m is excessive in traffic jam situations. It is therefore proposed to adopt a fixed notional lane width of 3 m and to fix the transverse wheel spacing to 2 m with no lateral movement within lanes. A notional lane width of 3 m further allows design lanes to be compared to actual traffic lanes.

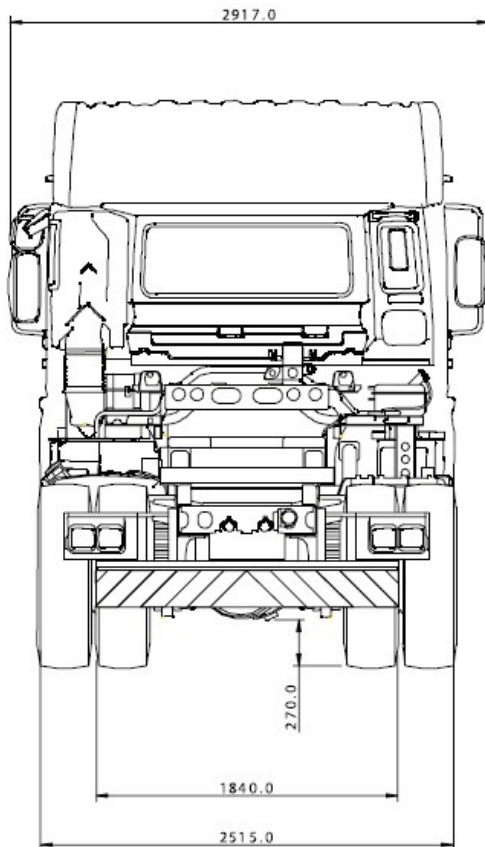


Figure 43 - Typical 7 axle truck width (UD Trucks South West Africa)

EN1991-2 (CEN, 2003) and AASHTO (AASHTO, 2007) both specify fixed lane widths of 3 m and 3.6 m respectively. It is only for deck widths between 5.4 m and 6 m for EN1991-2 and 6 m and 7.2 m for AASHTO where two notional lanes are specified which are narrower than the standard notional lane.

4.2 Methodology

This section performs the steps that are needed to derive a characteristic traffic load model for the reference lane, which is the lane with the heaviest, and usually the slowest traffic. First, the load model format is discussed after which the corresponding characteristic axle loads and UDLs are derived for all span lengths and load effects.

4.2.1 Choice of load model format

It became apparent that the standard load train from Figure 9 required substantial computational effort at the time to apply and that it was fairly inflexible with its defined axle spacings. With the introduction of the MOT load curve, the standard vehicle was replaced by a UDL and an axle load. This concept filtered through to other country's codes and is still standard practice today (Dawe, 2003). This is further clear from observing load models in different national norms in Section 2.4

A major benefit of using axle loads with UDLs is that it is easy to apply to a structure. It also means that the model is fairly flexible as it can accommodate a range of different vehicles and combination of vehicles. Moreover the use of UDLs do not model the effects of wheel loads and shear on short spans well, where axle loads are better suited. For longer span bridges, axle loads are less important and the UDL becomes much more critical for bending.

It is proposed to accept the concept of point loads corresponding to the axle loads along with an UDL, which is constant for the entire length of a loaded lane. This effectively removes the unpleasant concept of variable uniform load intensity according to the aggregate loaded lane length in TMH7 and addresses the concerns of practicing engineers described in Chapter 1.

4.2.2 Characteristic axle load

As it is accepted that a load model consists of distributed and axle loads, it is necessary to determine the axle load component for the new model. Daily maximum axle weights are fitted to a censored GEV distribution with MLE and evaluated at the characteristic 975 year return period. Figure 44 shows a quantile plot of the axle weights (in kN) fitted to a censored GEV distribution. There is good straight line adherence, indicating a good fit to the chosen distribution type. Groupings of measurements are due to the whole number measurement accuracy. The shape factor of the fitted distribution is $\xi = -0.418$ which is distinctly Weibull. This leads to a characteristic axle load of 158 kN which is essentially the upper bound of the distribution. The characteristic value is therefore at the bound and no uncertainty in the axle weight is expected when performing a reliability analysis. This result correlates well with the legal axle weight limit of 16 t and shows that, even though the GVW legal limit is regularly exceeded, the individual axles are not overloaded.

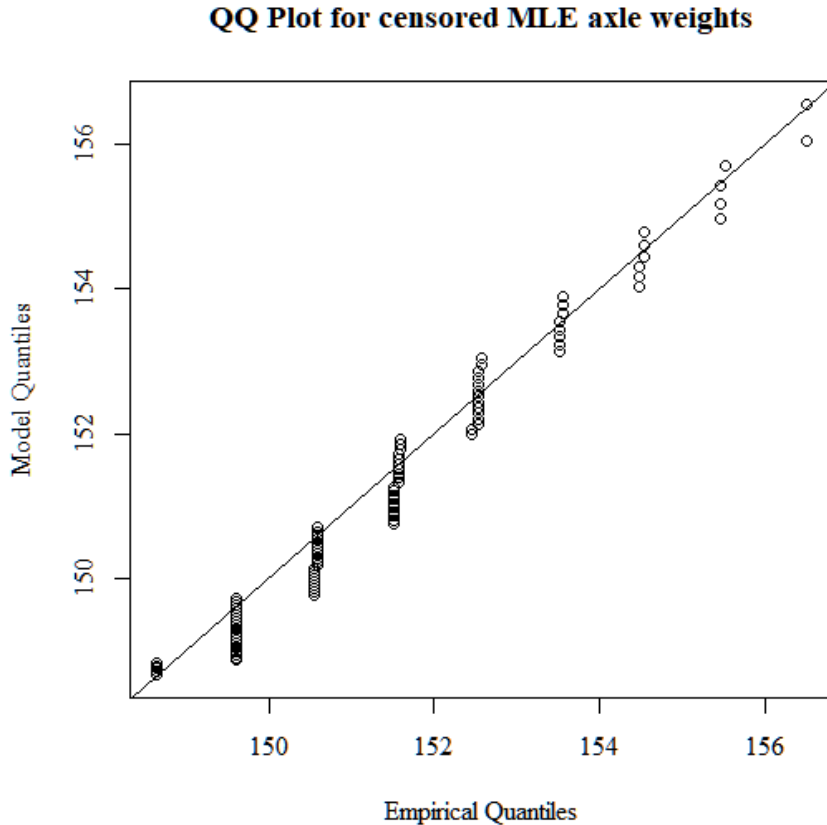


Figure 44 - Quantile plot for axle weights fitted to censored GEV distribution

4.2.3 Axle group configurations investigated

As noted previously, South African building and bridge design codes have historically been based mainly on the British codes which have since been superseded by the Eurocodes (Van der Spuy, 2014). In this study, a geometrical configuration similar to LM1 of EN1991-2 (CEN, 2003) is therefore tested initially. Other possible configurations that are investigated are a single axle similar to TMH7 (Committee of State Road Authorities, 1981), a triple axle similar to the Australian code (Standards Australia, 2004) and also a quad axle configuration for optimal performance of the intended load model. All axle spacings are taken as 1.2 m which is the same as specified in Eurocode LM1 and is further supported by the local WIM data where a consistent mean value of 1.2 m is found in axle group spacings of both tandems and tridem (Lenner *et al.*, 2017). The characteristic axle weight is not dependent on the number of axles in the load model configuration.

4.2.4 Calculation of distributed load

The extrapolated load effects from Table 8 that correspond to the 975 year return period values for the Roosboom station are used together with the characteristic axle weight of 158 kN to determine a distributed load necessary to achieve the characteristic load effects for different span lengths. Figure 45 shows an example of how the UDL is calculated by illustrating the procedure for sagging on a 30 m

span length with a single axle load. The characteristic bending moment of 6121 kNm is taken from Table 8.

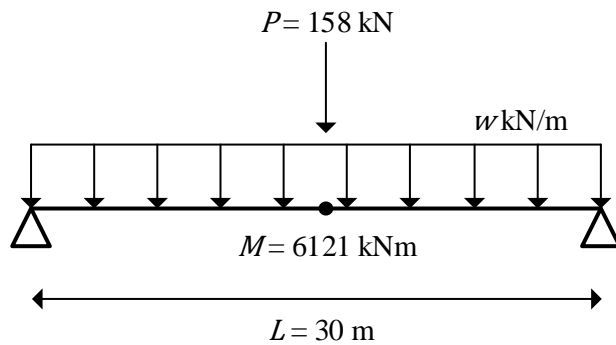


Figure 45 - UDL calculation example for sagging on a 30 m span length

$$w = \frac{8 \left(M - \frac{PL}{4} \right)}{L^2} = 44 \text{ kN/m}$$

≈ 15 kPa for a 3 m lane width

Similar calculations are performed for the different axle groupings. Figure 46 shows the distributed loads calculated for a single axle, tandem axle, tridem axle and quad axle configuration for all load effects and span lengths.

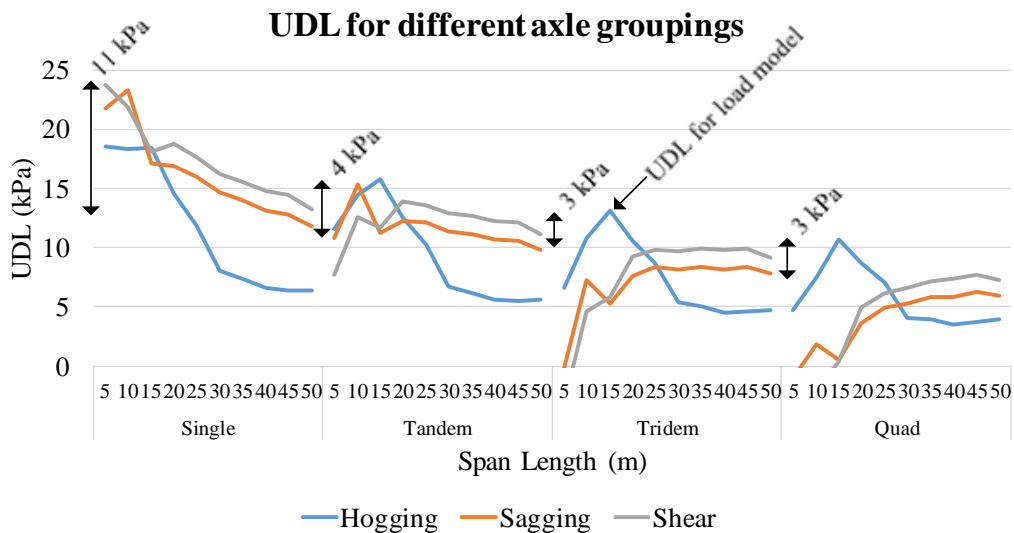


Figure 46 - UDL for various axle configurations

As can be expected, the value of the UDL decreases as the number of axles increases. A single axle configuration results in a maximum required distributed load of 24 kPa at 5 m span length and a minimum required of 13 kPa at a 50 m span length, with a difference of 11 kPa. A distributed load of 24 kPa results in a very conservative design for longer span lengths. Adopting a single axle, as currently

mandated by NA loading, therefore results in over design of most bridges and is not advisable from an economical perspective. As the number of axles increases, the difference between the highest required and lowest required distributed load decreases, leading to a more economical design. From Figure 46 the tridem and quad axle groups show the smallest difference between maximum and minimum of 3 kPa and are deemed the least conservative. Either can be adopted, but for simplicity the triple axle configuration is adopted. A tandem axle model is less economical which indicates that LM1 of EN1991-2 should not be adopted as is. Note that in the case where the load model consists only of a UDL and no axle, the difference between highest and lowest is 88 kPa, resulting in an extremely conservative design for long spans. This serves as further motivation to adopt a load model consisting of a UDL and axle loads.

The results show that current provisions in the NA model for variable distributed loading are in fact substantiated with the larger span lengths requiring lower UDL. This is especially apparent for the single axle configuration used in TMH7. Although the required UDL decreases with an increase in span length, the adoption of a constant value is not unreasonable as the ratio of dead load to live load for bridges increases at larger span lengths. Structures with long spans are dominated by dead loads therefore a slightly conservative live load model for longer spans is not of a great concern as it provides a higher safety margin at low additional cost. At the same time the UDL does become more constant for a tridem axle which is supported by Figure 49. A constant UDL greatly simplifies the application of the load model in practice and overcomes some of the challenges to the current model discussed in Chapter 1. It is therefore proposed to accept a constant UDL for the entire loaded length in order to simplify the load model.

4.2.5 Resulting load model

As discussed in the previous section a tridem axle configuration is adopted for the proposed model. Figure 47 shows the proposed load model with the UDL values taken from Figure 46. The axle load is rounded up to 160 kN and the UDL line load is rounded up to 40 kN/m.

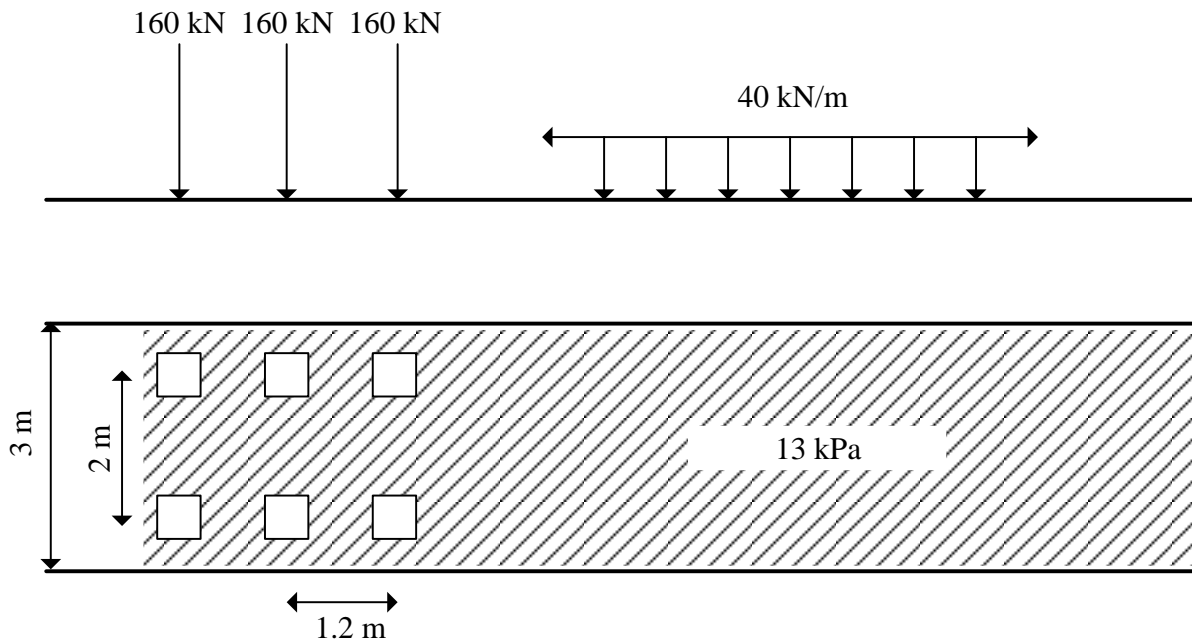


Figure 47 - Proposed load model for tridem and quad axle configurations

This load model is static and does not incorporate dynamic amplification or multiple lane presence, which are discussed in subsequent chapters.

4.3 Comparison of the new single lane model with measured load effects

The new model is governed by hogging on span lengths of 15 m and less and is therefore conservative for sagging and shear across all span lengths as shown in Figure 48. Figure 48 also shows that the proposed load model is conservative for longer spans, but as longer spans are dominated by dead loads this is deemed acceptable. This is a symptom of the constant UDL which is justified in the previous section. It does, however, offer the possibility of potentially deriving site specific models for long span structures. Figure 49 shows the same information, but normalised to WIM for easier interpretation.

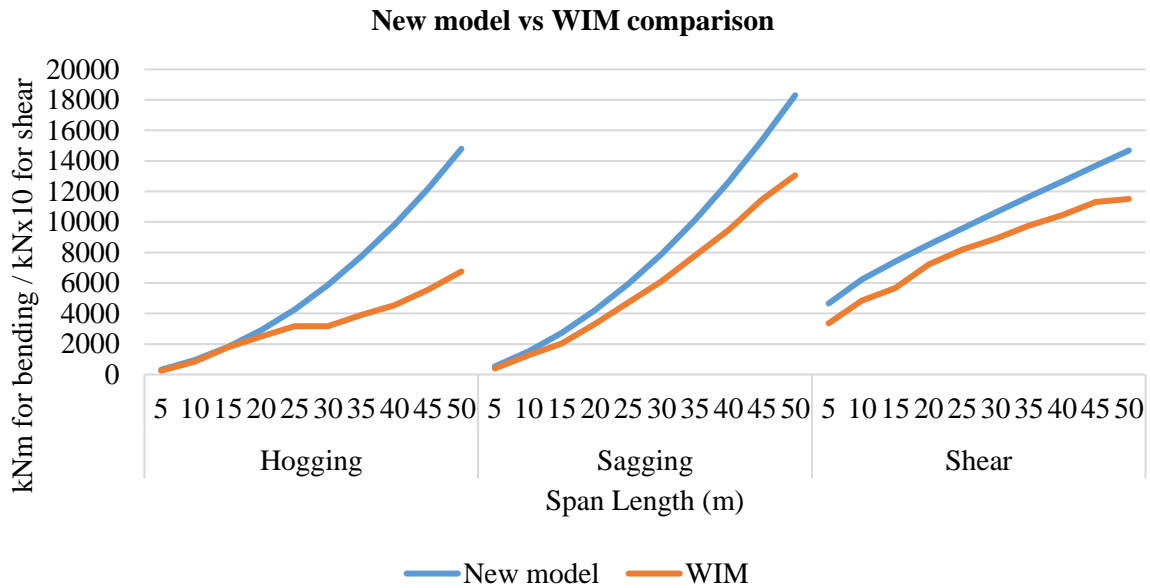


Figure 48 – Comparison of new model with characteristic measured WIM

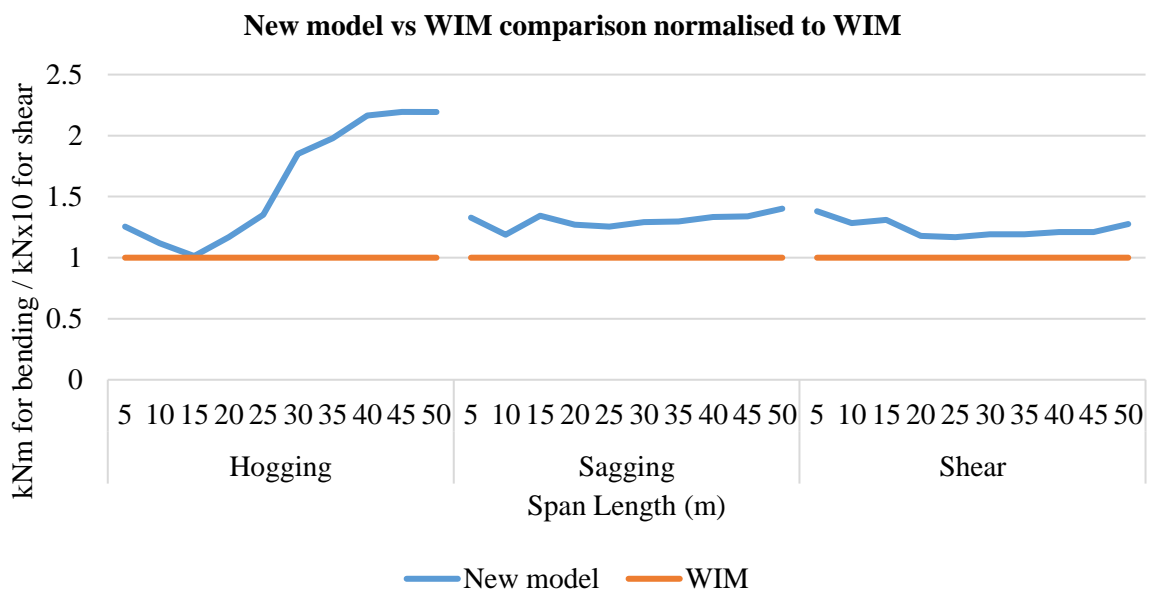


Figure 49 - Comparison of new model with characteristic measured WIM (normalised to WIM)

4.4 Conclusions

The current load model for design of bridges in South Africa shows deficiencies in both resulting internal forces for design and in the application of the load model itself. Simple adoption of a model from a different norm is deemed not advisable due to unique traffic characteristics of South Africa. It is therefore necessary to develop an updated probabilistic model based on WIM data. Furthermore, a preliminary load model for single lane traffic is derived based on the data collected at the Roosboom WIM station where seven years of data was used to calculate daily maximum hogging moments,

sagging moments and shear forces for span lengths up to 50 m. Characteristic values were determined at a return period of 975 years.

The resulting load model has a tridem axle group of 160 kN per axle, each spaced at 1.2 m apart with a distributed load of 13 kPa. The derived load model is limited to characteristic values only and does not incorporate multiple lane presence, dynamic amplification or reliability calibration as these are addressed in the following chapters.

5 Multiple lane presence

5.1 Introduction

MLFs are widely used in traffic load models for bridge design to account for the reduced probability of multiple heavy vehicles occurring simultaneously in adjacent lanes. A comprehensive treatment of the literature is provided in section 2.3. This chapter proposes a novel method to determine MLFs based on multiple lane WIM data by considering EV analysis of concurrent load effects in more than one lane, without prior knowledge of the superstructure type. The method maximises the characteristic load in any one lane, together with the characteristic concurrent total load, and does not need to consider dependence and multivariate extremes as proposed in the method by (Zhou *et al.*, 2018). Although the method is applied to free flowing traffic, it can also be applied to congested traffic if the LE data is available or artificially simulated, and considers the possibility of having more than one vehicle in any one lane. The method is thus suitable to any span length and can be extended to any number of lanes, as long as the load effects are *iid*. By not relying on the superstructure type, the method is well suited to the development of a design code as it results in a single set of MLFs. In deriving the MLFs, all permutations of combinations of all lanes are investigated which makes the method suitable for the concept of applying load in the most adverse manner. The method is first explored in detail and subsequently applied to WIM data from a station in South Africa to propose MLFs for the new slow lane model derived in Chapter 4.

The content of this chapter has been published in *Structures Volume 20: 543-549* under the title *Multiple lane reduction factors based on multiple lane weigh in motion data* (Van der Spuy, Lenner, de Wet & Caprani, 2019a) and published and presented at *SEMC 2019: The Seventh International Conference on Structural Engineering, Mechanics and Computation* under the title *Multilane reduction factors based on WIM data* (Van der Spuy, Lenner, de Wet & Caprani, 2019b).

5.2 MLF calculation methodology

To determine the largest LE in any bridge deck component due to traffic load, two phenomena need to be accounted for transversely:

- Transverse spatial arrangement of vehicles on the deck. This phenomena is dependent on the load pattern and captures the reduced probability of having multiple heavy vehicles on a bridge simultaneously side by side. This is determined through a statistical analysis of multiple lane WIM data as presented in this chapter
- Transverse load distribution being a function of the transverse stiffness of deck components. This is typically performed during the analysis stage of design through a grillage analysis or a finite element (FEA) model. Different superstructure elements combined carry the load imposed on a superstructure. It is natural that the elements closest to the load will attract most

of it and the amount of load carried by the other elements decreases with an increase in distance from the load and reduced stiffness. This effect is independent of the applied load intensity or configuration.

Some authors incorporate the transverse stiffness of a bridge deck in the definition of the lane factors (Enright *et al.*, 2011; OBrien & Enright, 2011; Fu *et al.*, 2013; Leahy, OBrien & O'Connor, 2015; Zhou *et al.*, 2018). In these approaches the stiffness and transverse traffic patterns are combined in one lane factor. This is achieved by performing a multitude of FEA with traffic loading which cover a range of deck types, widths and span lengths in order to represent most practical design situations. The factors are universally applicable to all deck types and may be conservative if decks are designed that are different to the critical ones that determine the lane factors. When this approach is used, care must be taken when a designer performs an analysis to ensure that the transverse stiffness in the design model does not lead to double transverse distribution as it may already have been taken into account in the derivation of the lane factors. It would be useful if a formulation can be derived where the loading and the stiffness distribution of a bridge deck can be combined after considering them separately. This avoids the one-size-fits-all approach to different deck types and is the novel contribution of this chapter.

In one of the first papers published on this topic, Jaeger & Bakht (1987) state that “*It is suggested that the load distribution characteristics of a bridge, which can be adequately handled separately by the methods of analysis for load distribution, should not have any influence on the reduction factors for multi-presence loading.*” This approach is followed here by treating the two phenomena separately and then to combine them when structural analysis is performed. This is convenient as it allows the determination of MLFs based on traffic only, without prior knowledge of the deck type and its transverse stiffness. A transverse stiffness of zero is assumed in the calculations of the MLFs with the transverse stiffness incorporated in the analysis model. It is well suited to design where the deck type does not affect the loading applied to it. To explain this concept in an example, Figure 50 shows how the MLFs are applied to create the largest load effect in Girder 1. For this example the number of girders and lanes is equal, but the concept can be extended to any number of lanes or girders, or for other bridge deck types. In this exercise the lanes are arranged so that the lane which has the largest influence on Girder 1 is located above Girder 1 with the load decreasing with reduced influence. The $Load_{rm} = (UDL + Axle)_{ref\ model}$ is the slow lane reference model. Of course Lane 1 carries the highest load due to the definition of the MLFs.

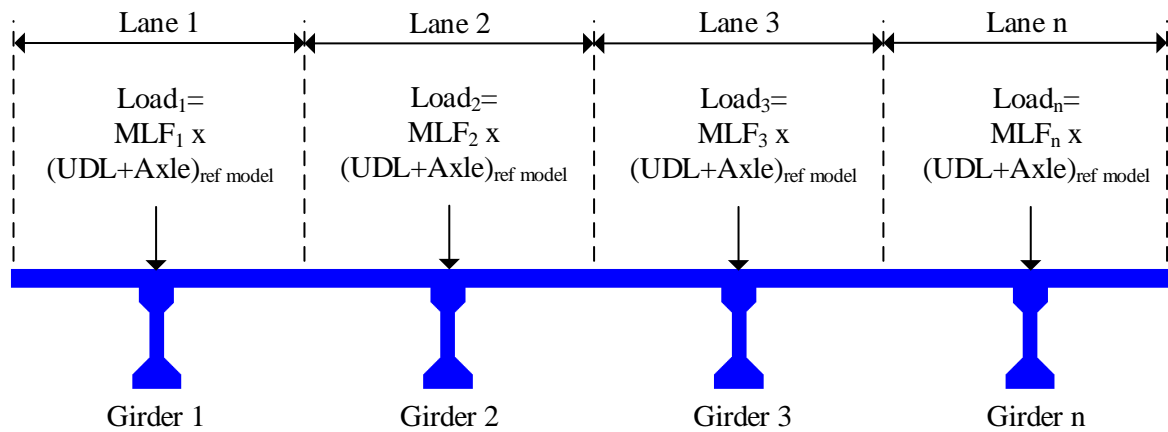


Figure 50 - Definition of MLF application

Due to the inherent transverse stiffness of the deck slab, some of the load applied to Girder 1 will be distributed to the other girders. The same applies for Girders 2 to n and the idea is illustrated in Figure 52 and summarised in Equation (98). Let

$\sum_{i=1}^n k_{1,i}$ be the portion of the load from Lane i which is carried by Girder 1

$\sum_{i=1}^n k_{2,i}$ be the portion of the load from Lane i which is carried by Girder 2

$\sum_{i=1}^n k_{3,i}$ be the portion of the load from Lane i which is carried by Girder 3

$\sum_{i=1}^n k_{n,i}$ be the portion of the load from Lane i which is carried by Girder n

These k factors, or distribution coefficients, are typically determined through a transverse influence line analysis. An example of such a transverse influence line is shown in Figure 51 for sagging at mid span for a 40 m span length with a point load applied in mid span on the edge beam. 51.2 % of the total moment generated by a 1000 kN point load is carried by the edge beam directly below it. This reduces to 6.9 % carried by the opposite edge beam.

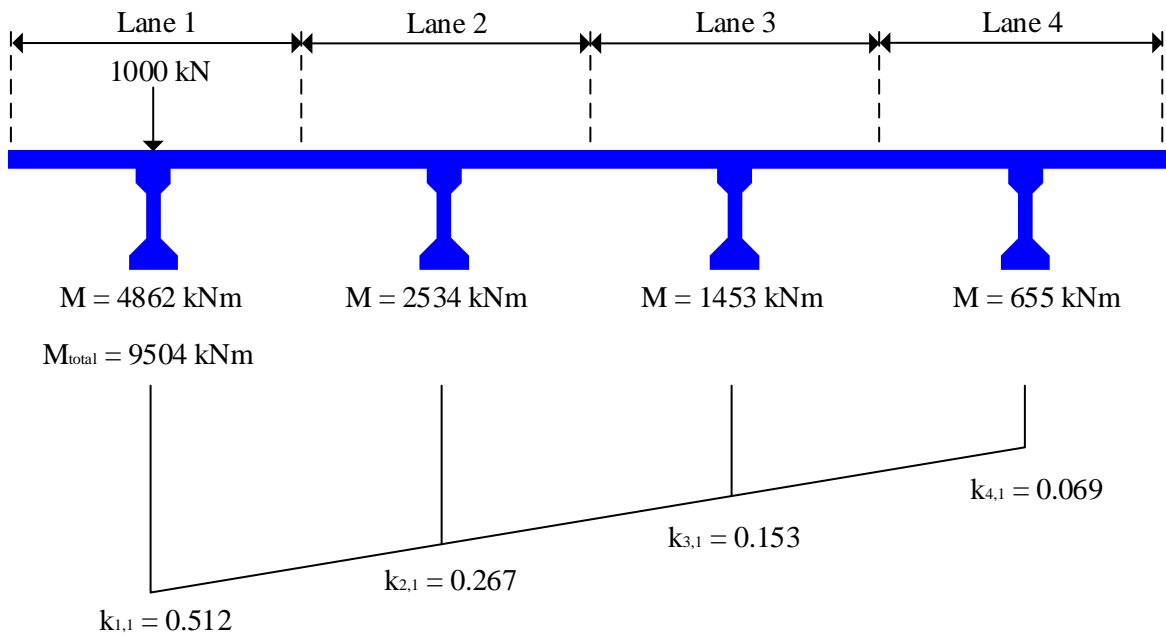


Figure 51 - Transverse influence line for 40 m sagging with load on edge beam

Let $LG_{1,2,\dots,n}$ be the total load on Girder 1, 2, ..., n , then

$$LG_1 = MLF_1 \times \text{Load}_{\text{rm}} \times k_{11} + MLF_2 \times \text{Load}_{\text{rm}} \times k_{12} + MLF_3 \times \text{Load}_{\text{rm}} \times k_{13} + MLF_n \times \text{Load}_{\text{rm}} \times k_{1n}$$

$$LG_2 = MLF_1 \times \text{Load}_{\text{rm}} \times k_{21} + MLF_2 \times \text{Load}_{\text{rm}} \times k_{22} + MLF_3 \times \text{Load}_{\text{rm}} \times k_{23} + MLF_n \times \text{Load}_{\text{rm}} \times k_{2n}$$

$$LG_3 = MLF_1 \times \text{Load}_{\text{rm}} \times k_{31} + MLF_2 \times \text{Load}_{\text{rm}} \times k_{32} + MLF_3 \times \text{Load}_{\text{rm}} \times k_{33} + MLF_n \times \text{Load}_{\text{rm}} \times k_{3n}$$

$$LG_n = MLF_1 \times \text{Load}_{\text{rm}} \times k_{n1} + MLF_2 \times \text{Load}_{\text{rm}} \times k_{n2} + MLF_3 \times \text{Load}_{\text{rm}} \times k_{n3} + MLF_n \times \text{Load}_{\text{rm}} \times k_{nn}$$

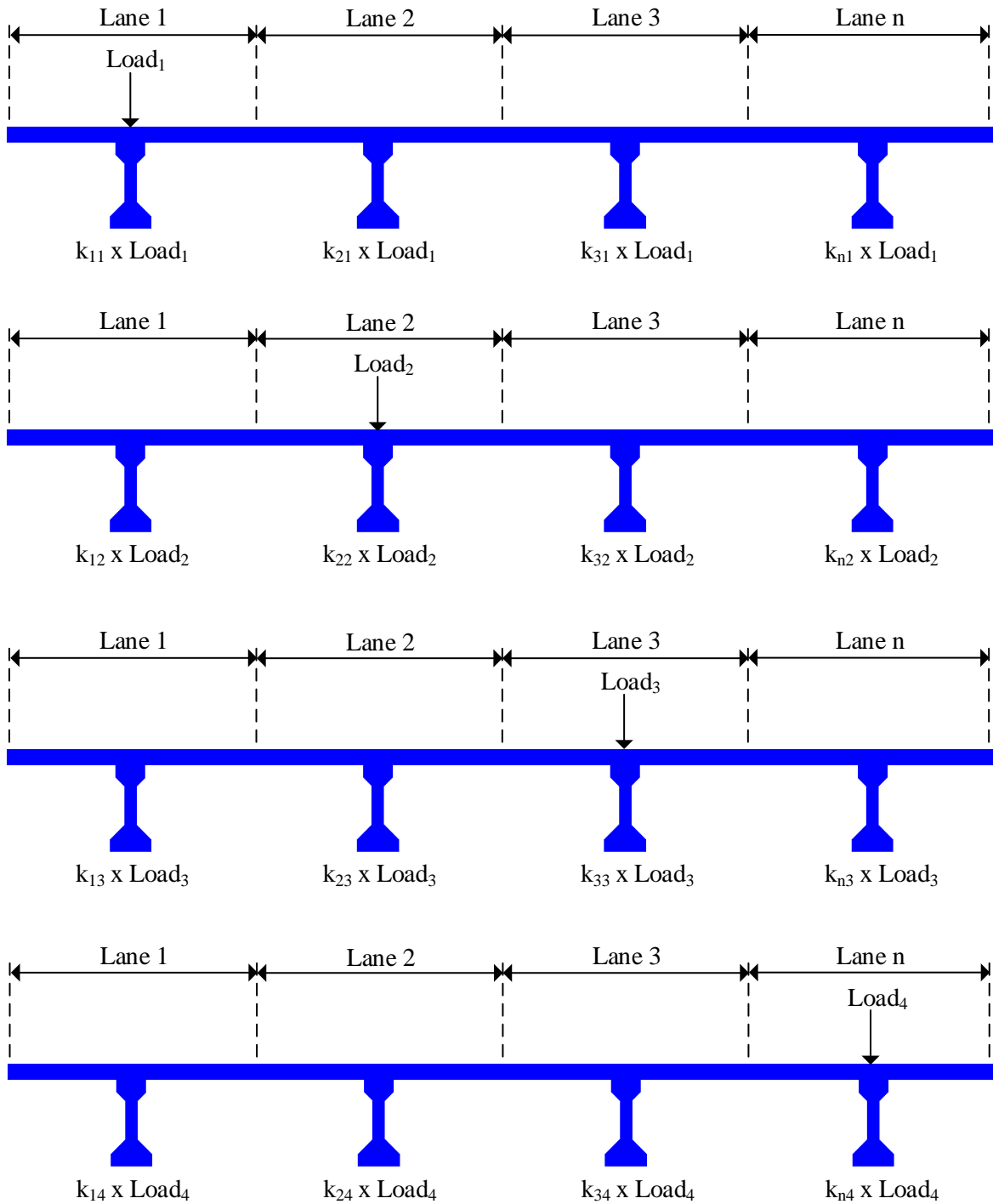


Figure 52 - Transverse distribution of lane loads

$$\begin{bmatrix} LG_1 \\ LG_2 \\ LG_3 \\ LG_n \end{bmatrix} = Load_{rm} \times \begin{bmatrix} k_{11} & k_{12} & k_{13} & k_{1n} \\ k_{21} & k_{22} & k_{23} & k_{2n} \\ k_{31} & k_{32} & k_{33} & k_{3n} \\ k_{n1} & k_{n2} & k_{n3} & k_{nn} \end{bmatrix} \begin{bmatrix} MLF_1 \\ MLF_2 \\ MLF_3 \\ MLF_n \end{bmatrix} \quad (98)$$

To apply the proposed method to calculate MLFs it is necessary to have either multiple lane recorded WIM data or congested traffic loading data. In order to assess the ratio of load effects in adjacent lanes

at EVs, it is necessary to predict extreme events at long return periods. The method proposed here is applicable to any number N of lanes, provided that N lanes of calculated load effect data are available. It is necessary to ensure that WIM data is cleaned and well calibrated, as set out in Van der Spuy & Lenner (2018, 2019). Time history of load effects are calculated for each lane assuming zero transverse stiffness between lanes. The time history of the lanes are used to identify occurrence of adjacent heavy vehicles in the traffic flow. A statistical procedure is then described to determine MLFs at characteristic level.

5.2.1 Time history of load effects

The first step in the proposed methodology is to calculate a time history of load effects for each of N lanes by applying WIM data or congested traffic data to influence lines of various lengths. This is done for each load effect and for each span length to be considered for all N lanes. It is proposed to start at a span length of 10 m and to increase the span length in increments of 10 m. It is necessary to create convoys of vehicles in order to capture the multiple vehicle occurrence in any single lane or adjacent lanes. As no acceleration or deceleration information is obtained from the WIM data it is not possible to obtain accurate vehicle gaps over time. For longer convoys this effect becomes more pronounced and the relative position of vehicles in adjacent lanes becomes inaccurate. For this reason shorter convoys can be built with only three following vehicles in any one lane which minimizes the potential error; as the critical vehicles are 22 m long, three vehicles are sufficient for short to medium span length bridges. This needs to be evaluated on a case specific basis. The LEs in any lane for any span length are then calculated as a function of time by moving the convoys over influence lines and assuming zero transverse stiffness. By studying the LE time history for each lane it is possible to determine concurrent lane LEs at any time t .

5.2.2 Extrapolation to characteristic values

To determine MLFs at characteristic level EV theory is used. All the LEs and span lengths considered in this work are evaluated again, but for multiple lanes. Calculating concurrent *daily* maxima LEs for multiple lanes and multiple years of WIM data, at 0.02 s time increments, is computationally very expensive in terms of the number of values that must be stored in the computer's Random Access Memory (RAM) and often not feasible, even with a High Performance Computer (HPC). A short time increment is necessary to capture the relative positions of vehicles accurately.

Section 3.3.7.2 shows that *monthly* blocks can also be used instead of *daily* blocks, although larger block sizes discard more extreme events. In order for computation to be possible with a time increment of 0.02 s, this is an accepted sacrifice for the application example shown in this chapter and is the same time increment used in the derivation of the reference lane model. The procedure is, however, formulated for any block size. Several studies, and Section 3.3.7.1 of this document, show that bridge

traffic LEs in a single lane are best described by the bounded Weibull extreme value distribution (Bailey, 1996; Caprani *et al.*, 2003; O'Brien *et al.*, 2015). However, to account for the possibility that the coincident lane load effects could approach the Gumbel extreme value distribution, a censored GEV distribution is used again. This is consistent with the rest of the work.

5.2.3 Procedure

Consider N lanes on which load effect data is available over a period of time. The method treats all load effects and span lengths identically and can be used for any span length or skew decks, provided that the load effects can be calculated for each. In this work, the procedure is applied as an example to span lengths between 10 m and 50 m in 10 m increments denoted by the set $L \{10,20,30,40,50\}$. It is necessary to have long run WIM data in order to have sufficient number of blocks so that a distribution can be fitted and that the extrapolation yields reasonable results.

The LE data can be blocked into B consecutive blocks and the maximum of each lane in every block can be calculated for each span length in the set. Denoting $M_{n;b;L}$ as the maximum of the load effect data of lane n for block b , where $n = 1, \dots, N$ and $b = 1, \dots, B$ and L is the span length under consideration. This yields a sequence of monthly block maxima given by $\mathbf{M}_{n;b;L}$. The Fisher-Tippet-Gnedenko theorem of extreme value theory and theorem 3.1.1 in Coles (2001) holds true for each lane sequence of block maxima, therefore the distribution of $\mathbf{M}_{n;b;L}$ can be approximated by a GEV distribution for every $n = 1, \dots, N$ and each L in the set. The parameters of each GEV distribution are estimated by MLE, using lane n 's block maxima.

Let ν be the number of blocks within a one year period, for example for monthly maxima $\nu = 12$. This leads to an exceedance probability, p , in the reference period given by Equation (99), with the probability of non-exceedance being $1 - p$.

$$p = \frac{1}{T\nu} \quad (99)$$

If each lane is evaluated individually at p , the return level for lane n is denoted by $m_{n;p;L}$ i.e. the $(1 - p)$ -th quantile of the GEV distribution fitted to the n lane block maxima for all L as per Equation (100). Parameters for each lane n are estimated by MLE.

$$m_{n;p;L} = \mu_{n;L} + [\sigma_{n;L}((- \ln(1 - p))^{-\xi_{n;L}} - 1)]/\xi_{n;L} \quad (100)$$

From the N quantiles $m_{n;p;L}$, the lane with the largest quantile is designated as Lane 1. This is the reference value of a single lane loading scenario and is the extrapolated load effect which is used to calibrate a load model for the lane experiencing the maximum load effect (Van der Spuy & Lenner, 2019). For Lane 1 the generic MLF is then given by Equation (101).

$$MLF_{1;p;L} = \frac{m_{1;p;L}}{m_{1;p;L}} = 1 \quad (101)$$

The single lane MLF is the maximum over all considered span lengths for all load effects, given by Equation (102).

$$MLF_1 = \max_{L \in \{10, \dots, 50\}} \{MLF_{1;hog}, MLF_{1;sag}, MLF_{1;shear}\} = 1 \quad (102)$$

Any two lanes can be considered by denoting them as r and s with $1 \leq r < s \leq N$. The sum, $S_L(t)$, of the load effects of these two lanes at every time instant is obtained according to Equation (103).

$$S_L(t) = LE_{r,L}(t) + LE_{s,L}(t) \quad (103)$$

$$M_{r+s;b;L} = \max_t S_L(t) \text{ for block } b \quad (104)$$

Considering the maximum, $M_{r+s;b;L}$, of $S_L(t)$ for each block b (Equation (104)), another sequence of block maxima data $\mathbf{M}_{r+s;b;L}_{b=1}^B$ is created consisting of the maximum concurrent LE sum of lanes r and s during each block b . Theorem 3.1.1 in Coles (2001), applied to this sequence leads to a GEV distribution, $GEV_{r+s;L}$, with parameters again estimated by MLE.

Denoting $(1-p)$ -th quantile of $GEV_{r+s;L}$ by $m_{r+s;L}$ and carrying out the analysis for all $\binom{N}{2}$ possible two lane combinations, let $m_{2;L}^*$ denote the combined maximum of these according to Equation (105) for each span length and load effect.

$$m_{2;L}^* = \max_{1 \leq r < s \leq N} m_{r+s;L} \quad (105)$$

The load effect in the second lane is obtained by subtracting the load effect of Lane 1 from the combined maximum $m_{2;L}^*$ according to Equation (106). This can be thought of as the value of the LE in Lane 2 when Lane 1 is at characteristic level.

$$m_{2;L} = m_{2;L}^* - m_{1;L} = m_{2;L}^* - m_{1;L} MLF_1 \quad (106)$$

The MLF relating the LE in Lane 2 to the reference lane is then given by Equation (107).

$$MLF_{2;L} = \frac{m_{2;L}}{m_{1;L}} \quad (107)$$

From a design code perspective which has to cover a range of span lengths, the maximum over span lengths is obtained by Equation (108).

$$MLF_2 = \max_{L \in \{10, \dots, 50\}} (MLF_{2;L}) \text{ per load effect} \quad (108)$$

This process is carried out for hogging, sagging and shear and calculates the MLF for the second lane according to Equation (109).

$$MLF_2 = \max\{MLF_{2,hog}, MLF_{2,sag}, MLF_{2,shear}\} \quad (109)$$

Iterating this process to obtain MLFs for any number of lanes it follows that for any $1 \leq n \leq N$ the n lane load effect is given by Equation (110).

$$m_{n;L} = m_{n;L}^* - m_{1;L} \sum_{i=1}^{n-1} MLF_{n-i}; \text{ for } 1 \leq n \leq N \text{ with } m_{1;L}^* = m_{1;L} \quad (110)$$

In this case the MLF is then given by Equation (111).

$$MLF_{n;L} \equiv \frac{m_{n;L}}{m_{1;L}} \quad (111)$$

The maximum over span lengths is taken to obtain

$$MLF_n = \max_{L \in \{10, \dots, 50\}} (MLF_{n;L}) \text{ per load effect} \quad (112)$$

The n -th lane MLF can be determined by Equation (113).

$$MLF_n = \max\{MLF_{n,hog}, MLF_{n,sag}, MLF_{n,shear}\} \quad (113)$$

The described procedure results in a set of MLFs derived for all considered span lengths and load effects. As the maximum MLF factor is retained for each individual lane, the set is suitable for application in a design code. All permutations are considered, which effectively means the heaviest lane ($MLF = 1$) can be applied in any position transversely and subsequent lanes with lower MLF factors can be applied in sequence according to the transverse influence line to achieve the most adverse effect.

5.3 Application to a WIM site in South Africa

The Kilner Park station on the N1 near Pretoria is the only station in South Africa that measures four lanes concurrently. The site has two lanes instrumented in each direction, shown in Figure 53. The time stamp resolution at this site is 0.01 s, however, to reduce computational effort 0.02 s was used as an increment for the LE calculation. Three years of data were recorded from 2015 to 2017 and cleaned and calibrated according to chapter 3; and are deemed to be sufficient in this work by yielding a sufficient number of blocks. Although this example illustrates free flowing traffic in opposing directions, the same procedure applies if all four lanes are recorded in the same direction. It also applies if congested traffic load effects are used, since the procedure requires only a spatial distribution of the recorded axle loads. It is expected that traffic in opposing directions will generally produce higher MLFs when compared to traffic in one direction, as two lanes of heavy traffic are recorded as opposed to only one. It is therefore more suitable for the implementation of the results in a design code.

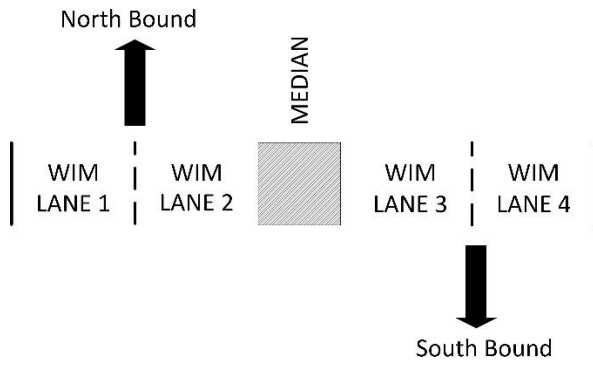


Figure 53 - WIM site lane arrangement

5.3.1 Calculation of MLFs

In this example, sets of monthly block maxima data are tested and shown to fit the censored GEV distribution well. To illustrate this, Figure 54 shows a quantile plot for the monthly maxima hogging moments in Lane 1 in kNm. Adherence of the measured data to a straight line confirms that the GEV distribution is a good fit to the monthly maxima and that the data is *iid*. The MLE fits to the data showed a negative shape factor for the GEV distribution, indicating that the data tends towards the bounded Weibull EV distribution.

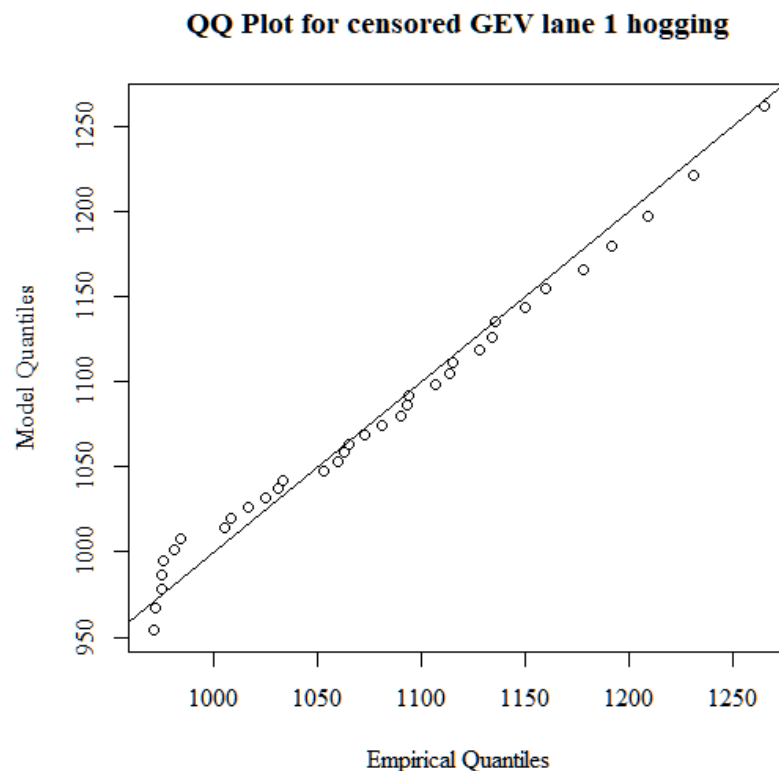


Figure 54 - Quantile plot for Lane 1 monthly maxima hogging moments

Table 11 shows extrapolated load effects for each lane with maximum values $m_{1;L}$ shown in bold denoting the reference values.

Table 11 - Extrapolated single lane load effects

Span length L (m)	Lane no	Hogging (kNm)	Sagging (kNm)	Shear (kN)
10	1	617	671	319
	2	692	1143	484
	3	548	893	503
	4	623	812	345
20	1	1434	2546	486
	2	1489	3071	564
	3	1374	2745	639
	4	1756	2528	468
30	1	1964	4457	596
	2	2470	5140	713
	3	2108	5441	767
	4	2166	4842	556
40	1	2646	6155	603
	2	3447	7924	760
	3	3287	6398	872
	4	3168	6999	648
50	1	3497	7793	627
	2	4276	9352	811
	3	4541	8824	719
	4	4041	8865	658

When compared to the Roosboom LEs from Table 8 it confirms that Roosboom is indeed a heavier station than Kilner Park.

For each permutation of two lanes loaded the combined monthly maxima is taken for each load effect and extrapolated to the return period. This gives the characteristic combined load effects for any two lanes loaded simultaneously. The results are shown in Table 12 with maximum values $m_{2;L}^*$ shown in bold.

Table 12 - Extrapolated two lane load effects

Span length L (m)	Lane no	Hogging (kNm)	Sagging (kNm)	Shear (kN)
10	1,2	853	1250	383
	1,3	784	1311	421
	1,4	932	1255	433
	2,3	752	1093	502
	2,4	875	1100	478
	3,4	1082	1508	445
20	1,2	2224	3625	703
	1,3	2310	3618	779
	1,4	2171	3596	614
	2,3	1888	3602	581
	2,4	1994	3316	695
	3,4	2814	4067	595
30	1,2	3064	5427	806
	1,3	3280	6995	946
	1,4	3332	7154	967
	2,3	3401	5973	739
	2,4	3415	6083	765
	3,4	4197	7728	840
40	1,2	4820	10667	1059
	1,3	4549	9909	1048
	1,4	4033	9843	1027
	2,3	4563	8905	919
	2,4	4215	9114	975
	3,4	6127	11696	1030
50	1,2	6227	13956	1063
	1,3	5567	12435	1034
	1,4	6664	11646	888
	2,3	6824	11652	893
	2,4	6395	12627	1047
	3,4	7433	15748	1044

For hogging on a 40 m span length it follows from Equation (100) that the characteristic values for single lane loading per lane are given by

$$m_{1,40} = \max\{2646, 3447, 3287, 3168\} = 3447$$

and from Equation (105) it follows that

$$m_{2,40}^* = \max\{4820, 4549, 4033, 4563, 4215, 6127\} = 6127$$

It follows from Equation (106) that

$$m_{2;40} = m_{2;40}^* - m_{1;40}MLF_1 = 6127 - 3447 \times 1$$

From Equation (107) the MLF for the second lane is calculated as

$$MLF_{2;40} = \frac{m_{2;40}}{m_{1;40}} = 0.777$$

Calculate the MLFs for each load effect and each span length and take the maximum, shown in Table 13. The maximum is the MLF to be applied to lane two throughout. An increase in the MLF with span length confirms the intuition of a higher probability of simultaneous occurrence of heavy vehicles on longer spans.

Table 13 - MLF values for two lanes loaded

Span length L (m)	MLF _{2;hog}	MLF _{2;sag}	MLF _{2;shear}
10	0.564	0.319	-0.002
20	0.603	0.324	0.219
30	0.699	0.420	0.109
40	0.777	0.476	0.214
50	0.637	0.684	0.219

From Equations (108) and (109) the MLF for the second lane loaded over all span lengths and load effects is

$$MLF_2 = \max\{MLF_{2,hog}, MLF_{2,sag}, MLF_{2,shear}\} = 0.777$$

The characteristic combined load effects for any three lanes loaded simultaneously are shown in Table 14 with maximum values $m_{3;L}^*$ shown in bold.

Table 14 - Extrapolated three lane load effects

Span length L (m)	Lane no	Hogging (kNm)	Sagging (kNm)	Shear (kN)
10	1,2,3	1189	1235	667
	1,2,4	1092	1259	481
	1,3,4	1214	1647	557
	2,3,4	1231	1720	505
20	1,2,3	3249	3500	747
	1,2,4	2422	4373	1038
	1,3,4	2516	3397	736
	2,3,4	2744	3828	899
30	1,2,3	3501	8131	1121
	1,2,4	4219	8556	1057
	1,3,4	4186	7574	999
	2,3,4	3861	7134	947
40	1,2,3	5471	11856	1398
	1,2,4	6147	11214	1073
	1,3,4	5472	12059	1128
	2,3,4	5433	11392	1153
50	1,2,3	7068	15464	1139
	1,2,4	8043	15147	1246
	1,3,4	7790	14804	1140
	2,3,4	7530	14697	1171

For example, for hogging on a 50 m span length it follows from Equation (100) that the characteristic values for single lane loading per lane are given by

$$m_{1;50} = \max\{3497, 4276, 4541, 4041\}$$

and

$$m_{3;50}^* = \max\{7068, 8043, 7790, 7530\}$$

From Equation (110) it follows that

$$m_{3;50} = m_{3;50}^* - m_{1;50}MLF_1 - m_{1;50}MLF_2 = 8043 - 4541 \times 1 - 4541 \times 0.777$$

Following from Equation (111) the MLF for the third lane is

$$MLF_{hogging;50} = \frac{m_{3;50}}{m_{1;50}} = -0.006$$

For each permutation of three lanes loaded take the combined monthly maxima for each load effect and extrapolate to the return period.

Calculate the MLFs for each load effect and each span length and take the maximum, shown Table 15. This maximum is the MLF to be applied to lane three throughout.

Table 15 - MLF values for three lanes loaded

Span length L (m)	MLF _{3;hog}	MLF _{3;sag}	MLF _{3;shear}
10	0.001	-0.273	-0.451
20	0.073	-0.354	-0.153
30	-0.069	-0.205	-0.492
40	0.006	-0.256	-0.174
50	-0.006	-0.124	-0.349

From Equations (112) and (113) the MLF for the third lane loaded over all span lengths and load effects is

$$MLF_3 = \max\{MLF_{3,hog}, MLF_{3,sag}, MLF_{3,shear}\} = 0.073$$

Negative values in Table 15 imply that the characteristic concurrent two lane load effects are larger than that for three lanes loaded simultaneously, and therefore the MLF must be taken as zero in that case. This occurs because the maxima for two and three lanes loaded are not necessarily caused by the same lanes. MLFs should be considered with the accompanying load effects to avoid the confusion of the negative values.

For four lanes loaded take the combined monthly maxima for each load effect and extrapolate to the return period. This gives the characteristic combined load effects for all four lanes loaded simultaneously. The results are shown in Table 16.

Table 16 - Extrapolated four lane load effects

Span length L (m)	Lane no	Hogging (kNm)	Sagging (kNm)	Shear (kN)
10	1,2,3,4	1277	1398	649
20	1,2,3,4	3640	4040	889
30	1,2,3,4	4388	7610	961
40	1,2,3,4	6878	13774	1359
50	1,2,3,4	7959	18230	1156

For example, for hogging on a 50 m span length it follows that $m_{4;50}^* = \max\{7959\}$ as there is only one possible combination of four lanes loaded.

From Equation (110) it follows that

$$m_{4;50} = m_{4;50}^* - m_{1;50}(MLF_1 + MLF_2 + MLF_3) = 7959 - 4541 \times (1 + 0.777 + 0.073)$$

Following from Equation (111) the MLF for the fourth lane is calculated as

$$MLF_{hogging;50} = \frac{m_{4;50}}{m_{1;50}} = -0.098$$

Calculate the MLFs for each load effect and each span length and take the maximum, shown in Table 17. This maximum is the MLF to be applied to lane four throughout.

Table 17 - MLF values for four lanes loaded

Span length L (m)	$MLF_{4;hog}$	$MLF_{4;sag}$	$MLF_{4;shear}$
10	-0.005	-0.627	-0.560
20	-0.276	-0.535	-0.459
30	-0.074	-0.452	-0.748
40	-0.135	-0.112	-0.292
50	-0.098	-0.244	-0.525

From Equations (112) and (113) the MLF for the fourth lane loaded over all span lengths and load effects is

$$MLF_4 = \max\{MLF_{4,hog}, MLF_{4,sag}, MLF_{4,shear}\} = -0.005$$

Negative values in Table 17 imply the fourth lane does not contribute to the global LEs. This occurs because MLF_2 and MLF_3 are derived for specific load effects and span lengths and are conservative for others. It must be emphasised that the total load effects are always applied with this method, although the distribution between lanes may differ between the load effects and span lengths.

This example, using WIM data from Kilner Park, results in a set of MLFs that cover all load effects for all span lengths between 10 m and 50 m and is summarised in Table 18. In this case, MLF values decrease rapidly with increased number of lanes. The effect of the fourth lane on characteristic load effects in girders supporting lane 1 is negligible and even the contribution from the third lane is small. This result is supported by Anitori *et al.* (2017) who argue that the probability of a third side-by-side truck contributing to the maximum effect in a main girder is very small due to the low probability of simultaneous presence.

Table 18 - Final MLFs

Lane no	MLF
1	1
2	0.78
3	0.07
4	0

As the procedure takes the maximum over all load effects, it results in conservative results for those that are not governing the resulting MLFs. This is a simplification for the sake of deriving a model for a design code. To quantify the implication of this simplification, the MLFs are given separately for hogging, sagging and shear and are shown in Table 19. These can be used in a refined analysis. The MLFs for sagging are smaller than those for hogging. This is expected as the total bridge length for hogging is twice than that for sagging and the probability of encountering concurrent side-by-side heavy vehicle events is higher. Shear is governed by axle loads which vary less between vehicles in adjacent lanes. Although vehicles with smaller GVWs are expected more frequently in the faster lanes, the axle weights are not necessarily smaller.

Table 19 - Final MLFs per load effect

Lane	Hogging	Sagging	Shear
1	1.00	1.00	1.00
2	0.78	0.68	0.62
3	0.07	0.00	0.16
4	0.00	0.00	0.00

5.4 Comparison with other codes

In order to compare the obtained MLF values with international codes, load effects are calculated for the Eurocode LM1 (CEN, 2003), Australian code (Standards Australia, 2004) and the American code (AASHTO, 2007) for hogging, sagging and shear for span lengths between 10 m and 50 m. The maximum ratios between load effects in adjacent lanes are calculated to compare with the results of this study. The values from the AASHTO code are normalised for comparison. Of the three codes, the Eurocode shows the largest reduction in MLFs with an increased number of loaded lanes. The Australian and AASHTO codes show high marginal factors even in the fourth loaded lane and beyond. Table 20 shows a comparison of the different code values.

Table 20 - Comparison of MLF values

Code	Lane Number			
	1	2	3	4
EN 1991-2	1.0	0.59	0.32	0.21
AS5100.2	1.0	0.80	0.40	0.40
AASHTO	1.0	0.83	0.71	0.54
This study	1.0	0.78	0.07	0.00

Even though this study shows that the contribution from the third lane and beyond is negligible for the data used, all these codes extend MLFs to the fourth lane and beyond. This can partly be explained by an absence of multiple lane WIM data to show that the contribution from these lanes may be much

smaller than the current values. Once these MLFs for the third lane and beyond are combined with the transverse distribution factors which reduce with an increase in the lane number from the critical lane, the contribution to LEs in the critical elements are small.

5.5 Comparison with Turkstra's rule

Turkstra's rule is a simple method of formulating a load combinations to combine several loading events which may occur concurrently on a structure and it is better suited for design codes than other more complicated methods. It is a *deterministic* oversimplification of the more complex Ferry Borges-Castanheta model (Ghosn *et al.*, 2003; Melchers & Beck, 2018). Although it is a simplification it was shown to perform well for probabilities of failure less than approximately 10^{-3} (Sykora & Holicky, 2011). Turkstra's rule is based on the *observation* that when one load component reaches an extreme, the other load components are acting at their average in a stationary process. This implies that the probability of having two load components at their respective extreme values are considered negligible (Nowak & Collins, 2002). The rule can lead to unsafe and inconsistent results when none of the actions are at their maxima, but *the most unfavourable situations are approximated closely nevertheless*.

The rule is typically used to combine different sources of loading, but is useful to combine the effect of several lanes within the traffic load loadcase and is used here for verification of the procedure proposed in this chapter. It should be emphasised that for reasons mentioned above, Turkstra's rule will only approximate the results obtained with the more refined methodology described in this chapter.

Let the load effects in lanes 1, 2, 3 and 4 be denoted as LE_1 , LE_2 , LE_3 and LE_4 respectively. LE_1 , LE_2 , LE_3 and LE_4 are random variables that vary with time. In practical situations, the load which is not at its maximum is taken as the mean (Ghosn *et al.*, 2003). Turkstra's rule states that the following must be satisfied

$$LE_T = \max \left\{ \begin{array}{l} \max(LE_1) + \overline{LE_2} + \overline{LE_3} + \overline{LE_4} \\ \overline{LE_1} + \max(LE_2) + \overline{LE_3} + \overline{LE_4} \\ \overline{LE_1} + \overline{LE_2} + \max(LE_3) + \overline{LE_4} \\ \overline{LE_1} + \overline{LE_2} + \overline{LE_3} + \max(LE_4) \end{array} \right\} \quad (114)$$

where

LE_T is the total load effect

$\max(LE_1)$ is the lifetime maximum load effect in lane 1

$\max(LE_2)$ is the lifetime maximum load effect in lane 2

$\max(LE_3)$ is the lifetime maximum load effect in lane 3

$\max(LE_4)$ is the lifetime maximum load effect in lane 4

\overline{LE}_1 the mean of LE_1

\overline{LE}_2 the mean of LE_2

\overline{LE}_3 the mean of LE_3

\overline{LE}_4 the mean of LE_4

The lifetime maximum load effect is commonly selected as the 95th percentile value (Melchers & Beck, 2018). For consistency with the rest of this work, this is chosen as the characteristic load level corresponding to a 5 % probability of exceedance in 50 years (or 95 % probability of non-exceedance). The censored GEV distributions from Section 5.3.1 are evaluated at the 50th percentile value for the mean and the 95th percentile values to evaluate Equation (114).

When calculating the MLFs using Turkstra's rule the resulting values are provided in Table 21.

Table 21 - MLFs calculated by Turkstra's rule

Lane	Hog	Sag	Shear
1	1	1	1
2	0.69	0.64	0.65
3	0.65	0.62	0.63
4	0.62	0.61	0.63

These values compare favourably to the values calculated by the proposed new method given in Table 19 for the second lane. However, for the third and the fourth lanes Turkstra overestimates the contribution of these lanes to the critical elements. This is a result of the formulation of Turkstra's rule where all other load components other than the primary component are at their mean in a stationary process. When studied more closely, as per the method described in this chapter, it can be shown that the contribution from other components can be much less than the mean values and approach zero. Turkstra's rule should be used with caution in these cases. In practical situations it may not be so much of a problem as a transverse influence analysis typically shows very little contribution past the second lane.

5.6 Conclusions

This section describes a novel procedure for derivation of MLFs. The method requires either multiple lane WIM recordings or congested traffic data and calculates MLFs based on characteristic single lane, and concurrent multiple lane, load effects using EV theory. All possible permutations of lane combinations are considered which makes the method well suited to design codes where it is custom to arrange the traffic loads to create the largest load effect in any one member.

The results, based on South African WIM data, show that the MLFs reduce rapidly with an increase in the number of loaded lanes and becomes negligible for more than three lanes loaded. The factors are based on envelope values so that all possible scenarios are covered for a live load model in a design code. There is thus a potential to reduce the MLF values if specific load effects and span lengths are evaluated. This is also beneficial for the assessment of existing bridges where conservatism can lead to demolition or costly strengthening and repair. MLFs for separate load effects are provided.

A load model is developed in Chapter 4 for the heaviest loaded lane for South African conditions and is referred to as the reference lane model in the overall load model. The MLFs, independent of superstructure type, are intended to be applied sequentially to any further lanes causing the maximum adverse load effect for the member under consideration. Transverse stiffness and load distribution are accounted for in the structural analysis model.

The proposed method does not require knowledge of dependence or independence between lanes which greatly simplifies the calculation of MLFs. If some dependence is present in the WIM data, the proposed method still holds as the time history of random variables in different lanes are added to create new random variables of concurrent load effects.

Turkstra's rule is evaluated for verification of the proposed method. The values obtained compare favourably with the MLFs calculated with the method formulated here-in for the second lane, but it should be used with caution for more than two lanes.

The methodology presented in this chapter is based on characteristic values. As the method is dependent on the return period for determining fractiles, it is reasonable to believe that the MLFs could be different at SLS and ULS which have different return periods to characteristic. This is an interesting observation as values in current codes are not specified for any specific limit state or return period, although dependence exists.

6 Dynamic amplification

This work thus far examined static loading and proposes a new static model for the design of bridges based on WIM data. However, the vehicle-structure interaction must be accounted for and dynamic amplification of static loads is hence investigated in this chapter.

To determine the dynamic amplification factors for bridge loading codes, two issues need to be considered:

- True dynamic amplification which can be measured or calculated with a VBI model
- Artificial dynamic amplification to ensure the validity of the free flow assumption in the derivation of the static load model

It is not the intention of this thesis to determine the true dynamic amplification and congested traffic behaviour for South African bridges. In the absence of a fully probabilistic VBI study, this chapter evaluates the applicability of the ARCHES D10 study (González *et al.*, 2009) to South African bridges and discusses the implication thereof on the free flow assumption.

The partial content of this chapter has been published and presented at *SEMC 2019: The Seventh International Conference on Structural Engineering, Mechanics and Computation* under the title *Dynamic amplification factor for South African bridges* (Van der Spuy, Lenner & Meyer, 2019).

6.1 Factors that influence DAF

Caprani (2017) and Deng *et al.* (2015) provide a comprehensive description of the various factors that influence VBI. The factors are summarised here.

6.1.1 Condition of the road surface

Studies show that dynamic impact increases as the road surface condition decreases through deterioration of the asphalt seal layer. The relationship between dynamic impact and pavement roughness is well correlated. Regular pavement maintenance therefore has a beneficial effect on the dynamic amplification and is a cost effective way to improve bridge safety.

The condition of the bridge approaches and position of expansion joints have a major impact on dynamic amplification. Cai, Shi, Araujo & Chen (2007) showed that settlement of the bridge approaches, with or without approach slabs, has a significant impact on the dynamic response of a bridge once the vehicle reaches and crosses the deck.

It is reasonable to assume that the effect of road surface defects on dynamic amplification will be limited because severe defects will cause a road to be closed and maintenance to be performed (Ludescher & Bruhwiler, 2009).

6.1.2 Span length and Eigen frequencies

Generally dynamic amplification is larger for shorter spans (Li, 2005). An exception to this is when there is frequency matching between the applied load and the first Eigen frequency of the bridge. This may occur at any span length and lead to increased dynamic amplification, even for longer spans.

6.1.3 Bridge type

Most studies focus on I-girder bridges for short to medium span structures. The main parameter influence by bridge type is the ratio of the mass of the bridge to the mass of the crossing vehicles. Heavier decks have more inertia and experience less dynamic amplification than for lighter bridges carrying the same traffic.

6.1.4 Bridge material and damping

Dynamic amplification decreases with an increase in damping (Azimi, Galal & Pekau, 2011). As different materials have different damping properties it is logical to assume that the dynamic amplification will also be different. As an example, timber bridges have been found to have more damping than steel bridges and hence lower dynamic amplification. This trend is not the case with newer materials like fibre-reinforced polymers and more research is needed in this area.

6.1.5 Vehicle velocity

The influence of speed on dynamic amplification is controversial as results from studies report contradictory results. Chang & Lee (1994) and Smith (1988) find that the dynamic amplification increases with an increase in vehicle speed. Increased dynamic amplification can occur when the speed of the vehicle is such that the loading frequency matches the first natural frequency of the bridge (Caprani, 2017). Yang, Liao & Lin (1995) investigated simply supported and continuous beams and found that the dynamic amplification is proportional to vehicle speed at mid span. However, a study by Laman, Pechar & Boothby (1999) found no correlation between dynamic amplification and speed.

There is strong evidence that dynamic amplification changes with acceleration and deceleration. Specifically, deceleration has been shown to increase the dynamic amplification due to the change in load distribution between the front and back wheels of a vehicle which could increase vibrations. Law & Zhu (2005) show that very large dynamic amplification can exist for short braking rise times.

It is clear that, although speed has an influence on dynamic amplification, it is difficult to predict this relationship due to the large amount of variables involved.

6.1.6 Vehicle weight

It has widely been shown that dynamic amplification reduces with an increase in static vehicle weight (Huang, Wang & Shahawy, 1993; Broquet, Bailey, Fafard & Brühwiler, 2004; Ashebo, Chan & Yu, 2007; González *et al.*, 2009; Caprani, 2017). Light vehicles cause the highest dynamic amplification, but this is insignificant as they also cause the smallest static load effects and hence smaller overall loads (Kwasniewski, Wekezer, Roufa, Li, Ducher & Malachowski, 2006).

Due to lateral load distribution in bridge decks the transverse position of a vehicle induces static load effects in all other girders under positive influence, also inducing dynamic amplification in these girders. It was again found that the dynamic amplification in these girders reduces with an increase in static load (Deng *et al.*, 2015).

6.1.7 Number of axles

Although some design codes specify dynamic amplification as a function of the number of axles, little evidence exists to support this correlation. Michael Schwarz & Laman (2001) and Ashebo *et al.* (2007) both found that there is nearly no statistical relationship between number of axles and dynamic amplification. The correlation between number of axles and vehicle weight is poor as vehicles with the same number of axles can vary greatly in weight. The fact that dynamic amplification reduces with an increase in vehicle weight does therefore not imply a reduction in dynamic amplification with an increase in the number of axles.

6.1.8 Number of vehicles

As noted in 6.1.6 the dynamic amplification reduces as the static vehicle weight increases. It is thus reasonable to assume that the dynamic amplification for following multi vehicle events will be lower than for single vehicle events. This has been confirmed by various studies (Hwang & Nowak, 1991; Wang, Huang & Shahawy, 1992; Humar & Kashif, 1995; Ashebo *et al.*, 2007). At the same time vehicles travelling next to each other exert much higher dynamic amplification than vehicles that are following or staggered (Humar & Kashif, 1995).

6.1.9 Vehicle suspension type

Vehicle suspension can be characterised by axles consisting of springs with a certain stiffnesses and dampers with a certain damping coefficients. Kirkegaard, Nielsen & Envoldsen (1997) found that lower suspension stiffness results in lower dynamic amplification and that changes in the damping coefficients have a very small impact. Kwasniewski *et al.* (2006) confirm these findings by showing in field tests that high suspensions stiffnesses cause high dynamic amplification. The findings are further confirmed by Szurgott, Wekezer, Kwasniewski, Siervogel & Ansley (2011).

6.1.10 Dynamic amplification at ULS

Analytical and experimental studies of dynamic amplification are based on the assumption that the structures behave elastically. This is the case for SLS and fatigue limit states, but not for ULS. At ULS a bridge behaves plastically and dynamic amplification factors based on elastic theory are no longer valid. Ductile deformations in bending at ULS act as highly effective dampers and VBI hence is completely different at ULS compared to SLS. Plastic hinges act as effective energy dissipating mechanisms and it has been shown that the energy dissipation capacity of the non-linear domain is sufficient to dissipate all the energy associated with dynamic effects. Further to this, increased amplification due to resonance is not applicable at ULS. This is because resonance is typically caused by single vehicle crossings on medium and long span bridges which do not correspond to the load scenarios that cause the highest load effects (Bruhwiler & Herwig, 2008; Ludescher & Bruhwiler, 2009).

It is thus concluded that dynamic amplification at ULS is considerably less than at SLS for ductile failures. Bruhwiler & Herwig (2008) show that the DAF can be taken as 1.0 at ULS for ductile failures. For brittle failures with small deformations, for example shear, the energy dissipation is not as pronounced as for ductile failures with larger deformation capacity. For these cases Bruhwiler & Herwig propose a DAF which starts at 1.3 up to a 5 m span and reduces linearly to 1.0 for spans in excess of 40 m.

6.2 Suggested DAF for South African traffic based on ARCHES report

In the absence of a fully probabilistic VBI study, which is a research project in its own right, the adaptability of the ARCHES project (Assessment and Rehabilitation of Central European Highway Structures) is investigated here for local conditions. The ARCHES project was commissioned to reduce the gap between the standard of highway infrastructure in Central and Eastern European countries. More specifically, ARCHES report D10 deals with the dynamic amplification to be applied in the assessment of existing structures, thereby reducing the conservative values typically provided in design codes.

The study performed site measurements, as well as simulations using Auxerre data, together with finite element analyses and, for the specific cases analysed in the report, the authors show that the dynamic amplification can be as low as 6 % at characteristic load effect level (González *et al.*, 2009). This is determined using the ADR concept first introduced by Caprani (2005) and in Section 2.2. The study confirms findings that heavier vehicles cause lower dynamic amplification.

ARCHES makes recommendations for dynamic allowance for bridge assessment, but these can be extended to the design of new bridges as well. The proposed dynamic allowance is a function of the road surface roughness, as prescribed in ISO8608. For ISO road class A, a DAF of 1.3 is prescribed for a span length of 5 m and reduces linearly to 1.15 for a 15 m bridge. For ISO road class B, the DAF is

given as 1.4 for a span length of 5 m reducing to 1.2 at 15 m. Beyond 15 m the DAFs remain constant. These recommendations are valid for one and two lane bridges and for both bending and shear load effects.

Based on the following it is reasonable to assume that the ARCHES recommendation for a class B road, shown in Figure 55, can be adopted for South Africa:

- It is shown in Section 6.1.6 that heavier vehicles exhibit lower dynamic amplification than lighter vehicles. In South Africa it was shown that the vehicles that cause the largest load effects are seven axle vehicles with a mean weight of 530 kN. In Europe the largest load effects are caused by five axle vehicles with a mean weight of 410 kN (Lenner *et al.*, 2017). It is thus reasonable to believe that, based on vehicle weight, the dynamic amplification at characteristic levels in South Africa will be lower than in Europe
- Bridge construction materials and bridge types in South Africa are similar to those in Europe
- Pavements on South African highways, where the heaviest vehicles are measured, are generally well maintained and should, at least, conform to ISO road class B

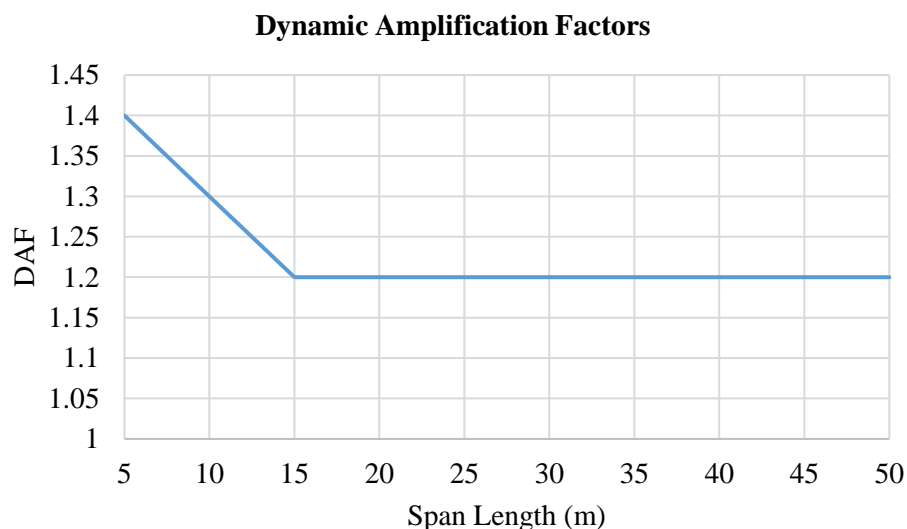


Figure 55 - Dynamic Amplification Factor based on ARCHES

It is important to note that ARCHES D-10 studies free flowing traffic only and does not consider that congested traffic may govern for some of the span lengths investigated.

6.3 Minimum DAF for the governing form of traffic

When deriving load models for bridge design, two traffic states need to be considered. Congested traffic is generally denser, but due to slow speeds, the dynamic interaction with a bridge is negligible. Free flowing traffic is less dense with vehicles spaced further apart, but for reasons discussed in Section 6.1,

significant VBI usually exists. It is the most unfavourable of these two cases that governs the calibration of a load model.

$$E_{govern} = \max(\hat{E}_s \times DAF, \hat{E}_{congested}) \quad (115)$$

where

E_{govern} is the largest LEs of static with DAF and congested traffic states

\hat{E}_s is the characteristic static LE from Equation (83)

$\hat{E}_{congested}$ is the characteristic congested LE

It has been shown that free flowing traffic with dynamic amplification governs on shorter spans with congested traffic being more onerous on longer spans (Caprani & OBrien, 2010a). The span length where the governing traffic state changes from free flow to congested is of particular interest and is influenced by the DAF that is allowed for. Various assumptions have been made regarding the maximum span length for which free flowing traffic governs the load effects. Miao & Chan (2002) investigated span lengths up to 40 m where Enright (2010) investigated span lengths up to 45 m. Jaeger & Bakht (1987) and Bakht & Jaeger (1990) assumed that moving vehicles govern up to a span length of 125 m.

This study is based on WIM and free flowing traffic, hence short to medium span lengths between 5 m and 50 m are investigated based on the assumption that free flowing traffic governs for these span lengths (Caprani & OBrien, 2010a). Work by Caprani (2013) and experiments by González *et al.* (2009) have shown that the high DAFs that are historically assumed in design codes may not necessarily be true. This implies that the transition span length may be much shorter than assumed by previous authors or in this study. The transition span length can be shifted to longer spans by artificially inflating the DAF. By dividing the congested model results by the free flow results, a required minimum DAF can be determined to ensure that free flow governs (Enright *et al.*, 2011). It is therefore critical that the DAF suggested for the load model is high enough to ensure that the load model derived on the free flowing assumption governs up to the assumed span length of 50 m.

In the absence of congested traffic LEs it may, in some cases, be necessary to artificially inflate the DAF from Section 6.2 to ensure that the governing free flow assumption still holds. This inflation process is described by Enright *et al.* (2011) and Caprani & OBrien (2008). The authors, while investigating various span lengths using the Eurocode Auxerre data, show that the effect is most pronounced in longer span lengths, where an artificial DAF of up to 1.6 is required for the hogging LE and a 50 m span length. This is based on measurements of five European countries, shown in Figure 56.

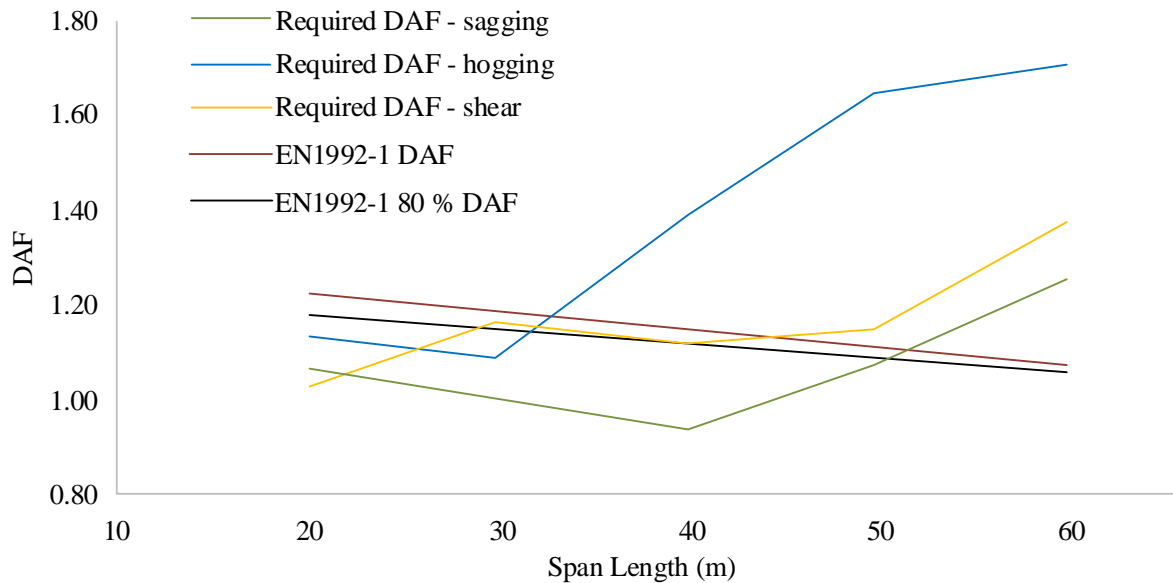


Figure 56 - Required DAF for European traffic

Without characteristic load effects for congested traffic in South Africa, it is not possible to determine if such artificial inflation is necessary for the span lengths considered in this work. However, it was shown in Section 4.3 that the suggested static load model is governed by hogging for a span length of 15 m. The model is conservative for all other span lengths for all load effects. Figure 57 shows a comparison between:

1. The new static characteristic model from Chapter 4, amplified by the DAFs from Section 6.2. This gives the total load effect predicted by the model (blue line)
2. The measured static characteristic load effects (orange line)
3. The required DAF for European traffic from Figure 55 (green line)

The comparison is for a single lane. The values have been normalised to the measured static characteristic load effects, \hat{E}_S , for easier interpretation.

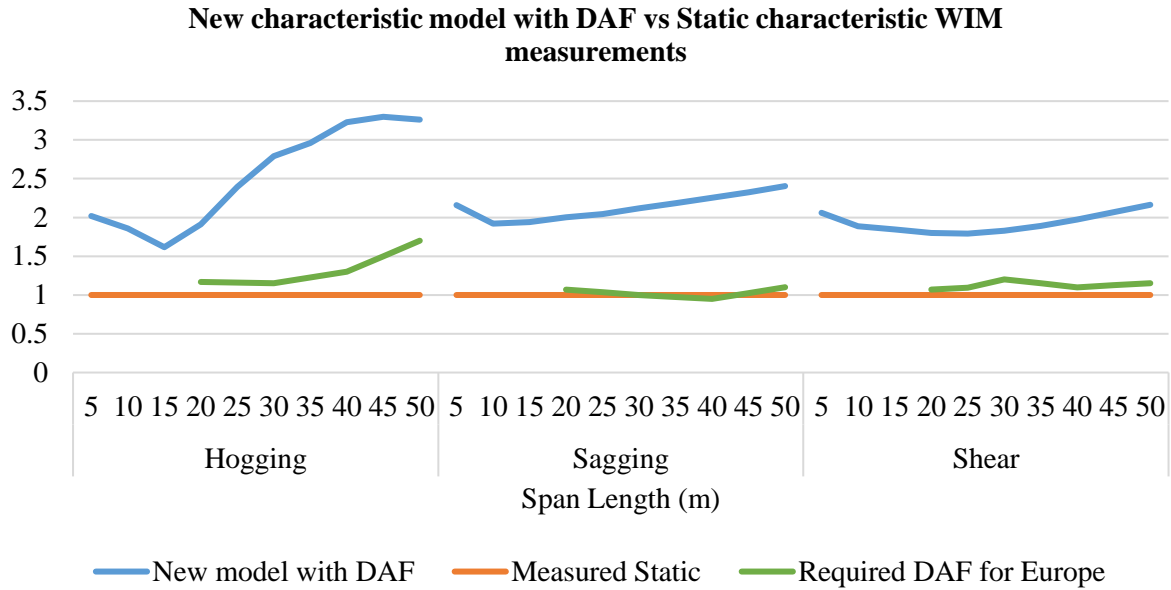


Figure 57 - New model with DAF compared to static measurements

The ratio of congested LEs to measured static characteristic free flow LEs need to exceed the ratios shown in Figure 57 for the new model with dynamic amplification for congested traffic to become governing. This is explained by Equations (116) and (117).

$$\frac{\hat{E}_{congested}}{\hat{E}_S} > \frac{New\ model + DAF}{\hat{E}_S} \quad (116)$$

$$\hat{E}_{congested} = \hat{E}_S \times Required\ DAF \quad (117)$$

For example, for hogging on a 50 m span length the new static model, multiplied by the suggested DAFs from ARCHES, exceeds the measured static load effects by a factor of $\frac{New\ model + DAF}{\hat{E}_S} = 3.3$. For congested traffic to govern in this case would require a ‘required DAF’ of at least 3.3. For the Eurocode Auxerre data Enright *et al.* (2011) and Caprani & O’Brien (2008) show that the ‘required DAF’ or $\frac{\hat{E}_{congested}}{\hat{E}_S} = 1.7$. This shows that the congested traffic LEs are only 1.7 times the measured static free-flow LEs. Equations (116) and (117) are thereby satisfied and the new model with the ARCHES DAFs exceeds the LEs caused by congested traffic.

The ratios from Figure 57 are well in excess of the required ratios for European traffic, shown in Figure 56 and Figure 57. This implies that, if the ratios between congested and measured free flow load effects are assumed similar than for Europe, then the DAFs from Section 6.2 can be used without the need for artificial inflation.

7 Partial factor calibration

For the implementation of the load model in a design code it is necessary to calibrate PFs for SLS and ULS. This section discusses the derivation of PFs for the live load model derived in this document. A background of the methodology is provided in Section 2.1.2. The PF investigation is split into the PFs for the static load effect, model uncertainty and statistical uncertainty. The expression for the total PF is shown in Equation (118)

$$\gamma_E = \gamma_{Ed,M} \gamma_{Ed,S} \gamma_e \quad (118)$$

where

γ_e is the reliability based PF

$\gamma_{Ed,M}$ is the model uncertainty PF

$\gamma_{Ed,S}$ is the statistical uncertainty PF

7.1 Reference period and design life

The design working life is an assumed period of time for which a structure is to be used for its intended purpose without any major repair being necessary. The concept of a reference period is therefore fundamentally different from the concept of design working life. This is especially relevant to bridges where the reference period for β and the design life are typically not equal, as shown in the following sections.

7.2 Design life for bridges

It is difficult to predict the exact working life of a structure as the behaviour of materials and structures over long periods of time can only be estimated. The idea of a design working life is still useful for:

- Choosing design loads and determining material property deterioration for reliability
- Comparing different structural solutions
- Determining strategies for maintenance and renovation

ISO2394, EN1990, TMH7 and Holicky (2009), however, specify a design working life of 100 years for large or major bridges. It is worth noting that a structure is not abandoned at the end of its service life, but rather that significant repairs or maintenance needs to be performed for the structure to remain serviceable. Routine maintenance should still be performed during the design working life. On a bridge, routine maintenance can include replacement of expansion joints, bearings and surfacing. Table 22 shows the design working life for various types of structures (ISO, 2015).

Table 22 - Design working life of structures according to ISO2394

Class	Notional design working life (years)	Examples
1	1 to 5	Temporary structures
2	25	Replacement structural parts e.g. gantry girders, bearings
3	50	Buildings and other common structures, other than those listed below
4	100 or more	Monumental buildings, and other special or important structures. Large bridges

SANS10160 does not cover bridges, but specifies a design working life of 100 years for structures described as

“Building structures designated as essential facilities such as having post-disaster functions (hospitals and communication centres, fire and rescue centres), having high consequences of failure or having another reason for an extended design working life”

Bridges are often essential to access essential facilities during natural disasters. Bridges which are on routes leading to hospitals are especially critical. Failure of a bridge can often disrupt economical activities on major routes and lead to large economic losses. An example of this is the collapse of the Morandi bridge in Genoa, Italy in 2018. Not only were 43 people killed and 600 left homeless, but the major route through Genoa was disrupted. The collapse of a pedestrian bridge at Florida International University in 2018 left six dead, eight injured and crushed eight vehicles. It is clear that bridge failures can have great consequences for human life and economical activities.

7.3 Target reliability

Based on the cost of safety measures and the consequences of failure, an acceptable, or target, maximum probability of failure within a certain reference period or lifetime can be decided upon to satisfy the minimum performance targets of a structure. This target probability of failure within a reference period is related to a target reliability index, β_T , through Equation (62).

ISO2394 (2015) specifies β_T values which are the minimum values needed to provide adequate safety based on a cost optimisation analysis to minimise the lifetime cost of a structure (Van Coile, Hopkin, Bisby & Caspeele, 2017). The procedure is described by Rackwitz (2000) and includes consideration of the construction cost, obsolescence cost, ULS failure cost and inspection and maintenance cost. Benefit from a structure’s existence, SLS failure cost and ageing failure cost are not included in the optimization. The values, shown in Table 23, are given lifetime values and not constrained to a reference period (ISO, 2015).

Table 23 - ISO2394 target beta values (lifetime values)

Relative cost of safety measures	Consequences of failure			
	small	some	moderate	great
High	0	A 1.5	2.3	B 3.1
Moderate	1.3	2.3	3.1	C 3.8
Low	2.3	3.1	3.8	4.3

A for SLS use 1.5 for irreversible and 0 for reversible

B for FLS use 2.3 to 3.1¹

C for ULS use 3.1, 3.8 and 4.3

EN1990 (CEN, 2002), influenced by ISO2394 (1998), defines consequence classes from CC1 to CC3, shown in Table 24. These are based on minimum requirements for human safety from an individual, economical, environmental or societal point of view when the expected number of fatalities are taken into account.

Table 24 – EN1990 consequence classes

Consequences Class	Description	Examples of buildings and civil engineering works
CC3	High consequence for loss of human life, or economic, social or environmental consequences very great	Grandstands, public buildings where consequences of failure are high (e.g. a concert hall)
CC2	Medium consequence for loss of human life, economic, social or environmental consequences considerable	Residential and office buildings, public buildings where consequences of failure are medium (e.g. an office building)
CC1	Low consequence for loss of human life, and economic, social or environmental consequences small or negligible	Agricultural buildings where people do not normally enter (e.g. storage buildings), greenhouses

CC2 β_T values are typically used in design of normal structures and are shown in Table 25. For highway bridges it is argued here that bridges fall into the CC3 class as there is a high consequence for the loss of human life and potentially large economic consequences of failure. The values are attached to a reference period of 1 or 50 years. It should be noted that 1 year and 50 year values correspond to the same reliability level.

¹ Depending on the possibility of inspection

Table 25 – EN1990 target beta values for CC2

Limit state	Target reliability index	
	1 year	50 year
Ultimate	4.7	3.8
Fatigue		1.5 to 3.8*
Serviceability (irreversible)	2.9	1.5

* Depends on degree of inspectability, reparability and damage tolerance

It is clear that the values of target reliabilities in EN1990 and ISO2394 (2015) are similar, but that they are based on different criteria. The former is based on the cost and consequence of the loss of human life, and the latter on a cost optimisation analysis to minimise the total lifetime cost of structures.

Dunaiski & Retief (2009) motivate a 50 year ULS β_T value for South Africa of 3.0 which is implemented in SANS10160-1 (SABS, 2018) for Reliability Class 2 (RC2). RC2 specifies moderate for loss of human life, economic, social or considerable environmental consequences. RC2 corresponds to CC2 in EN1990, although EN1990 specifies a higher value for β_T . The South African β_T of 3.0 is a significant deviation from the Eurocode value of 3.8, but that

- There is agreement with ASCE-7 procedures indicating that the suggested value of the reliability index is similar to international practice.
- There is rationale for the difference with the Eurocode in that the structures in more developed countries are potentially used for longer and require a longer design life and higher reliability.
- An upwards adjustment of the reliability level, for example in the Eurocode, is indicative of increasing conservatism
- There is no reason to believe that the current reliability implemented in SABS0160-1989 is not sufficient anymore

It was previously motivated that bridge failures may have high consequence for loss of human life and economic activities. It can therefore be concluded that the bridges considered in this work fall in the RC3 category in SANS10160 which carries a β_T of 3.5 for a 50 year reference period.

A β_T of 1.5 is specified for the irreversible SLS, similar to ISO2394 and EN1990. It is, however, unclear how this value was derived and values vary considerably according to cost parameters in the reliability optimisation (van Nierop, Viljoen & Lenner, 2017).

7.4 Target reliability for design of new bridges in South Africa

There is a disconnect between the reference period of 50 years in SANS10160 and the design working life for bridges of 100 years. This is in contrast with ISO2394 (2015) which provides lifetime β_T values.

Holicky (2011) describes the problem in greater detail. He shows that the optimum β_{opt} from a cost optimisation exercise is dependent on the cost ratio between the malfunctioning cost C_f and the cost per unit of the decision parameter C_1 , the discount rate q and the design working life n . The discount rate is used to determine the present value of future cash flow. However, it is shown in Figure 58 that n has an insignificant effect on β_{opt} between $n = 50$ and $n = 100$. The discount rate q has an insignificant influence on β_{opt} (Holicky, 2011) over the typical range of 0.01 – 0.05.

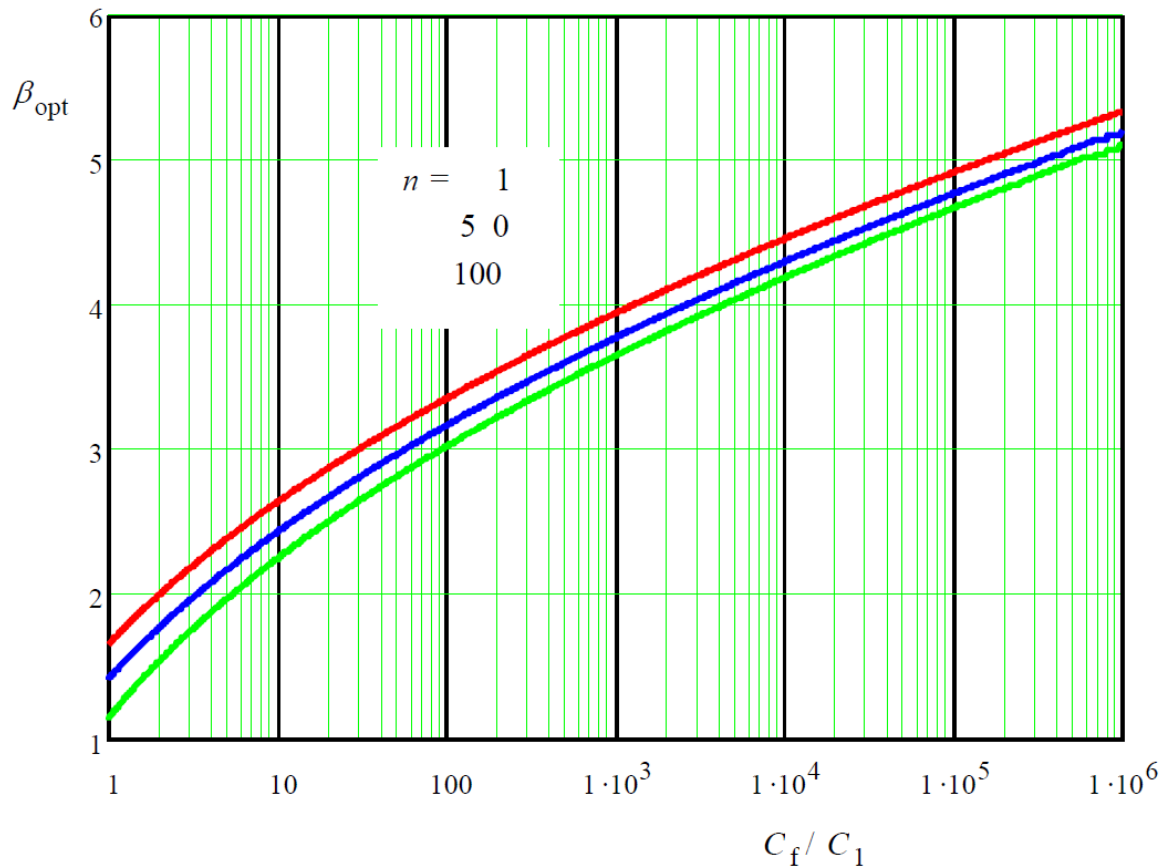


Figure 58 - Variation of reliability index with cost ratio for selected working life (Holicky, 2011)

The β_T can not be set to β_{opt} if the cost ratio is unknown. A conservative value for a lower bound of the design working life, for example 50 years, can be used in these cases for longer design working lives, in this case 100 years. It was argued in the previous section that a $\beta = 3.5$ should be used for bridges in South Africa, and according to the arguments presented in this section this value is applied for a design life of 100 years. It is therefore taken as a lifetime value. The $\beta = 1.5$ for SLS is adopted for the same reasons for 100 years.

7.5 Return periods and non-exceedance probabilities for SLS and ULS

In accordance with Equation (81) it is necessary to determine the design values for both SLS and ULS to arrive at a PF for each. The design values are fractiles determined according to Equation (79) which is a function of the sensitivity factor for loading and the respective β values for SLS and ULS.

The return period for characteristic loads, denoted here as T_C , is determined in Section 3.3.4 as 975.3 years. The FORM sensitivity factor for traffic load effects, α_E , is taken as -0.7 from Section 2.1.2.3 and used to calculate the return periods for SLS and ULS.

The return periods for ULS, T_{ULS} , and SLS, T_{SLS} , are found from Equation (55) using the β_T values from Section 7.4 above.

$$\begin{aligned} T_{SLS} &= \frac{t_{ref}}{p} = \frac{t_{ref}}{\phi(\alpha_E \beta_{T,SLS})} \\ &= \frac{100}{\phi(-0.7 \times 1.5)} = 435 \text{ years} \end{aligned}$$

$$\begin{aligned} T_{ULS} &= \frac{t_{ref}}{p} = \frac{t_{ref}}{\phi(\alpha_E \beta_{T,ULS})} \\ &= \frac{100}{\phi(-0.7 \times 3.5)} = 5040 \text{ years} \end{aligned}$$

It is worth noting that EN1990 specifies a $\beta_T = 3.8$ in 50 years, or in this case taken for 100 years. This translates to a $T_{ULS} = 16000$ years (Vrouwenvelder & Waarts, 1993), indicating that the return period at ULS of South African codes is significantly lower than for Europe, and the probabilities of failure are therefore higher.

If one is to compare the design values for SLS and ULS with the characteristic load effects determined in Section 3.3.7, it is imperative that the same censored GEV distributions are used for SLS and ULS that are used for the derivation of the characteristic load effects. The distributions are based on daily maximum values. To evaluate Equation (79) it is therefore necessary to determine the daily probabilities of non-exceedance, p , so that the quantiles can be evaluated at SLS, p_{SLS} , and ULS, p_{ULS} .

$$\begin{aligned} p_{ULS} &= 1 - \frac{1}{5040 \times 365} \\ p_{SLS} &= 1 - \frac{1}{435 \times 365} \end{aligned}$$

From Equation (96), the daily probability of non-exceedance for characteristic loads, p_C , is

$$p_C = 1 - \frac{1}{975 \times 365}$$

7.6 PFs for the static load effect

The method is first illustrated for the case of shear on a 30 m span length. Thereafter the design values and accompanying PFs for the static load are given for other load effects and span lengths.

7.6.1 MLE for evaluation of quantiles

The same censored GEV distributions that were fitted to determine characteristic load effects are used here. The design values are quantiles of these censored GEV distributions.

For the case of shear for a 30 m span length, the censored GEV fit in *R* produces the following location, scale and shape parameter estimates

$$\mu = 432.830$$

$$\sigma = 63.602$$

$$\xi = -0.101$$

leading to a quantile function, Q , from Equation (97)

$$Q(p; \mu, \sigma, \xi) = 432.830 + \frac{63.602}{-0.101} [(-\ln(p))^{0.101} - 1]$$

The quantile function, Q , is equivalent to the inverse CDF, F^{-1} , of the same distribution function, necessary to evaluate Equation (79). From this equation it follows that

$$V_{D,SLS} = Q(p_{SLS}; \mu, \sigma, \xi) = 875 \text{ kN}$$

$$V_C = Q(p_C; \mu, \sigma, \xi) = 890 \text{ kN}$$

$$V_{D,ULS} = Q(p_{ULS}; \mu, \sigma, \xi) = 917 \text{ kN}$$

From Table 9 the bound for this case is located at 1064 kN. From Equation (81) it follows that the reliability based partial factors for the static load, or the γ_e factors, are calculated as

$$\gamma_{e,SLS} = \frac{V_{D,SLS}}{V_C} = 0.983$$

$$\gamma_{e,ULS} = \frac{V_{D,ULS}}{V_C} = 1.030$$

These reliability based partial factors are close to 1.0, indicating small uncertainty in design values at the return periods considered. This is due to the negative shape factor of the GEV distribution, showing an underlying Weibull distribution which is heavy-tailed and bounded in the right tail. The bounds are

shown in Table 9. By using a bounded distribution for the load effects, with small uncertainty in the tail, may contradict the very purpose of a reliability calibration which is done to quantify uncertainties in design and characteristic values. This effect is quantified for other span lengths and load effects to investigate the implications thereof.

Table 26,

Table 27 and Table 28 show the reliability based partial factors for hogging, sagging and shear respectively for all span lengths considered in this study. The largest partial factor for ULS occurs for the sagging and hogging cases on a 25 m span with a value of 1.07. The largest partial factor for SLS occurs for the shear case on a 5 m and 10 m span with a value of 1.00. These values are, however, still close to 1.00, which practically implies similar partial factors for SLS and ULS for all load effects and span lengths. This is not intuitive, but a result of the large characteristic return period of 5 % in 50 years and the bounded nature of the underlying Weibull distribution (implied by the negative shape factor of the GEV distribution). It is shown in the following section that the dominant uncertainty is model uncertainty.

Table 26 - Reliability based partial factors for hogging

Hogging (kNm)					
Span length (m)	$M_{D,SLS}$	M_C	$M_{D,ULS}$	$\gamma_{e,SLS}$	$\gamma_{e,ULS}$
5	248	250	253	0.99	1.01
10	822	841	877	0.98	1.04
15	1743	1779	1845	0.98	1.04
20	2436	2490	2589	0.98	1.04
25	3052	3160	3379	0.97	1.07
30	3117	3178	3301	0.98	1.04
35	3840	3907	4043	0.98	1.04
40	4482	4547	4680	0.99	1.03
45	5458	5557	5758	0.98	1.04
50	6602	6749	7049	0.98	1.04

Table 27 - Reliability based partial factors for sagging

Sagging (kNm)					
Span length (m)	$M_{D,SLS}$	M_C	$M_{D,ULS}$	$\gamma_{e,SLS}$	$\gamma_{e,ULS}$
5	395	401	411	0.99	1.03
10	1248	1269	1307	0.98	1.03
15	2011	2034	2073	0.99	1.02
20	3233	3315	3472	0.98	1.05
25	4568	4729	5055	0.97	1.07
30	5922	6121	6527	0.97	1.07
35	7563	7808	8301	0.97	1.06
40	9180	9461	10021	0.97	1.06
45	11094	11459	12189	0.97	1.06
50	12665	13061	13851	0.97	1.06

Table 28 - Reliability based partial factors for shear

Shear (kN)					
Span length (m)	$V_{D,SLS}$	V_C	$V_{D,ULS}$	$\gamma_{e,SLS}$	$\gamma_{e,ULS}$
5	336	336	337	1.00	1.00
10	482	485	489	1.00	1.01
15	561	566	575	0.99	1.02
20	708	722	747	0.98	1.04
25	805	819	844	0.98	1.03
30	875	890	917	0.98	1.03
35	957	976	1013	0.98	1.04
40	1022	1045	1090	0.98	1.04
45	1098	1130	1194	0.97	1.06
50	1119	1151	1211	0.97	1.05

7.7 Time invariant uncertainties

Time invariant uncertainties mainly consist of model uncertainties and statistical uncertainties which do not vary with time.

7.7.1 Model uncertainty

Model uncertainty occurs when real phenomena are represented by simplified models (Melchers & Beck, 2018). When calculating load effects from traffic data, beams are idealised with constant stiffness, typically supported by pins. In reality the supports are spread over an area, which changes the moment distribution and shear forces. Supports can also provide some rotational restraint to a deck, which is not

accounted for when the idealised load effects are calculated. It often occurs in bridge decks that the stiffness varies along the length of the bridge. In statically indeterminate structures this can change the distribution of internal forces. These uncertainties are known as model uncertainties and are addressed here by applying an additional partial factor. Figure 59 illustrates the concept of model uncertainty where the load model underpredicts the real LEs experienced by a structure. The partial factor for model uncertainty compensates for this underprediction by applying an additional model uncertainty PF larger than 1.0.

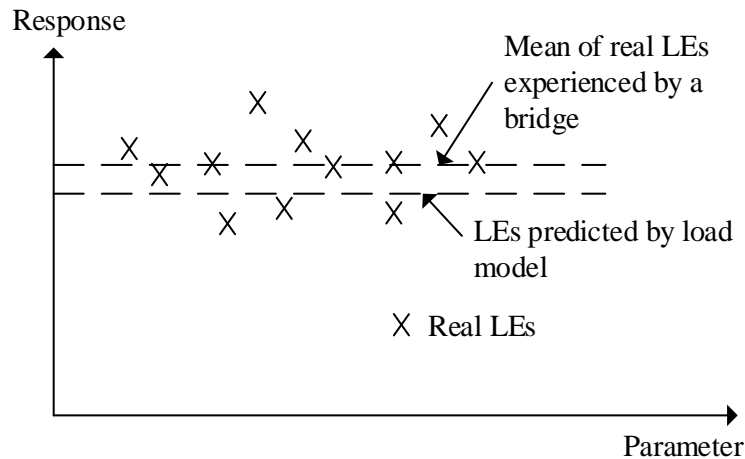


Figure 59 - Model uncertainty concept

Fib Bulletin 80 (fib, 2016) states that $\gamma_{Ed,M}$ is normally taken as 1.12 for unfavourable variable actions. This is a blanket value that covers the typical range of β values for limit state design. Alternatively it can be determined as a fractile of LN(1.0, 0.1) where the fractile is dependent on β . Sykora *et al.* (2013) recommend a value of 1.1.

7.7.2 Statistical uncertainty in parameter estimates

An additional uncertainty, $\gamma_{Ed,S}$, is added in this study to account for statistical uncertainty in the fitted distribution parameters. This uncertainty, termed the statistical uncertainty, is based on a method employed in wind engineering (Hong, Ye & Li, 2016) where samples are particularly small, leading to large uncertainty in distribution parameters. A PF is determined based on this statistical uncertainty, $\gamma_{Ed,S}$, which is multiplied by the reliability based PF and the model uncertainty PF.

A method of quantifying this uncertainty is presented here. Thereafter the statistical uncertainty is calculated for all load effects and span lengths to determine a partial factor due to this phenomenon.

7.7.2.1 Procedure

When fitting the censored GEV distributions in Section 7.6.1, the MLE method was used to calculate the location, shape and scale parameters. Due to the inherent uncertainty with small samples, there

necessarily exists uncertainty in the distribution parameters as well. These uncertainties influence the return period values for SLS, characteristic and ULS. To determine $\gamma_{Ed,S}$ the following procedure is followed:

1. For each load effect and span length, a censored GEV distribution is fitted to the tail using MLE and the location, shape and scale parameters for each is noted. The quantile is then evaluated at the desired return period
2. For each load effect and span length, use the fitted distribution and randomly sample v values
3. Fit a new censored GEV distribution to the sample from step 2 and evaluate the quantile at the desired return period
4. Repeat steps 2 and 3 V amount of times for each load effect and span length
5. Take the mean and standard deviation of the V quantiles determined in step 4

The standard deviation from step 5 is an indication of the statistical uncertainty. The mean from step 5 should be a nearly unbiased estimator of the quantile determined in step 1. As the quantiles are different for SLS and ULS, the statistical uncertainty will also be different with larger uncertainties at ULS due to the longer return period. As the V samples are sampled from the same parent distribution, the quantiles of the samples will be normally distributed according to the central limit theorem (Montgomery & Runger, 2010).

7.7.2.2 Results

In this section the procedure is first illustrated as an example for shear for a 30 m span length after which the results are given for the other load effects and span lengths.

Section 7.6.1 shows that the location, shape and scale parameters for shear on a 30 m span are equal to 432.830, -0.101 and 63.602 respectively, leading to a quantile function and inverse CDF of

$$Q(p; \mu, \sigma, \xi) = 432.830 + \frac{63.602}{-0.101} [(-\ln(p))^{0.101} - 1] \quad (119)$$

Serviceability limit state

By applying Equation (119), it is shown in Section 7.6.1 that the quantile at the SLS return period is equal to

$$Q(p_{SLS}) = 875 \text{ kN}$$

$v = 2537$ values are sampled $V = 1000$ times from Equation (119). The sample size of 2537 is chosen as it is equal to the number of daily maxima used in the analysis. A GEV distribution is fitted to each of the samples and evaluated at p_{SLS} as per Section 7.5. These quantiles are normally distributed as

shown by the Figure 60 which shows a histogram of the quantiles with a normal distribution fit. This is in accordance with the Central Limit Theorem (CLT) which states that the distribution of the samples must be normally distributed. The goodness of fit of the quantiles to a normal distribution is influenced by the number of samples, V . The size of the samples, v , influences the standard deviation of the quantiles. The larger v is, the smaller the standard deviation is and hence also the statistical uncertainty.

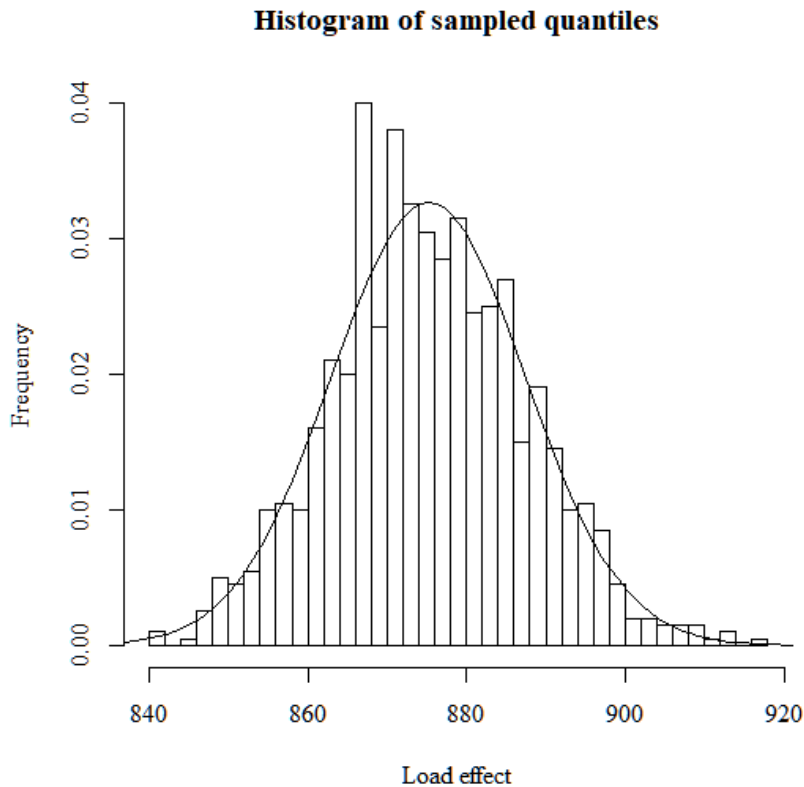


Figure 60 - Normal plots of the sample quantiles at SLS (shear in kN)

The mean and the standard deviation for the one thousand quantiles are

$$\mu_{Q,sampled} = 876 \text{ kN}$$

$$\sigma_{Q,sampled} = 13 \text{ kN}$$

$\mu_{Q,sampled}$ is nearly identical to $Q(p_{SLS})$, showing that it is an unbiased estimator.

The corresponding normal quantile function, evaluated at p_{SLS} , is given by

$$Q_{norm}(p; \mu, \sigma) = \mu_{Q,sampled} + \sigma_{Q,sampled} \phi^{-1}(p_{SLS}) \quad (120)$$

The partial factor for statistical uncertainty, $\gamma_{Ed,S}$, can now be determined as

$$\gamma_{Ed,S} = \frac{Q_{norm}(p_{SLS}; \mu_{Q,sampled}, \sigma_{Q,sampled})}{Q(p_{SLS})} \quad (121)$$

Therefore

$$\gamma_{Ed,S} = \frac{933}{876} = 1.065$$

Ultimate limit state

The same procedure is followed for ULS with the following result:

By applying equation (119) it is shown in Section 7.6.1 that the quantile at the ULS return period is equal to

$$Q(p_{ULS}) = 917 \text{ kN}$$

The mean and the standard deviation for the sampled quantiles are

$$\mu_{Q,sampled} = 917 \text{ kN}$$

$$\sigma_{Q,sampled} = 16 \text{ kN}$$

Once again, $\mu_{Q,sampled}$ is identical to $Q(p_{ULS})$, showing that it is an unbiased estimator. The sampled quantiles are again normally distributed as shown in Figure 61.

Histogram of sampled quantiles

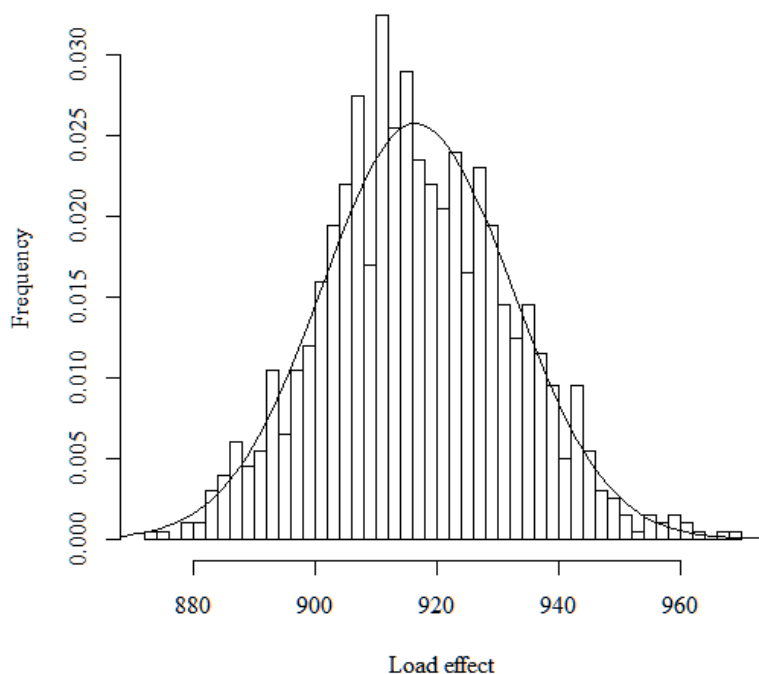


Figure 61 - Normal plots of the sample quantiles at ULS (shear in kN)

The corresponding normal quantile function, evaluated at p_{ULS} , is given by

$$Q_{norm}(p; \mu, \sigma) = \mu_{Q,sampled} + \sigma_{Q,sampled} \phi^{-1}(p_{ULS}) \quad (122)$$

The partial factor for statistical uncertainty, $\gamma_{Ed,S}$, can now be determined as

$$\gamma_{Ed,S} = \frac{Q_{norm}(p_{ULS}; \mu_{Q,sampled}, \sigma_{Q,sampled})}{Q(p_{ULS})} \quad (123)$$

Therefore

$$\gamma_{Ed,S} = \frac{987}{917} = 1.076$$

The statistical uncertainty is marginally more for ULS compared to SLS.

Other load effects and span lengths

Table 29 provides a summary of the statistical uncertainty PFs for all load effects and span lengths. The values vary between 2 % and 12 % which are not trivial and higher than the uncertainty for static LEs.

Table 29 - Statistical uncertainty partial factors for all load effects and span lengths

Span length (m)	Hogging		Sagging		Shear	
	$\gamma_{Ed,S,SLS}$	$\gamma_{Ed,S,ULS}$	$\gamma_{Ed,S,SLS}$	$\gamma_{Ed,S,ULS}$	$\gamma_{Ed,S,SLS}$	$\gamma_{Ed,S,ULS}$
5	1.04	1.05	1.04	1.06	1.04	1.04
10	1.07	1.09	1.06	1.07	1.05	1.06
15	1.07	1.09	1.05	1.06	1.05	1.06
20	1.08	1.09	1.08	1.10	1.07	1.08
25	1.04	1.04	1.04	1.04	1.06	1.07
30	1.02	1.02	1.04	1.04	1.07	1.08
35	1.02	1.02	1.09	1.12	1.07	1.09
40	1.02	1.02	1.08	1.11	1.07	1.09
45	1.02	1.02	1.09	1.12	1.08	1.11
50	1.02	1.03	1.08	1.11	1.09	1.11

7.8 Partial load factors

The final partial factors are a product of the reliability based partial factor, the model uncertainty partial factor and the statistical uncertainty partial factor. Table 30, Table 31 and Table 32 provide the final partial factors, γ_E , for all load effects, span lengths and limit states.

Table 30 - Partial factors for hogging

Hogging								
Span Length (m)	SLS				ULS			
	γ_e	$\gamma_{Ed,M}$	$\gamma_{Ed,S}$	γ_E	γ_e	$\gamma_{Ed,M}$	$\gamma_{Ed,S}$	γ_E
5	0.99	1.12	1.04	1.15	1.01	1.12	1.05	1.19
10	0.98	1.12	1.07	1.17	1.04	1.12	1.09	1.27
15	0.98	1.12	1.07	1.18	1.04	1.12	1.09	1.27
20	0.98	1.12	1.08	1.18	1.04	1.12	1.09	1.28
25	0.97	1.12	1.04	1.12	1.07	1.12	1.04	1.25
30	0.98	1.12	1.02	1.12	1.04	1.12	1.02	1.19
35	0.98	1.12	1.02	1.12	1.04	1.12	1.02	1.18
40	0.99	1.12	1.02	1.12	1.03	1.12	1.02	1.17
45	0.98	1.12	1.02	1.12	1.04	1.12	1.02	1.19
50	0.98	1.12	1.02	1.12	1.04	1.12	1.03	1.20

Table 31 - Partial factors for sagging

Sagging								
Span Length (m)	SLS				ULS			
	γ_e	$\gamma_{Ed,M}$	$\gamma_{Ed,S}$	γ_E	γ_e	$\gamma_{Ed,M}$	$\gamma_{Ed,S}$	γ_E
5	0.99	1.12	1.04	1.15	1.03	1.12	1.06	1.22
10	0.98	1.12	1.06	1.17	1.03	1.12	1.07	1.24
15	0.99	1.12	1.05	1.17	1.02	1.12	1.06	1.21
20	0.98	1.12	1.08	1.18	1.05	1.12	1.10	1.29
25	0.97	1.12	1.04	1.12	1.07	1.12	1.04	1.25
30	0.97	1.12	1.04	1.12	1.07	1.12	1.04	1.24
35	0.97	1.12	1.09	1.18	1.06	1.12	1.12	1.33
40	0.97	1.12	1.08	1.18	1.06	1.12	1.11	1.31
45	0.97	1.12	1.09	1.18	1.06	1.12	1.12	1.33
50	0.97	1.12	1.08	1.18	1.06	1.12	1.11	1.32

Table 32 - Partial factors for shear

Shear								
Span Length (m)	SLS				ULS			
	γ_e	$\gamma_{Ed,M}$	$\gamma_{Ed,S}$	γ_E	γ_e	$\gamma_{Ed,M}$	$\gamma_{Ed,S}$	γ_E
5	1.00	1.12	1.04	1.16	1.00	1.12	1.04	1.17
10	1.00	1.12	1.05	1.18	1.01	1.12	1.06	1.20
15	0.99	1.12	1.05	1.17	1.02	1.12	1.06	1.21
20	0.98	1.12	1.07	1.17	1.04	1.12	1.08	1.25
25	0.98	1.12	1.06	1.17	1.03	1.12	1.07	1.24
30	0.98	1.12	1.07	1.17	1.03	1.12	1.08	1.24
35	0.98	1.12	1.07	1.17	1.04	1.12	1.09	1.26
40	0.98	1.12	1.07	1.18	1.04	1.12	1.09	1.27
45	0.97	1.12	1.08	1.18	1.06	1.12	1.11	1.31
50	0.97	1.12	1.09	1.18	1.05	1.12	1.11	1.31

7.9 Discussion of partial factors

This chapter derives the PFs for all span lengths and load effects, based on the literature described in Section 2.1.2. The partial factors are based on the same censored GEV distributions fitted in Section 3.3.7 for consistency, and extrapolated to the return periods corresponding to the reliability indices described in this chapter. By using the 100 year reliability indices of 1.5 for SLS and 3.5 for ULS for South Africa, the corresponding return periods were shown to be 435 and 5040 years respectively for a 100 year reference period. With a shorter SLS return period compared to characteristic, it is found that the reliability based partial factors for SLS are smaller than one, but close to unity for both SLS and ULS. After multiplication with the model and statistical uncertainty partial factors, the final partial factors, γ_E , fall between 1.12 – 1.18 for SLS and 1.16 – 1.33 for ULS. It is therefore suggested to adopt a PF of 1.2 for SLS and 1.35 for ULS.

It is further worth noting that the partial factors at ULS, although close to the PF of the Eurocode, are smaller than those typically used in other codes. The lower values for the ULS partial factors are governed by the small reliability based partial factors, γ_e , which are influenced by the characteristic load effects and β_T and the bounded nature of the Weibull distribution (negative shape factor for the GEV distribution). EN1991-2 and AASHTO are both based on a normal distribution for load effects which is unbounded and leads to larger PFs. For traffic loads, the characteristic return period is located at a probability of non-exceedance of close to 1.0. This leads to very small differences in load effects between characteristic and ULS return periods, especially for bounded distributions, and is indicative of very small time variant uncertainty. The premise of a 5 % probability of exceedance in a 50 year reference period for characteristic load effects should perhaps be adjusted to a shorter return period. A possible solution is to tie the characteristic return period to the SLS return period to yield a PF of 1.0,

with model and statistical uncertainties included. This can lead to a more conventional PF at ULS. For a probability of non-exceedance of the static LE of practically 1.0 at ULS, it implies that the β value can be increased substantially with a negligible increase in the PF. This implies that a higher reliability can be achieved for a small increase in design load effects at ULS and a small additional monetary investment. With low uncertainty in the loading indicated by the small reliability based PFs, the assumed FORM sensitivity factor $\alpha_E = -0.7$ for the load should be revisited, as it is possible that the resistance contributes more to the uncertainty than assumed. If the characteristic load effects are at the bound of the fitted distributions, then $\alpha_E \approx 0.0$ for the static load and $\alpha_R \approx 1.0$, which implies that almost all of the reliability based uncertainty in the calibration is located in the resistance. This would not be the case for the unbounded Gumbel distribution.

A procedure was introduced to assess statistical uncertainty in the estimation of the distribution parameters. As this study is based on seven years of well cleaned and calibrated WIM data it was expected that the influence of statistical uncertainty would be small. The largest statistical uncertainty of 11.7 % was found for sagging at ULS for a 45 m span length which is not trivial. As the statistical uncertainty is a function of the return period, the values differ for SLS and ULS.

8 Model validation

This section serves as a parametric validation of the proposed model. It presents the characteristic and ULS load effects caused by the load model proposed herein for varying deck widths and span lengths. The deck width is varied from 3 m to 9 m, as the notional lane width is taken as 3 m. Deck widths more than 9 m are not analysed here as the traffic loading beyond the third lane is typically negligible to the critical elements. This leads to a maximum of three loaded lanes, for which MLFs are calculated in Chapter 5. Span lengths are varied from 10 m to 50 m in 10 m increments, which fall within the bounds of this study.

The load effects from the proposed model are compared to characteristic and ULS TMH7 NA, NB and NC loading and LM1 of the Eurocode. The load effects that are calculated are sagging and shear on single span structures and hogging on two span structures. These are the same LEs investigated in the derivation of the model.

8.1 Summary of load model

The new static load model derived in this work is shown in Figure 62. It is important to note that different permutations of the lane numbers must be investigated to obtain the maximum effect on any element. For the derivation of the MLFs only four lanes of concurrent WIM data was available and therefore the load model only extends to four lanes, although the contribution of the fourth lane to the characteristic global LEs is negligible. From the negligible MLF for the fourth lane, it is concluded that any loading due to the derived load model in a fourth lane or more will not have a noteworthy effect on the critical characteristic and ULS LEs in any elements.

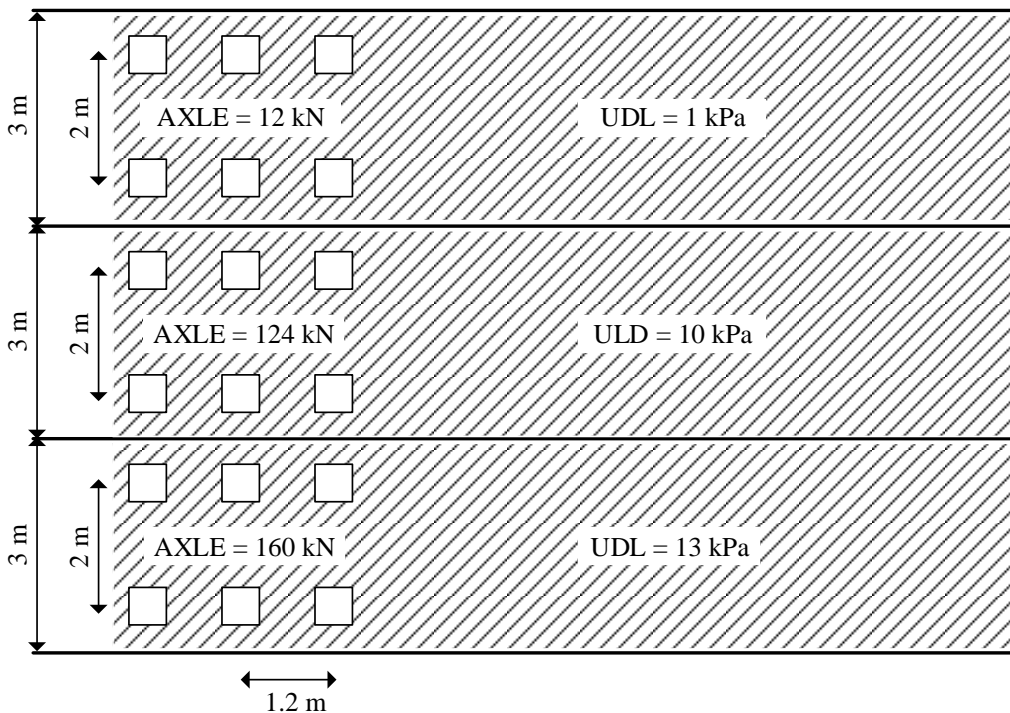


Figure 62 - New static load model

Beyond the static load model shown in Figure 62, dynamic amplification is applied in accordance with Chapter 6 which is based on recommendations from the ARCHES study. It specifies a DAF of 1.4 for a 5 m span, reducing to 1.2 for a 15 m span and remaining constant thereafter. The DAF is applied to the total LE. ULS partial factors are taken as 1.65 for NA loading and 1.32 for both NB and NC loading (Committee of State Road Authorities, 1981). For the new model, the ULS PF is rounded to 1.35. The PF for LM1 is taken as 1.35.

8.2 Analysis type and deck configurations

In this example, the maximum load effects in critical elements are determined, rather than global load effects. In bridge design it is typical to perform a grillage analysis to determine the forces in the main structural members. This analysis model takes into account transverse stiffness of the bridge deck to apportion the applied live loads to the individual longitudinal beams. A typical deck slab thickness of 200 mm is used, supported by concrete I-beams, spaced at 3 m c/c. Transverse distribution of the loads is achieved through transverse bending in the slab only, as no crossbeams are provided. Figure 63 shows the grillage model for a single span structure. The loads shown are applied in such a manner to obtain the maximum sagging moment in girder 1. To obtain the maximum shear forces the axle loads are moved adjacent to the supports.

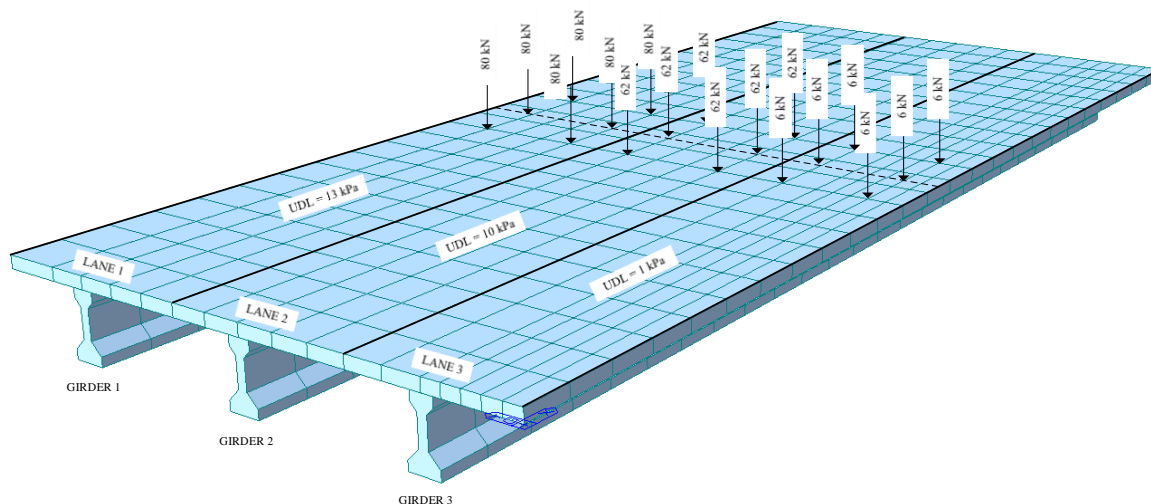


Figure 63 – Typical single span grillage model for sagging and shear

Figure 64 shows the grillage model for a two span structure with supports indicated in green. The loads shown are applied in such a manner to obtain the maximum hogging moment in girder 1. The centroid of the axle loads is placed at 60 % of the span length where the influence line peaks for hogging on a two span structure.

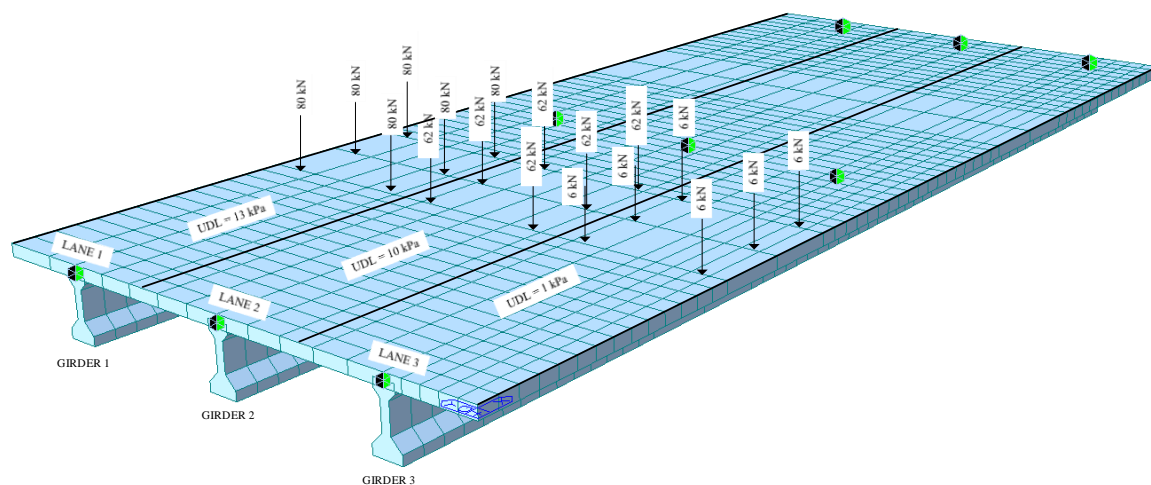


Figure 64 - Typical two span grillage model for hogging

The loading for TMH7 NA, NB and NC and Eurocode LM1 is applied in MIDAS Civil automatically.

8.3 Results

The results from the grillage analyses are presented here, first by fixing the deck width and varying the span length, and then by fixing the span length and varying the deck width. Results are presented in tabular form for characteristic and ULS load effects. Figures referred to in this section are located in the Appendix. Note that ‘NM’ refers to the New Model.

8.3.1 Fixed deck width - Characteristic

In this section characteristic load effects for deck widths of 3 m, 6 m and 9 m are investigated for varying span lengths.

8.3.1.1 9m Deck width - Characteristic

Table 33 and Figure 65 show the results for a 9 m deck width for span lengths varying from 10 m to 50 m. The deck consists of three traffic lanes with three supporting girders and is symmetrical along its centreline, therefore only the results of girders 1 and 2 are presented here. For girder 2 the loads are arranged such that the heaviest loading is in lane 2.

Table 33 – Results table for 9 m deck width

Sagging										
Span Length	Girder 1					Girder 2				
	NM	LM1	NA	NB	NC	NM	LM1	NA	NB	NC
10	1802	1521	765	1177	486	1538	1287	675	791	777
20	4276	3363	2284	2813	2301	3125	2617	2074	1580	2445
30	7116	5260	4190	4117	5298	5592	4349	3917	2651	5303
40	10409	7386	6397	5241	9446	8795	6412	6124	3787	9407
50	14313	9815	8930	6321	14170	12692	8872	8666	4911	14131
Shear										
Span Length	Girder 1					Girder 2				
	NM	LM1	NA	NB	NC	NM	LM1	NA	NB	NC
10	594	595	293	525	181	544	546	256	372	317
20	824	788	509	813	434	654	677	426	488	548
30	1070	936	678	916	684	797	774	548	533	785
40	1308	1068	820	973	933	938	858	649	555	1025
50	1544	1193	948	1008	1132	1078	936	739	570	1217
Hogging										
Span Length	Girder 1					Girder 2				
	NM	LM1	NA	NB	NC	NM	LM1	NA	NB	NC
10	1147	872	582	1110	454	1076	663	506	811	853
20	3234	2208	1864	2051	2155	2418	1689	1498	1234	2791
30	6152	3825	3378	2750	4391	4401	2855	2753	1514	4913
40	9683	5719	5090	3294	6488	7127	4330	4269	1820	6838
50	13830	7903	7004	3691	8461	10586	6190	6087	2170	8726

The new model exceeds NA, NB and NC for all load effects and span lengths for girder 1. NC exceeds the new model for hogging up to a span length of 40 m in girder 2 as well as sagging and shear above 30 m span length. This is expected, as the NC load is placed directly above girder 2 on a 9 m wide deck.

It is concluded that, when compared to the new model, TMH7 is conservative for girders close to centre of a deck above a 30 m span length, where the effect of NC loading is most pronounced. For all edge beams, TMH7 is unconservative when compared to the new model. The new model exceeds NA, NB and Eurocode LM1 loading for all load effects and span lengths, although for shear in girder 2 the difference between the new model and LM1 is marginal for shorter spans.

8.3.1.2 6m Deck width - Characteristic

Table 34 and Figure 66 show the results for a 6 m deck width for span lengths varying from 10 m to 50 m. The deck consists of two traffic lanes with two supporting girders and is symmetrical along its centreline, therefore only the results of girder 1 are presented here.

Table 34 – Results table for 6 m deck width

Sagging					
Span Length	Girder 1				
	NM	LM1	NA	NB	NC
10	1777	1516	738	1044	891
20	4404	3446	2303	2708	3548
30	8056	5631	4448	4336	7677
40	12688	8215	7008	5991	14177
50	18308	11217	9951	7661	21262
Shear					
Span Length	Girder 1				
	NM	LM1	NA	NB	NC
10	586	595	278	468	341
20	800	774	467	764	710
30	1037	926	640	867	1079
40	1268	1067	803	920	1447
50	1411	1203	945	956	1742
Hogging					
Span Length	Girder 1				
	NM	LM1	NA	NB	NC
10	1137	850	558	974	888
20	3176	2237	1852	1907	3563
30	6250	3982	3480	2657	6827
40	10290	6097	5340	3309	9929
50	15306	8604	7450	3886	12845

The new model exceeds NA, NB and LM1 loading for all load effects and span lengths. NC loading exceeds the new model for sagging and shear on span lengths in excess of 30 m and for hogging on all span lengths.

8.3.1.3 3m Deck width - Characteristic

Table 35 and Figure 67 show the results for a 3 m deck width for span lengths varying from 10 m to 50 m. The deck consists of one traffic lane with one supporting girder. Although the results are given here, it is not likely that a bridge deck width of only 3 m will be constructed.

Table 35 – Results table for 3 m deck width

Sagging					
Span Length	Girder 1				
	NM	LM1	NA	NB	NC
10	1804	1557	741	1378	1070
20	4684	3940	2358	4174	4258
30	8807	6946	4824	7566	9573
40	14036	10596	8112	10952	17013
50	20370	14883	11940	14347	25465
Shear					
Span Length	Girder 1				
	NM	LM1	NA	NB	NC
10	587	585	277	553	409
20	806	791	465	933	852
30	1047	929	646	1082	1294
40	1283	1072	823	1159	1736
50	1517	1212	974	1206	2090
Hogging					
Span Length	Girder 1				
	NM	LM1	NA	NB	NC
10	1143	852	555	1223	1066
20	3265	2376	1960	2600	4277
30	6572	4526	3889	3896	8197
40	10982	7310	6176	5114	11917
50	16497	10730	8807	6372	15416

As expected for a narrow bridge, NC exceeds the new model for sagging and hogging for most span lengths. The new model only exceeds NC for shear on short span lengths. For these narrow bridges, NC could be retained, but as it exceeds the measured values and a bridge width of only 3 m being unlikely, a complication of this sort should be avoided.

8.3.2 Fixed span lengths - Characteristic

By rearranging the data from Table 33, Table 34 and Table 35, the width can be varied by keeping the span length constant. This provides an indication of the influence of deck width on load effects.

8.3.2.1 10 m Span length - Characteristic

Figure 68 shows the results for a 10 m span length, by varying the deck width from 3 m to 9 m. Only the edge beam, which is critical, is considered. As NC loading is restricted to the centre of the deck, its effect on girder 1 diminishes as the deck width increases. The new model exceeds NA, NB, NC and LM1 for all deck widths and load effects. LM1 exceeds NA, NB and NC for sagging and shear, but is exceeded by NB and NC in hogging.

8.3.2.2 20m Span length - Characteristic

Figure 69 shows the results for a 20 m span length, by varying the deck width from 3 m to 9 m. The new model exceeds NA, NB, NC and LM1 for all deck widths and load effects, except for hogging and shear on narrower deck widths.

8.3.2.3 30 m Span length - Characteristic

Figure 70 shows the results for a 30 m span length, by varying the deck width from 3 m to 9 m. The new model exceeds NA, NB and LM1 for all load effects and deck widths. NC exceeds the new model for narrower deck widths.

8.3.2.4 40 m Span length - Characteristic

Figure 71 shows the results for a 40 m span length, by varying the deck width from 3 m to 9 m. The new model exceeds NA, NB and LM1 for all load effects and deck widths. NC exceeds the new model for narrower deck widths. LM1 generally exceeds NA and NB loading.

8.3.2.5 50 m Span length - Characteristic

Figure 72 shows the results for a 50 m span length, by varying the deck width from 3 m to 9 m. The new model exceeds NA, NB and LM1 for all load effects and deck widths and for both girders. NC exceeds the new model for all deck widths, except for wider decks in shear where the new model exceeds NC.

8.3.3 Characteristic summary

The findings from the analysis of characteristic loads are:

- The new model exceeds NA, NB and LM1 for all span lengths, deck widths and load effects

- For spans shorter than 20 m the new model governs, but as the span length increases NC becomes more pronounced
- NC is most critical on narrow decks due to the geometric limitation on its location

8.3.4 Fixed deck width - ULS

In this section ULS load effects for deck widths of 3 m, 6 m and 9 m are investigated at varying span lengths.

8.3.4.1 9 m Deck width - ULS

Table 36 and Figure 73 show the results for a 9 m deck width for span lengths varying from 10 m to 50 m. The new model exceeds NA, NB, NC and LM1 loading for girder 1 for all span lengths and load effect. For girder 2 NC generally governs due to its proximity to the centreline of the deck.

Table 36 – Results table for 9 m deck width

Sagging										
Span Length	Girder 1					Girder 2				
	NM	LM1	NA	NB	NC	NM	LM1	NA	NB	NC
10	2433	2054	1262	1554	641	1923	1737	1114	1045	1025
20	5773	4540	3769	3713	3037	3906	3533	3422	2086	3228
30	9607	7101	6914	5435	6993	6990	5871	6464	3499	7000
40	14052	9971	10555	6918	12468	10994	8656	10105	4999	12417
50	19323	13250	14734	8344	18704	15865	11977	14298	6483	18652
Shear										
Span Length	Girder 1					Girder 2				
	NM	LM1	NA	NB	NC	NM	LM1	NA	NB	NC
10	802	803	483	693	239	680	737	422	491	418
20	1112	1064	840	1074	573	818	914	703	645	723
30	1445	1264	1119	1208	903	996	1045	905	704	1036
40	1766	1442	1353	1284	1231	1173	1158	1072	733	1353
50	2084	1610	1564	1330	1494	1348	1264	1219	752	1607
Hogging										
Span Length	Girder 1					Girder 2				
	NM	LM1	NA	NB	NC	NM	LM1	NA	NB	NC
10	1548	1177	959	1465	599	1345	895	834	1070	1126
20	4366	2980	3076	2707	2844	3023	2281	2472	1629	3684
30	8305	5163	5573	3630	5796	5501	3854	4542	1999	6485
40	13072	7720	8399	4348	8564	8909	5846	7044	2402	9026
50	18671	10669	11557	4872	11169	13233	8356	10044	2865	11518

8.3.4.2 6 m Deck width - ULS

Table 37 and Figure 74 show the results for a 6 m deck width for span lengths varying from 10 m to 50 m. The new model exceeds NA, NB and LM1, except for NC which generally exceeds the new model on longer spans.

Table 37 – Results table for 6 m deck width

Sagging					
Span Length	Girder 1				
	NM	LM1	NA	NB	NC
10	2399	2047	1217	1377	1176
20	5945	4652	3800	3574	4684
30	10876	7601	7339	5723	10133
40	17129	11090	11564	7908	18713
50	24716	15143	16419	10113	28066
Shear					
Span Length	Girder 1				
	NM	LM1	NA	NB	NC
10	791	804	458	618	450
20	1080	1044	770	1009	937
30	1400	1250	1056	1144	1424
40	1712	1440	1324	1214	1911
50	1905	1624	1560	1262	2300
Hogging					
Span Length	Girder 1				
	NM	LM1	NA	NB	NC
10	1535	1148	921	1286	1172
20	4288	3020	3056	2517	4704
30	8438	5375	5742	3508	9012
40	13892	8231	8811	4368	13106
50	20663	11616	12292	5130	16955

8.3.4.3 3 m Deck width - ULS

Table 38 and Figure 75 show the results for a 3 m deck width for span lengths varying from 10 m to 50 m. NC exceeds the new model for all span lengths and load effects, except shear on shorter spans and hogging on longer spans. The new model exceeds NA, NB and LM1 for all load effects and span lengths. For these narrow bridges, NC could be retained, but as it exceeds the measured values and a bridge width of only 3 m being unlikely, a complication of this sort should be avoided.

Table 38 – Results table for 3 m deck width

Sagging					
Span Length	Girder 1				
	NM	LM1	NA	NB	NC
10	2435	2102	1223	1819	1412
20	6323	5320	3890	5510	5621
30	11889	9376	7960	9988	12636
40	18949	14304	13384	14457	22457
50	27500	20092	19702	18938	33614
Shear					
Span Length	Girder 1				
	NM	LM1	NA	NB	NC
10	792	790	456	729	540
20	1088	1068	767	1232	1124
30	1413	1254	1066	1429	1708
40	1732	1447	1358	1530	2292
50	2048	1636	1608	1591	2759
Hogging					
Span Length	Girder 1				
	NM	LM1	NA	NB	NC
10	1543	1150	916	1614	1407
20	4408	3207	3234	3432	5646
30	8872	6110	6416	5143	10819
40	14826	9869	10191	6750	15730
50	22271	14485	14531	8411	20349

8.3.5 Fixed span lengths - ULS

By rearranging the data from Table 36, Table 37 and Table 38, the width is varied by keeping the span length constant. This provides an indication of the influence of deck width on load effects.

8.3.5.1 10 m Span length - ULS

Figure 76 shows the results for a 10 m span length, by varying the deck width from 3 m to 9 m. The new model exceeds NA, NB, NC and LM1 for hogging, sagging and shear for all deck widths, except for hogging on very narrow decks.

8.3.5.2 20 m Span length - ULS

Figure 77 shows the results for a 20 m span length, by varying the deck width from 3 m to 9 m. The new model exceeds NA, NB, NC and LM1 in sagging for all deck widths. For narrow deck widths in shear and hogging NC exceeds the new model due to the location of the load application with relation to girder 1. This effect diminishes as the width increases.

8.3.5.3 30 m Span length - ULS

Figure 78 shows the results for a 30 m span length, by varying the deck width from 3 m to 9 m. NC generally exceeds the new model for deck widths below 9 m for all load effects in girder 1. This effect diminishes as the width of the deck increases and for 9 m decks the new model exceeds NC.

8.3.5.4 40 m Span length - ULS

Figure 79 shows the results for a 40 m span length, by varying the deck width from 3 m to 9 m. For widths below 9 m the new model is exceeded by NC loading for all load effects. The new model exceeds NC and governs for a deck width of 9 m.

8.3.5.5 50 m Span length - ULS

Figure 80 shows the results for a 50 m span length, by varying the deck width from 3 m to 9 m. NC exceeds the new model for deck widths less than 9 m in sagging and shear. For hogging the new model exceeds NA, NB, NC and LM1 for all widths.

8.3.6 ULS summary

A typical bridge configuration is investigated for TMH7 loads and the new model at ULS. The PFs at ULS are different for TMH7 compared to the new model, and different cases are critical when compared to characteristic loads only.

The findings from the analysis of ULS loads are that the new model governs for all load effects and span lengths except

- Narrow bridge decks where NC typically governs for span lengths of 20 m and longer for all load effects
- The internal girder for a 9 m deck width where NC generally governs
- This implies that NC could be retained for these situations, but keeping in mind that NC significantly exceeds the measured load effects, this would be overly conservative
- It is further unlikely to encounter NC loading on narrow bridges, as NC is classified as super loading

8.4 Example discussion

The results consistently show that NC exceeds the new model for characteristic and ULS loads on narrow decks. The significance thereof is questionable as it is unlikely to get NC, which is classified as super loading, on narrow bridges. For decks of 9 m wide, where NC loads could be encountered, the new model exceeds the load effects in the edge girder for all span lengths at characteristic level and ULS. Even though NA loading carries a higher PF when compared to the new model, the new model still exceeds NA for all load effects, span lengths and deck widths for characteristic and ULS.

The new model therefore exceeds NA, NB and NC loading for all load effects, span lengths and reasonable deck widths at characteristic and ULS levels except for longer spans where NC governs on narrow decks. For this specific example, it proves to be a worthy replacement for TMH7, and it addresses the concerns about the current load model raised in Chapters 1 and 3. These concerns did not include deficiencies for longer spans, but due to the desire to derive a model which is easier to apply than the current model, conservatism also occurs in longer spans. However, Lenner (2014) showed that the LEs on longer spans are dominated by dead loads and hence it is concluded that some conservatism on the side of the traffic loading is not unreasonable. Given the increase in the legal limits for GVW and axle loads and the increase in traffic volumes since the publication of TMH7 it is reasonable to expect larger load effects from the new model.

A comparison between the new model and LM1 of the Eurocode shows that the new model exceeds LM1 in all cases. This is not surprising when it is considered that the legal limit for GVW in South Africa is 40 % higher than in Europe. This is compounded by the high amount of overloading in South Africa, shown in Chapter 3, and the inclusion of potential permit vehicles in the new model. LM1 only considers normal traffic and allows for special vehicles in LM3.

9 Conclusions

This study set out to derive a new traffic load model for the design of short to medium span highway bridges in South Africa, with novel contributions to the field of bridge traffic loading. The current code for bridge design in South Africa, TMH7, was published in 1981 and was shown by previous studies, and by this study, to be deficient at characteristic level. This is especially true for shorter spans, but it should be kept in mind that the characteristic return period used in TMH7 and that used for the new model are probably different as TMH7 does not give any indication of the levels of safety used to calibrate the code for SLS, characteristic or ULS. It was therefore not clear whether the code is still providing the necessary safety margins, but a comparison was performed in Chapter 8 which is discussed later.

A station along the N3 at Roosboom was chosen for this study, as seven years of traffic from 2010 to 2016 were available and the station is located along the heaviest loaded route in the country. A comparison was performed with other WIM stations to confirm this premise. WIM sensors in South Africa have an accuracy of 0.01 s. An accuracy of at least 0.02 s is necessary to obtain an accurate spatial arrangement of vehicles, especially for multiple presence where accurate transverse positioning is required. The model developed herein is valid for span lengths up to 50 m as free flowing traffic load effects exceed congested load effects within this bound. To ensure that this condition holds, DAFs are investigated in Chapter 6 which indicate that typical DAFs from ARCHES are high enough for the free flowing assumption to be true when European and South African traffic are compared.

In contrast with the current TMH7 and the concept of aggregate loaded length, it is typical in international codes to provide a load model for the slow, or heavy, lane which is reduced transversely by MLFs. A slow lane model was derived based on the seven years of data at the Roosboom station. A study of the vehicle type distribution showed that the tail of the GVW distribution for South Africa is governed by seven axle vehicles. In Europe the GVW tail is dominated by five axle trucks. The GVW limit in South Africa is 40 % higher than the general limit of 40 t in Europe, but the local vehicles have more axles and hence smaller axle loads. It was therefore expected that the UDL component of the load model would be larger than that for the Eurocode LM1, but that the axle load would be lower. Through the use of censored GEV distributions the daily maxima load effects were extrapolated to the characteristic return period of 975.3 years corresponding to a 5 % probability of exceedance in a 50 year reference period as per EN1991-2. The characteristic axle load amounted to 158 kN, which was used to calculate a UDL to replicate the characteristic load effects. The axle load was rounded to 160 kN, resulting in a slow lane load model with a UDL of 13 kPa and a triple axle of 160 kN, spaced at 1.2 m, shown in Figure 62. The critical LE for the calibration of the new model is hogging on a 15 m span length. As the model should cover all load effects, it necessarily implies that the model is conservative for other load effects and span lengths. The effect is most pronounced on span lengths approaching 50

m, but as it is shown the LEs on these span lengths are dominated by selfweight. The conservatism of the traffic load model on longer spans is therefore accepted at this stage. The UDL can be refined through a future probabilistic cost optimization study to reduce the conservatism on longer spans.

To distribute the slow lane model transversely, MLFs were derived which take into account the reduced probability of simultaneous heavy vehicles in adjacent lanes. A novel method was presented in this work in which multiple lane WIM data is used to calculate MLF factors. This is the main contribution of this work to the state of the art. The maximum load effects are caused by the heaviest vehicles and it was therefore necessary to calculate MLFs based on concurrent occurrence of very heavy vehicles at characteristic level. The monthly maxima for all load effects and span lengths were calculated for all lanes and extrapolated to the characteristic return period. The next step was to calculate a time history of load effects for each lane and all span lengths at 0.02 s resolution. The high resolution was necessary to accurately determine the spatial arrangement of vehicles in adjacent lanes. By studying concurrent characteristic load effects in adjacent lanes it was possible to determine MLFs, first for two lanes loaded, then three lanes loaded and finally for four lanes loaded. The transverse distribution from the superstructure takes place at the analysis step and does not have an effect on the MLFs. The resulting MLFs are 1.0; 0.78; 0.07; 0, indicating that the fourth lane does not contribute to the global LE at characteristic level. It should be noted, however, that these MLFs are based on a single station only and that more stations need to be evaluated as more multiple lane data becomes available. Turkstra's rule was used to verify the proposed method and produced favourable results for the first two lanes. Beyond the second lane, Turkstra continues to assume that LEs are at their mean and hence the MLFs do not reduce substantially as the number of lanes increases. MLF values in other international norms show this same trend, but by studying the concurrent LEs more closely with multiple lane WIM data at characteristic level, the method proposed in this work provides a rational approach which is based on measured data.

Vehicles that travel at speed, referred to as free flowing traffic, cause additional forces on bridge decks due to dynamic interaction between the vehicles and a bridge (VBI). To account for these increased loads, it is typical to multiply the static loads by a DAF which is defined as the ratio between the total load effect to the static load effect. It was not the aim of this study to do an in depth investigation of dynamic amplification for South African bridges and it was therefore decided to adopt the values given in the ARCHES report D10, which was based on European traffic.

Partial factors were calibrated in accordance with structural reliability theory. Target 50 year β values were taken in accordance with the South African building design codes, which are based on extensive studies of historical practice in South Africa. For ULS the 50 year β value was taken as 3.5 and for SLS as 1.5. The SLS value is in accordance with international standards. As a bridge has a service life of 100 years, the β values were taken as lifetime values as per ISO2394 (2015). For traffic loads, the

characteristic return period is located at a probability of non-exceedance close to 1.0. This leads to very small differences in load effects between characteristic and ULS return periods, especially for bounded Weibull (GEV with negative shape) distributions. The premise of a 5 % probability of exceedance in a 50 year reference period for characteristic load effects should perhaps be adjusted to a shorter return period. A possible solution is to tie the characteristic return period to the SLS return period to yield a PF of 1.0, with uncertainties included. This will lead to a more conventional PF at ULS. With low uncertainty indicated by the reliability based PFs, the assumed FORM sensitivity factor $\alpha_E = -0.7$ for the load should be revisited, as it is possible that the resistance is contributing more to the uncertainty than assumed. If the SLS, characteristic and ULS fractiles are located at the distribution bound, then there is almost no uncertainty in the load ($\alpha_E = 0.0$), and all the uncertainty in the reliability calibration is in the resistance ($\alpha_R = 1.0$). The model uncertainty partial factor was taken as 1.12 in accordance with the fib Bulletin 80. A new approach was introduced to address statistical uncertainty in the estimation of distribution parameters. Final partial factors are a function of reliability based partial factors, model uncertainty and statistical uncertainty. These amount to 1.18 for SLS and 1.33 for ULS. Chapter 8 presents a worked example for a typical bridge configuration for various widths and span lengths and considered both characteristic loads and ULS. The findings from this section are that the new model is almost always critical for deck widths of 9 m, for all span lengths and load effects. For deck widths less than 9 m NC is often critical. NC loading is positioned centrally on a bridge deck without any other loading present. It is therefore plausible that it would cause the highest load effects on internal girders. It is, however, unlikely to encounter NB or NC on narrow bridges as they are referred to abnormal and super loading respectively. The new model generally exceeds NA and NB loading at characteristic and ULS level. The results are valid for this specific example and further studies need to be performed to determine the implications on other deck types.

A comparison between the new model and LM1 of the Eurocode shows that the new model exceeds LM1 in all cases. This is not surprising when it is considered that the legal limit for GVW in South Africa is 40 % higher than in Europe, together with a higher frequency of heavy vehicles and a higher percentage of loaded vehicles. This is compounded by the high amount of overloading in South Africa, shown in Chapter 3, and the inclusion of potential permit vehicles in the new model. LM1 only considers normal traffic and allows for special vehicles in LM3.

In summary, this document presents a new traffic load model for bridge design in South Africa. Although this is a perfectly valid load model given all the discussed constraints and assumptions made, further refinements are suggested in the next section.

10 Recommendations for future research

This study has identified the need for further research, not only for South African bridge traffic loading, but for bridge traffic loading in general as well. These needs are discussed here.

- The load model derived herein is based on the assumption that free flowing traffic conditions govern up to span lengths of 50 m. Although this is a reasonable assumption if the DAFs are sufficiently high, a study must be performed to derive a congested traffic load model for longer spans where DAFs are no longer applicable. In combination with this work, it will give an indication of where the threshold lies between free flowing traffic with DAF and congested traffic without DAF.
- A comprehensive probabilistic study must be performed to determine the true dynamic amplification for South African traffic and bridges. A study of this nature is likely to indicate that current DAFs applied in codes worldwide are conservative and can lead to expensive designs and less expensive strengthening of existing bridges. An accurate DAF is also necessary to determine the true threshold between free flowing and congested traffic.
- The load model presented here has been calibrated for global effects. A simple load model needs to be derived for local effects at expansion joints, over supports and cantilevers of box girder bridges.
- The Roosboom station used in this study provided seven years of WIM data. Some stations in South Africa have measured considerably shorter periods, implying more statistical uncertainty at longer return periods. The effect of this statistical uncertainty should be quantified and compared to other stations with longer measurement periods. Aggregating WIM stations should also be investigated.
- In bridge traffic loading, many assumptions have been made regarding the length of the distribution tails for extrapolation. By increasing the length of a tail until the statistical uncertainty reaches acceptable levels will give an indication of an adequate tail length and should be investigated. The tail should also not be too long such that it violates the *iid* assumption if EV theory is used.
- On longer bridge lengths the load effects are often governed by more than one heavy vehicle in a lane on a bridge simultaneously. These vehicles are mostly distributed differently in terms of the load effects that they cause and should be separated before extrapolating to longer return periods. A statistical investigation should be performed to decouple these load effects and then adding them together at the return level.
- A load model for fatigue must be derived.

- The MLFs are based on a single site on the N1 at Kilner Park, measuring four lanes of traffic. The processing of concurrent loading in four lanes at 0.02 s time increments make the process computationally expensive if daily maxima are considered. In this study, monthly maxima were used to reduce the computational effort, but as computational capacity increases with time, it would be worthwhile to perform the same exercise for daily maxima as well. To gain further confidence in the MLFs it is recommended to investigate more measuring stations as they become available. As the MLFs are dependent on the return period it is a possibility to derive separate MLFs for SLS and ULS.
- PFs have been calibrated based on a 5 % probability of exceedance in 50 years for characteristic loads, equating to a return period of 975.3 years. As this characteristic return period is already high, indicating considerable safety at characteristic level, the resulting partial factors are small. Further to this the load effects are bounded which leads to small PFs if the SLS, characteristic and ULS quantiles are close to the bound. The return period for SLS is lower than that for characteristic, leading to reliability based partial factors smaller than 1.0. The characteristic return period should be reinvestigated. A possibility is to tie the SLS return period to the characteristic return period which will result in a more conventional PF for SLS.
- The partial factors for loading at SLS and ULS indicate small uncertainty in the load effects. This could imply that the resistance is contributing more to the reliability than assumed and the continued validity of $\alpha_E = -0.7$ should be investigated.

Appendix

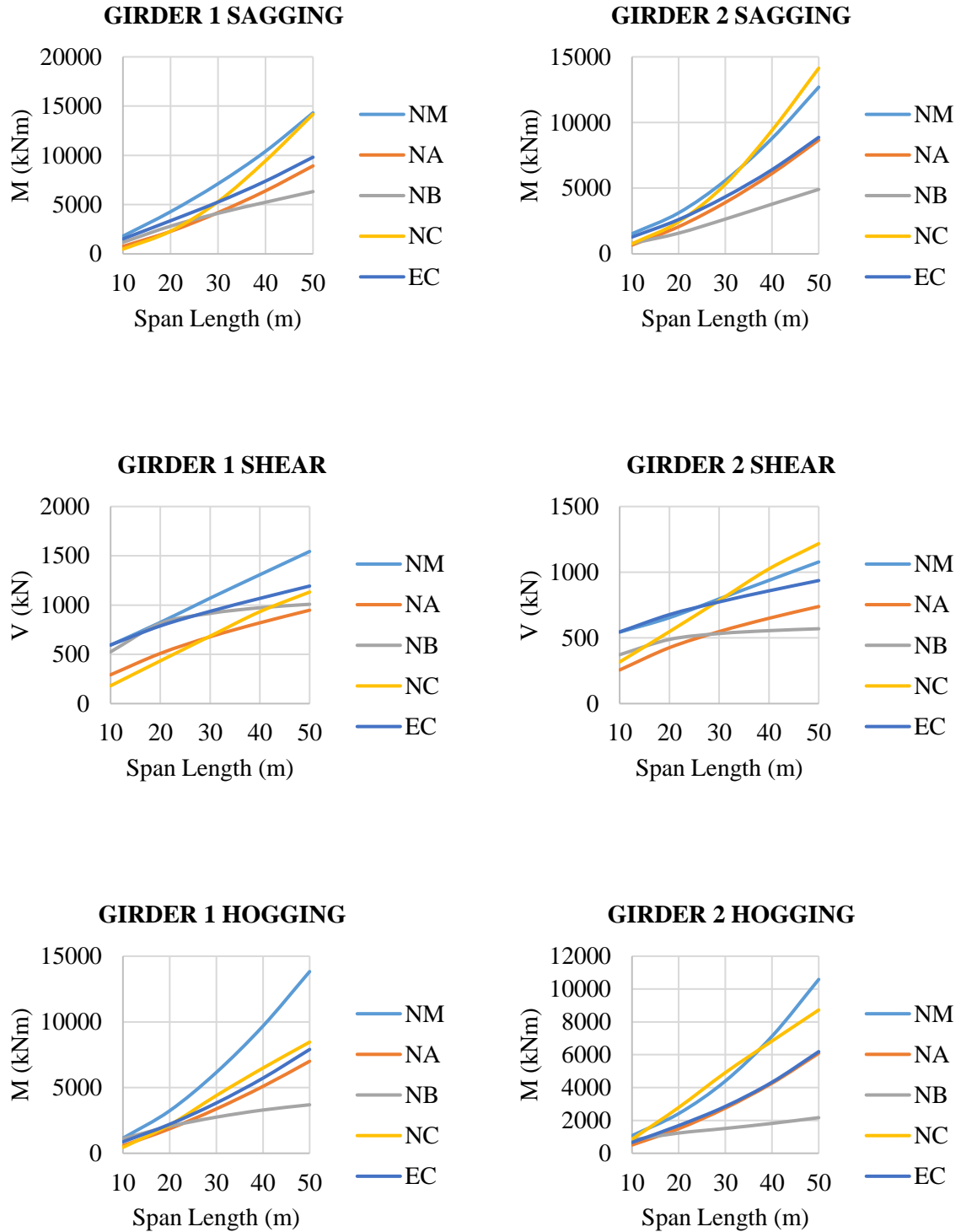


Figure 65 - Graphical results for 9 m deck width characteristic

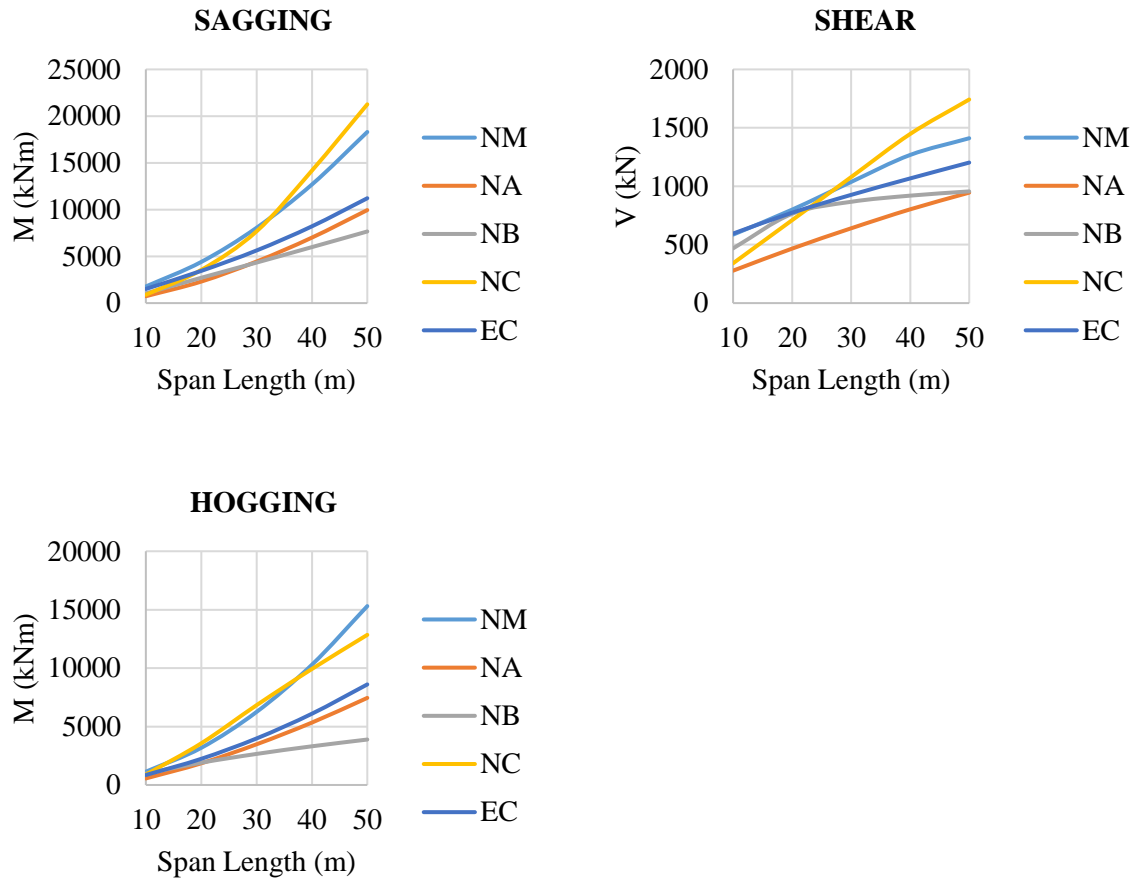


Figure 66 - Graphical results for 6 m deck width characteristic

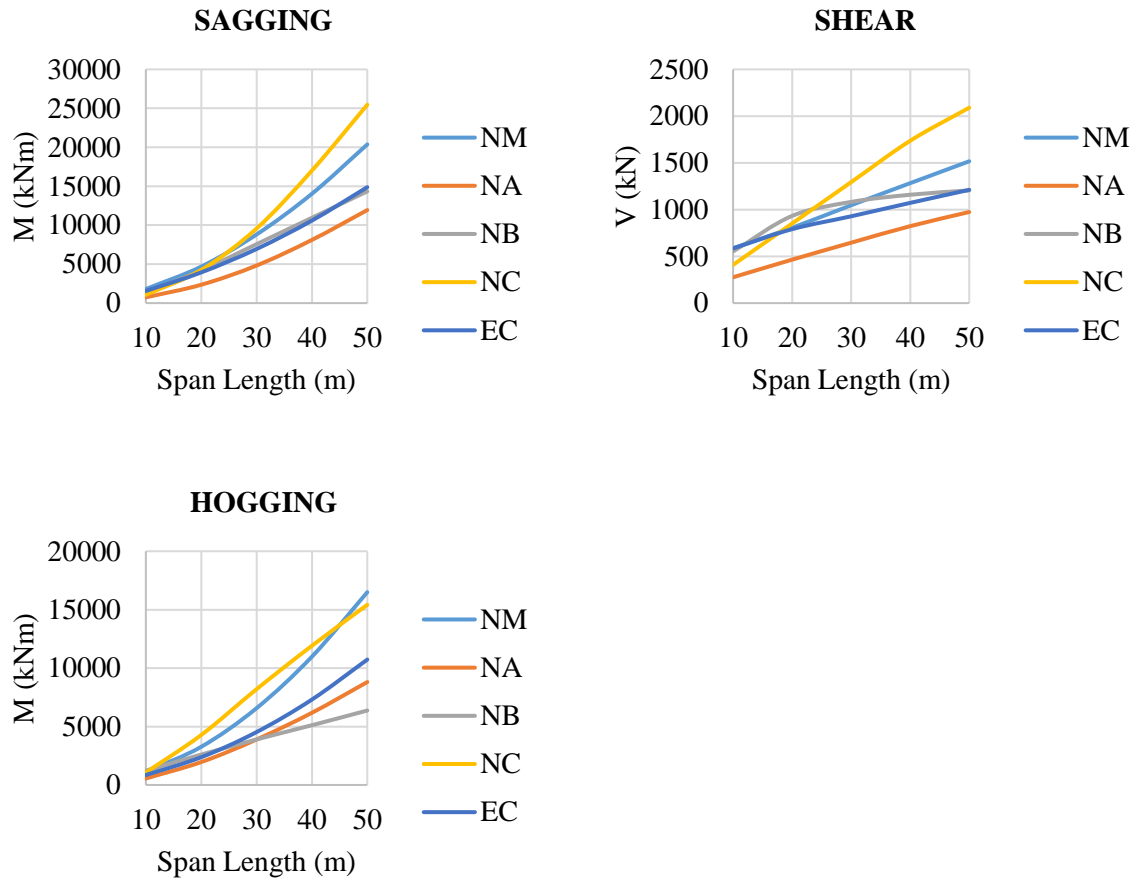


Figure 67 - Graphical results for 3 m deck width characteristic

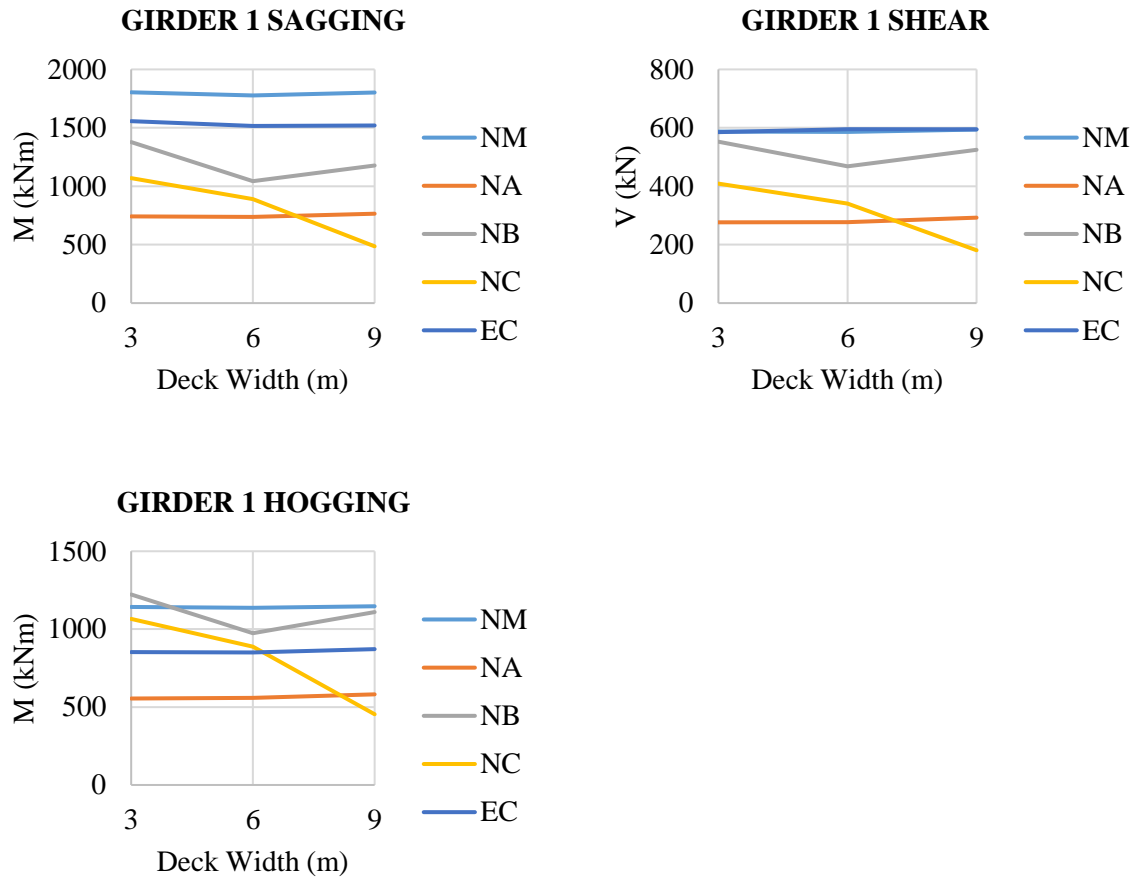


Figure 68 - Graphical results for 10 m span length characteristic

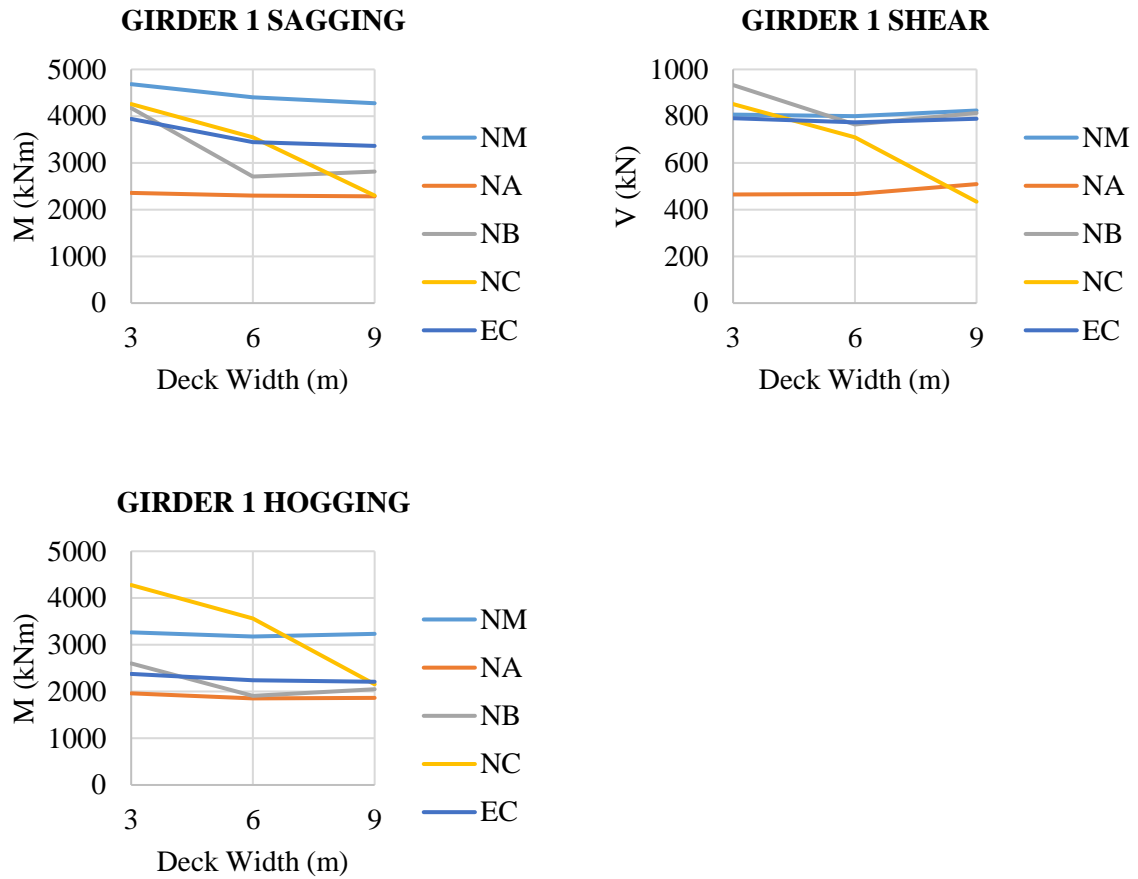


Figure 69 - Graphical results for 20 m span length characteristic

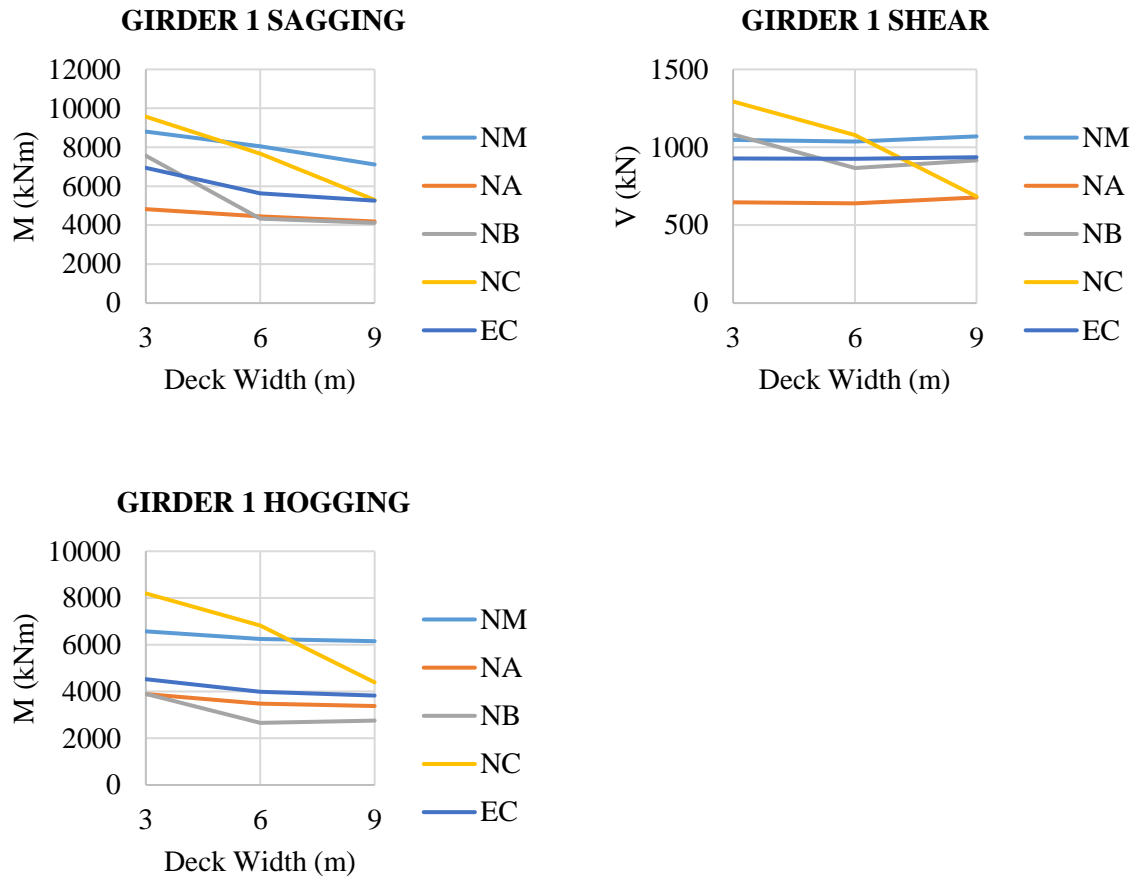


Figure 70 - Graphical results for 30 m span length characteristic

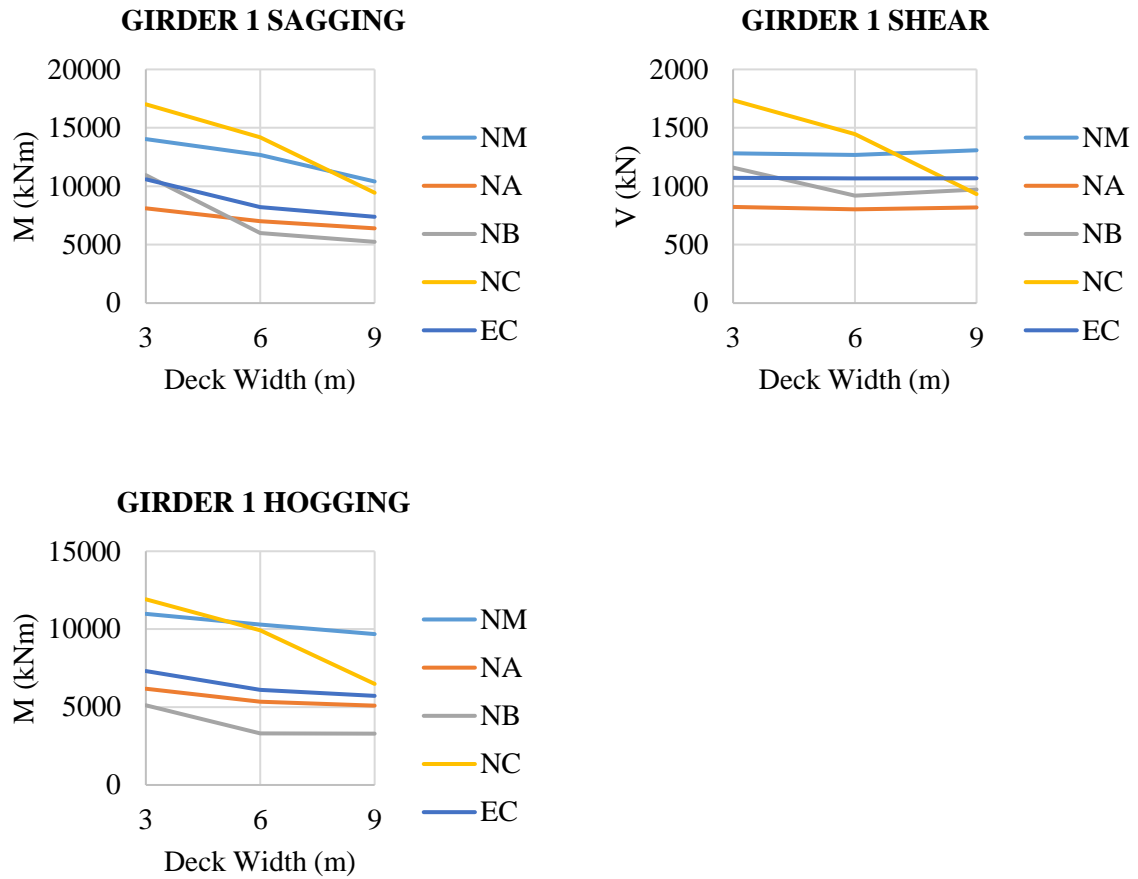


Figure 71 - Graphical results for 40 m span length characteristic

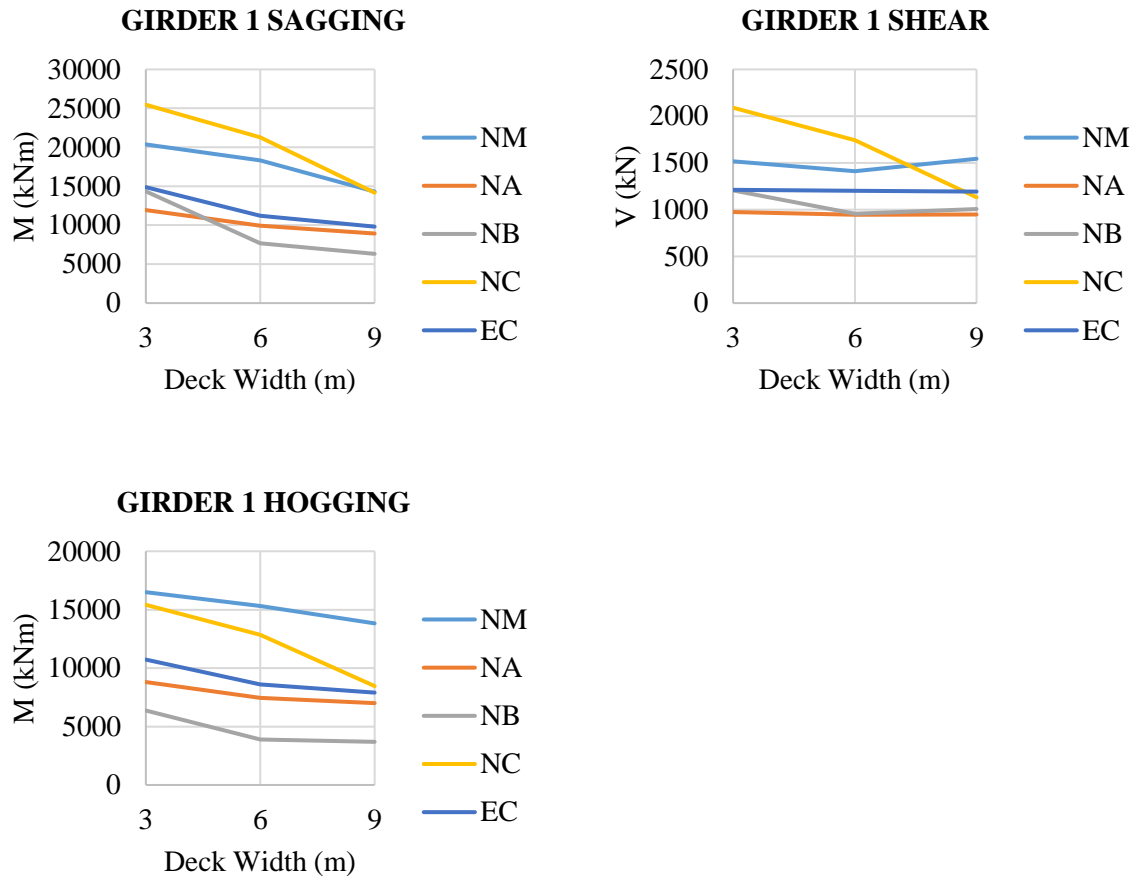


Figure 72 - Graphical results for 50 m span length characteristic

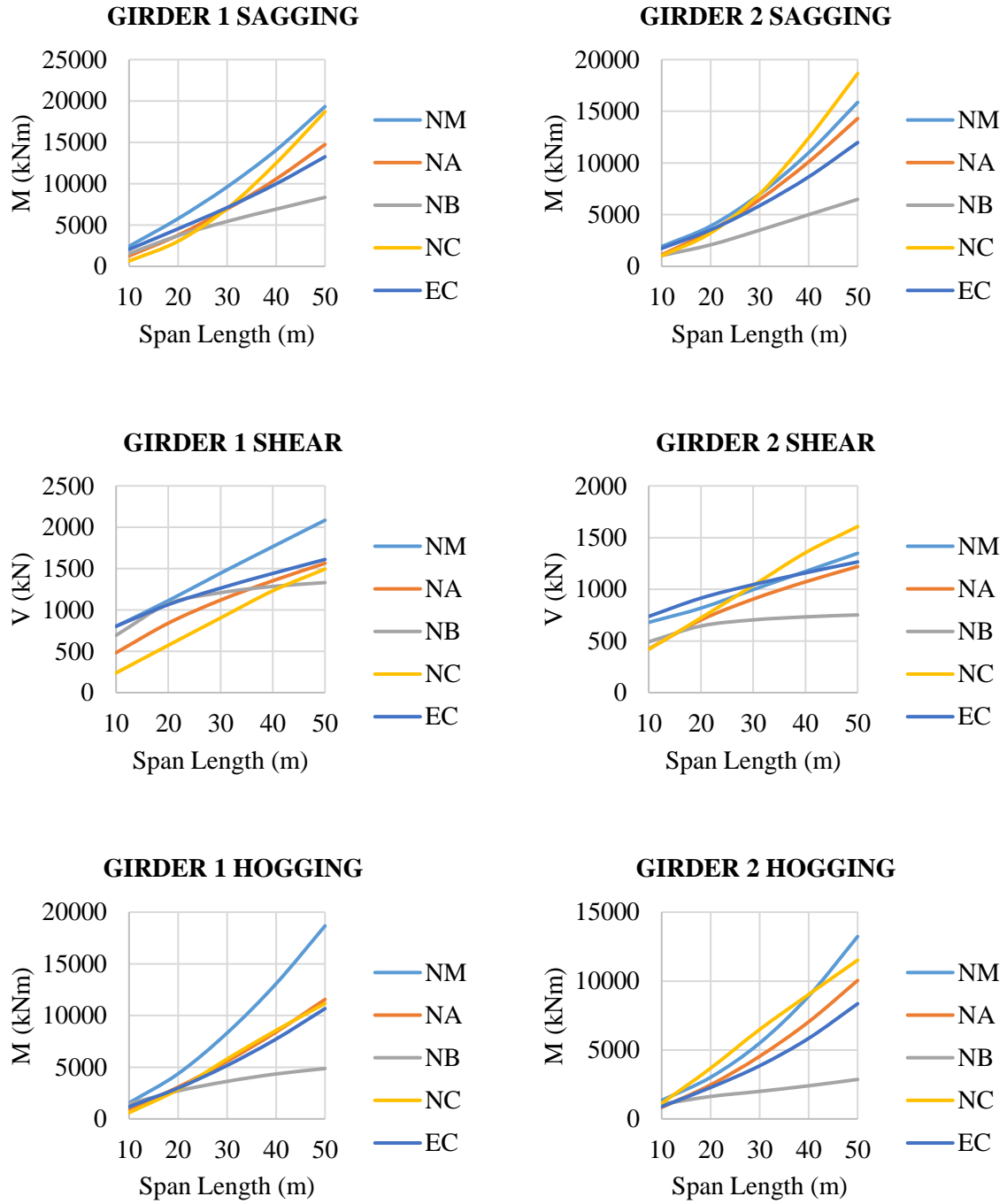


Figure 73 - Graphical results for 9 m deck width ULS

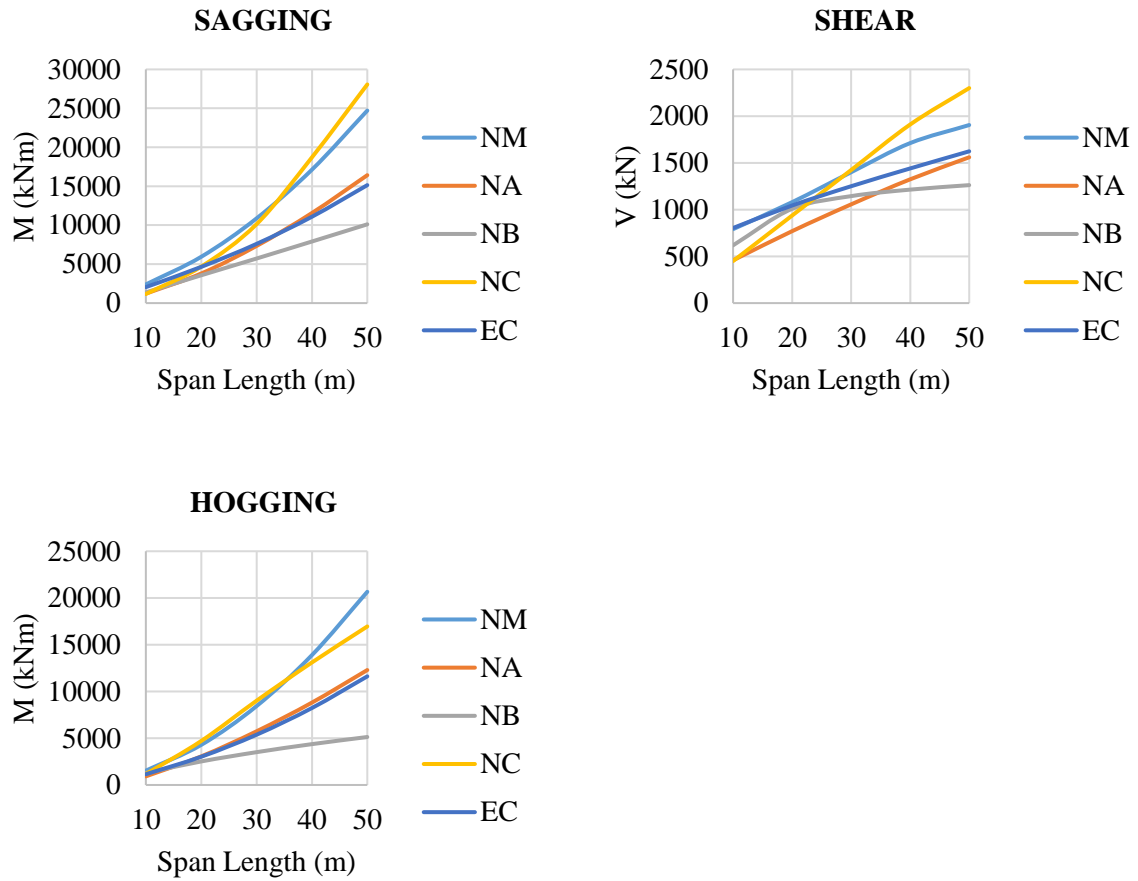


Figure 74 - Graphical results for 6 m deck width ULS

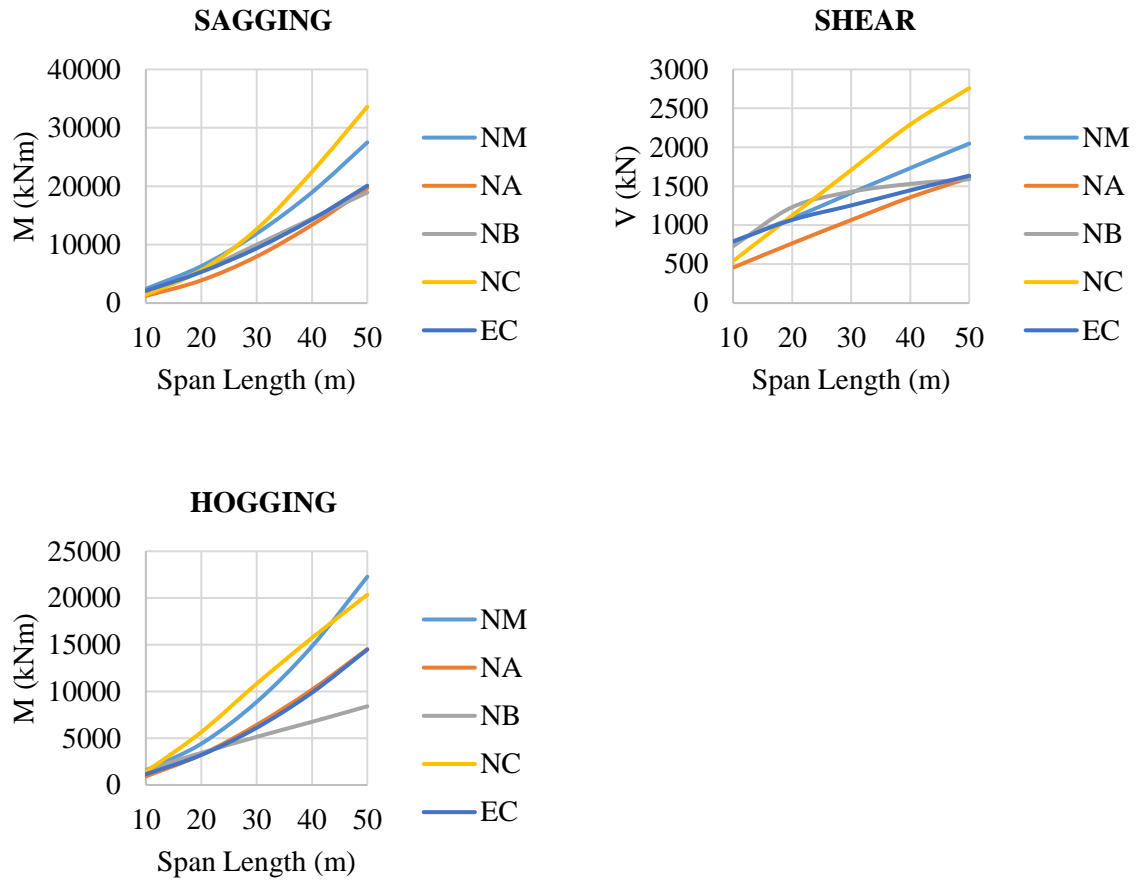


Figure 75 - Graphical results for 3 m deck width ULS

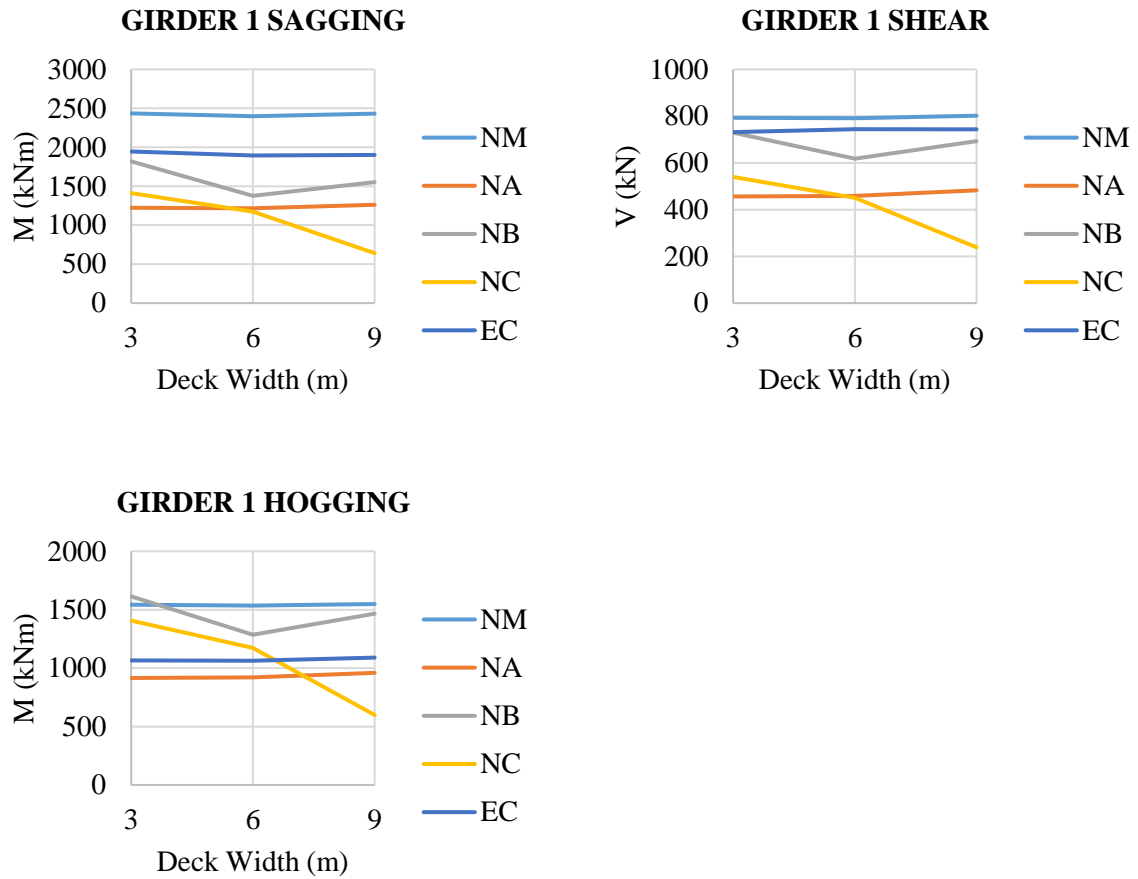


Figure 76 - Graphical results for 10 m span length ULS

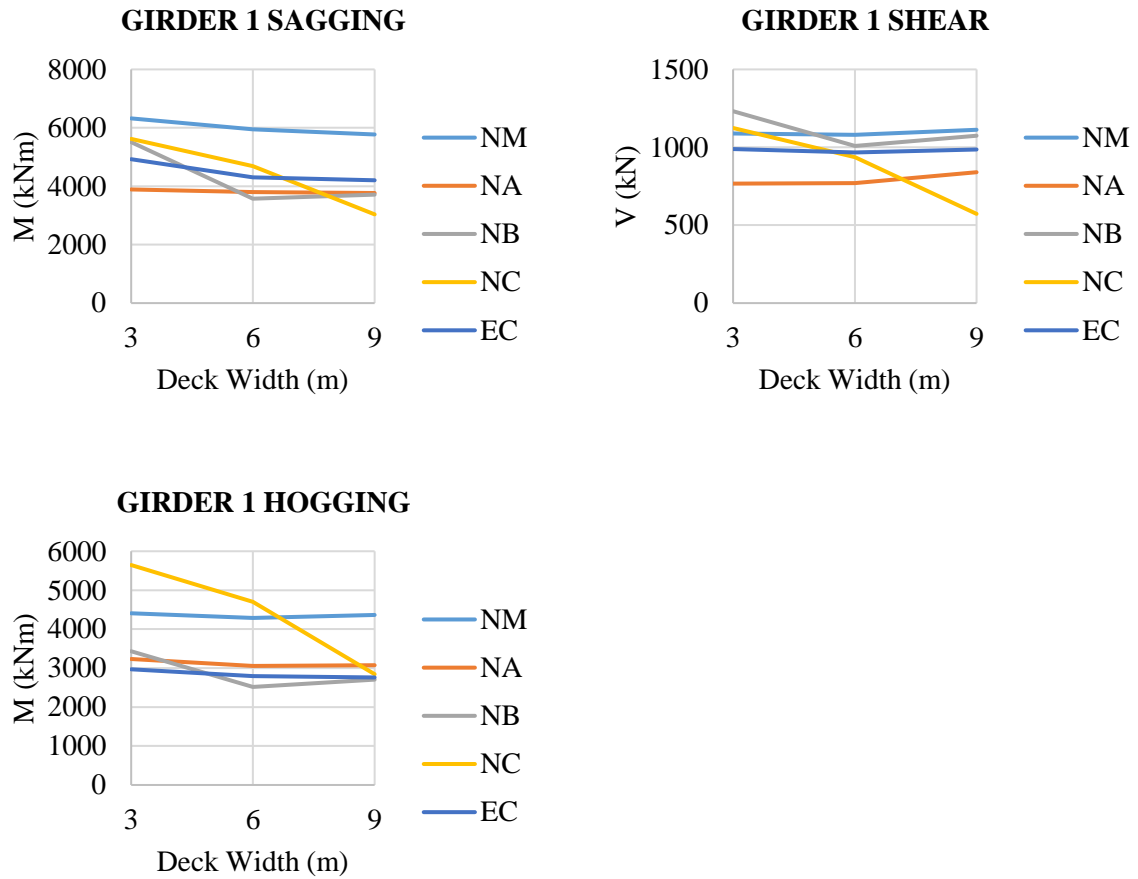


Figure 77 - Graphical results for 20 m span length ULS

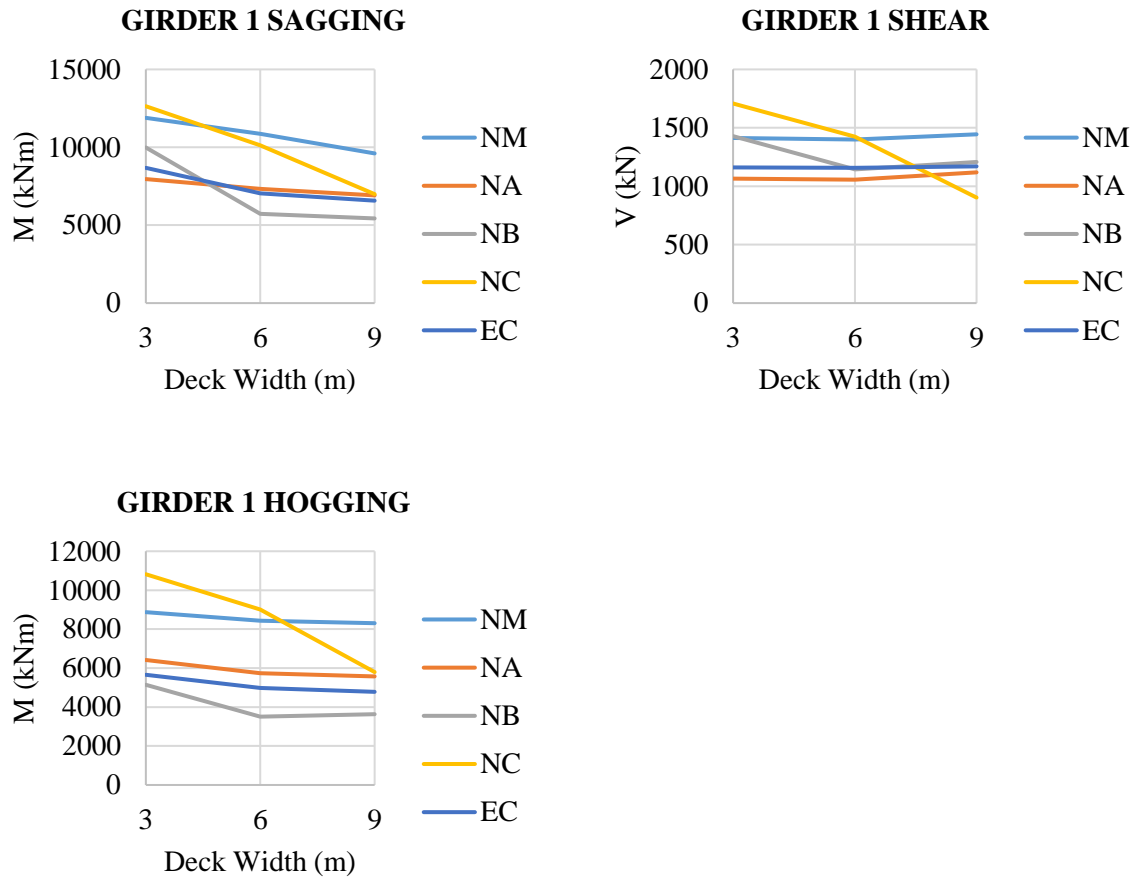


Figure 78 - Graphical results for 30 m span length ULS

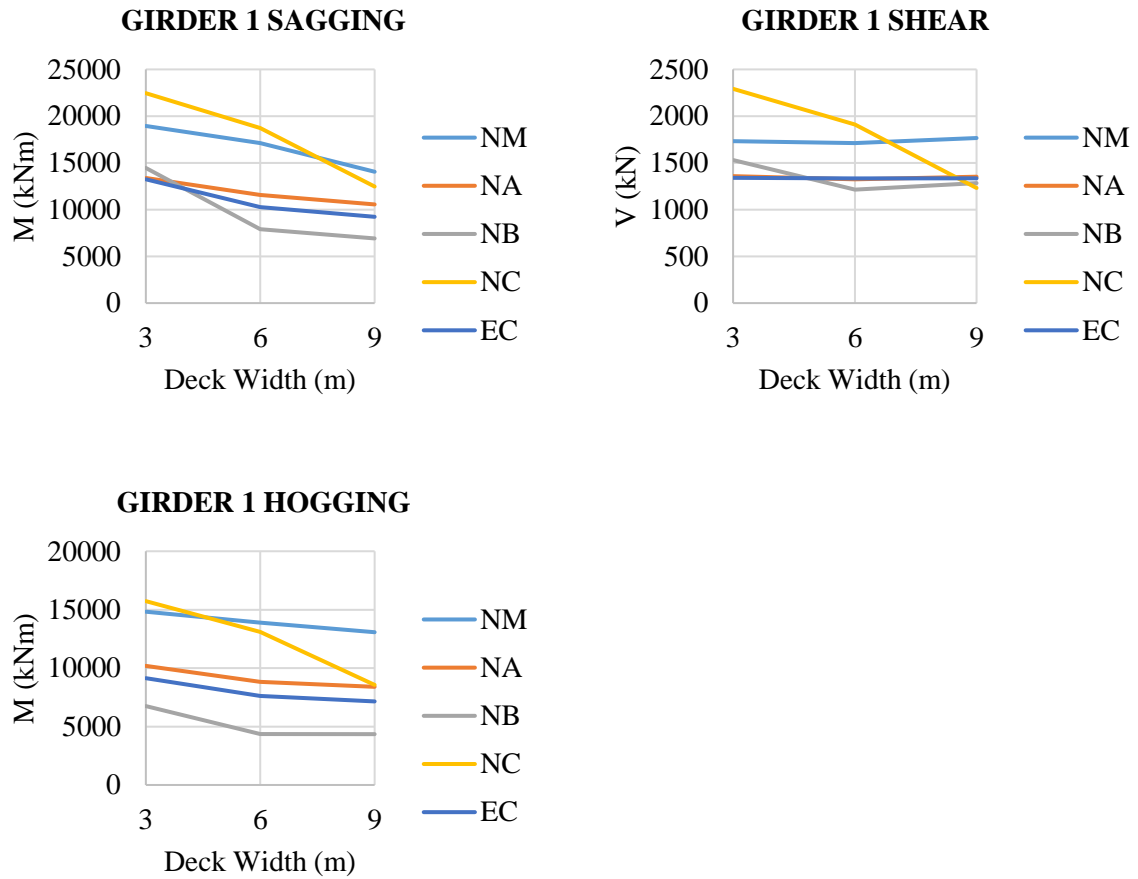


Figure 79 - Graphical results for 40 m span length ULS

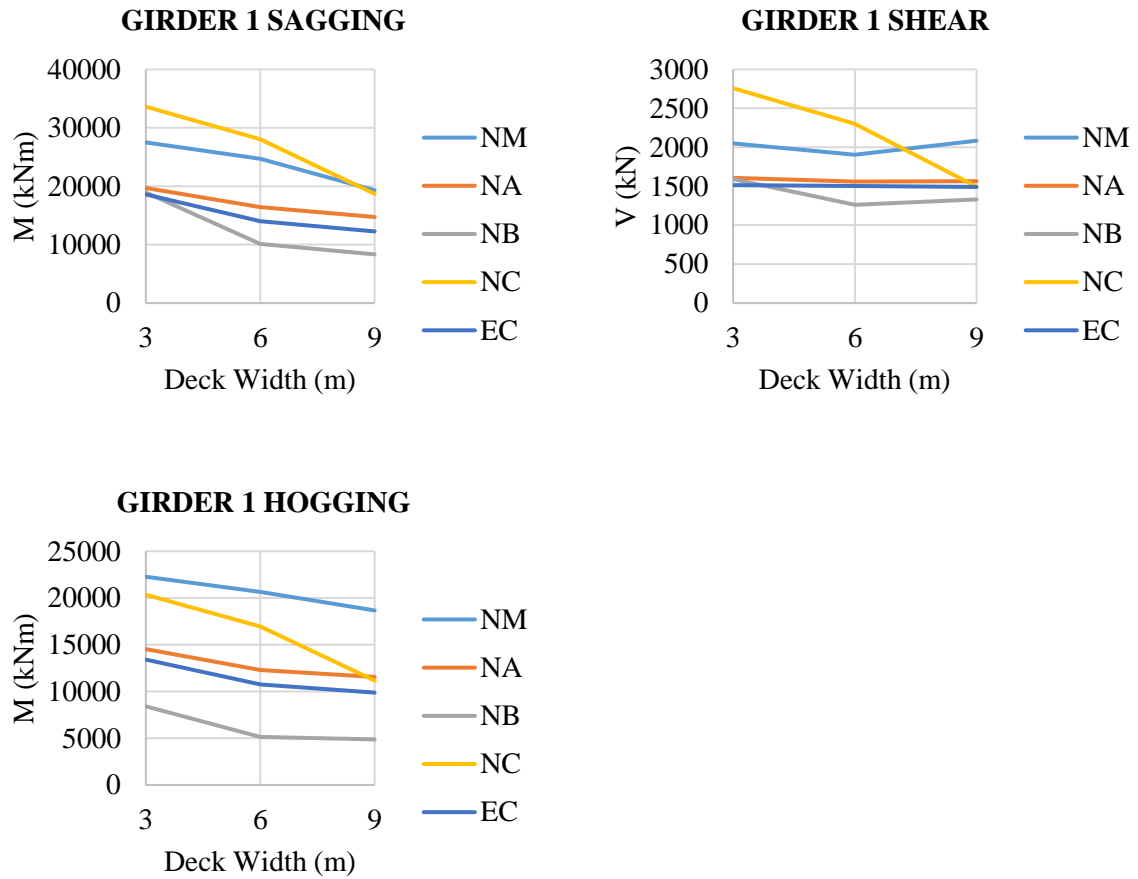


Figure 80 - Graphical results for 50 m span length ULS

Bibliography

- AASHTO. 2007. *AASHTO LRFD Bridge Design Specifications*. 4th ed. Washington.
- Abbas, K. & Tang, Y. 2013. Estimation of Parameters for Frechet Distribution Based on Type II Censored Samples. *Caspian Journal of Applied Sciences Research*. 2(7):36–43.
- Agarwal, A. & Cheung, M. 1987. Development of loading-truck model and live-load factor for the Canadian Standards Association CSA-S6 code. *Canadian Journal of Civil Engineering*. 14(1):58–67.
- Allaix, D.L. 2007. Bridge Reliability Analysis with an Up-to-Date Traffic Load Model. Politecnico di Torino. PhD Thesis.
- Anderson, J.R.B. 2006. Review of South African Live Load Models for Traffic Loading on Bridge and Culvert Structures Using WIM Data. University of Cape Town. Masters Thesis.
- Ang, A.H. & Tang, W.H. 1975. *Probability Concepts in Engineering Planning and Design: Basic principles*. Vol. 1. New York: Wiley.
- Anitori, G., Casas, J.R. & Ghosn, M. 2018. Methodology for development of live load models for refined analysis of short and medium-span highway bridges. *Structure and Infrastructure Engineering*. 14(4):477–490.
- Anitori, G., Casas, J.R. & Ghosn, M. 2017. WIM-Based Live-Load Model for Advanced Analysis of Simply Supported Short- and Medium-Span Highway Bridges. *Journal of Bridge Engineering*. 22(10):1–11.
- Ashebo, D.B., Chan, T.H.T. & Yu, L. 2007. Evaluation of dynamic loads on a skew box girder continuous bridge Part II: Parametric study and dynamic load factor. *Engineering Structures*. 29(6):1064–1073.
- Azimi, H., Galal, K. & Pekau, O.A. 2011. A modified numerical VBI element for vehicles with constant velocity including road irregularities. *Engineering Structures*. 33(7):2212–2220.
- Bailey, S.F. 1996. Basic Principles and Load Models for the Structural Safety Evaluation of Existing Road Bridges. EPFL. PhD Thesis.
- Bailey, S.F. & Bez, R. 1999. Site specific probability distribution of extreme traffic action effects. *Probabilistic Engineering Mechanics*. 14(1–2):19–26.

- Bakht, B. & Jaeger, L. 1990. Bridge Evaluation for Multipresence of Vehicles. *Journal of Structural Engineering*. 116(3):603–618.
- Banerjee, A., Merugu, S., Dhillon, I. & Ghosh, J. 2005. Clustering with Bregman Divergences. *Journal of Machine Learning Research*. 6:1705–1749.
- Basson, S. & Lenner, R. 2019. Reliability verification of bridges designed according to TMH7. In A. Zingoni (ed.). Cape Town: CRC Press *SEMC 2019: The Seventh International Conference on Structural Engineering, Mechanics and Computation*. 1–6.
- Bhattacharya, P. 2011. *Weibull Distribution for Estimating the Parameters*. P. Bhattacharya (ed.). Rijeka: Intech.
- Borman, S. 2004. *The Expectation Maximization Algorithm A short tutorial*. University of Utah. Lecture Notes.
- Bosman, J. 2004. Traffic loading characteristics of South African heavy vehicles. In *Proceedings of the 8th international symposium on heavy vehicle weights and dimensions, roads and the information highway*. 14–18.
- Broquet, C., Bailey, S.F., Fafard, M. & Brühwiler, E. 2004. Dynamic Behavior of Deck Slabs of Concrete Road Bridges. *Journal of Bridge Engineering*. 9(2):137–146.
- Bruhweiler, E. & Herwig, A. 2008. Consideration of dynamic traffic action effects on existing bridges at ultimate limit state. In H. Koh & D.M. Frangopol (eds.). Seoul: Taylor & Francis *Bridge Maintenance, Safety, Management, Health Monitoring and Informatics - IABMAS2008: Proceedings of the Fourth International IABMAS Conference*. 3675–3682.
- Cai, C.S., Shi, X.M., Araujo, M. & Chen, S.R. 2007. Effect of approach span condition on vehicle-induced dynamic response of slab-on-girder road bridges. *Engineering Structures*. 29(12):3210–3226.
- Canadian Standards Association. 2014. *CSA S6-14 Canadian Highway Bridge Design Code*.
- Caprani, C.C. 2005. Probabilistic Analysis of Highway Bridge Traffic Loading. University College Dublin. PhD Thesis.
- Caprani, C.C. 2017. Dynamic Load Allowance - A synthesis of the state of the art. In Melbourne: Austroads *10th Austroads Bridge Conference*. 1–10.
- Caprani, C.C. 2013. Lifetime Highway Bridge Traffic Load Effect from a Combination of

- Traffic States Allowing for Dynamic Amplification. *Journal of Bridge Engineering*. 18(9):901–909.
- Caprani, C.C. 2012. Calibration of a congestion load model for highway bridges using traffic microsimulation. *Structural Engineering International*. 22(3):342–348.
- Caprani, C.C. & O'Brien, E.J. 2010a. Estimating Extreme Highway Bridge Traffic Load Effects. In *Safety, reliability and risk of structures, infrastructures and engineering systems : proceedings of the Tenth International Conference on Structural Safety and Reliability (ICOSSAR2009), Osaka, Japan*. 3053–3060.
- Caprani, C.C. & O'Brien, E.J. 2010b. The use of predictive likelihood to estimate the distribution of extreme bridge traffic load effect. *Structural Safety*. 32(2):138–144.
- Caprani, C.C. & O'Brien, E.J. 2008. The governing form of traffic for highway bridge loading. In E. Cannon, R. West, & P. Fanning (eds.). *Galway Proceedings of 4th Symposium on Bridge and Infrastructure Research in Ireland*. 53–60.
- Caprani, C.C., O'Brien, E.J. & McLachlan, G.J. 2008. Characteristic Traffic Load Effects From a Mixture of Loading Events on Short to Medium Span Bridges. *Structural Safety*. 30(5):394–404.
- Caprani, C.C., Belay, A. & O'Connor, A.J. 2003. Site-specific Probabilistic Load Modelling for Bridge Reliability. In *Proceedings of the 3rd. International Conference on Current and Future Trends in Bridge Design*. 341–348.
- Caprani, C.C., González, A., Rattigan, P. & O'Brien, E.J. 2011. Assessment dynamic ratio for traffic loading on highway bridges. *Structure and Infrastructure Engineering*. 8(3):295–304.
- Carrillo, C., Cidrás, J., Díaz-Dorado, E. & Obando-Montaña, A.F. 2014. An approach to determine the weibull parameters for wind energy analysis: The case of Galicia (Spain). *Energies*. 7(4):2676–2700.
- Castillo, E. 1988. *Extreme value theory in engineering*. First edit ed. Academic Press Inc.
- CEN. 2002. *EN1990: Basis of structural design*. Brussels.
- CEN. 2003. *EN1991-2: Traffic loads on bridges*. Brussels.
- Chang, D. & Lee, H. 1994. Impact Factors for Simple-Span Highway Girder Bridges. *Journal*

of Structural Engineering. 120(3):704–715.

- Van Coile, R., Hopkin, D., Bisby, L. & Caspeepele, R. 2017. The meaning of Beta: Background and applicability of the target reliability index for normal conditions to structural fire engineering. In *6th International Workshop on Performance, Protection & Strengthening of Structures under Extreme Loading*. 528–536.
- Coles, S.G. 2001. *An introduction to Statistical Modeling of Extreme Values*. London: Springer.
- Committee of State Road Authorities. 1981. *TMH7 Parts 1 and 2: Code of Practice for the Design of Highway Bridges and Culverts in South Africa*.
- Committee of Transport Officials South Africa. 2016. *TMH3 Specifications for the Provision of Traffic and Weigh-in-Motion Monitoring Services*.
- Committee of Transport Officials South Africa. 2014. *TMH8 Traffic and Axle Load Monitoring Procedures*.
- Committee of Transport Officials South Africa. 2013. *TMH14 South African Standard Automatic Traffic Data Collection Format*.
- Cremona, C. 2001. Optimal Extrapolation of Traffic Load Effects. *Structural Safety*. 23(1):31–46.
- Crespo-Minguillón, C. & Casas, J.R. 1997. A Comprehensive Traffic Load Model for Bridge Safety Checking. *Structural Safety*. 19(4):339–359.
- Croce, P., Sanpaolesi, L. & Bruls, A. 1996. *ENV1991 - part 3 : Traffic Loads on Bridges : Calibration of Road Load Models for Road Bridges*. Zurich.
- Dawe, P. 2003. *Traffic loading on highway bridges*. 1st ed. London: Thomas Telford.
- Dempster, A.P., Laird, N.M. & Rubin, D.B. 1977. Maximum likelihood from incomplete data via the EM algorithm. *Journal of the Royal Statistical Society Series B Methodological*. 39(1):1–38.
- Deng, L., Yu, Y., Zou, Q. & Cai, C.S. 2015. State-of-the-Art Review of Dynamic Impact Factors of Highway Bridges. *Journal of Bridge Engineering*. 20(5):1–14.
- Ditlevsen, O. & Madsen, H. 2007. *Structural reliability methods*. First ed. Denmark: John Wiley & Sons.

- Doan, K., Sparling, B. & Feldman, L. 2016. Methods of Comparing Extreme Load Effects Based on Weigh-in-Motion Data. In *London Resilient Infrastructure, London, UK*. 1–11.
- Dunaiski, P. & Retief, J. 2009. *Background to SANS10160*. First ed. J. Retief & P. Dunaiski (eds.). Stellenbosch: SUN MEDIA.
- Enright, B. 2010. Simulation of Traffic Loading on Highway Bridges. University College Dublin. PhD Thesis.
- Enright, B. & OBrien, E.J. 2012. Monte Carlo Simulation of Extreme Traffic Loading on Short and Medium Span Bridges. *Structure and Infrastructure Engineering*. 9(12):1267–1282.
- Enright, B. & OBrien, E.J. 2011. *Cleaning Weigh-in-Motion Data: Techniques and Recommendations*. University College Dublin.
- Enright, B., Caprani, C.C. & OBrien, E.J. 2011. Modelling of Highway Bridge Traffic Loading: Some Recent Advances. In *Zurich 11th International Conference on Applications of Statistics and Probability in Civil Engineering (ICASP11), Zürich, Switzerland*. 397–405.
- Faber, M. 2009a. *Basics Of Structural Reliability*. ETH Zurich. Lecture Notes.
- Faber, M. 2009b. *Risk and Safety in Engineering*. ETH Zurich. Lecture Notes.
- fib. 2016. *Partial factor methods for existing concrete structures - Bulletin 80*. Lausanne.
- Figueiredo, M. & Jain, A.K. 2002. Unsupervised learning of finite mixture models. *Pattern Analysis and Machine Intelligence, IEEE Transactions on*. 24(3):381–396.
- Flint, A.R. & Jacob, B. 1996. Extreme Traffic Loads on Road Bridges and Target Values of Their Effects for Code Calibration. *Proceedings of IABSE Colloquium*. 469–478.
- Fu, G. & You, J. 2009. Truck Loads and Bridge Capacity Evaluation in China. *Journal of Bridge Engineering*. 14(5):327–335.
- Fu, G., Liu, L. & Bowman, M.D. 2013. Multiple Presence Factor for Truck Load on Highway Bridges. *Journal of Bridge Engineering*. 18(3):240–249.
- Garcia, V., Nielsen, F. & Nock, R. 2010. Levels of details for Gaussian mixture models. In Vol. 5995 LNCS. Xi'an *Lecture Notes in Computer Science (including subseries Lecture Notes in Artificial Intelligence and Lecture Notes in Bioinformatics)*. 514–525.
- Genschel, U. & Meeker, W.Q. 2010. A Comparison of Maximum Likelihood and Median-

- Rank Regression for Weibull Estimation. *Quality Engineering*. 22:236–255.
- Getachew, A. 2003. Traffic Load Effects on Bridges. Royal Institute of Technology Stockholm. PhD Thesis.
- Getachew, A. & OBrien, E.J. 2007. Simplified site-specific traffic load models for bridge assessment. *Structure and Infrastructure Engineering*. 3(4):303–311.
- Ghosn, M. & Moses, F. 1986. Reliability Calibration of Bridge Design Code. *Journal of Structural Engineering*. 112(4):745–763.
- Ghosn, M., Moses, F. & Wang, J. 2003. *NCHRP Report 489 - Design of highway bridges for extreme events*. Washington DC.
- Gindy, M. & Nassif, H. 2007. Multiple Presence Statistics for Bridge Live Load Based on Weigh-in-Motion Data. *Transportation Research Record: Journal of the Transportation Research Board*. 2028(14):125–135.
- González, A., Dowling, J., OBrien, E.J. & Znidaric, A. 2010. Experimental determination of dynamic allowance for traffic loading in bridges. In Washington DC: Transportation Research Board *TRB 89th Annual Meeting*.
- González, A., Znidaric, A., Casas, J.R., Enright, B., OBrien, E.J., Lavric, I. & Kalin, J. 2009. *ARCHES Recommendations on dynamic amplification allowance*. Brussels.
- Grave, S. 2001. Modelling of Site-Specific Traffic Loading on Short to Medium Span Bridges. Trinity College Dublin. PhD Thesis.
- Hanswille, G. & Sedlacek, G. 2007. *Background Report Traffic loads on road bridges - Basis of the load models in EN1991-2 and DIN-Report 101*. Aachen.
- Harman, D. & Davenport, A. 1976. *The formulation of vehicular loading for the design of highway bridges in Ontario*. Ontario.
- Heitner, B., OBrien, E.J., Schoefs, F., Yalamas, T., Décatoire, R. & Leahy, C. 2016. Evaluation of bridge safety based on Weigh-in-Motion data. *Civil Engineering Research in Ireland 2016*.
- Hellebrandt, L., Blom, C.B.M. & Steenbergen, R.D.J.M. 2014. Probabilistic Traffic Load Model for Short-span City Bridges. *Heron*. 59(2/3):147–168.
- Heywood, R., Gordon, R. & Bouilly, G. 2000. Australia's bridge design load model: Planning

- for an efficient road transport industry. *Transportation Research Record: Journal of the Transportation Research Board*. 1696(1):1–7.
- Holicky. 2009. *Reliability analysis for structural design*. First ed. Stellenbosch: SUN meDIA.
- Holicky, M. 2011. The target reliability and design working life. In Antwerp *Fourth international conference on safety and security engineering*. 161–170.
- Hong, H.P., Ye, W. & Li, S.H. 2016. Sample size effect on the reliability and calibration of design wind load. *Structure and Infrastructure Engineering*. 12(6):752–764.
- Huang, D., Wang, T. & Shahawy, M. 1993. Impact Studies of Multigirder Concrete Bridges. *Journal of Structural Engineering*. 119(8):2387–2402.
- Humar, J. & Kashif, A. 1995. Dynamic response analysis of slab-type bridges. *Journal of Structural Engineering*. 121(1):48–62.
- Huynh, N.P. & Fang, T.E. 1989. Parameter estimation for the general extreme value distribution. *Water SA*. 15(2):57–64.
- Hwang, E. & Nowak, A.S. 1991. Simulation of Dynamic Load for Bridges. *Journal of Structural Engineering*. 117(5):1413–1434.
- ISO. 2015. *General Principles on Reliability for Structures ISO2394*. Geneva.
- Jacob, B. & Feypell-de La Beaumelle, V. 2010. Improving truck safety: Potential of weigh-in-motion technology. *IATSS Research*. 34(1):9–15.
- Jacob, B., OBrien, E.J. & Jehaes, S. 2002. *COST 323 Weigh-in-Motion of Road Vehicles*. Paris.
- Jaeger, L. & Bakht, B. 1987. Multiple Presence Reduction Factors for Bridges. In Orlando *Bridge and transmission line structures*. 47–59.
- Kantar, Y.M. 2015. Generalized least squares and weighted least squares estimation methods for distributional parameters. *Revstat*. 13(3):263–282.
- Kernane, T. & Raizah, Z. 2010. Estimation of the Parameters of Extreme Value Distributions from Truncated Data Via the EM Algorithm. *HAL*. 1–6.
- Kirkegaard, P.H., Nielsen, S.R.K. & Envoldsen, I. 1997. *Heavy vehicles on minor highway bridges*. Aalborg.
- Konig, G. & Hosser, D. 1982. *The simplified level II method and its application on the*

derivation of safety elements for level I - CEB Bulletin no 147 Conceptual preparation of future codes (Progress report). Paris.

Kozikowski, M. 2009. WIM Based Live Load Model for Bridge Reliability. University of Nebraska. PhD Thesis.

Kulicki, J., Prucz, Z., Clancy, C., Mertz, D. & Nowak, A.S. 2007. *Updating the calibration report for AASHTO LRFD code*.

Kwasniewski, L., Wekezer, J., Roufa, G., Li, H., Ducher, J. & Malachowski, J. 2006. Experimental Evaluation of Dynamic Effects for a Selected Highway Bridge. *Journal of Performance of Constructed Facilities*. 20(3):253–260.

Laman, J.A., Pechar, J.S. & Boothby, T.E. 1999. Dynamic Load Allowance for Through-Truss Bridges. *Journal of Bridge Engineering*. 4(4):231–241.

Law, S.S. & Zhu, X.Q. 2005. Bridge dynamic responses due to road surface roughness and braking of vehicle. *Journal of Sound and Vibration*. 282(2005):805–830.

Leahy, C., O'Brien, E.J. & O'Connor, A.J. 2015. Traffic Load Effect Forecasting for Bridges. In Geneva: IABSE *IABSE Conference Geneva 2015: Structural Engineering: Providing Solutions to Global Challenges*. 994–1001.

Leahy, C., O'Brien, E.J., Enright, B. & Hajializadeh, D. 2015. Review of HL-93 Bridge Traffic Load Model Using an Extensive WIM Database. *Journal of Bridge Engineering*. 20(10):04014115-1–8.

Lenner, R. 2014. Safety Concept and Partial Factors for Military Assessment of Existing Concrete Bridges. Universitat der Bundeswehr Munchen. Dr-Ing Thesis.

Lenner, R., de Wet, D.P.G. & Viljoen, C. 2017. Bridge Loading and Traffic Characteristics in South Africa. *Journal of the South African Institution of Civil Engineering*. 59(4):34–46.

Lenner, R., Keuser, M. & Sykora, M. 2014. Safety Concept and Partial Factors for Bridge Assessment under Military Loading. *Advances in Military Technology*. 9(2):5–20.

Li, H. 2005. Dynamic response of highway bridges subjected to heavy vehicles. Florida State University. PhD Thesis.

Lucic, M., Bachem, O. & Krause, A. 2015. Strong Coresets for Hard and Soft Bregman Clustering with Applications to Exponential Family Mixtures. In Vol. 51 *AISTATS*.

- Ludescher, H. & Bruhwiler, E. 2009. Dynamic amplification of traffic loads on road bridges. *Structural Engineering International: Journal of the International Association for Bridge and Structural Engineering (IABSE)*. 19(2):190–197.
- Mahdi, S. 2005. Estimating Parameters of Gumbel Distribution Using the Methods of Moments, Probability Weighted Moments and Maximum Likelihood. *Mahdi – M.Cenac Rev.Mate.Teor.Aplic.* 12(12):151–156.
- Malan, A. & Van Rooyen, G.C. 2013. Critical normal traffic loading for flexure of skew bridges according to TMH7. *Journal of the South African Institution of Civil Engineering*. 55(3):86–95.
- Marušić, M. & Markovic, D. 2010. Least squares fitting the three-parameter inverse Weibull density. *Math. Commun.* 15(2):539–553.
- McLachlan, G.J. & Peel, D. 2000. *Finite Mixture Models*. Queensland: John Wiley & Sons.
- Melchers, R. & Beck, A. 2018. *Structural reliability analysis and prediction*. Third ed. Hoboken: John Wiley & Sons.
- Messervey, T.B., Frangopol, D.M. & Casciati, S. 2011. Application of the statistics of extremes to the reliability assessment and performance prediction of monitored highway bridges. *Structure and Infrastructure Engineering*. 7(1–2):87–99.
- Miao, T.J. & Chan, T.H.T. 2002. Bridge Live Load Models From WIM Data. *Engineering Structures*. 24(8):1071–1084.
- Montgomery, D.C. & Runger, G.C. 2010. *Applied Statistics and Probability for Engineers*. 4th Editio ed. Arizona: John Wiley & Sons.
- van Nierop, S., Viljoen, C. & Lenner. 2017. Target reliability of concrete structures governed by serviceability limit state design. In Dresden *15th International Probabilistic Workshop*. 1–10.
- Nowak, A.S. 1993. Load model for highway bridges. *Structural Safety*. 13(1–2):53–66.
- Nowak, A.S. 1994. Load Model for Bridge Design Code. *Canadian Journal of Civil Engineering*. 21(1):36–49.
- Nowak, A.S. & Collins, K. 2002. *Reliability of Structures*. 1st Editio ed. McGraw-Hill Higher Education.

- Nowak, A.S. & Grouni, H. 1984. Calibration of the Ontario highway bridge design code 1983 edition. *Canadian Journal of Civil Engineering*. 11:760–770.
- Nowak, A.S. & Grouni, H.N. 1994. Calibration of the Ontario highway bridge design code 1991 edition. *Canadian journal of civil engineering*. 21(1):25–35.
- Nowak, A.S. & Hong, Y. 1991. Bridge Live-Load Models. *Journal of Structural Engineering*. 117(9):2757–2767.
- Nowak, A.S. & Iatsko, O. 2017. Revised load and resistance factors for the AASHTO LRFD Bridge Design Specifications. *PCI Journal*. 62(3):46–58.
- Nowak, A.S. & Rakoczy, P. 2013. WIM-based live load for bridges. *KSCE Journal of Civil Engineering*. 17(3):568–574.
- Nowak, A.S. & Szerszen, M.M. 1998. Bridge Load and Resistance Models. *Engineering Structures*. 20(11):985–990.
- Nowak, A.S. & Szerszen, M.M. 2000. Structural reliability as applied to highway bridges. *Progress in Structural Engineering and Materials*. 2(2):218–224.
- Nowak, A.S., Nassif, H. & DeFrain, L. 1993. Effect of truck loads on bridges. *Journal of Transportation Engineering*. 119(6):853–867.
- Nwobi, F.N. & Ugomma, C.A. 2014. A Comparison of Methods for the Estimation of Weibull Distribution Parameters. *Metodološki Zvezki - Advances in Methodology and Statistics*. 11(1):65–78.
- O'Connor, A.J. & O'Brien, E.J. 2003. An Assessment of the Influence of Dynamic Interaction Modelling on Predicted Characteristic Load Effects in Bridges. In Shanghai: Thomas Telford *3rd International Conference on Current and Future Trends in Bridge Design*.
- O'Connor, A.J. & O'Brien, E.J. 2005. Traffic Load Modelling and Factors Influencing the Accuracy of Predicted Extremes. *Canadian Journal of Civil Engineering*. 32(1):270–278.
- O'Connor, C. & Shaw, P. 2000. *Bridge Loads - An International Perspective*. First ed. London: Spon Press.
- O'Brien, E.J. & Enright, B. 2013. Using Weigh-In-Motion Data to Determine Aggressiveness of Traffic for Bridge Loading. *Journal of Bridge Engineering*. 18(3):232–239.
- O'Brien, E.J. & Enright, B. 2011. Modeling same-direction two-lane traffic for bridge loading.

- Structural Safety*. 33(4–5):296–304.
- O'Brien, E.J., Schmidt, F., Hajializadeh, D., Zhou, X.Y., Enright, B., Caprani, C.C., Wilson, S. & Sheils, E. 2015. A review of probabilistic methods of assessment of load effects in bridges. *Structural Safety*. 53:44–66.
- O'Brien, E.J., O'Connor, A.J. & Arrigan, J.E. 2012. Procedures for Calibrating Eurocode Traffic Load Model 1 for National Conditions. In Lake Maggiore *Bridge Maintenance, Safety, Management, Resilience and Sustainability - Proceedings of the Sixth International Conference on Bridge Maintenance, Safety and Management*. 2597–2603.
- O'Brien, E.J., Hajializadeh, D., Donovan, O. & Enright, B. 2012. Bridge traffic load estimation of lifetime maximum distributions of bridge effects. In Stresa *IABMAS 2012*. 1482–1488.
- O'Brien, E.J., Enright, B. & Getachew, A. 2010. Importance of the Tail in Truck Weight Modeling for Bridge Assessment. *Journal of Bridge Engineering*. 15(2):210–213.
- O'Brien, E.J., Rattigan, P., González, A., Dowling, J. & Žnidarič, A. 2009. Characteristic dynamic traffic load effects in bridges. *Engineering Structures*. 32(2009):1607–1612.
- O'Brien, E.J., Cantero, D., Enright, B. & González, A. 2010. Characteristic Dynamic Increment for extreme traffic loading events on short and medium span highway bridges. *Engineering Structures*. 32(2010):3827–3835.
- Oosthuizen, A.P.C., Meintjies, C.J., Trumpelmann, V., Peters, D., Ullmann, K.K.A.B. & Oppermann, G.H.P. 1991. *TMH7 Part 2: Traffic Loading (1991) Proposed Substitution of Section 2.6*. Cape Town.
- Paultre, P., Chaallal, O. & Proulx, J. 1992. Bridge dynamics and dynamic amplification factors - a review of analytical and experimental findings. *Canadian Journal of Civil Engineering*. 19(2):260–278.
- Phien, H.N. & Fang, T.S. 1989. Maximum likelihood estimation of the parameters and quantiles of the general extreme-value distribution from censored samples. *Journal of Hydrology*. 105(1989):139–155.
- Picard, F. 2007. *An Introduction to mixture models*. University d'Evry. Lecture Notes.
- Pobocikova, I. & Sedliackova, Z. 2014. Comparison of four methods for estimating the Weibull Distribution Parameters. *Applied Mathematical Sciences*. 8(83):4137–4149.

- Quilligan, M. 2003. Bridge weigh in motion. Royal Institute of Technology Stockholm. Licentiate.
- Rackwitz, R. 2000. Optimization — the basis of code-making and reliability verification. *Structural Safety*. 22(1):27–60.
- SABS. 2011. *Basis of structural design and actions for buildings and industrial structures Part 1*. Pretoria: SABS.
- SABS. 2018. *SANS 10160-1:2018 Basis of structural design and actions for buildings and industrial structures*. Pretoria.
- Schneider, J. 1997. *Introduction to safety and reliability of structures*. First ed. Zurich: IABSE.
- Schwarz, M. & Laman, J.A. 2001. Response of Prestressed Concrete I-Girder Bridges to Live Load. *Journal of Bridge Engineering*. 6(1):1–8.
- Sedlacek, G., Merzenich, G., Paschen, M., Bruls, A., Sanpaolesi, L., Croce, P., Calgaro, J.A. & Pratt, M. 2008. *Background document to EN 1991- Part 2 - Traffic loads for road bridges - and consequences for the design*.
- Sivakumar, B., Ghosn, M. & Moses, F. 2011. *NCHRP 683 Protocols for Collecting and Using Traffic Data in Bridge Design Prepared for NCHRP*. Washington DC.
- Sivakumar, B., Moses, F. & Ghosn, M. 2008. *Protocols for Collecting and Using Traffic Data in Bridge Design Prepared for NCHRP*. Paramus.
- Slavik, M. 2007. Weigh-in-motion: Years of South African experience. *Journal of the South African Institution of Civil Engineering*. 49(1):11–16.
- Slavik, M. 1998. Weighing of Trucks in Motion: Calibration of Equipment and Correction of Measurements. In Durban, South Africa *4th International Conference on Managing Pavements*.
- Smith, J. 1988. *Vibration of structures : applications in civil engineering*. New York: Chapman and Hall.
- Soriano, M., Casas, J.R. & Ghosn, M. 2016. Simplified Probabilistic Model for Maximum Traffic Load From Weigh-In-Motion Data. *Structure and Infrastructure Engineering*. 13(4):454–467.
- Van der Spuy, P.F. 2014. A Comparative Study Between the South African and European

- Bridge Design Codes for Bending and Shear. University of Cape Town. MEng Thesis.
- Van der Spuy, P.F. & Lenner, R. 2019. Towards a new bridge live load model for South Africa. *Structural Engineering International*. 29(2):292–298.
- Van der Spuy, P.F. & Lenner, R. 2018. Developing a new bridge live load model for South Africa. In Powers, Frangopol, Al-Mahaidi, & Caprani (eds.). Melbourne: Taylor & Francis *Proceedings of the ninth international conference on bridge maintenance, safety and management (IABMAS)*. 1405–1410.
- Van der Spuy, P.F., Lenner, R., de Wet, T. & Caprani, C.C. 2019a. Multiple lane reduction factors based on multiple lane weigh in motion data. *Structures*. 20:543–549.
- Van der Spuy, P.F., Lenner, R., de Wet, T. & Caprani, C.C. 2019b. Multilane Reduction Factors Based on WIM Data. In A. Zingoni (ed.). Cape Town: CRC Press *SEMC 2019: The Seventh International Conference on Structural Engineering, Mechanics and Computation*. 1–6.
- Van der Spuy, P.F., Lenner, R. & Meyer, M.M. 2019. Dynamic amplification factor for South African bridges. In A. Zingoni (ed.). Cape Town: CRC Press *SEMC 2019: The Seventh International Conference on Structural Engineering, Mechanics and Computation*. 1–6.
- Standards Australia. 2004. *AS5100.2-2004 Bridge Design Part 2: Design loads*. Sydney.
- Steenbergen, R.D.J.M. & Morales Napoles, O. 2012. Traffic Load Model Based on Weigh-In-Motion Measurements. In Vol. 2 *11th International Probabilistic Safety Assessment and Management Conference and the Annual European Safety and Reliability Conference 2012, PSAM11 ESREL 2012*. 933–945.
- Stutterheim, C. 1988. *Loadings and Codes*. University of Pretoria. Course Notes.
- Sykora, M. & Holicky, M. 2011. Comparison of load combination models for probabilistic calibrations. In Zurich: Taylor & Francis *ICASP11*.
- Sykora, M., Holicky, M. & Markova, J. 2013. Verification of existing reinforced concrete bridges using the semi-probabilistic approach. *Engineering Structures*. 56(2013):1419–1426.
- Szurgott, P., Wekezer, J., Kwasniewski, L., Siervogel, J. & Ansley, M. 2011. Experimental assessment of dynamic responses induced in concrete bridges by permit vehicles. *Journal of Bridge Engineering*. 16(1):108–116.

- Tiryakioğlu, M. 2008. On estimating Weibull modulus by moments and maximum likelihood methods. *Journal of Materials Science*. 43(2):793–798.
- Vrouwenvelder, T. & Waarts, P.H. 1993. Traffic Loads on Bridges. *Structural Engineering International*. 3(3):169–177.
- Wang, T., Huang, D. & Shahawy, M. 1992. Dynamic Response of Multigirder Bridges. *Journal of Structural Engineering*. 118(8):2222–2238.
- de Wet, D.P.G. 2010a. Post-Calibration and Quality Management of Weigh-in-Motion Traffic Data. Stellenbosch University. MScEng Thesis.
- de Wet, D.P.G. 2010b. WIM Calibration and Data Quality Management. *Journal of the South African Institution of Civil Engineering*. 52(2):70–76.
- Yang, Y.-B., Liao, S.-S. & Lin, B.-H. 1995. Impact Formulas for Vehicles Moving over Simple and Continuous Beams. *Journal of Structural Engineering*. 121(11):1644–1650.
- Zhang, H. & Huang, Y. 2015. Finite Mixture Models and Their Applications: A Review. *Austin Biom and Biostat*. *Austin Biom and Biostat*. 2(2):1013–1.
- Zhou, X.Y. 2013. Statistical Analysis of Traffic Loads and Traffic Load Effects on Bridges. Universite Paris Est. PhD Thesis.
- Zhou, J., Shi, X., Caprani, C.C. & Ruan, X. 2018. Multi-lane factor for bridge traffic load from extreme events of coincident lane load effects. *Structural Safety*. 72:17–29.
- Zhou, X.Y., Schmidt, F. & Jacob, B. 2012. Extrapolation of Traffic Data for Development of Traffic Load Models: Assessment of Methods Used During Background Works of the Eurocode. In *Bridge Maintenance, Safety, Management, Resilience and Sustainability - Proceedings of the Sixth International Conference on Bridge Maintenance, Safety and Management*. 1503–1509.
- Zhou, X.Y., Schmidt, F., Toutlemonde, F. & Jacob, B. 2016. A mixture peaks over threshold approach for predicting extreme bridge traffic load effects. *Probabilistic Engineering Mechanics*. 43:121–131.